Dissertation

Comprehensive metabolome analysis of the marine microalga *Emiliania huxleyi* regarding calcification status, growth phase and nutrient-starvation response

zur Erlangung des akademischen Grades
Doktor der Naturwissenschaften (Dr. rer. nat.)

vorgelegt von
Robin Wördenweber

angefertigt an der Fakultät für Biologie der Universität Bielefeld
Lehrstuhl für Algenbiotechnologie und Bioenergie
unter der Betreuung von Herrn Prof. Dr. Olaf Kruse
Januar 2017

II

Eigenständigkeitserklärung

Hiermit versichere ich, dass ich die vorliegende Dissertation selbstständig verfasst und keine anderen als die angegebenen Quellen und Hilfsmittel verwendet habe. Alle aus der Literatur ganz oder teilweise entnommenen Stellen habe ich als solche kenntlich gemacht.

Weiterhin erkläre ich, dass die vorliegende Dissertation weder vollständig noch teilweise einer anderen Fakultät zur Erlangung eines akademischen Grades vorgelegt wurde.

Bielefeld, den 30.01.2017

Robin Wördenweber

Contents

Abbreviations

1N	haploid life-cycle stage (*E. huxleyi* RCC 1217)
2N	diploid life-cycle stage (*E. huxleyi* RCC 1216)
3-NPH	3-nitrophenylhydrazine
β-caro	β-carotene
BLL	betaine-like lipid (betaine lipid)
but-fucoxanthin	19'-butanoyloxy-fucoxanthin
CAD	charged aerosol detector
caro	carotenoids
chl a	chlorophyll a
chl c	chlorophyll c
chl c_2	chlorophyll c_2
chl c_2-MGDG	chlorophyll c_2-monogalactosyldiacylglycerol
chl c_3	chlorophyll c_3
CT	cultivation temperature
ddx	diadinoxanthin
DGCC	diacylglyceryl carboxyhydroxymethylcholine
DGDG	digalactosyldiacylglycerol
DGTS	diacylglyceryl trimethylhomoserine
DIC	dissolved inorganic carbon
DMSP	dimethylsulfoniopropionate
dtx	diatoxanthin
E. huxleyi	*Emiliania huxleyi*
EDC	1-ethyl-3-(3-dimethylaminopropyl)carbodiimide hydrochloride
Eq.	equation
ESAW	enriched seawater, artificial water
EI	electron impact ionization
ESI	electrospray ionization
FAME	fatty acid methyl esters
FCP	fucoxanthin-chlorophyll a/c-binding protein
FID	flame-ionization detection
FTIR	Fourier transform infrared spectroscopy
fuco	fucoxanthin
F_v/F_m	maximum quantum efficiency of photosystem II photochemistry
GC	gas chromatography
GC-FID	gas chromatography-flame ionization detection
GC-MS	gas chromatography-mass spectrometry
GMD	Golm Metabolome Database
GSL	glycosphingolipid
h4k-fuco/h4k-fucoxanthin	19'-hexanoyloxy-4-ketofucoxanthin
hex-fuco/hex-fucoxanthin	19'-hexanoyloxyfucoxanthin
hGSL	host-glycosphingolipid (sphingolipid)
HPLC	high-performance liquid chromatography
LC	liquid chromatography
LC-MS/MS	liquid chromatography-tandem mass spectrometry
LC-MS/MS	liquid chromatography coupled with tandem mass-spectrometry
LED	light-emitting diode

MGDG	monogalactosyldiacylglycerol
MS	mass spectrometry
MSTFA	N-Methyl-N-(trimethylsilyl)trifluoroacetamide
m/z	mass-to-charge ratio
N	nitrogen
NIST	National Institute of Standards and Technology
NL/NLF	neutral lipid fraction
P	phosphorus
PC	phosphatidylcholine
PDPT	phosphatidyl-S,S-dimethylpropanethiol
PE	phosphatidylethanolamine
PG	phosphatidylglycerol
PL/PLF	polar lipid fraction
PS I/PS II	photosystem I, photosystem II
PULCA	polyunsaturated long-chain alkenones, alkenoates, alkenes
RCC	Roscoff Culture Collection
ROS	reactive oxygen species
RT	retention time
SD	standard deviation
SEM	scanning electron microscopy
sGSL	sialic-glycosphingolipid
SQDG	sulphoquinovosyldiacylglycerol
SST	sea surface temperature
TAG	triacylglyceride
TLC	thin layer chromatography
$U^{K'}_{37}$	alkenone unsaturation index
UV-vis	ultraviolet-visible spectroscopy

1. Summary

Emiliania huxleyi is the most abundant calcifying microalgae in the ocean, and plays an important role in the global carbon and sulfur cycle, as well as constituting feed for animal plankton. The microalga has attracted much interest due to its ability to form complex calcite structures, so called coccoliths.

This thesis presents a comprehensive metabolome analysis of two life-cycle stages of the *E. huxleyi* species complex, with regard to growth phase and nutrient starvation. *E. huxleyi* naturally occurs in a diploid, calcifying and a haploid, non-calcifying stage. Therefore, comparison of these stages on metabolomic level could allow identification of `key metabolites´ involved in calcification. Knowledge of such metabolites could help elucidate the coccolith formation process, and facilitate *in vitro* coccolith production for industrial application as custom-designed nanoparticles. Furthermore, metabolomes can differ dependent on the organism's growth phase. Therefore, metabolomic analysis during different growth phases could allow further interpretation regarding physiology of these life-cycle stages. An additional factor for comparative metabolome analysis is nutrient limitation, as this is a common scenario in oceanic waters, proposed to enhance with advancing climate change. How microalgae respond to environmental changes will determine their success in the ocean, and therefore have implications on the ecosystem.

In the first part of this thesis, growth phase-dependent profiles of pigments and lipid associated fatty acids were obtained for both life-cycle stages. Highest cellular pigment and fatty abundances were observed in the metabolically most active early-exponential growth phase, whereas they decreased prior to cell numbers in the late-exponential phase, indicating restriction of photosystems and membrane structures before other cellular components, adapting to the decreased energy demand of non-dividing cells. These results underpin the importance of analyzing several time points to draw physiological conclusions. In the later growth phases, especially the diploid stage of *E. huxleyi* displayed exceptional capability of fine-tuning its photosynthetic machinery on pigment level, by activating photoprotection via xanthophyll cycle-mediated non-photochemical quenching, and changing absorption spectra by interconversions of fucoxanthin and chlorophyll c derivatives. These results extend the knowledge of *E. huxleyi*'s exceptional photosynthetic capacity, which include no photo-inhibition under extremely high light for the diploid stage. Responses were not as pronounced in the haploid stage, supporting less efficient photosynthesis previously reported for this stage. This result could possibly back up the hypothesis of distinct ecological niche occupation of the two life-cycle stages, which has been suggested previously.

In the second part of this thesis, a comprehensive metabolome analysis was conducted, focusing on *E. huxleyi*'s responses towards phosphorus (P) and nitrogen (N) starvation. Eleven different metabolome analysis methods were applied, based on gas and liquid chromatography, coupled to mass spectrometry, flame ionization, UV-vis, or charged aerosol detection, to obtain information regarding primary metabolites, and more specifically amino acids, carboxylic acids, osmolytes and polyamines, as well as pigments, polar and neutral lipid fatty acids, triacylglycerides (TAG), alkenes and alkenones (long chain polyunsaturated ketones). P-starvation resulted in a `metabolic overflow´ for both life-cycle stages, including increased abundances for many generic and especially N-rich metabolites, such as pigments, osmolytes and lipids. Results indicate that P-starvation mainly arrests the cell-cycle, as P is needed for nucleic acid synthesis, but enzymatic functionality is not affected. Diploid *E. huxleyi* cells also showed an upregulation of xanthophyll cycle-mediated photoprotection via non-photochemical quenching, as observed in the later growth phases. Results further underpin the highly effective adaptation of photosynthetic machinery of the diploid stage, possibly contributing to its success in P-limited waters. N-starvation had a severe effect on the diploid stage, resulting in a decrease of most central metabolites. The haploid stage was also affected, although it showed different priorizations in response to N-starvation than the diploid stage, again highlighting possible niche separation. As previously reported transcriptomic responses suggested the down-regulation of metabolism regarding both P- and N-starvation, the data presented in this work underlines the importance of instantaneous biochemical flux, which determines the metabolomic phenotype.

The data obtained under nutrient replete conditions highlight differences between the calcifying and non-calcifying stage, which could be connected to calcification, such as higher osmolyte, polar lipid fatty acid and alkenone abundance in the diploid, calcifying stage. These are most likely required for osmolytic regulation in connection with Ca^{2+} import and additional vesicle structures for calcification. However, the connection between alkenones and coccolith vesicles is still under debate. No further metabolites were identified that could be specific for the calcification process.

In conclusion, the data obtained in this thesis extends the knowledge of differences between *E. huxleyi* life-cycle stages on the metabolomic level, and highlights the diploid *E. huxleyi*'s capacity to survive in oligotrophic waters, due to efficient scavenging, recycling and storage of limiting nutrients, as well as efficient adaptation of photosynthesis. The established metabolomic analysis methods applied in this work provide a valuable tool for metabolome analysis in other microalgal species.

2. Introduction

In the first section of this chapter, the microalga *Emiliania huxleyi*, analyzed in this thesis, will be reviewed regarding phylogeny, origin, occurrence, life-cycle, ecological implication and calcification (2.1). In the second section, the role of pigments in microalgal photosynthesis will be introduced, with additional focus on *E. huxleyi*'s pigment composition (2.2). The third section will cover the central carbon metabolism (2.3). The fourth section consists of the description of microalgal lipids (2.4). In the fifth section, the effect of macronutrient limitation on microalgae will be elucidated (2.5). The sixth section summarizes state of the art of metabolomic analysis methods (2.6).

2.1 The organism *Emiliania huxleyi*

2.1.1 Taxonomical classification

Emiliania huxleyi is a marine microalga, which belongs to the haptophytes, more specifically to the order of Isochrysidales (Lee, 2008; Lee, 2016). It is also classified as a coccolithophore, as it produces coccoliths, which are highly structured calcium carbonate shells that cover the cell (Figure 1 a) (Paasche, 2001). *E. huxleyi* is the most abundant coccolithophore and has been extensively studied because of its capacity to form large blooms (Holligan, 1983; Brown & Yoder, 1994; Tyrrell & Merico, 2004). Due to light scattering on the coccoliths, blooms can be easily monitored by satellite (Figure 1 b), as cells shed their coccoliths in late stages of the bloom (Holligan, 1983; Balch, 1996; Vardi, 2012; Lehahn, 2014).
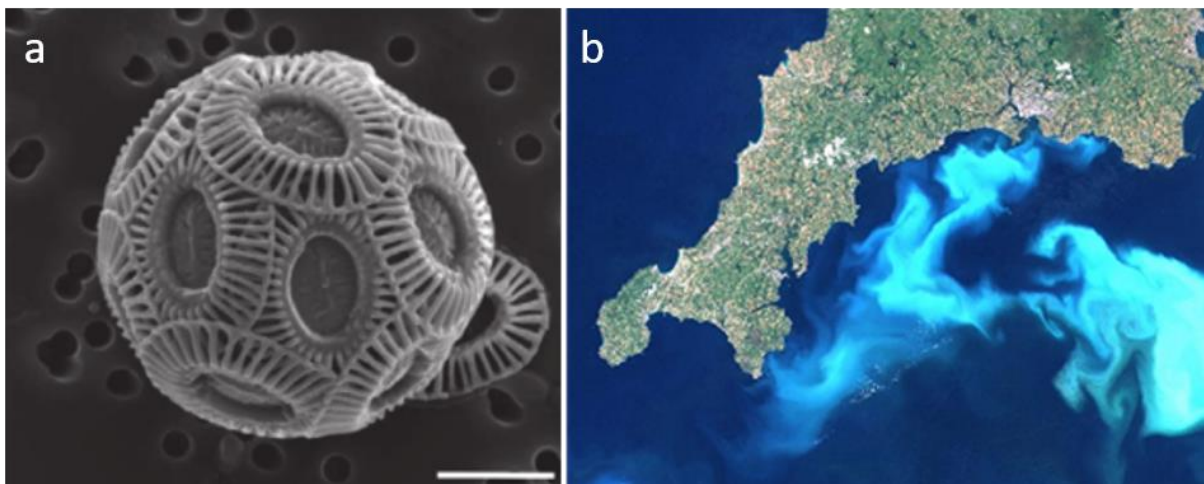
Figure 1: *E. huxleyi* cell and bloom. (a) SEM image of *E. huxleyi* PLY-B92/11 (Durak, 2016) (image license CC BY 4.0). (b) LANDSAT satellite image of an *E. huxleyi* bloom in the English Channel, 24 July 1999 (image courtesy of Andrew Wilson & Steve Groom, NASA).

Oxygen isotope records show the first appearance of *E. huxleyi* around 270,000 years ago (Thierstein, 1977). *E. huxleyi* is thought to have evolved during the cretaceous epoch (Latin

creta, meaning chalk), naturally sequestering carbon as coccoliths and removing it from the CO_2 rich atmosphere (Tyson & Funnell, 1987). It has existed through the two latest glacial-interglacial cycles (Paasche, 2001), and became dominant among coccolithophores around 70,000 years ago, a time in which atmospheric pCO_2 was low (Bijma, 2001). *E. huxleyi*'s closest relation is *Gephyrocapsa oceanica*, and these two are phylogenetically isolated from the other coccolithophores (Edvardsen, 2000; Fujiwara, 2001). The next closest relative is the non-calcifying *Isochrysis galbana* (Edvardsen, 2000; Fujiwara, 2001).

The reference genome of the *E. huxleyi* strain CCMP 1516 was recently published by Read and coworkers (2013), along with sequences from 13 other *E. huxleyi* strains. So far, *E. huxleyi* was considered a single species, however these results revealed a pan genome, a core genome (~two-thirds of the genome) with variably distributed genes in different strains, highlighting that *E. huxleyi* is a species complex. Authors state that this is reflected by the ability of different *E. huxleyi* strains to form blooms from arctic to tropical temperatures. Sequencing revealed an estimated genome size of 141.7 Mb (97 % complete) for the haploid genome of strain CCMP 1516, with a high GC content (~65 %), as well as a high proportion of repetitive elements (>64 %). 30,569 proteins were predicted, of which the majority has transcriptomic evidence (93 %) (Read, 2013).

E. huxleyi is not genetically accessible. However, the availability of the genome sequence has been of great value for genomic, transcriptomic, proteomic and metabolomic approaches (Jones, 2011; Rokitta, 2011; Bochenek, 2013; Obata, 2013; Jones, 2013; Rokitta, 2014; Mausz & Pohnert, 2015; McKew, 2015; von Dassow, 2015; Zhang, 2016; Rokitta, 2016). The genome of the two life-cycle stages analyzed in this work (*E. huxleyi* RCC 1216 and RCC 1217) has not been sequenced. However, this is one of the few strains where two stable life-cycle stages exist in laboratory culture, allowing comparison of the calcifying and non-calcifying stage with identical genetical background (Houdan, 2005; von Dassow, 2009; Rokitta, 2011; Mausz & Pohnert, 2015).

2.1.2 Life-cycle stages of *E. huxleyi*

E. huxleyi drives a haplo-diplontic life-cycle (Klaveness & Paasche, 1971; Klaveness, 1972b; Green, 1996; Paasche, 2001), as illustrated in Figure 2. A diploid (2N), coccolith-bearing non-motile stage (C for coccolith, 2N) and a haploid (1N), non-calcifying, motile stage (S for scales, 1N) exist, which is covered in organic scales (Green, 1996; Paasche, 2001). Diploid cells have a diameter of 4-5 µm (Paasche 1967; Klaveness 1972b), haploid cells appear smaller due to the missing coccoliths (Paasche, 2001). A diploid, non-calcifying naked stage (N for naked, 2N) can be found in laboratory cultures (Klaveness, 1972b; Green, 1996). This stage can develop

from C, 2N cells if the media is not changed regularly (Paasche, 2001), or under low nitrogen and phosphorus concentrations (Nanninga & Tyrrell, 1996). All three stages can exist independently, reproducing vegetatively by mitosis (Billard, 1994). The occurrence of two ploidy stages suggests the possibility of sexual reproduction, however this has not been confirmed (Billard, 1994).
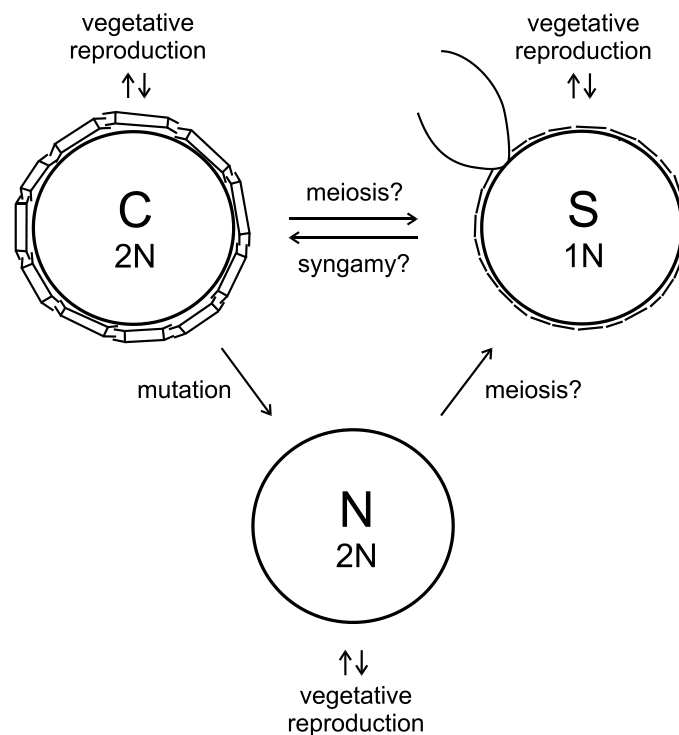
Figure 2: The haplo-diplontic life-cycle of *E. huxleyi*. In nature, a diploid (2N), calcified (C), non-motile life-cycle stage and a haploid (1N), motile, scale-covered (S) life-cycle stage exist. A naked (N), diploid (2N) stage can develop in laboratory culture. All three stages can exist individually and reproduce vegetatively. Transitions between C and S cells have been observed. Question marks indicate that the exact process of interconversion has not been elucidated. Syngamy describes the fusion of two haploid gametes to form a diploid zygote. Image from Paasche, 2001, redrawn with permission from Phycologia (license no. 4021410463644).

The haploid life-cycle stage is poorly investigated in its natural surroundings (Mausz & Pohnert, 2015). Field studies show that blooms of *E. huxleyi* are dominated by calcified diploid cells, as haploid non-calcifying cells only account for a minor fraction (Frada, 2012). These blooms typically occur during early summer, after the spring diatom bloom (Holligan, 1993), which leaves the water depleted in macronutrients (Tyrrell & Taylor, 1996). Blooms develop in up to 30 m depth (Lehahn, 2014), in high-latitude seas with relatively shallow mixed layers, and are characterized by high light intensities (Iglesias-Rodríguez, 2002). Cell densities can reach up to 10,000 cells mL^{-1} (Holligan, 1983; Holligan, 1993), and blooms can span up to hundreds of thousands of square kilometers (Holligan, 1983; Brown & Yoder, 1994; Tyrrell &

Merico, 2004). Viruses typically terminate *E. huxleyi* blooms (Bratbak, 1993; Schroeder, 2002; Wilson, 2002; Lehahn, 2014). These are large, lytic double stranded DNA viruses, specific to *E. huxleyi*, belonging to the family of phycodnaviridae (van Etten, 2002), typically 170-190 nm in diameter (Wilson, 2002). Viruses selectively infect and lyse only the diploid life-cycle stage of *E. huxleyi* (Frada, 2008). Also, virus-induced changes of life-cycle stage from diploid to haploid stage have been observed, leading to the hypothesis of an escape strategy, ensuring survival of the species in a time-space independent manner (Frada, 2008). This hypothesis implies that both life-cycle stages could occupy distinct ecological niches.

It has previously been speculated that haplo-diplontic life cycles could have evolved in an environment that is either seasonally variable or contains two different niches (Stebbins & Hill, 1980). As the haploid stage has long been overlooked by research, evidence on field level is lacking. However, the morphological differences of the two life-cycle stages, containing either calcification machinery or flagella, already suggest differences, i.e. regarding energy distribution (Rokitta, 2011). Transcriptome analyses have confirmed that the diploid and haploid life-cycle stages of *E. huxleyi* analyzed in this work (RCC 1216 and RCC 1217), utilize different parts of their genetic repertoire, with regard to calcification and motility (von Dassow, 2009; Rokitta, 2011). Results also suggested that the haploid stage has a more streamlined nitrogen and general metabolism, indicating the ability to thrive in post-bloom waters, containing limited nutrients (Rokitta, 2011).

The hypothesis of distinct ecological niche occupation has been postulated for other haplo-diplontic microalgal species (Houdan, 2006). For example, the haploid, motile, holococcolith-bearing stages of *Coccolithus braarudii* and *Calcidiscus leptoporus* thrive in low-nutrient, low-turbulent regimes, whereas their diploid, non-motile heterococcolith-bearing stages cope better with high nutrient, high-turbulence regimes (Houdan, 2006). This is in line with Margalef's 2-dimensional niche space model, in which haploid dinoflagellates thrive in low-nutrient, low-turbulence environments, whereas diploid diatoms prefer high-nutrient, high-turbulence habitats (Margalef, 1978).

2.1.3 Ecological implications of *E. huxleyi*

Marine microalgae are responsible for the majority of primary production in the ocean (Falkowski & Raven, 2007), and for ~50 % of global photosynthesis (Field, 1998; Friend, 2009), thereby supporting aquatic animals (Muller-Feuga, 2000). *E. huxleyi* is the most abundant coccolithophore (Okada & McIntyre, 1979; Winter, 1994; Iglesias-Rodriguez, 2008; Mohan, 2008), and plays a role in the global carbon, oxygen and sulfur cycle, exerting an important impact on the environment (Charlson, 1987; Westbroek, 1993; Malin & Steinke, 2004; Rost & Riebesell, 2004; Poulton, 2007).

Through photosynthesis, *E. huxleyi* produces organic carbon that is consumed by zooplankton grazers (Sikes & Wilbur, 1982; Hansen, 1996; Nejstgaard, 1997). Studies have estimated the fixation of up to 24,000 tons of organic carbon from a large *E. huxleyi* bloom, the majority of which was consumed by grazers or exported to depth within one week (Lehahn, 2014). Next to carbon fixation via photosynthesis, the process of coccolith formation sequesters carbon, reducing atmospheric CO_2 and therefore global warming (Salter, 2007). Inorganic carbon is fixed long term, as coccoliths are deposited on the ocean floor after cell death, and are fossilized (Buitenhuis, 1996). These aggregates form major chalk formations, such as the cliffs of Dover or Rügen (Saruwatari, 2008). Coccolithophores can account for 2 % of total carbon fixation on some systems (Poulton, 2007). However, calcification also leads to CO_2 production, therefore making the influence on the carbon cycle more complex (Frankignoulle, 1994).

Furthermore, *E. huxleyi* produces dimethylsulfoniopropionate (DMSP) (Turner, 1988; Gage, 1997; Keller, 1999; Spielmeyer, 2011; Gebser & Pohnert, 2013). This is an osmolyte with cryoprotective and antioxidative properties (Sunda, 2002). DMSP is cleaved to dimethylsulfoxide (DMS) intracellularly and secreted (Alcolombri, 2015). DMS is a gas that has been proposed to be involved in cloud nucleus formation (Shaw, 1983; Charlson, 1987), however, this process seems to be more complex and is possibly not regulated by DMS (Quinn & Bates, 2011).

2.1.4 The coccolith formation process

E. huxleyi's cellular components are those of a typical eukaryotic microalga, apart from a special compartment in the diploid life-cycle stage, the coccolith vesicle (Figure 3) (Paasche, 2001). As a descendent from secondary endosymbiosis, it contains four chloroplast membranes (Falkowski, 2004; Reyes-Prieto, 2007). *E. huxleyi* is surrounded by a coccosphere, made of several interlocking coccolith layers which are held together by polysaccharides (Young, 2003; Hoffmann, 2015). Haploid cells lack this coccolith producing machinery (Paasche, 2001).
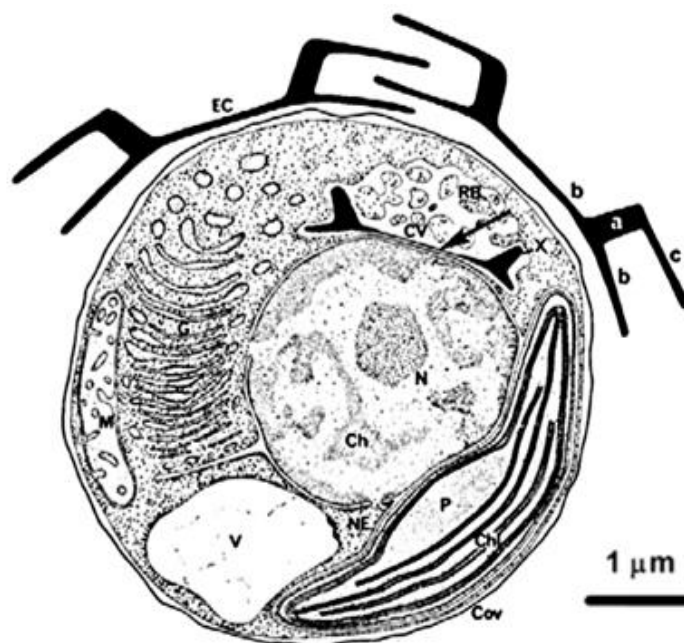
Figure 3: Cross section of calcifying *E. huxleyi* strain. Intracellular structures are chromatin (Ch), chloroplast (Chl), coccolith vesicle (CV), endoplasmatic reticulum (ER), Golgi complex (G), mitochondrion (M), nucleus (N), nuclear envelope (NE), reticular body (RB), vacuole (V), christalline matter (X). Extracellular coccoliths (EC) can be divided into a connecting wall (a) between the lower (b) and upper element (c). Image from (Moheimani, 2012), reproduced with permission from Elsevier (license no. 4021350274687).

E. huxleyi's coccoliths are composed of calcium carbonate in the form of calcite (Mann & Sparks, 1998, Didymus 1994). The precipitation reaction can be described by the following equation (Falkowski & Raven, 2007):

$$Ca^{2+} + 2HCO_3^- \rightarrow CaCO_3 + CO_2 + H_2O \quad \text{Eq. 1}$$
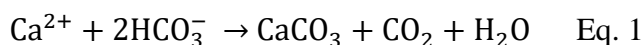
Calcite in coccoliths does not exclusively crystalize in the typical rhombohedral form (Figure 4 a), but forms complex crystal units (Young, 1999). The overall coccolith structure resembles a shirt stud, composed of two rings with spokes, held together by a tubular middle section (Figure 4 b) (Paasche, 2001). A coccolith is composed of 30-40 segments, each representing a single crystal (Young, 1992; Young, 1999), consisting of four parts; the central area element, inner tube element and the proximal and distal shield elements (Figure 4 c)

(Young, 1992). Coccoliths are produced (Figure 4 d, e) in the coccolith vesicle, which is connected to the nucleus. In a first step, an organic baseplate forms in the coccolith vesicle, on which the crystallization takes place (Klaveness, 1972a; Westbroek, 1984). Next, the proximal shield/protococcolith ring appears (van der Wal, 1983; Westbroek, 1984), which crystallizes in rhombohedral shape, typical of calcite (Mann & Sparks, 1988; Young, 1992). The crystal then however grows upwards and inwards, deviating from the rhombo-hedical structure, creating the inner tube and central area element (Paasche, 2001). In a last step, the distal shield element is formed (Paasche, 2001). The coccolith is subsequently turned out through the cell envelope and inserted between older coccoliths on the cell surface, however, details of this process are unknown (Paasche, 2001). Only one coccolith is formed at a time (Paasche, 2001), the process can take less than one hour (Paasche, 1962). Coccolith vesicles and reticular bodies are found in naked, non-calcifying diploid cells (N, 2N) as well, although slightly deformed and inactive (Klaveness & Paasche, 1971; van der Wal, 1983).

The underlying mechanism for the cell's control on crystal growth is so far unknown. However, organic components in the coccolith vesicle seem to be involved (Paasche, 2001). Polysaccharides line the base plate and the inner wall of the coccolith vesicle (Figure 4 f), representing an organic `skin´ around the crystals and baseplate (van der Wal, 1983). An acidic polysaccharide, named coccolith polysaccharide, is thought to be involved, as it binds calcium ions and prevents calcium carbonate precipitation in supersaturated solutions (Westbroek, 1984; de Vrind-de Jong, 1986; de Vrind-de Jong, 1994). In *in vitro* crystallization, it binds to calcite crystal surfaces (Didymus, 1993; Henriksen, 2005) and induces the change from rhombohedral to tubular, elongated calcite formation (Kayano, 2011).

a

A-axis

A-axis

A-axis

Ca++

CO₃⁻⁻

C-axis

b

c

DISTAL SHIELD
ELEMENT

INNER TUBE
ELEMENT

PROXIMAL SHIELD
ELEMENT

V-UNIT

CENTRAL AREA
ELEMENT

d

COMPLETE GROWTH

INCOMPLETE
GROWTH

PROTO-
COCCOLITH RING

e

cv

n

B

rb

cv

n

C

rb

cv

n

D

cv

n

E

f

(c)

skin

p.t.

n.e.
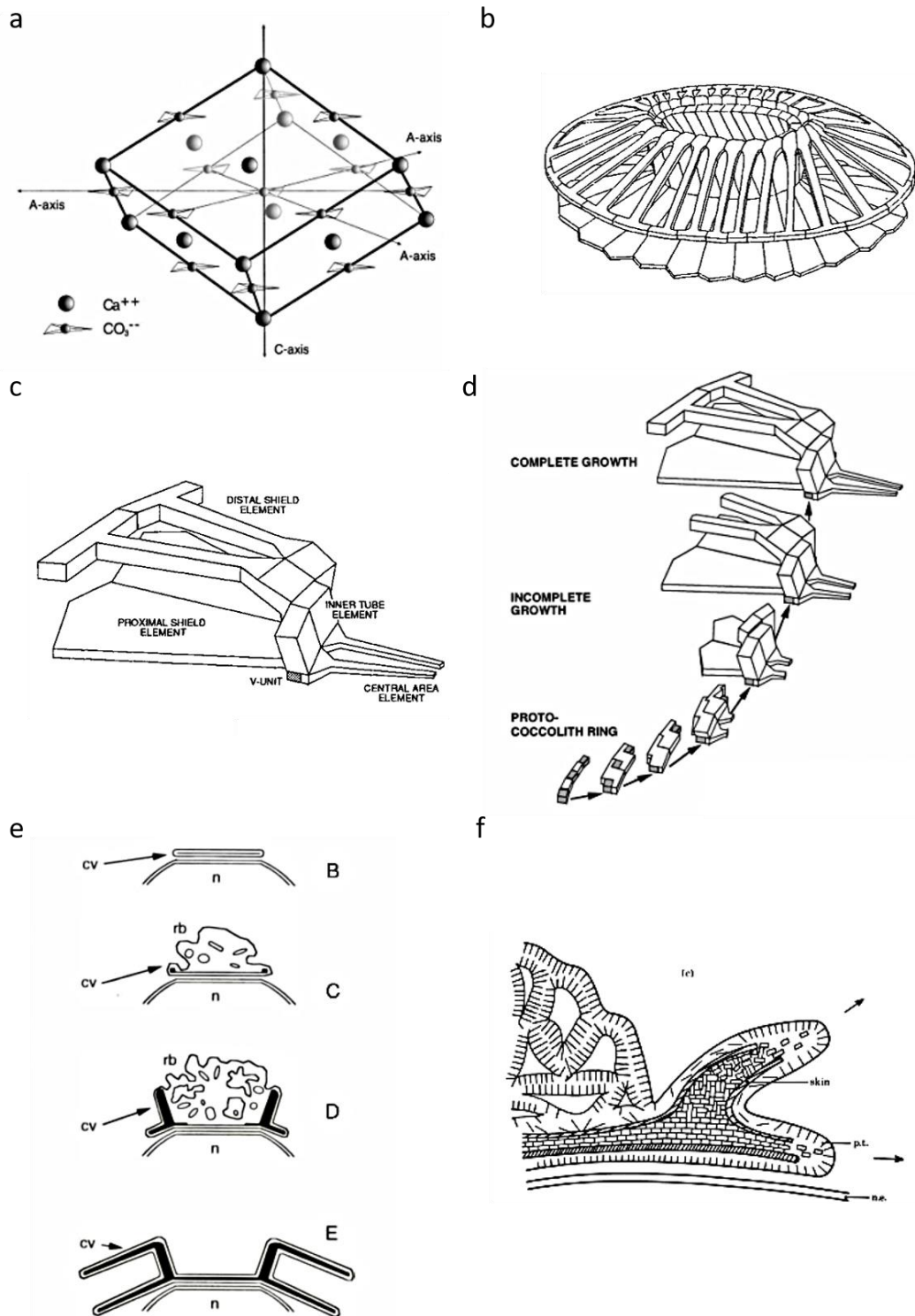
Figure 4: The process of coccolith formation in the coccolithophore *E. huxleyi*. (a) The typical rhombohedral calcite crystal structure. Calcite crystals formed by *E. huxleyi* are more complex (Young, 1999). (b) Complete coccolith and (c) the four elements of a coccolith calcite crystal (Young, 1992). (d) Steps of coccolith crystallization, starting from a protococcolith ring, ending with a complete complex crystal (Young, 1999). (e) Steps of coccolith formation illustrated in coccolith vesicle (cv) with reticular body (rb) and nucleus (n) (Paasche, 2001). (B) A base plate forms in the coccolith vesicle. (C) The reticular body expands and the proximal shield/protococcolith ring appears. (D) The crystal grows upwards and inwards. (E) The finished coccolith. (f) Illustration of coccolith formation controlled by polysaccharides, which are suggested to form a `skin´ around the coccolith (Westbroek, 1984). All images were reproduced with permission of the publishers. Image a, image d, Elsevier, licence no. 4020870847225; image b, image c, Nature Publishing Group, license no. 4021360061139; image e, International Phycological Society, license no. 4021361471858; image f, The Royal Society, license no. 4021370348299.

Calcification is an energy consuming process that competes with other cellular processes (Paasche, 2001). Evolution of calcifying species indicates beneficial properties of this trait. Several hypotheses were proposed, trying to underpin purposes or advantages of calcification in *E. huxleyi*.

For example, it was hypothesized that the coccolith shell protects the cell and creates a suitable microenvironment around the cell surface (Young, 1994). The fact that naked diploid life-cycle stages (N, 2N) have not been identified in *E. huxleyi* blooms could support this assumption, as they possess neither coccoliths nor organic scales that could be necessary for survival in the ocean (Paasche, 2001). In line with cell protection, coccoliths have been suggested to protect against predators (Sikes & Wilbur, 1982). However certain zooplankton grazers are not disturbed by the presence of coccoliths (Sikes & Wilbur, 1982; Hansen, 1996; Nejstgaard, 1997) and furthermore the calcifying diploid life-cycle stage is infected by viruses, whereas the non-calcifying, haploid stage is not (Bratbak, 1996; Frada, 2008). Therefore this theory does not seem to be valid (Paasche, 2001). However, coccoliths have recently been proven to play a role in mechanical protection against harsh environmental conditions, as the polysaccharide matrix and the interlocking architecture of coccoliths stabilize calcified cells regarding hydrostatic pressure, thereby even outperforming technical ceramics in strength to weight ratio (Jaya, 2016).

A further hypothesis suggested that coccoliths could aid in light protection, as diploid, calcifying *E. huxleyi* strains don't show any signs of photoinhibition under high light intensities (Nanninga & Tyrrell, 1996; Ragni, 2008; Loebl, 2010). This hypothesis was disproven, as cells without coccoliths did not show signs of photoinhibition (Nanninga & Tyrrell, 1996). However, it has been shown that coccoliths protect the cell against ultra violet (UV) radiation (Gao, 2009; Guan & Gao, 2010; Gao, 2012), especially UV-B (Xu, 2016).

It was also suggested that calcification presents a form of carbon concentrating mechanism, as coccolith production produces CO_2, enhancing CO_2 supply to the Calvin cycle for carbon fixation. However, it has been shown that this CO_2 is not obligatory for photosynthesis and cannot drive the observed concentration mechanism (Raven & Crawfurd, 2012; Beardall & Raven, 2016).

Another hypothesis proposed that coccoliths could help the non-flagellated diploid stage regulate its sinking rate (Linschooten, 1991; Young, 1994; Lecourt, 1996). Evidence supports this assumption on several levels. Calcium carbonate has a higher density than organic matter and seawater (Paasche, 2001) and it has been shown that cells sink faster, the more coccoliths they carry (Lecourt, 1996). Furthermore, senescent or nutrient limited cells have more

coccoliths (Linschooten, 1991; Lecourt, 1996; Paasche, 1998) and could therefore sink to deeper nutrient-rich water levels (Linschooten, 1991; Young, 1994; Lecourt, 1996). In line with this argument, light limited cells have less coccoliths (Balch, 1996), theoretically allowing them to rise to lighter areas in the water column (Paasche, 2001). However, sinking rate is also influenced by the cellular lipid content, as *E. huxleyi* contains many poly-unsaturated fatty acids (Pond & Harris, 1996) and alkenones (Yamamoto, 2000) which enhance buoyancy (Fernández, 1994; Fernández, 1996; Paasche, 2001).

2.2 Pigments in microalgae

2.2.1 The role of pigments in oxygenic photosynthesis

Photosynthetic organisms convert energy from light into chemical bonds, with the help of water and CO_2. This requires two reactions, which take place in the chloroplast. The light reaction comprises absorption of light energy, subsequently leading to production of NADPH and ATP, which are used in the dark reaction to fix CO_2 in form of carbohydrates in the Calvin cycle (Falkowski & Raven, 2007).

Pigments can be divided into light harvesting pigments (chlorophylls and some carotenoids) and photoprotective pigments (carotenoids). The first step in the light reaction is performed by light harvesting pigments. These are located in light harvesting protein complexes (LHC), which are part of the photosystem I (PS I) and photosystem II (PS II) complexes. In the process of light harvesting, a chlorophyll molecule is excited by a photon, lifting the molecule from its ground state (S_0) into an excited state (S_3). Rapid relaxation to a lower state (S_1) allows transport of excitation energy to another chlorophyll molecule, typically chlorophyll a. Via several chlorophyll a molecules, excited energy is transferred to the reaction center of the photosystem, where it initiates charge separation in special chlorophylls (P680 or P700). In PS II, the reaction center chlorophyll P680 releases an electron to pheophytin, causing linear electron flow from PS II via plastoquinone, the cytochrome b_6f complex and plastocyanin to PS I. Here P700 is excited, which donates an electron to ferredoxin, subsequently leading to the reduction of $NADP^+$ to NADPH. The electron in P680 is replaced by an electron extracted from water, thereby releasing oxygen and protons. Together with protons from linear and cyclic electron flow, this causes a proton gradient in the thylakoid lumen, fueling the ATP synthase for ATP production (Ke, 2001; Croce & van Amerongen, 2014).

Plants and green algae typically contain chlorophyll a as main light-harvesting pigment, and chlorophyll b as accessory pigments. Diatoms, dinoflagellates and haptophytes, such as *E. huxleyi*, contain chlorophyll a and chlorophyll c. Other accessory chlorophylls exist, such as

chlorophyll d and chlorophyll e (Croce & van Amerongen, 2014). In some microalgae, carotenoids also function in light harvesting (Blankenship, 2014). Because light consists of a broad spectrum of wavelengths, pigments differ in their absorption capacity, to ensure capture of as much light as possible (Ke, 2001).

Photoprotective carotenoids are important under stress conditions, such as high light, where reaction centers of photosystems can be saturated, preventing fast energy transfer. This can cause excited chlorophylls to go into a harmful triplet states, leading to production of phototoxic singlet oxygen species (reactive oxygen species, ROS). Carotenoids quench triplet chlorophylls or singlet oxygen species, emitting energy as heat, so that chlorophyll can return to its ground state. Some carotenoids, xanthophylls, can also prevent excited chlorophylls from going into triplet state, by non-photochemical quenching, also emitting energy as heat (Pogson, 2005).

This particular type of non-photochemical quenching is performed via the xanthophyll cycle, involving dissipation of excess energy (Llewellyn, 2007). Two types of this cycle exist, dependent on the species-specific pigment repertoire (Figure 5). Higher plants, Chlorophyceae and other individual species (i.e. Rhodophyceae, Chrysophyceae, Xantophyceae) use the violaxanthin-dependent cycle, while marine microalgae, such as *E. huxleyi*, rely on the diadinoxanthin-dependent pathway (Demmig-Adams & Adams III, 1993).
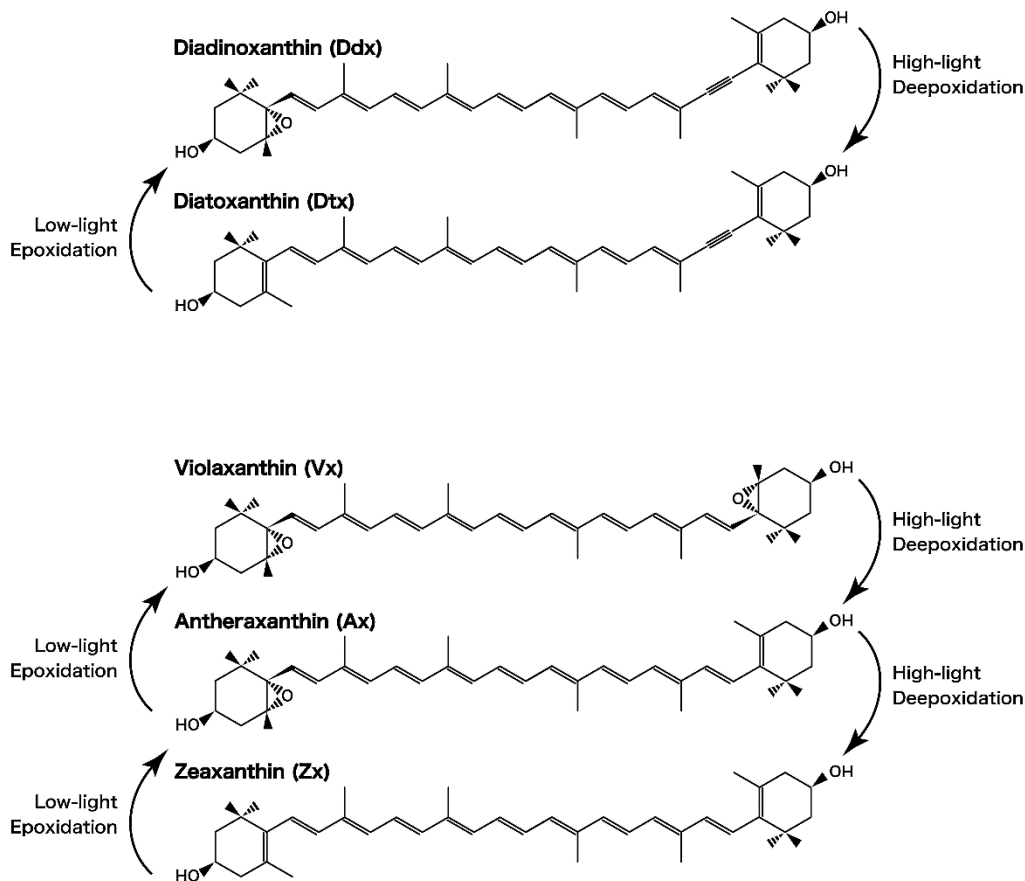
Figure 5: The two different xanthophyll cycles in microalga. (a) The diadinoxanthin cycle. (b) The violaxanthin cycle. Image from (Tanabe, 2011), license CC BY 4.0.

2.2.2 *E. huxleyi*'s pigment composition

Strains of the *E. huxleyi* species complex possesses a highly unique pigment profile (Stolte, 2000; Zapata, 2004). Next to chlorophyll a *E. huxleyi* contains the accessory chlorophyll c (Green & Durnford, 1996; Jeffrey, 1997), allowing extension of the spectral absorption towards blue light (Larkum, 1994; Green & Durnford, 1996), which is important in deeper oceanic waters (Brunet, 2011; Kirk, 2011; Croce & van Amerongen, 2014). Chlorophyll c is structurally similar to chlorophyll a and chlorophyll b, however, it does not contain a phytol chain and ring D is not reduced (Jeffrey, 1997). Different *E. huxleyi* strains can contain several different chlorophyll c pigments, such as chlorophyll c_2, chlorophyll c_3, divinyl chl c_3, monovinyl c_3 and chlorophyll c_2-MGDG (Garrido, 2000; Garrido, 2016). All chlorophyll c derivatives have a similar yet not identical spectral absorption (Jeffrey, 1972; Fawley, 1989; Saitoh, 1993; Zapata, 2006).

Next to light-harvesting, chlorophyll c pigments may play a role in LHC stabilization (Jeffrey & Anderson, 2000; Hoober & Eggink, 2001). As oxidized chlorophylls, it is proposed that chlorophyll c forms strong coordination bonds with ligands of LHC apoproteins, due to the higher lewis strength of the central Mg atom, therefore aiding in LHC assembly, similar to

chlorophyll b (Hoober & Eggink, 2001). Chlorophyll c molecules are proposed to be noncovalently attached to fucoxanthin-chlorophyll a/c polypeptides, as occurs in the chlorophyll a/b complex of PS II in plants (Kühlbrandt, 1994). Non-polar chlorophyll c_2-MGDG additionally allows hydrophobic interactions, and could therefore act as a space filler in the thylakoid membrane (Jeffrey & Anderson, 2000). Furthermore, a transporting role has been proposed for this chlorophyll, as the lipid component could help deliver chlorophyll c_2 from the inner chloroplast membrane to the light-harvesting antenna in the thylakoids (Jeffrey & Anderson, 2000).

To aid absorption of the limited light spectrum in oceanic waters, *E. huxleyi* also contains various light-harvesting fucoxanthins (Stolte, 2000; Zapata, 2004; Garrido, 2016). Strains can contain several different fucoxanthins, such as fucoxanthin, 19'-hexanoyloxy-fucoxanthin (hex-fucoxanthin), 19'-hexanoyloxy-4-ketofucoxanthin (h4k-fucoxanthin), 19'-butanoyloxy-fucoxanthin (but-fucoxanthin), cis-fucoxanthin and cis-199-19'-hexanoyloxyfucoxanthin (Stolte, 2000; Zapata, 2004; Airs & Llewellyn, 2006). The derivatives differ marginally in their absorption features (Egeland, 2000; Airs & Llewellyn, 2006). It is not clear whether fucoxanthins also function as secondary carotenoids in photoprotection (Kim, 2012).

Additionally, *E. huxleyi* contains further carotenoids functioning in photoprotection, such as diadinoxanthin, diatoxanthin, and α- and β-carotene (Stolte, 2000; van Lenning, 2004; Zapata, 2004; Garrido, 2016).

2.3   The central carbon metabolism in microalgae

After light absorption by pigments and subsequent linear electron flow in the light reaction, the produced ATP and NADPH are used in the dark reaction, the Calvin cycle. Here CO_2 is fixed in form of glyceraldehyde-3-phosphate, which is subsequently converted to hexoses by gluconeogenesis (Oesterhelt & Wachtveitl, 2012). This reaction takes place in the chloroplast stroma (Falkowski & Raven, 2007). Hexoses can be stored in form of different glucans (Barsanti & Gualtieri, 2006). *E. huxleyi*'s carbon storage glucan is a 1,6-linked β-D-glucan with branching at position 3, and 1,6-linkages in the side chains (Vårum, 1986).

Carbon allocation seems unique in *E. huxleyi* compared to other algae. For example, ^{14}C-labeling experiments showed that in the strain NIES 837, only a small amount of β-glucan was formed as a photosynthetic product in both nutrient-replete exponential and stationary phase cultures (Tsuji, 2015). The majority of carbon/energy storage was performed by alkenones (long chain ketones) and low molecular-mass compounds, including mannitol (Tsuji, 2015). Mannitol had been proposed to be a major storage compound in *E. huxleyi* previously (Obata, 2013; Mausz & Pohnert, 2015). In contrast, β-glucan is the major carbon storage molecule

haptophytes and diatoms that don't produce alkenones, also under nutrient replete conditions (Myklestad, 1989; Hirokawa, 2008).

Energy and biosynthesis intermediates are generated in a process termed dark respiration, as it can function in the absence of light. It involves glycolysis, pentose phosphate pathway, the tricarboxylic acid cycle and oxidative phosphorylation. In microalgae this process is thought to have the same role as in other aerobic organisms (Raven & Beardall, 2003; Buchanan, 2015).

Glycolysis is a key pathway of metabolism, where hexoses from carbon fixation, storage, or import are converted to pyruvate, thereby producing energy and reducing equivalents in form of ATP and NADH. Further compounds are formed that can be used for biosynthesis (i.e. glycerol 3-phosphate, acetyl-CoA, alanine). It can be assumed that glycolysis is compartmentalized between the chloroplast and the cytosol for microalgae (Raven & Beardall, 2003; Khozin-Goldberg, 2016), as this has been observed in the chlorophyte *Chlamydomonas reinhardtii* (Klein, 1986; Klöck & Kreuzberg, 1991; Johnson & Alric, 2013), as well as in diatoms (Smith, 2012). However, diatoms have additional glycolytic capabilities in the mitochondria (Liaud, 2000; Kroth, 2008; Fabris, 2012). The exact location of glycolysis in *E. huxleyi* has not been elucidated. Furthermore, *E. huxleyi* has not been shown to import sugars, it only grows photoautotrophically. The pentose phosphate cycle is a competing pathway of glycolysis, which converts glucose to pentoses and tetroses needed for biosynthesis of nucleosides and amino acids. In the process, reducing equivalents in the form of NADPH are produced (Raven & Beardall, 2003; Wünschiers, 2012a).

The largest part of energy generation takes place in the mitochondria, involving the tricarboxylic acid cycle (TCA), electron transfer reactions and oxidative phosphorylation. In the TCA, carbon chains from carbohydrates, fatty acids (both entering as acetyl-CoA) and several amino acids are oxidized to CO_2 and water, yielding NADH, $FADH_2$, ATP (Raven & Beardall, 2003; Wünschiers, 2012a). The cycle also provides intermediates for amino acid and porphyrin synthesis (Wünschiers, 2012a). In oxidative phosphorylation, electrons from NADH and $FADH_2$ are passed through an electron transport chain to O_2, reducing it to water. The transporting complexes are located in the inner mitochondrial matrix, and transfer protons into the intermembrane space. The created proton gradient fuels an ATPase to generate ATP. The majority of energy from hexoses is generated by oxidative phosphorylation (Le Williams & del Giorgio, 2005; Jahn & Jahn, 2012).

In microalgae, fatty acid synthesis is presumed to take place in the chloroplast, although enzymes have been predicted to be targeted to both the mitochondrion and chloroplast (Riekhof, 2005; Li-Beisson, 2016). Fatty acids are synthesized from malony-CoA, which is obtained by

carboxylation of acetyl-CoA, using NADPH and ATP (Khozin-Goldberg, 2016). They can subsequently be esterified to form lipid molecules in the chloroplast and endoplasmatic reticulum (Wünschiers, 2012c; Li-Beisson, 2016). Fatty acids can be recycled to acetyl-CoA by β-oxidation (Li-Beisson, 2015), which can subsequently be used for energy and intermediate generation in the TCA cycle or can be converted to back to hexoses in gluconeogenesis, in a series of steps partly resembling reverse glycolysis. Some amino acids as well as glycerol can also be recycled in gluconeogenesis (Wünschiers, 2012a).

2.4 Lipids in microalgae

2.4.1 General classification of lipids

Lipids represent a major subcellular component, playing many essential roles, such formation of biological membranes, storage and signaling molecules (Li-Beisson, 2016). The strict definition of the term `lipid´ is under debate. However, the general understanding is that lipids are hydrophobic or amphipathic small molecules that are solvable in organic solvents, yet not in water (Li-Beisson, 2016). This applies to several different compounds, such as fatty acids and their derivatives, as well as chlorophylls, carotenoids, terpenes, steroids and bile acids (Christie, 2013). Further, they can be categorized into `polar´ and less polar lipids, termed `neutral´. This allows easy differentiation of microalgal lipids, as polar lipids mostly represent membrane structures, whereas neutral lipids compose storage lipids, such as triacylglycerides (TAG), hydrocarbons, ketones, as well as wax and sterol esters (Volkman, 1981; Christie, 2013; Li-Beisson, 2015).

2.4.2 Membrane lipids in microalgae

Polar lipids form lipid bilayer structures that compose cellular membranes (Harwood, 1998). These structures provide matrices for interactions of membrane associated proteins (Han & Gross, 2005) as well as subcompartments which contribute to cellular functions (Falkowski & Raven, 2007; Shevchenko & Simons, 2010). Important membrane lipids in microalgae are phosphoglycerides, such as phosphatidylcholine (PC), phosphatidylethanolamine (PE), phosphatidylglycerol (PG) and phosphatidylinositol (PI); glycosyl-glycerides, such as mono-galactosyldiacylglycerol (MGDG), digalactosyldiacylglycerol (DGDG) and sulfoquinovosyl-diacylglycerol (SQDG); and betaine lipids, such as diacylglyceryltrimethylhomoserine (DGTS), diacylglycerylhydroxymethyltrimethyl-β-alanine (DGTA) and diacylglyceryl-carboxylhydroxymethylcholine (DGCC) (Guschina & Harwood, 2006; Li-Beisson, 2016). *E. huxleyi* has been reported to additionally contain the phospholipid phosphatidyl-S,S-dimethylpropanethiol (PDPT), as well as an abundance of glycosphingolipids (GSL) and

betaine-like glycerolipids (Fulton, 2014; Hunter, 2015; Malitsky, 2016). Phospholipids, sphingolipids and betaine lipids generally constitute a large proportion of extraplastidial lipids in microalgae, next to sterols (Murata, 1998; Khozin-Goldberg, 2016). Major components of microalgal chloroplast thylakoid membranes are the glycosylglycerides MGDG, DGDG and SQDG, the phospholipid PG, as well as betaine lipids, such as DGTS, DGTA or DGCC (Murata, 1998; Guschina & Harwood, 2006; Li-Beisson, 2016). Next to forming the lipid bilayers necessary for photosynthesis to take place, they aid in folding and assembly of protein subunits in photosynthetic complexes, and are therefore highly important for efficient photosynthesis (Murata, 1998; Kobayashi, 2016).

2.4.3 Storage lipids in microalgae

Microalgae are able to store energy in form of lipids (Hu, 2008). The role of neutral lipid storage in microalgae is typically performed by TAG, which accumulate under stress conditions (Fidalgo, 1998; Rodolfi, 2009). In *E. huxleyi*, only small amounts of TAG have been detected (Volkman, 1986; Bell & Pond, 1996; Malitsky, 2016). *E. huxleyi* produces polyunsaturated long chain alkenones (ketones), alkenoates and alkenes, which are often abbreviated as PULCA. Alkenones accumulate under stress conditions and have therefore proposed to be metabolic storage lipids (Bell & Pond, 1996; Epstein, 2001; Prahl, 2003; Eltgroth, 2005; Pan & Sun, 2011), which was confirmed by isotope labeling (Tsuji, 2015). The reason for this difference could be the higher photostability of alkenones (Rontani, 1997), which would be advantageous in *E. huxleyi*'s high-light habitat (Eltgroth, 2005). Alkenones have been investigated intensively, as they are relevant for paleoclimatic temperature reconstructions, due to the fact that double bond positions are influenced by temperature and alkenones are highly resistant to decomposition (Brassell, 1986; Prahl & Wakeham, 1987; Conte, 1998; Müller, 1998; Conte, 2006). PULCA seem to be present as membrane-unbound lipids (Mouzdahir, 2001; Sawada & Shiraiwa, 2004; Eltgroth, 2005). Results about the exact location are contradicting, as Sawada and coworkers (2004) stated they were highly abundant in an ER and coccolith vesicle fraction, whereas Eltgroth and coworkers (2005) did not find PULCA associated with the coccolith vesicle fraction, but in lipid droplets. PULCA are also proposed to play a role in regulating buoyancy (Fernández, 1994; Fernández, 1996; Paasche, 2001).

2.5 The effect of nutrient limitation on microalgae

2.5.1 Natural occurrence of nutrient limitation for *E. huxleyi*

Nutrient limitation is common in the ocean, as areas are naturally limited by different macronutrients, such as nitrogen, phosphorus, silicate, iron and nickel (Moore, 2013; Palenik, 2015). Climate change, next to causing ocean acidification (Caldeira, 2005) by increased CO_2 partial pressure (Solomon, 2007), is proposed to increase nutrient limitation, due to increased stratification in warmer waters (Doney, 2006; Cermeno, 2008; Beman, 2011).

2.5.2 Phosphorus-starvation in microalgae

Phosphorus is an important nutrient, which constitutes ATP, coenzymes, DNA, RNA and phospholipids (Barsanti & Gualtieri, 2006). It is involved in energy transfer, signal transduction, macromolecule biosynthesis, photosynthesis and respiration (Plaxton & Carswell, 1999; Raghothama, 1999). In microalgae, P-starvation has been shown to decrease growth rate (Dugdale, 1967; Latasa & Berdalet, 1994; Falkowski, 1997; Kozlowska-Szerenos, 2004; Hou, 2007; McKew, 2015; Kamalanathan, 2016). Comprehensive metabolome data regarding P-starvation in microalgae is so far lacking, as studies often only assess certain metabolic groups, complicating statements concerning general responses of microalgae to P-starvation. Furthermore, responses appear non-generic, as different microalgal strains show diverging patterns. For example, proteins have been shown to either decrease and not change under P-starvation in *Skeletonema costatum* and *Prorocentrum donghaiense*, respectively, while carbohydrates increased in both strains (Zhao, 2009). In *Chlamydomonas reinhardtii* and *Chlorella vulgaris*, P-starvation did not affect chlorophyll a abundance (Kozlowska-Szerenos, 2004; Kamalanathan, 2016), whereas photoprotective carotenoids were increased selectively in *Chlorella vulgaris* (Kozlowska-Szerenos, 2004). P-starvation resulted in lipid accumulation in *Phaeodactylum tricornutum*, *Chaetoceros* sp., *Pavlova lutheri* (Reitan, 1994) and *Prorocentrum donghaiense* (Zhao, 2009). No change was observed for *Skeletonema costatum* (Zhao, 2009), whereas decreased lipid abundances were found in other species, such as *Nannochloris atomus* and *Tetraselmis* sp. (Reitan, 1994).

These results indicate that some microalgae can cope better with P-starvation than others. For example, marine microalgae efficiently scavenge, recycle and store phosphorus under conditions where P is scarce, thereby prolong survival (Twining, 2010). Many marine microalgae, including *E. huxleyi*, substitute phospholipids by non-P-containing betaine lipids and galactolipids under P-starvation, thereby saving 10-30 % of P (van Mooy, 2009; Shemi, 2016). Furthermore, phytoplankton can accumulate polyphosphates as P-storage (Martin,

2014). Also, P-starvation can lead to increased coccolith production in *E. huxleyi* (Paasche & Brubak, 1994; Paasche, 1998; Kayano & Shiraiwa, 2009; Satoh, 2009). However, it appears this effect is coupled to ceased cell division. When cells become P-limited, they eventually stop dividing, but coccolith production proceeds unperturbed, forming further layers around the cell, making it appear bigger (Shiraiwa, 2003).

E. huxleyi has been shown to bloom and become the dominant species in low-phosphorus waters (Riegman, 1992; Egge & Heimdal, 1994; Tyrrell & Taylor, 1996; Riegman, 2000), often after diatoms have bloomed (Holligan, 1993), leaving the water devoid of nutrients (Tyrrell & Taylor, 1996). Therefore, it has been hypothesized that P-limitation is a key for *E. huxleyi's* bloom formation (Lessard, 2005). This could be explained by its exceptional ability to scavenge inorganic P from external sources, as the number of phosphate transporters and alkaline phosphatases is highly increased in *E. huxleyi* under P-starvation (Riegman, 2000; McKew, 2015; Shemi, 2016). Alkaline phosphatases are cell surface proteins which cleave phosphate off dissolved organic material, such as DNA, RNA, nucleotides and proteins (Dyhrman & Palenik, 2003; Landry, 2006; McKew, 2015). Other microalgae also use alkaline phosphatases to scavenge external P (Kuenzler & Perras, 1965; Sakshaug, 1984; Dyhrman & Palenik, 1997; Dyhrman & Palenik, 2003; Wurch, 2011). However, alkaline phosphatases in *E. huxleyi* have been shown to have the highest affinity ever reported for phytoplankton species (Riegman, 2000), and are produced in higher abundance compared to other microalgae (Kuenzler & Perras, 1965).

2.5.3 Nitrogen-starvation in microalgae

Nitrogen is an element present in many cellular components, as it is part of all proteinogenic amino acids. N-starvation in microalgae directly affects amino acid synthesis (Barsanti & Gualtieri, 2006), and therefore protein production (McKew, 2015). Photosynthetic proteins seem to be more strongly affected than cytoplasmic proteins (Rhiel, 1986; Kolber, 1988; Falkowski, 1989; Geider, 1993), leading to a decreased PS II efficiency (Berges, 1996; Zhang, 2013), in line with decreases of N-containing chlorophylls (Latasa & Berdalet, 1994; Berges, 1996; Li, 2008; Zhang, 2013; McKew, 2015; Kamalanathan, 2016). At the same time photoprotective pigments can be increased, for example in *Phaeodactylum tricornutum*, *Thalassiosira weissflogii*, *Dunaliella tertiolecta* and *Parietochloris incisa* (Geider, 1993; Berges, 1996; Solovchenko, 2008). As a result of N-starvation, carbon and nitrate assimilation are affected (Hipkin, 1983; Kaffes, 2010). In many algae, N-starvation leads to increased lipid accumulation, especially in form of triacylglycerides (TAG) (Fidalgo, 1998; Rodolfi, 2009), as photosynthetate is channeled into storage molecules (Scott, 2010).

E. huxleyi efficiently scavenges external inorganic and organic N sources under N-limitation, as observed on proteomic level (McKew, 2015). It can grow well on various forms of organic nitrogen, such as urea, purines, acetamide and formamide (Antia, 1975; Ietswaart, 1994; Palenik & Henson, 1997; Bruhn, 2010; McKew, 2015). Next to viral termination, N-starvation is thought to be the main reason for bloom termination (Bratbak, 1993; Egge & Heimdal, 1994; van der Wal, 1995).

2.6 Metabolome analysis methods

2.6.1 Common approaches for metabolome analysis

A metabolite is an intermediate or a product of biochemical pathways, representing the endpoint of the `omics cascade´, consisting of genome, transcriptome, proteome and metabolome (Dettmer, 2007). The sum of all metabolites in a cell is termed `metabolome´. Metabolite levels represent the ultimate response of a biological system to genetic or environmental changes (Fiehn, 2002). Due to the complexity of the metabolome, consisting of numerous metabolites with diverse physico-chemical properties in different abundance levels, no single-instrument platform can currently analyze all metabolites (Dettmer, 2007). Furthermore, due to the highly dynamic nature of metabolites, metabolomics can only represent a `snap-shot´ of the metabolic constellation of a particular time point (Villas-Bôas, 2007).

Two approaches that can be chosen for metabolome analysis, namely metabolic fingerprinting and metabolic profiling. Metabolic fingerprinting is an untargeted analysis of a sample, allowing comparison of metabolite patterns, whereas metabolomic profiling represents targeted analysis of specific metabolite classes, providing quantitative data for physiological interpretations (Dettmer & Hammock, 2004; Villas-Bôas, 2007). In this work, only metabolomic profiling was applied. Here methods can be utilized to analyze a broad range of metabolites. If specific analytes cannot be identified with the applied method, additional approaches can be performed to identify specific metabolite groups. Both approaches require separation of compounds, e.g. by capillary electrophoresis, gas or liquid chromatography (GC or LC) and detection by e.g. ultraviolet-visual (UV) spectrophotometers, nuclear magnetic resonance spectroscopy or mass spectrometry (MS) (Dettmer, 2007; Villas-Bôas, 2007).

Performance of high quality metabolome analysis requires proper sampling and sample handling (van Gulik, 2010). As metabolites have a very fast turnover, sample quenching needs to be performed to stop metabolic activities. This can be performed by cold shock (freezing in liquid nitrogen), cold quenching (i.e. injecting sample into cold methanol), freeze clamping, or acid treatment (Dettmer, 2007). For cells that only reach low cell densities, additional

enrichment through centrifugation or filtration may be necessary prior to sample quenching. This is the case for *E. huxleyi*, which additionally does not separate well by centrifugation. Therefore, it is necessary to perform quick filtration at unchanged light and temperature conditions, followed by cold shock in liquid nitrogen (Obata, 2013). Analysis of metabolites from complex biological samples requires metabolite extraction and separation from interfering components, which can contribute to metabolite loss (Dettmer, 2007). For microalgal cells liquid-liquid-phase extraction is often applied, involving homogenization of frozen sample, followed by extraction with organic solvents (Roessner, 2000; Doebbe, 2010).

2.6.2 Principles of gas chromatography

GC is often applied to analyze a broad range of metabolites (Marriott, 2004; Villas-Bôas, 2007). Analytes are required to be volatile and thermally stable for GC analysis. Small molecules with low boiling points (<200-300 °C) can easily be evaporated. However, non-volatile compounds, such as amino acids, sugars, small organic acids, and other polar metabolites, as well as large apolar metabolites such as fatty acids and sterols, need to be chemically derivatized to increase volatility (Villas-Bôas, 2007). This is often achieved by silylation or methylation, which `covers´ i.e. carboxylic, hydroxylic and amino groups with apolar functionality, resulting in more volatile compounds (Dettmer, 2007; Villas-Bôas, 2007). Samples are commonly injected into the column in gas or liquid form. In liquid injection systems, the sample is injected into a hot liner, where analytes evaporate. A carrier gas (i.e. He, H_2 or N_2) transports analytes from the injector to the column. Here they are retained based on interactions with the stationary phase and differences in vapor pressure, and are eluted with a temperature gradient. Long capillary columns (10-100 m) commonly contain a polymer stationary phase and allow separation of a broad array of analytes (Marriott, 2004; Villas-Bôas, 2007). Universal detectors used for GC include MS, flame ionization detectors (FID), Fourier transform infrared spectrometers (FTIR) and thermal conductivity detectors (Marriott, 2004).

2.6.3 Principles of liquid chromatography

LC is commonly performed as high-performance liquid chromatography (HPLC). This technique allows separation of compounds solvable in a mobile phase, from apolar to ionic, small to very large, acidic to alkaline (Villas-Bôas, 2007). In contrast to GC, non-volatile or thermally labile high molecular compounds can be separated (Forcisi, 2013). The separation principle involves a pump sending a pressurized mobile phase and the sample over a column containing a stationary phase (Smith, 2004). Analytes are retained due to their individual interaction with the stationary phase material, and are eluted subsequently, leading to separation

of analyzes by retention time (van der Meeren & Vanderdeelen, 2013). Numerous different stationary phases can be combined with different mobile phases, thereby expanding separation possibilities compared to GC (Smith, 2004; Villas-Bôas, 2007). Analytes eluting from HPLC are commonly detected by MS, UV and fluorescence spectroscopy detectors, refractive-index detectors, light-scattering detectors, electro-chemical amperometric/coulometric detectors, conductivity and suppressed-conductivity detectors or chiral detectors (Smith, 2004).

2.6.4 Principles of mass spectrometry

Mass spectrometry allows the determination of molecular mass of free ions under high vacuum (Gross, 2004). A mass spectrometer consists of an ion source, which ionizes analytes, a mass filter that separates ions according to their mass-to-charge ratio (m/z), and a detector, that measures the ion current (Villas-Bôas, 2007). Results are represented as a mass spectrum, showing ion abundance and their m/z ratios (Hart-Smith & Blanksby, 2012).

The first step includes ionization of analytes that are introduced into the system, e.g. from the GC or LC column. For gas phase analytes, the source of these ions is typically electron impact ionization (EI), in which energetic electrons ionize compounds (Gross, 2004; Niessen, 2004). For liquid phase analytes (i.e. from LC), these need to be brought into the gaseous phase as well as be ionized, for example by action of a strong electrical field, in electron spray ionization (ESI) or by application of a heated nebulizer, in atmospheric-pressure chemical ionization (Niessen, 2004). Ionized analytes are subsequently sorted by mass analyzers, such as quadrupole mass filters, ion traps, time of flight mass analyzers, Fourier transform ion cyclotron resonance mass analyzers and orbitraps (Hart-Smith & Blanksby, 2012). Quadrupole mass analyzers and ion traps will be described in more detail, as they are of relevance for the measurements in this work.

The quadrupole mass filter consists of four electrodes, to which a combination of alternating and direct voltages is applied. This allows selection for analytes with specific m/z-values or wide m/z ranges, which pass through the quadrupole on stable flight paths, whereas others collide with the electrodes and are neutralized (Villas-Bôas, 2007; Hart-Smith & Blanksby, 2012). The quadrupole ion trap (Paul trap) is very similar to a quadrupole mass filter, although it doesn't continuously transmit ions, but stores and ejects them when required (Villas-Bôas, 2007). It consists of a ring electrode and two electrodes at either end, resulting in a chamber in the shape of a hyperbola. Through alternating voltage an oscillating quadrupole electrical field is formed, focusing ions, which can then be analyzed by mass (Villas-Bôas, 2007; Hart-Smith & Blanksby, 2012).

ESI does not produce many fragment ions with structural information, which is why tandem MS (i.e. LC-MS/MS) can be applied (Kruve, 2015). This includes selection of ions of a particular m/z in the first MS, which are subsequently fragmented by collision with an inert gas. A second MS separates these ions, which are then detected, allowing more advanced analysis for structure elucidation or obtaining high specificity and sensitivity in target analysis (Villas-Bôas, 2007; Hart-Smith & Blanksby, 2012; Kruve, 2015).

2.6.5 Metabolomic analysis of lipids

Several different methods can be applied to analyze lipids. Most analyses require the extraction of lipophilic compounds with organic solvents before measurement. Typical methods are based on the `Folch´ or `Bligh & Dyer´ extraction protocols (Folch, 1957; Bligh & Dyer, 1959), which involve different proportions of methanol and chloroform to extract lipids of various polarities, including a phase separation with water, to separate contaminants (Christie & Han, 2010). The dry weight of this total lipid extract can be determined, however it is important to note that this fraction also contains triterpenoids, pigments and non-lipid contaminants (Li-Beisson, 2016).

The easiest and cheapest way to further analyze the lipid composition is via thin layer chromatography (TLC). TLC allows 1D- or 2D separation of complex lipid samples due to their polarity, resulting in separated lipid classes (i.e. MGDG, DGDG, PC, PE, PG, TAG). These can then be stained (i.e. with primuline), and visualized with UV (Li-Beisson, 2016). Quantification of lipids can be performed densiometrically by comparison with standards, or by analysis of recovered lipids via GC or LC (Christie, 2011a). Joint systems exist, consisting of automatic TLC coupled to HPLC (HPTLC), allowing higher accuracy of this method (Fuchs, 2011).

The most commonly used lipid analysis method is detection of lipid fatty acid composition via GC-MS or GC-FID (Dodds, 2005). This requires derivatization of fatty acids to fatty acid methyl esters (FAME), to neutralize carboxyl groups, thereby preventing hydrogen bond formation, which negatively impacts stationary phase interaction (Christie, 2011b). Derivatization can be performed by acid- or base-mediated catalysis. Both methods have disadvantages, as acid-based catalysis can be too strong for fatty acids with epoxy, cyclopropane or cyclopropene rings (Bao, 1998), and base-catalysis is not affective on free fatty acids or fatty acids in sphingolipids, due to the amide-bond (Li-Beisson, 2016). Normally these methods derivatize all lipids in the sample, so that differentiation between fatty acids from lipids and naturally occurring free fatty acids is not possible. However, free fatty acids can be separated from the total lipid extract and derivatized separately (Kaczmarzyk & Fulda, 2010), or analyzed by fractional derivatization (Kail, 2012). The resulting FAME are separated and quantified via GC-FID or GC-MS (Li-Beisson, 2016). While GC-FID is more commonly used,

GC-MS is a powerful alternative, as it offers the additional value of clear compound identification, whereas GC-FID only renders retention time and instrument response (Dodds, 2005). This can lead to misidentification of FAME due to coeluting compounds, contaminants or artifacts (Ackman, 1990; Dodds, 2005).

The charged aerosol detection is a comparably new development (Dixon & Peterson, 2002) which can be applied to detect TAG, after separation via HPLC (Moreau, 2006; Lísa, 2007). The detection principle is based on nebulizing the effluent from the HPLC column using a nitrogen flow, and evaporating resulting volatile analytes and solvents. Aerosol particles are then charged with secondary stream of nitrogen that has passed a high-voltage platinum wire, and the charged particle flux is measured by an electrometer (Moreau, 2006; Vehovec & Obreza, 2010). This principle allows detection of many different analytes with great reproducibility (Vehovec & Obreza, 2010).

A highly promising method for lipid analysis is termed `lipidomics´, as it allows analysis of all lipids in a sample, providing information of the exact molecular species of each lipid (Han & Gross, 2005). Analysis platforms include direct infusion ESI-MS/MS and LC-MS/MS (Li-Beisson, 2016). This method requires analytical standards of each lipid, which is why studies are often only comparative, as standards are not available for every lipid species (Shevchenko & Simons, 2010). Lipidomics is not a standard analysis tool yet, due to expensive instruments and requirement of specialist knowledge for handling and data processing (Li-Beisson, 2016). However, it is a powerful tool used for elucidation of lipid composition in biological systems (Welti, 2002; Yoon, 2012), and is highly promising in health and disease (Shevchenko & Simons, 2010; Murphy & Nicolaou, 2013).

Furthermore, lipids can be analyzed *in situ*, without extraction, i.e. by staining with lipophilic dyes (i.e. Nile red) and following microscopical visualization (Chen, 2009), or directly by using electron microscopic techniques (Glauert, 1968; Fujita, 2010). Both chemical-based lipidomics and *in situ* visualization are integrated by mass spectrometry imaging, allowing insights to spatial compartmentation of the lipid metabolism (Passarelli & Winograd, 2011; Gorzolka, 2016). Here, typically three detection types are used, such as secondary ion MS, desorption electrospray ionization and matrix-assisted laser desorption/ionization MS (Horn & Chapman, 2014).

2.7 Objective

Due to the natural occurrence of two life-cycle stages, of which only one stage calcifies, the first objective was to compare the metabolome of these stages, to find life-cycle specific differences that could possibly be connected to the calcification process. Only few *E. huxleyi* strains exist where both diploid, calcifying (C, 2N) and haploid, non-calcifying (S, 1N) life-cycle stages grow in stable individual cultures in the laboratory. Therefore *E. huxleyi* RCC 1216 (2N) and RCC 1217 (1N) were chosen for comparison.

Furthermore, it was important to analyze the effect of harvesting time point with regard to metabolome analysis. Therefore, the metabolome of both life-cycle stages was analyzed at three different growth phases; the early-exponential, late-exponential and stationary growth phase. The focus was set on pigment and lipid analysis, to allow physiological comparison of both life-cycle stages and growth phase-dependency of each stage.

A further interesting scenario for metabolome analysis is nutrient limitation. P- and N-limitation is a quite common scenario in the ocean, and diploid *E. huxleyi* strains shows great capacity to cope with P-starvation. Therefore, comprehensive metabolome analysis under these nutrient-starvation scenarios would allow further elucidation about how the life-cycle stages cope with nutrient starvation.

3. Materials and Methods

3.1 Strains and cultivation conditions

3.1.1 Analyzed strains/life-cycle stages

The diploid, calcifying strain *E. huxleyi* RCC 1216 (C, 2N) and its haploid, non-calcifying life-cycle stage *E. huxleyi* RCC 1217 (S, 1N) were obtained from the Alfred Wegener Institute, Helmholtz Centre for Polar and Marine Research, Bremerhaven (S. Rokitta). They were originally obtained from the Roscoff Culture Collection (Roscoff, France). RCC 1216 is also known as AC 472, TQ 26, NIES-2697 and CCMP 3266. According to the culture collection, this strain was isolated from the Tasman Sea in the Pacific Ocean, ~90 km from New Zealand's west coast (42.3° S 169.8° E), on the September 1, 1998, by I. Probert. (Roscoff Culture Collection, 2017). As RCC 1216 and RCC 1217 are genetically identical, but present in different ploidy stages, they will be referred to as diploid (2N) and haploid (1N) life-cycle stages throughout this work.

3.1.2 Cultivation conditions

E. huxleyi was cultivated in a climate control chamber (Model SE-41 with 2 E-LBS lamp benches and phenol-coated evaporator, PFL Plant Climatics). Temperature was set to 20 °C. Cultures were illuminated with 350 µmol m^{-2} s^{-1} on a 16:8 h light/dark cycle using tubular fluorescent lamps (Master TL-D 18W/840, Philips). The absorption spectrum of the light source is shown in Supplementary Figure 2. Cells were resuspended twice a day by gently shaking by hand.

E. huxleyi can to be non-axenic, as bacteria are naturally associated with the strain (van Oostende, 2013; Green, 2015). Therefore, pre-cultures were checked for contaminations before main cultivations. If associated bacteria were found (one specific rod-shaped type of bacterium), an antibiotic treatment with kanamycin was conducted (0.5 mg mL^{-1}), after which another round of pre-culture growth in media without antibiotics was conducted. Only axenic cultures were used to inoculate main cultures, which were regularly monitored with regard to contamination, by microscopical observation and plating on ESAW and LB-plates (Lysogeny broth agar plates: 10 g L^{-1} bacto-tryptone, 5 g L^{-1} yeast extract, 10 g L^{-1} sodium chloride, 15 g L^{-1} agar, pH 7.0).

3.1.3 Cultivation media

E. huxleyi was cultivated in photoautotrophic ESAW media, which is short for `enriched seawater-artificial water´. The recipe was slightly modified from (Berges, 2001). Salt solutions

I and II were freshly prepared and solved in deionized water (Table 1). The three main nutrients, nitrate, phosphate and silicate, the two metal solutions, and vitamins were added from prepared stock solutions (Table 2-Table 4). For main cultivations, media was directly sterile filtered (sterile filters from Sartorius), as the C-source $NaHCO_3$ outgasses slightly when autoclaving. For stock cultures, autoclaved media was used, here vitamins were added afterwards.

Table 1: Composition of salt solutions I and II for ESAW media. c, concentration.

Solution	Component	Net weight / g L^{-1}	M/ g mol^{-1}	c_{final} / mM L^{-1}
salt solution I	NaCl	21.19	58.44	363
	Na_2SO_4	3.55	142.04	25
	KCl	0.599	74.55	8.04
	$NaHCO_3$	0.174	84.01	2.07
	KBr	0.0863	119.01	$725 \cdot 10^{-3}$
	H_3BO_3	0.023	61.83	$372 \cdot 10^{-3}$
	NaF	0.0028	41.99	$65.7 \cdot 10^{-3}$
salt solution II	$MgCl_2 \cdot 6H_2O$	9.592	203.3	47.2
	$CaCl_2 \cdot 2H_2O$	1.344	147.02	9.14
	$SrCl_2 \cdot 6H_2O$	0.0218	266.62	$82 \cdot 10^{-3}$

Table 2: Composition of different stock solutions for ESAW media. Prepare 100 mL of each of these four stock solutions with deionized water. sol., solution; c, concentration.

Stock solution	Component	Stock sol. / g L^{-1}	M / g mol^{-1}	c_{final} / mM L^{-1}
nitrate, 1 mL L^{-1}	$NaNO_3$	46.7	84.99	$549 \cdot 10^{-3}$
phosphate, 1 mL L^{-1}	$NaH_2PO_4 \cdot H_2O$	3.09	137.99	$21 \cdot 10^{-3}$
silicate, 1 mL L^{-1}	$Na_2SiO_3 \cdot 5H_2O$	11.2	212.16	$105 \cdot 10^{-3}$
metal I, 1 mL L^{-1}	FeEDTA	2.408	367.1	$6.56 \cdot 10^{-3}$

Table 3: Composition of metal stock solution II for ESAW media. Prepare 100 mL. c. concentration.

Stock solution	Component	Net weight / g L^{-1}	M / g mol^{-1}	c_{final} / mM L^{-1}
metal II, 1 mL L^{-1}	$ZnSO_4 \cdot 7H_2O$	0.073	287.53	$254 \cdot 10^{-6}$
	$CoSO_4 \cdot 7H_2O$	0.016	281.1	$5.69 \cdot 10^{-6}$
	$MnSO_4 \cdot 1H_2O$	0.409	169.02	$2.42 \cdot 10^{-3}$
	$Na_2MoO_4 \cdot 2H_2O$*	$1.48 \cdot 10^{-3}$	241.95	$6.1 \cdot 10^{-6}$
	Na_2SeO_3*	$1.73 \cdot 10^{-4}$	172.94	$1 \cdot 10^{-6}$
	$NiCl_2 \cdot 6H_2O$*	$1.49 \cdot 10^{-3}$	237.7	$6.3 \cdot 10^{-6}$
	$Na_2EDTA \cdot 2H_2O$	3.09	372.24	$8.29 \cdot 10^{-3}$

*Stock solutions of individual metals can be prepared:

$Na_2MoO_4 \cdot 2H_2O$ stock solution: 148 mg / 100 mL, add 1 mL to metal II solution

$Na_2SeO_3 \cdot 2H_2O$ stock solution: 17.3 mg / 100 mL, add 1 mL to metal II solution

$NiCl_2 \cdot 6H_2O$ stock solution: 149 mg / 100 mL, add 1 mL to metal II solution

Table 4: Composition of vitamin stock solution for ESAW media. Prepare 100 mL, filter sterilize and freeze aliquots at -20 °C. c, concentration.

Stock solution	Component	Net weight / g L^{-1}	M / g mol^{-1}	c_{final} / mM L^{-1}
vitamin, 1 mL L^{-1}	thiamin·HCl (B_1)	0.1	337.27	$297 \cdot 10^{-6}$
	biotin (B_7)	0.002	244.31	$4.09 \cdot 10^{-6}$
	cyanocobalamin (B_{12})	0.001	1355.37	$1.47 \cdot 10^{-6}$

Biotin stock solution: 20 mg/ 20 mL, add 1 mL to vitamin solution
B12- stock solution: 20 mg/ 10 mL, add 1 mL to vitamin solution

3.2 Main cultivation setups for generation of metabolomic samples

3.2.1 Growth phase-dependent metabolome analysis

In this experiment, both *E. huxleyi* life-cycle stages were cultivated in nutrient-replete ESAW media. Pre-cultures were grown under identical conditions and used as inoculum when in exponential growth. Per life-cycle stage, six biological replicates were inoculated at 2000 cells mL^{-1}, in 2 L glass bottles containing ESAW-media with no headspace. Cell number was monitored daily in triplicate (Z2 Coulter® Particle Counter and Size Analyzer, Beckman Coulter). At three chosen time points, two biological replicates were harvested for metabolome analysis. The media was analyzed with respect to pH (Metrohm) and total alkalinity, using a photometric test (Sarazin, 1999).

3.2.2 Metabolome analysis under nutrient-starvation

To analyze the effect of nutrient starvation, two separate cultivations were conducted. In each setup, both life-cycle stages were grow in nutrient replete media (n=3), and P- or N-starved media (n=3), which contained either 22.4 µM or 2.24 µM phosphate for the P-starvation setup, or 549 µM or 54.0 µM nitrate, for the N-starvation setup. Cells were inoculated from nutrient-replete exponential pre-cultures at 2000 cells mL^{-1} in 2 L glass bottles containing the respective ESAW media without any headspace. Cell numbers were monitored daily in triplicate (Z2 Coulter® Particle Counter and Size Analyzer, Beckman Coulter). Additionally, samples for nutrient concentration in the media were taken daily, therefore triplicate samples of culture were centrifuged (14,000 g, 2 min) at 4 °C and frozen at -20 °C until analysis. Nutrient concentrations were analyzed with commercial photometric tests, for nitrate in seawater and o-phosphate (Spectroquant®, Merck).

3.3 Measurement of total alkalinity

Total alkalinity (TA) is defined as the excess of proton acceptors over proton donors (Dickson, 1981), and therefore indicates how much dissolved inorganic carbon can be taken up by the media. At the initial pH of seawater or ESAW media (pH=8.2), HCO_3^- is the major proton

acceptor, with smaller amounts of CO_3^{2-}. Total alkalinity can be roughly seen as the amount of protons that can be accepted by these acceptors. It is measured by acidic titration to the alkalinity equivalence point, where TA equals 0 (pH ~4.3). The amount of added acid to reach this point can be used to estimate the TA (Wolf-Gladrow, 2007). Total alkalinity was determined according to Sarazin (Sarazin, 1999).

3.4 Metabolome analysis

3.4.1 Harvest of cells for metabolome analysis

Cells for metabolome samples were harvested by vacuum filtration, applying -500 mbar to filtrate aliquots of culture onto polycarbonate filters (Whatman® Nuclepore™ Track-Etched Membranes). Different filter pore sizes were used for the life-cycle stages, 3.0 µm for diploid, and 0.4 µm for haploid stages. For the growth phase experiment, 200 mL aliquots were harvested for pigment and lipid samples. For the N-starvation setup, GC-MS metabolome analysis required 500 mL of culture, filtered in smaller volumes to ensure filtration did not take longer than two minutes, as metabolites have high turnover. For pigment and lipid analyses, 250 mL were harvested. LC-MS/MS analyses only required 20 mL of culture volume. All filters were instantly frozen in liquid nitrogen and stored at -80 °C until analysis.

3.4.2 Cellular content analysis via FTIR

Diploid and haploid life-cycle stages were cultivated in nutrient replete ESAW media, as described above (3.2.1), and harvested in late-exponential phase (3.4), so that ~$1.4 \cdot 10^8$ cells were present per filter. Using 3 mL 5 M sodium chloride solution (analytical grade, Sigma-Aldrich) cells were removed from the filter and centrifuged (2,500 g, 2 min). The supernatant was decanted, and cells of both life-cycle stages were resuspended in 2 mL 0.2 M hydrochloric acid (analytical grade, Fisher Chemicals), to remove coccoliths. After direct centrifugation (20,238 g, 2 min), the supernatant was carefully removed with a pipette. A washing step followed with 1 mL of the 5 M sodium chloride solution. After repeated centrifugation and removal of the supernatant, the pellet was shock frozen in liquid nitrogen and lyophilized (-55 °C, 0.03 mbar, Alpha-14, Christ).

Fourier transform infrared (FTIR) analysis was performed by J. L. Klocke and T. Kottke (Physical and Biophysical Chemistry Group, Department of Chemistry, Bielefeld University). FTIR spectra were measured on a spectrometer (IFS 66/S, Bruker) equipped with a photoconductive mercury cadmium telluride detector and an attenuated total reflection setup (DuraSampl*IR* II, diamond crystal, Smiths) with nine active reflections. Lyophilized biomass was pressed onto the crystal and absorption spectra were recorded with air as reference. The

scanning velocity was set to 150 mHz, and the spectral resolution to $2\,cm^{-1}$. Fourier transformation was performed with Mertz phase correction, a zerofilling factor of 2 and Blackman-Harris-3-term apodization. For every sample, multiple measurements were totaled and averaged to a total number of 6144 scans. OPUS 5.5 (Bruker) was used to correct baselines, and spectra were normalized to the amide II band ($1539\,cm^{-1}$). Reference spectra of hexatriacontane (98 %, Sigma-Aldrich), tetradecane (99 %, Acros organics), trans-7-tetradecene (97 %, Sigma-Aldrich) and calcium carbonate (>99 %, Sigma-Aldrich) were recorded, to validate the contribution of alkenes and calcium carbonate to the bands. Literature comparison was used to identify the other bands.

3.4.3 GC-MS based metabolome analysis

In order to extract metabolites, filters were allowed to thaw on ice. Cells were gently removed from the filter with 1 mL ice-cold methanol (80 % v/v, HPLC-grade) containing 10 µM of internal standard ribitol (≥99 %, Sigma-Aldrich). The metabolite extract was transferred to screw cap vials containing 0.1 mm silica beads (Carl Roth), up to the 0.4 mL mark. Cells were subsequently homogenized in a ribolizer (Precellys 24 homogenizer, Peqlab), using three cycles of 45 sec at 6,500 rpm with incubation on ice in between cycles. After centrifugation at room temperature (5 min, 14,000 rpm), 700 µL of the supernatant were dried under nitrogen gas. Derivatization was carried out as reported by (Doebbe, 2010). In detail, 100 µL of a methoxylamine hypochloride (Sigma-Aldrich)-pyridine solution (20 mg/mL) was added, samples were incubated while stirring at 37 °C for 90 min. After addition of 100 µL N-Methyl-N-(trimethylsilyl)trifluoroacetamide (Macherey-Nagel) samples were incubated a further 30 min. The mixture was centrifuged (4 min, 2,500 rpm) and the supernatant was transferred to GC-sampling vials for subsequent GC-MS analysis.

Analysis was performed using a TraceGC gas chromatograph and ITQ ion trap mass spectrometer equipped with an AS 3000 autosampler (Thermo Scientific, Germany), as reported previously. (Doebbe, 2010). In short, 1 µL of sample was injected in splitless mode onto a 30 m x 0.25 mm VF-5 ms column coated with 0.25 µm of 5 % diphenyl and 95 % dimethylsiloxane (Varian Deutschland GmbH, Darmstadt, Germany). Injector and interface temperature were set to 250 °C, ion source to 220 °C. Helium as a carrier gas was set to $1\,mL\,min^{-1}$. The oven temperature was held at 80 °C for 1 min and then raised to 300 °C at 6 °C min^{-1}. Mass spectra were recorded at 20 scans s^{-1} in the scanning range of 50-750 m/z. The resulting chromatograms were evaluated with Xcalibur software (Version 2.0.7, Thermo Scientific, Germany). Identification of metabolites was performed with previously measured standards and data base comparison NIST 05 library, National Institute of Standards and

Technology, Gaithersburg, MD, Thermo Finnigan and the Golm Metabolome Data base (GMD), Max Planck Institute of Molecular Plant Physiology, Golm, Germany (Kopka, 2005)). Metabolites were reported as identified compound (level 1), or putatively identified compound (level 2) according to (Sumner, 2007). Normalization was performed to the internal standard and number of cells in the sample. All chromatograms were additionally reviewed manually, to increase data-confidence.

3.4.4 Pigment analysis via UV-vis-HPLC

All work was carried out in a preferably dark environment. Cells from thawed filters were removed with 1 mL of 90 % (v/v) acetone (analytical grade), saturated with calcium carbonate. The extract was transferred to screw cap vials containing 0.1 mm silica beads (Carl Roth), up to the 0.4 mL mark. Cells were disrupted in a ribolizer (Precellys 24 homogenizer, Peqlab), using three cycles of 45 sec at 6,500 rpm, including 15 sec break between each cycle, followed by centrifugation of samples (14,000 rpm, 5 min). The supernatant was transferred to a HPLC vial. If not immediately measured, samples were coated with N_2 gas and stored at -20 °C.

Pigment separation and detection was performed via HPLC (Frommolt, 2001). The system from Thermo Finnigan consisted of a TSP degasser, TSP AS 3000 autosampler, TSP P4000 pump, TSP column oven and TSP UV6000 detector. 20 µL of pigment sample was separated on a AccucoreTM Polar Premium RP-C18 column (150 mm x 4,6 mm, 2.6 µm particle size, Thermo Scientific) with a pre-column Accucore C8 filter (10 mm x 4.6 mm, 2.6 µm). Eluent A consisted of 0.1 M ammonium acetate/methanol (15:85, v/v), eluent B of methanol/acetonitrile/acetone (44:43:13, v/v). All solvents were HPLC-grade, except for acetone (analytical grade). The column was equilibrated for 5 min with 100 % A and a flow rate of 0.5 mL min^{-1}. The solvent composition changed to 75 % A and 25 % B at 31 min, and then to 100 % B at 47 min, which was held until the end of the run at 70 min. The UV-vis-detector scanned the wavelength-range 190-800 nm with a bandwidth of 1 nm and a scan rate of 1 Hz. Additionally, a discrete channel was recorded at 440 nm. The resulting chromatograms were evaluated with Xcalibur software (Version 2.0.7, Thermo Scientific, Germany). Identification of pigments was performed by comparison with commercially available pigment standards (DHI group) (Supplementary Table 2). Peak areas were normalized to the number of cells in the sample. Values were stated as relative abundance, as quantification was not possible, due to the limited concentration of internal standards.

3.4.5 Lipid isolation and separation

Cells were removed from the thawed filters with 1 mL of methanol (HPLC grade) and vortexing. The extract was transferred to screw cap vials containing 0.1 mm silica beads (Carl Roth), up to the 0.4 mL mark. Cells were disrupted in a ribolizer (Precellys 24 homogenizer, Peqlab), using three cycles of 45 sec at 6,500 rpm, including 15 sec break between each cycle. Lipids were extracted using a modified Folch protocol (Bogen, 2013). Briefly, lipids were extracted twice with 4 mL methanol and 8 mL chloroform in total, initiating phase separation by addition of 3 mL of deionized water, with which contaminants were eliminated. The extract was evaporated to dryness with nitrogen gas.

Column chromatographies were performed to separate the neutral from the polar lipid fraction as described previously (Chen, 2009). In short, single-use chromatography columns were built in glass pipettes, containing cotton wool and silica gel (Silica gel 60 for column chromatography, 0.063-0.200 mm, 70-230 mesh ASTM, Merck). The column was equilibrated with chloroform (HPLC grade), the sample was dissolved in chloroform and loaded onto the column and the neutral lipids were eluted into a glass vial (Supelco) with 7 mL chloroform. Then a new vial was placed under the column, and polar lipids were eluted with the same amount of methanol (HPLC grade). Subsequently, all fractions were evaporated to dryness under a nitrogen gas stream and stored at -20 °C until further use.

Obtained neutral and polar lipid fractions were further analyzed regarding their fatty acid composition (FAME), as described in 3.4.6. The neutral lipid fraction was divided into two halves, to analyze FAMEs, as well as triacylglycerides (3.4.7), alkenes (3.4.8) and alkenones (3.4.9).

3.4.6 FAME analysis via GC-MS

Half of the neutral and polar lipid fractions were derivatized to gain fatty acid methyl esters (FAMEs) as described by Jaeger et al. (Jaeger, 2016) and analyzed via GC-MS. Briefly, lipids were dissolved in chloroform containing internal standard glycerol triheptadecanoate (Sigma-Aldrich). 1.1 mL of methanol and hydrochloric acid (10:1 v/v) were added. After vortexing, samples were heated for 2 hours at 80 °C in sealed glass vials. FAMEs were extracted by addition of 1.0 mL hexane and chloroform (4:1 v/v), after 10 min of gentle shaking, the upper phase was taken for analysis via GC-MS, as described in section 3.4.3. Fatty acids were identified and quantified with calibration curves (Supplementary Table 1) of the Supelco 37 Component FAME Mix (Sigma-Aldrich) and additional database comparison (NIST 05 library, National Institute of Standards and Technology, Thermo Finnigan).

3.4.7 TAG analysis via CAD-HPLC

The internal standard glycerol triheptadecanoate (≥99 %, Sigma-Aldrich) was added to the non-derivatized half of the neutral lipid fraction, which was analyzed with regard to its TAG abundance via charged aerosol detector HPLC (CAD-HPLC). The Ultimate 3000 SD system contained a dual gradient pump with a Corona ultra RS detector (Thermo Scientific™ Dionex™ Corona™ ultra RS™ Charged Aerosol Detector). The detector's nebulizer was set to 15 °C, the corona filter to 4. Samples were separated on an Accucore C8-column (150 x 4.6 mm, 2.6 µm, Thermo Scientific), heated to 40°C, using eluent A (methanol/water, 65:35 v/v, both LC-MS grade), eluent B (acetonitrile, LC-MS grade) and eluent C (isopropanol, GC-MS grade). The flow rates of the gradient eluent and inverse gradient pumps were aligned to 0.8 mL min^{-1} and 1.2 mL min^{-1}, respectively. The gradient eluent pump was equilibrated with 100 % A 10 min pre-run, the gradient was set to 50 % A and 50 % B at 2 min, 45 % A and 55 % B at 15 min, 100 % B at 23 min, holding until 30 min, then 35 % B and 65 % C at 60 min. The inverse gradient pump was equilibrated with 66,7 % B and 33 % C 10 min pre-run. The gradient was set to 33.3 % of A, B and C at 2 min, 40 % A, 26.7 % B and 33.3 % C at 15 min, 66.7 % A and 33.3 % C at 23 min, holding until 30 min, 66.7 % A and 33.3 % B until 60 min. Chromatograms were evaluated with Chromeleon 7.0 (Thermo Scientific), integrated peak areas were normalized to the internal standard and the number of cells in the sample.

3.4.8 Alkene analysis via GC-MS

The non-derivatized neutral lipid fraction, analyzed regarding its TAG content as described in 3.4.7, was further analyzed via GC-MS according to 3.4.3, after addition of the internal standard hexatriacontane (analytical standard grade, Sigma-Aldrich). Comparison of resulting peaks with literature revealed alkenes (Volkman, 1980b). The peak area was normalized to the number of cells present in the analyzed sample.

3.4.9 Alkenone analysis via GC-FID

Alkenone analysis was performed by K. Fahl (Marine Geology and Paleontology, Alfred Wegener Institute, Helmholtz Centre for Polar and Marine Research, 27570 Bremerhaven, Germany). The non-derivatized neutral lipid fraction was subjected to a further purification step, via single-use chromatography. In contrast to instruction in 3.4.5, finer silica gel was used (Silica gel 60 extra pure for column chromatography, 0.063-0.200 mm, 70-230 mesh ASTM, Merck), which had been baked at 350 °C for three hours and kept in a desiccator three days before use. Column equilibration was performed with dichloromethane (GC-MS grade) and hexane (GC-MS grade). Samples were dissolved and loaded with hexane. The first fraction was

eluted with dichloromethane/hexane (1:1 v/v) and contained unwanted lipids, such as TAGs. Pure dichloromethane was used to elute the alkenone fraction. Fractions were collected in glass tubes, dried with nitrogen gas and kept at -20 °C. For GC-FID analysis samples were diluted in 100 µL hexane with internal standard hexatriacontane (analytical standard grade, Sigma-Aldrich).

Measurements were performed with a Hewlett Packard gas chromatograph (HP6890, column 30 m x 0.25 mm; film thickness 0.25 µm; liquid phase: HP 5). 1 µL of sample was injected using a cold injection system, which was set to 60 °C, then went to 105 °C at 3 °C s^{-1}, then to 320 °C at 10 °C s^{-1}, holding there for 60 s. The GC temperature profile started at 60 °C, after one minute went to 270 °C at 20 °C min^{-1}, further to 320 °C at 1 °C min^{-1}, holding there for 20 min. Alkenones were identified by comparison of retention time and previously measured standards. Peak areas were normalized to the internal standard and number of cells present in the sample. Further, alkenone-related parameters were calculated from the obtained data. The alkenone unsaturation index indicates the proportion of unsaturation among alkenones (Brassell, 1986; Prahl & Wakeham, 1987):

$$U_{37}^{K'} = \frac{C_{37:2}Me}{C_{37:2}Me + C_{37:3}Me} \qquad \text{Eq. 2}$$

Based on the U$^{K'}_{37}$, calculation of sea surface temperature (SST) is possible, as an alkenone-producing organism produces more less unsaturated alkenones at higher water temperatures. Several different calibrations have been reported, describing the relationship between unsaturation of alkenones and the temperature of the surrounding waters. A global summer calibration was reported for waters of a temperature range of 1-30 °C . (Müller, 1998), reflected in equation 3. More specific calibrations were published for *E. huxleyi* B92/21 (equation 4) and *E. huxleyi* G1779Ga (equation 5) (Conte, 1998). All three calibrations were applied in this work.

$$U_{37}^{K'} = 0.005 + 0.033 \cdot SST \qquad \text{Eq. 3}$$

$$U_{37}^{K'} = 0.053 + 0.009 \cdot SST + 0.001 \cdot SST^2 \qquad \text{Eq. 4}$$

$$U_{37}^{K'} = 0.025 + 0.001 \cdot SST + 0.001 \cdot SST^2 \qquad \text{Eq. 5}$$

3.4.10 Metabolite extraction for LC-MS/MS analyses

The following metabolite analyses via LC-MS/MS were performed by the project partners (ZeBiCa[2] project) E. Heidenreich and F. Kirschhöfer (Analytical Biochemistry, Department of Bioengineering and Biosystems, Institute of Functional Interfaces, Karlsruhe Institute of Technology, 76344 Eggenstein-Leopoldshafen, Germany). The extraction of metabolites was identical for all four methods, and included addition of 1 mL 80 % (v/v) methanol (LC-MS grade) to thawed filters. Ultrasonication was used to homogenize cells (15 min, room temperature), after which filters were removed. The sample was centrifuged (13,000 g, 10 min) and the supernatant was transferred to a fresh glass vial for further analysis.

3.4.11 Amino acid analysis via LC-MS/MS

This analysis was performed by E. Heidenreich and F. Kirschhöfer (Analytical Biochemistry, Department of Bioengineering and Biosystems, Institute of Functional Interfaces, Karlsruhe Institute of Technology, 76344 Eggenstein-Leopoldshafen, Germany). Free amino acids were derivatized to amino acid butyl esters analyzed via LC-MS/MS as described previously (Casetta, 2000; Harder, 2011). Samples were spiked with isotope labeled standards (labeled amino acid standards set A, Cambridge Isotope Laboratories). Briefly, samples were dried with nitrogen gas and then derivatized with 300 µL butanol/HCl, including incubation at 65 °C and 450 rpm for 20 min in a thermoshaker. After derivatization samples were dried again and resolved in 500 µL 0.1 % trifluoroacetic acid (≥99 %, Sigma-Aldrich) in deionized water. 20 µL of sample were separated on an Agilent 1100 HPLC system (Agilent), using a Multospher 120 RP18 AQ-5µm column (Chromatographie Service) with 0.1 % trifluoroacetic acid in water (eluent A) and 0.1 % trifluoroacetic acid in acetonitrile (eluent B). The gradient was run at 0.6 mL min^{-1}, starting with 15 min equilibration with 90 % A before each run. The eluent changed to 70 % A at 15 min, holding until 19 min, changing to 50 % at 26 min, holding until 28 min, and ending at 30 min with 90 % A. Amino acids were detected on an API 4000 quadrupole mass spectrometer (Applied Biosystems/MDS Sciex), equipped with an electrospray ionization (ESI) source. Peaks were analyzed with Analyst software (Version 1.6, AB Sciex), and amino acids were quantified with calibration curves of the standards and normalized to internal standard recovery as well as number of cells in the sample.

3.4.12 Small organic acid analysis via LC-MS/MS

This analysis was performed by E. Heidenreich and F. Kirschhöfer (Analytical Biochemistry, Department of Bioengineering and Biosystems, Institute of Functional Interfaces, Karlsruhe Institute of Technology, 76344 Eggenstein-Leopoldshafen, Germany). Analysis of small organic acids was performed using a modified version of a published derivatization method (Han, 2013). The derivatization reagent contained a 1:1 mixture of 50 mM 3-nitrophenylhydrazine (98 %, Sigma-Aldrich) in methanol and 30 mM 1-ethyl-3-(3-dimethylaminopropyl)carbodiimide hydrochloride (EDC, crystalline, Sigma-Aldrich) in methanol. 10 µL succinic acid-d3 (Sigma-Aldrich, internal standard, 5 µg mL^{-1} in methanol), 10 µL of 10 % (v/v) pyridine (dried, Merck) in methanol and 50 µL derivatization reagent were added to 30 µL sample. Samples were incubated for 60 min at room temperature and diluted 1:10 with methanol/10 mM ammonium acetate (50/50, v/v). LC-MS/MS analysis was performed with the same instruments as described in 3.4.11, however separation differed. A Lichrosper 100 Å RP-C18 EC column was used (125 mm x 4 mm, 5 µm, Merck), and methanol (eluent A) and 10 mM ammonium acetate in water (eluent B) were used with a flow rate of 0.5 mL min^{-1}. Column equilibration was performed with 30 % A for 15 min before each run. 30 µL of sample were injected, and the gradient changed to 80 % A at 20 min, holding until 25 min, then returning to 30 % A at 30 min. Organic acids were quantified with calibration curves of standards and normalized to internal standard recovery as well as number of cells in the sample.

3.4.13 Osmolyte analysis via LC-MS/MS

This analysis was performed by E. Heidenreich and F. Kirschhöfer (Analytical Biochemistry, Department of Bioengineering and Biosystems, Institute of Functional Interfaces, Karlsruhe Institute of Technology, 76344 Eggenstein-Leopoldshafen, Germany). Osmolyte analysis did not require derivatization. Samples were diluted in acetonitrile/10 mM ammonium acetate (50:50, v/v) and analyzed via LC-MS/MS using the instruments described in 3.4.11. Separation of 20 µL of sample was performed using a Luna NH2 100 Å LC column (250 mm x 2 mm, 5 µm, Phenomenex), with acetonitrile (eluent A) and 10 mM ammonium acetate (eluent B). The flow rate was set to 0.4 mL min^{-1}, and the column was equilibrated before each run with 80 % A for 2 min. The gradient changed to 50 % A at 1 min, holding until 6 min, then going back to 80 % A, which was held until 18 min. Standards for comparison were bought (DMSP, Biozol Diagnostica) or synthesized in the analytical biochemistry group (Institute of Functional Interfaces, Karlsruhe Institute of Technology) according to (Gebser & Pohnert, 2013) (dimethylsulfonioacetate, homarine, trimethylammonium propionate and trimethylammonium

butyrate standards), including substance validation via LC-MS/MS and NMR. Identified compounds were quantified with calibration curves of standards, values were normalized to the number of cells.

3.4.14 Polyamine analysis via LC-MS/MS

This analysis was performed by E. Heidenreich and F. Kirschhöfer (Analytical Biochemistry, Department of Bioengineering and Biosystems, Institute of Functional Interfaces, Karlsruhe Institute of Technology, 76344 Eggenstein-Leopoldshafen, Germany). A modified version of Escribano's derivatization method (Escribano & Legaz, 1988) was applied to derivatize polyamines. 250 µL deionized water, 250 µL saturated sodium bicarbonate solution and 400 µL 0.02 M dansylchloride (≥99 %, Fluca) in acetone (HPLC grade) were added to 100 µL of sample. Samples were incubated at 60 °C for 30 min. Dansyl derivatives were extracted with cyclohexane (99.9 %, Merck), the organic phase was recovered and dried with nitrogen gas. Samples were dissolved in 1 mL acetonitrile/water (50:50 v/v) with 0.1 % acetic acid for LC-MS/MS analysis using the instruments described in 3.4.11. Separation was achieved on a Gemini 100 RP-18-3µ column (Phenomenex), using water with 0.1 % acetic acid (eluent A) and acetonitrile (LC-MS grade) (eluent B). The flow rate was 0.4 mL min^{-1} and 20 µL of sample were injected. Column equilibration was performed with 50 % A for 15 min before each run, followed by a change to 10 % A at 9 min, holding until 14 min, and returning to 50 % A at 15 min. Polyamine standards measured were putrescine (1,4-diaminobutane, 99 %, Sigma-Aldrich), cadaverine (purum, ≥97.0 % (GC), Sigma-Aldrich), spermidine (≥99 % (GC), Sigma-Aldrich) and spermine (≥99.0 % (GC), Sigma-Aldrich). At this point it is important to note that no polyamines were detected in the samples analyzed in this work.

3.5 Statistical analysis

To determine whether changes between different treatments were statistically significant, a two-tailed t-test was performed. Significance was determined if p-values were below 0.05, differentiating two levels, as indicated by the number of asterisks (≤0.05 (*) and ≤0.01 (**)). Discussed results represent mean values or fold-changes of mean values, with standard deviation (SD).

4. Results

In this work the diploid, calcifying (C, 2N) strain *E. huxleyi* RCC 1216, and its haploid, non-calcifying (S, 1N) life-cycle stage RCC 1217 were analyzed. They will be referred to as diploid (2N) and haploid (1N) life-cycle stages hereafter. Cultivation of *E. huxleyi* was established in pretests not discussed in detail this work. The metabolome harvesting method and several analysis methods were adapted, to allow metabolome analysis of a microalga that grows to comparably low cell densities and cannot be harvested by centrifugation.

In this chapter, results regarding optimization of fatty acid analysis are presented in the first section (4.1). In the second section, results from non-invasive FTIR measurements are reported, elucidating differences in cellular composition of the diploid and haploid *E. huxleyi* life-cycle stages, regarding proteins, carbohydrates and lipids (4.2). In a third section, growth phase-dependent pigment and fatty acid profiles are presented for both life-cycle stages grown under nutrient-replete conditions (4.3). In the last section, a comprehensive metabolome analysis of both life-cycle stages under nutrient replete, as well as nutrient-starvation conditions (P, N), is presented, including analysis of primary metabolites, osmolytes, pigments, fatty acids, TAGs, alkenes and alkenones (4.4).

4.1 Optimization of FAME analysis

It is common to analyze lipids as their respective fatty acid methyl esters (FAME), enabling their detection and quantification via GC-MS or GC-FID and classification regarding fatty acid chain length (Dodds, 2005). However, it is important to note that for both instruments, the detector's response varies with regard to the number of carbons and double bonds in a FAME molecule (Ackman & Sipos, 1964; Ulberth, 1999; Ackman, 2002; Dodds, 2005), underlining the necessity of calibration (Marriott, 2004).

To test the response of the instrument used in this work (TraceGC gas chromatograph and ITQ ion trap mass spectrometer, Thermo Scientific), FAME calibration curves were measured using commercially available FAME standards. The individual FAMEs showed varying non-linear responses and calibration curves were best fitted by second degree polynomial regression (quadratic polynominal) (Figure 6, shown for each FAME individually in Supplementary Figure 1). Unsaturated FAME, especially with shorter chains, had low responses (Figure 6 a), whereas some unsaturated, some mono- and all polyunsaturated FAME showed medium responses (Figure 6 b). Longer chain saturated and unsaturated FAME had the highest responses (Figure 6 c).
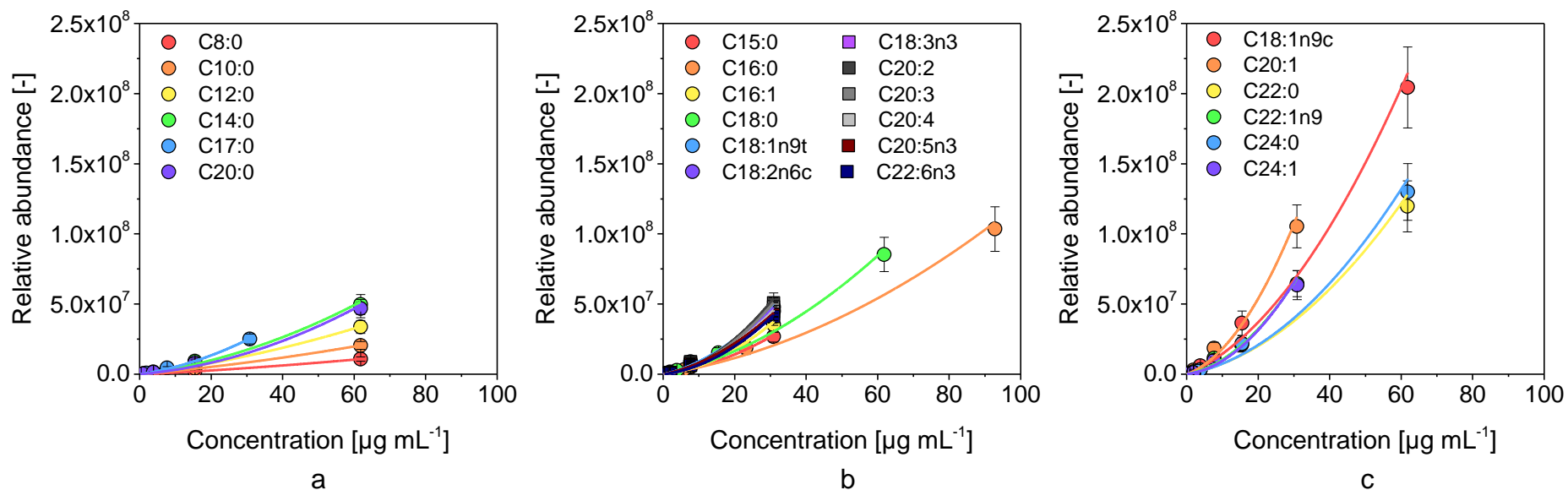
Figure 6: Calibration curves for individual FAMEs measured via GC-MS (ITQ), fitted by second degree polynomial regression (y=ax²+bx+c). Dilutions of a commercially available FAME mix (Supelco) containing 37 individual FAMEs in different concentrations. Curves are grouped in different categories regarding detection response. (a) FAMEs with small response. (b) FAMEs with medium response. (c) FAMEs with high response. Y-axis is fixed for all diagrams for better comparison. Mean values and standard deviation (SD) of four technical replicates.

Especially in the lower concentration range, FAME calibration curves were not linear in the measurements (Figure 7 and Supplementary Figure 1). Furthermore, the instrument was particularly sensitive regarding short-chain fatty acids, such as $C_{8:0}$ (Figure 7). Here, the limit of detection was 3.9 µg mL^{-1}, higher compared to the other FAME.
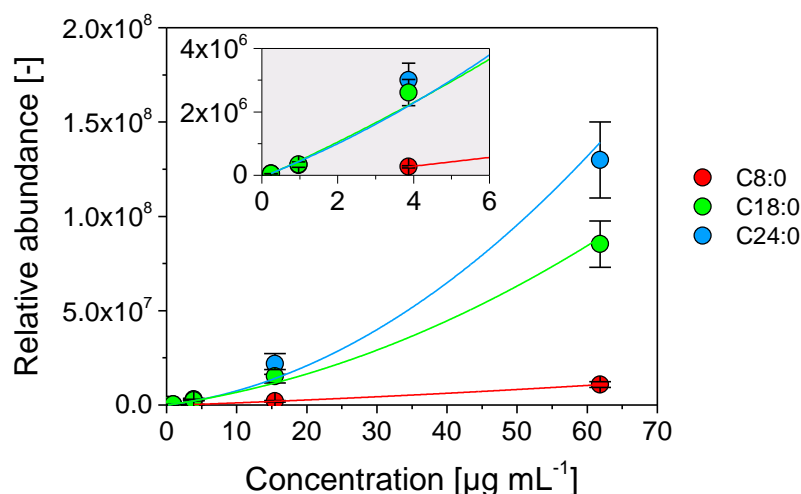
Figure 7: Representative FAME from each of the three groups. Box shows zoomed in proportion. Mean values and SD of four technical replicates.

To avoid misinterpretation, second degree polynomial regression (Supplementary Table 1) was applied to correct FAME abundance data post-run. An example for non-corrected and corrected FAME abundance is shown in Figure 8 for fatty acids belonging to *E. huxleyi*'s polar lipid fraction, highlighting the differences of the resulting fatty acid profile.
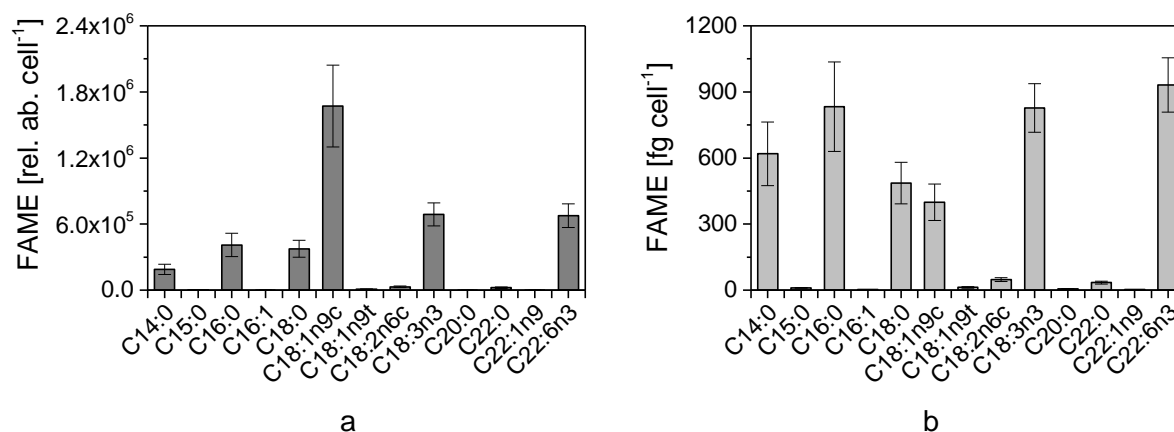
Figure 8: The effect of post-run FAME correction. (a) Uncorrected FAME concentration, normalized to internal standard and cell number. (b) Corrected FAME concentrations, using quadratic calibration equations for each individual FAME before normalizing to cell number. Mean values and SD of one biological replicate measured in technical triplicate.

Throughout this work, the misinterpretation of short-chain FAMEs via GC-MS became clear on a further level. While analyzing the triacylglycerols via CAD-HPLC, $C_{8:0}$ TAG was

detected in *E. huxleyi* samples. As these belong to the neutral lipid fraction, $C_{8:0}$ FAME should also be detected in the neutral lipid FAME, analyzed via GC-MS. This, however, was not the case. A test with different TAG standards revealed discrepancies between HPLC and GC-MS, as illustrated in Figure 9 for $C_{8:0}$ TAG/FAME. Based on a calibration curve with eight dilution steps (200-1.6 ng μL^{-1}), only the highest five concentrations were detectable via GC-MS. This was partly due to the added dilution (factor 8) introduced by the FAME derivatization procedure.
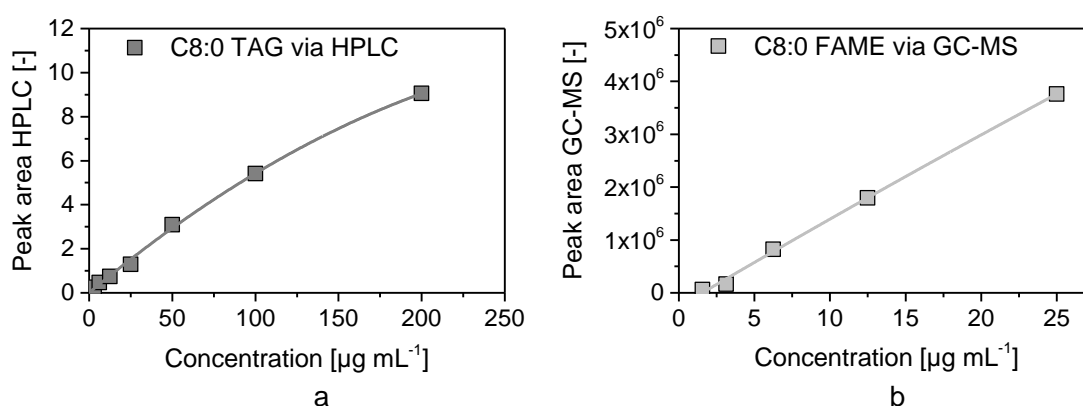
Figure 9: Comparison of TAG detection via CAD-HPLC and GC-MS. Curves were fitted by second degree polynomial regression. (a) Dilution curve of $C_{8:0}$ TAG standard (200-1.6 ng μL^{-1}, glyceryl-trioctanoat, Supelco) measured as whole TAG via HPLC. (b) Measurement of the same samples after derivatization to FAME via GC-MS. Note dilution (factor 8) introduced by derivatization step. Only the five highest concentrations of eight in total were detectable via GC-MS. n=1.

4.2 Cellular composition of *E. huxleyi* determined via FTIR

The results described in this section were submitted as part of a manuscript:

> Wördenweber, R., Rokitta, S. D., Heidenreich, E., Corona, K., Kirschhöfer, F., Fahl, K., Klocke, J. L., Kottke, T., Brenner-Weiß, G., Rost, B., Mussgnug, J. H., Kruse, O. (submitted): Phosphorus and nitrogen starvation reveal life-cycle specific responses in the metabolome of *Emiliania huxleyi* (Haptophyta).

Fourier transform infrared (FTIR) spectroscopy is a method allowing quick determination of a cell's composition, with respect to proteins, carbohydrates and lipids (Naumann, 1991; Giordano, 2001). It can be especially advantageous in high-throughput screening of different species, as it requires only a small amount of biomass and no time- and labor-intensive extraction or derivatization methods, as the whole cell is analyzed (Johnson, 2004).

To determine whether the diploid (2N) and haploid (1N) *E. huxleyi* life-cycle stages differed with respect to their cellular content, Fourier transform infrared (FTIR) spectroscopy was carried out using cells from the mid-exponential growth phase. FTIR analysis was performed

by J. L. Klocke and T. Kottke (Physical and Biophysical Chemistry Group, Department of Chemistry, Bielefeld University, Bielefeld, Germany).

First tests showed that it was not possible to detect cellular components via FTIR for the diploid cells, as their coccoliths interfered with the measurements (Figure 10 a). This was verified by comparison with the spectrum obtained with calcium carbonate, of which coccoliths are made (Figure 10 a, red discontinuous line). The haploid non-calcifying stage was assessed without problems (Figure 10 b). Extension of the protocol by an acidification step proved to successfully remove coccoliths (Figure 11 a). For sake of comparison, the haploid, non-calcified stage was treated accordingly (Figure 11 b). The effect of acidification on the overall cellular composition of this stage proved to be minor, with slight deviations at 1730 cm^{-1} and at around 1200 cm^{-1} because of the change in pH (Figure 10 b, Figure 11 b).

Peaks were identified by comparison with measured standards and literature. The left side of the spectrum showed an unspecific region, peaks originating from O-H, N-H and C-H stretching vibrations (3700-3100 cm^{-1} and 3000-2800 cm^{-1}). The peak at ~1730 cm^{-1} derived from C=O vibrations of ester groups (Giordano, 2001; Stehfest, 2005), mainly indicating phospholipids. These were also indicated by contributions of phosphodiester vibrations at 1230 and ~1085 cm^{-1} (Giordano, 2001; Naumann, 2001; Stehfest, 2005; Pelusi, 2016). Proteins were indicated by amide I and II bands at 1650 and 1538 cm^{-1} (Giordano, 2001; Stehfest, 2005). An unspecific region originating from C-H bending vibrations was found at 1470-1350 cm^{-1}. Carbohydrates were indicated by associated coupled stretching and bending vibrations at 1200-900 cm^{-1} (Stehfest, 2005). The peaks at 3013 and 963 cm^{-1} showed =C-H stretching modes and hydrogen-out-of-plane modes of trans double bonds of unsaturated hydrocarbons, such as alkenones (Pelusi, 2016).

Comparison of spectra for both life-cycle stages showed high similarities (Figure 11 c, d). The contribution of alkenones was slightly larger for the diploid stage (1.1-fold), and this difference was significant (*t*-test, p-value=0.01). Other than that, no differences were observed for the cellular content of both life-cycle stages, regarding proteins, carbohydrates and lipids. Therefore, both life-cycle stages did not differ significantly on this level of analysis.

In the following parts of this thesis, further in-depth metabolomic analysis is applied, to obtain a more detailed picture of biochemical pathways, with regard to growth phase (section 4.3) and nutrient-starvation (section 4.4).
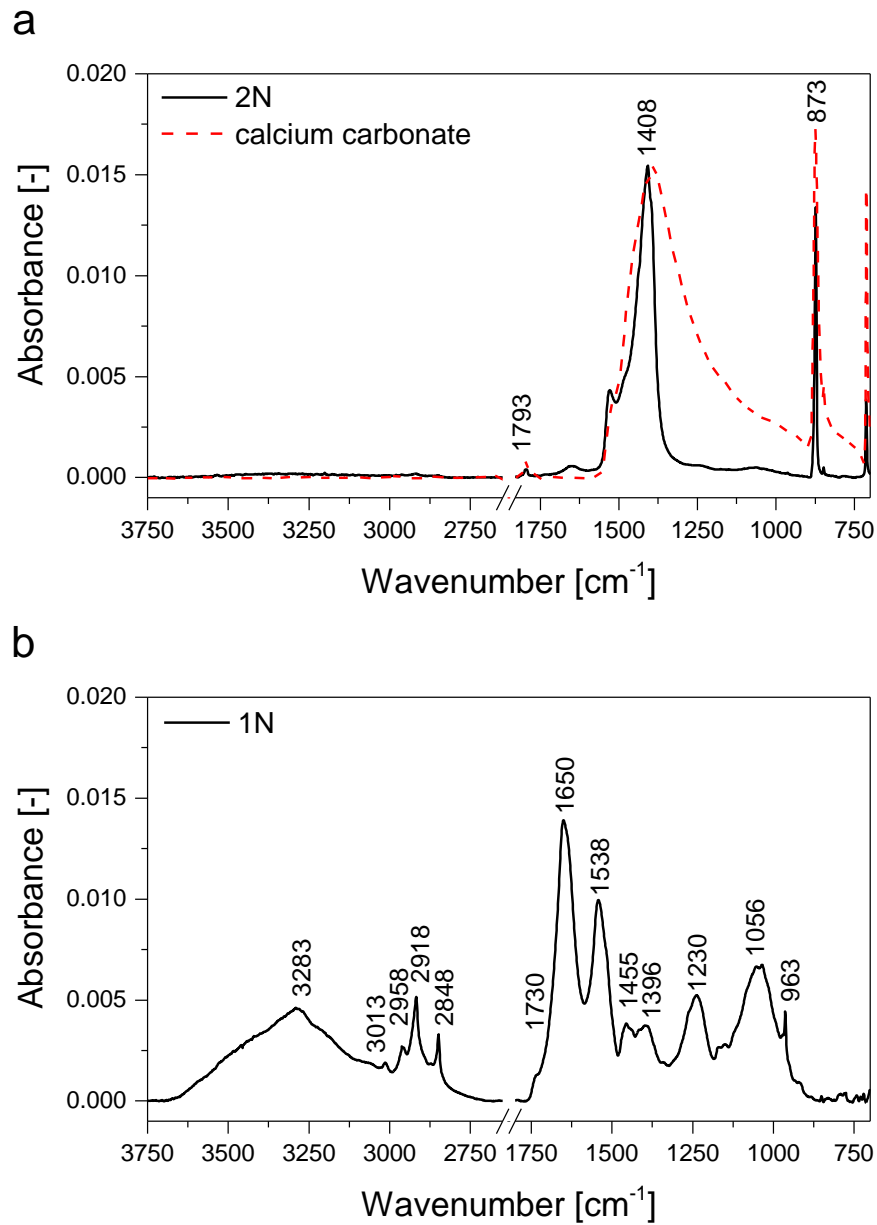
Figure 10: FTIR spectra of the diploid (2N) and haploid (1N) *E. huxleyi* **life-cycle stages without further pretreatment. (a) The dominant signals in the diploid sample (black line) at 1408 and 873 cm^{-1} are assigned to calcium carbonate (red discontinuous line) of the coccoliths, which interfere with the measurement. (b) The haploid, non-calcifying life-cycle stage can be assessed without further treatment. Mean values of six technical measurements are denoted.**
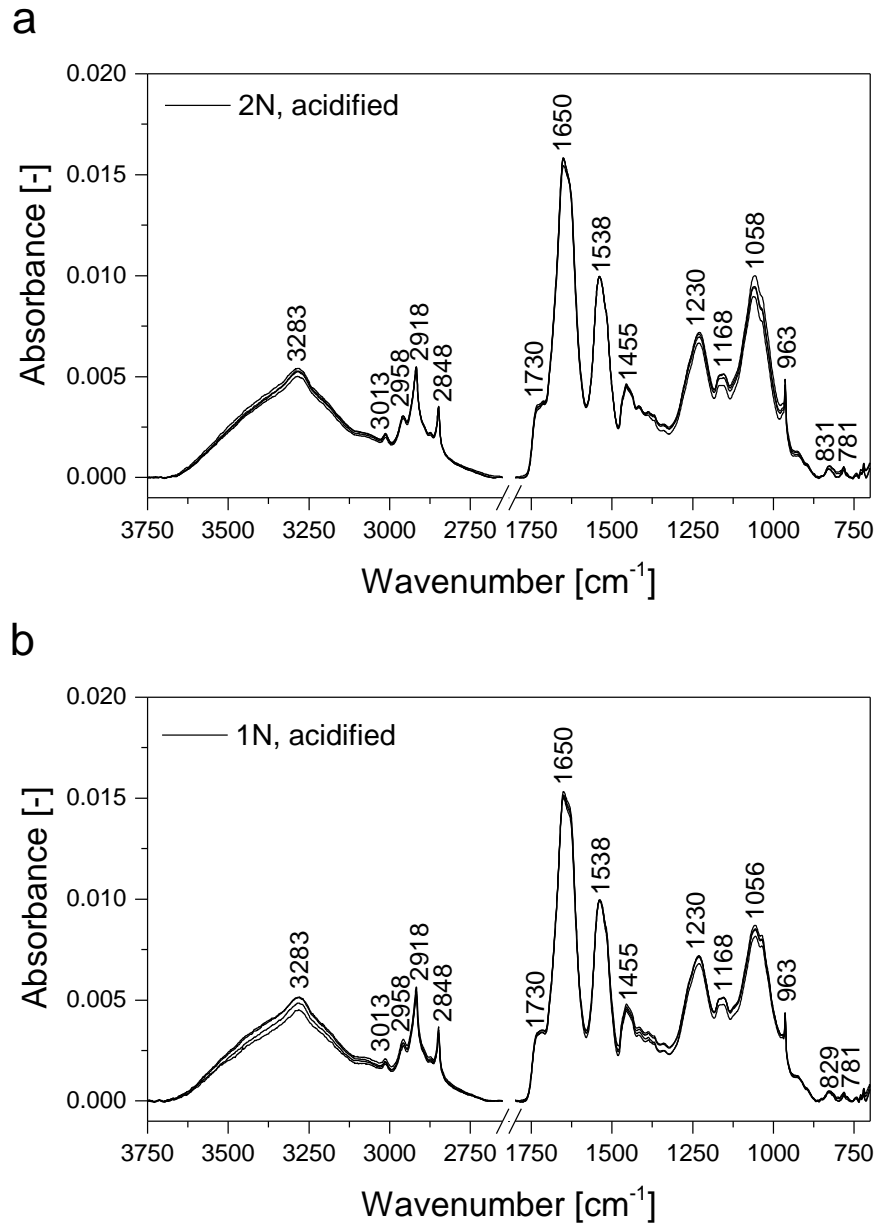
Figure 11: FTIR spectra of the diploid (2N) and haploid (1N) *E. huxleyi* life-cycle stages with acidification treatment. Analysis of acidified lyophilized biomass harvested in the late exponential growth phase (n=4). (a) FTIR spectra of four biological replicates of the 2N life-cycle stage. (b) FTIR-spectra of four biological replicates of the 1N life-cycle stage. Mean values of six technical measurements are denoted.

4.3 Growth phase-dependent metabolomic analysis of *E. huxleyi* life-cycle stages

The metabolome is highly dynamic, as concentrations of numerous metabolites change in the time frame of seconds (Dettmer, 2007). In microalgae, growth phase-dependent changes in the metabolome have been observed, including highest abundances for numerous primary metabolites in the exponential growth phase (Vidoudez & Pohnert, 2012), and accumulation of assimilation products (storage lipids, sugars) with ceasing cell growth (Hodgson, 1991; Kluender, 2009; Vidoudez & Pohnert, 2012). These changes can influence microalgal food quality (regarding predators), chemical defenses and signal molecule production of the microalgae, and are therefore ecologically relevant (Vidoudez & Pohnert, 2012; Mausz & Pohnert, 2015).

Growth phase-dependency of the metabolome has been reported for the haploid and diploid life-cycle stages of *E. huxleyi* analyzed in this work, however only primary metabolites that are derivatizable to trimethylsilyl-esters were measured via GC-MS (Mausz & Pohnert, 2015). In this work, the focus was set on pigments and lipids (more specifically fatty acids), to allow precise conclusions about the physiological status of the cell during various stages of growth.

To reach this goal, *E. huxleyi* was grown under nutrient-replete conditions and harvested at three different time points, in order to analyze the growth phase-dependent pigment and fatty acid content. The diploid (2N) and haploid (1N) life-cycle stages were inoculated at 2000 cells mL^{-1} and grown in nutrient-replete ESAW media (Figure 12 a). Cell numbers were assessed daily.
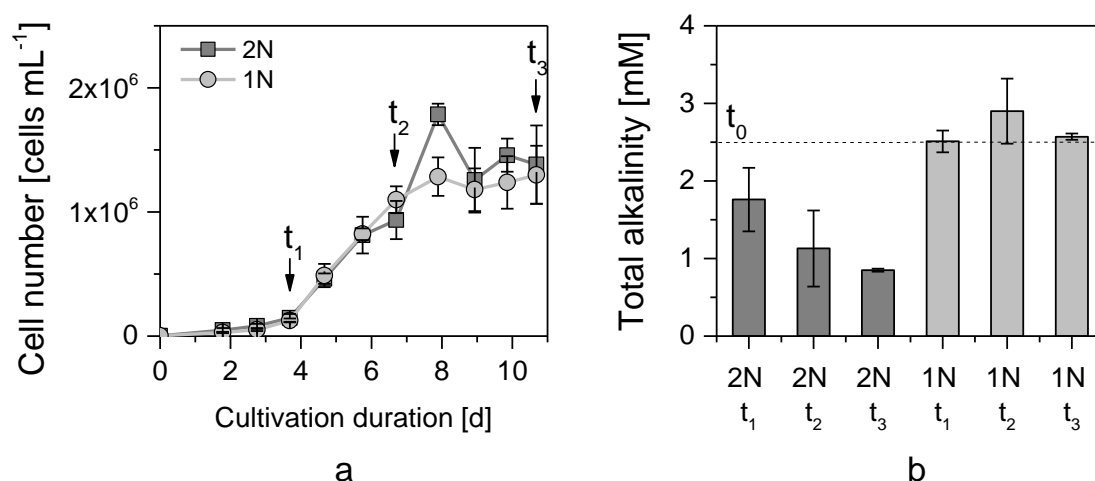
Figure 12: Growth characteristics for two life-cycle stages of *E. huxleyi* under nutrient-replete conditions. (a) Cell numbers for 2N (dark grey boxes) and 1N (light grey circles) stages grown in ESAW media. Arrows indicate harvesting time points t_1-t_3. (b) Total alkalinity analyzed in harvested samples at respective harvesting time point. Dashed line indicates the value at the beginning of the cultivation. Mean values and standard deviations (SD) of triplicate technical measurements of six (t_0-t_1), four (t_1-t_2), or two biological replicates (cell number) and of two biological replicates (total alkalinity).

Both stages grew similarly until the late-exponential phase, where the diploid strain reached a higher cell number on day seven, after which cell numbers converged again, entering stationary growth phase. Maximal cell numbers were $1.7 \cdot 10^6 \pm 8.7 \cdot 10^4$ cells mL^{-1} for the diploid and $1.3 \cdot 10^6 \pm 2.3 \cdot 10^5$ cells mL^{-1}. Metabolome samples were harvested at three time points, as indicated by the arrows. These can be defined as early-exponential (t_1), late-exponential (t_2) and stationary phase (t_3). Cell numbers at these harvesting time points, for the diploid and haploid life-cycle stages, respectively, were $1.3 \cdot 10^5 \pm 2.0 \cdot 10^4$ and $1.1 \cdot 10^5 \pm 7.1 \cdot 10^3$ cells mL^{-1} at t_1, $1.1 \cdot 10^6 \pm 4.8 \cdot 10^4$ and $1.1 \cdot 10^6 \pm 5.5 \cdot 10^4$ cells mL^{-1} at t_2, as well as $1.4 \cdot 10^6 \pm 3.2 \cdot 10^5$ and $1.3 \cdot 10^6 \pm 2.3 \cdot 10^5$ cells mL^{-1} at t_3. At the end of the cultivation, particle counting indicated a higher number of small particles (~1 µm), which were confirmed by light microscopy to be shed coccoliths.

There was no significant difference (p=0.207, determined via two-tailed *t*-test) for the maximal specific growth rates reached on day 4 in both life-cycle stages (2N: 1.1 ± 0.2 vs. 1N 1.3 ± 0.1 d^{-1}). At harvesting time points, growth rates for 2N and 1N, respectively, were 0.6 ± 0.2 d^{-1} and 1.0 ± 0.1 d^{-1} for the t_1, 0.15 ± 0.26 and 0.30 ± 0.05 d^{-1} for t_2, and -0.09 ± 0.3 and 0.05 ± 0.02 d^{-1} for t_3.

At the pH of seawater (~8.2), most dissolved inorganic carbon exists in form of bicarbonate (HCO_3^-), which is why many marine microalgae rely on HCO_3^- as their carbon source. As the diploid *E. huxleyi* stage takes up more HCO_3^- for calcification (Kottmeier, 2016), limitation might occur. Measurement of total alkalinity (TA) of the media allows a rough estimation of dissolved inorganic carbon (DIC) uptake capacity of the media (Wolf-Gladrow, 2007). TA decreased in the diploid life-cycle stage with progressing growth (0.85 ± 0.02 mM at t_3), due to calcification, but it was not depleted (Figure 12 b). No significant changes were observed for the haploid stage. The pH of the media increased to 8.5 at the end of the cultivation for the diploid stage, whereas the increase was even more prominent for the haploid stage (Table 5).

Table 5: pH of nutrient-replete *E. huxleyi* diploid (2N) and haploid (1N) cultures harvested in early-exponential (t_1), late-exponential (t_2) and stationary growth phase (t_3) (n=1).

	pH [-]	
Growth phase	**2N**	**1N**
early-exponential	8.24	8.14
late-exponential	8.28	8.96
stationary	8.51	9.17

Metabolome analysis with regard to pigments and fatty acids was performed with the samples collected from each time point (Figure 12). Extractions were performed separately, and

pigment abundance was measured via UV-vis-HPLC. Extracted lipids were separated into neutral and polar lipid fractions and analyzed as their respective FAMEs via GC-MS.

4.3.1 Pigment composition in different growth phases

In this result section, the general pigment content and differences between both life-cycle stages at each respective time point will be described first. In a second step, the differences between growth phases will be addressed.

It is important to note that pigment results are presented in relative abundance per cell, as quantification via external standard calibration curves was not possible due to limited concentration of many commercially available standards. This is a common issue for marine microalgae, as they contain many uncommon pigments (Egeland, 2011). As analytes can give variable responses in UV-vis-spectrometers, it is possible that the abundance of one pigment is not necessarily comparable to another pigment (Jeffrey, 1997; Smith, 2004). For example, chlorophyll a is known to give a smaller response compared to fucoxanthin, at the same injected weight (Jeffrey, 1997). Studies have reported that fucoxanthin derivatives give comparable responses, the same is true for chlorophyll c derivatives (Egeland, 2011; Garrido, 2016). This does not influence conclusions about relative changes between life-cycle stages and growth phases.

Ten pigments could be detected in both life-cycle stages and all growth phases (Figure 13). They were identified as chlorophyll a, chlorophyll c_2, chlorophyll c_2-MGDG, chlorophyll c_3, diadinoxanthin, diatoxanthin, fucoxanthin, h4k-fucoxanthin, hex-fucoxanthin and β-carotene, based on comparison of retention times and absorption spectra from commercially available standards (Supplementary Table 2).
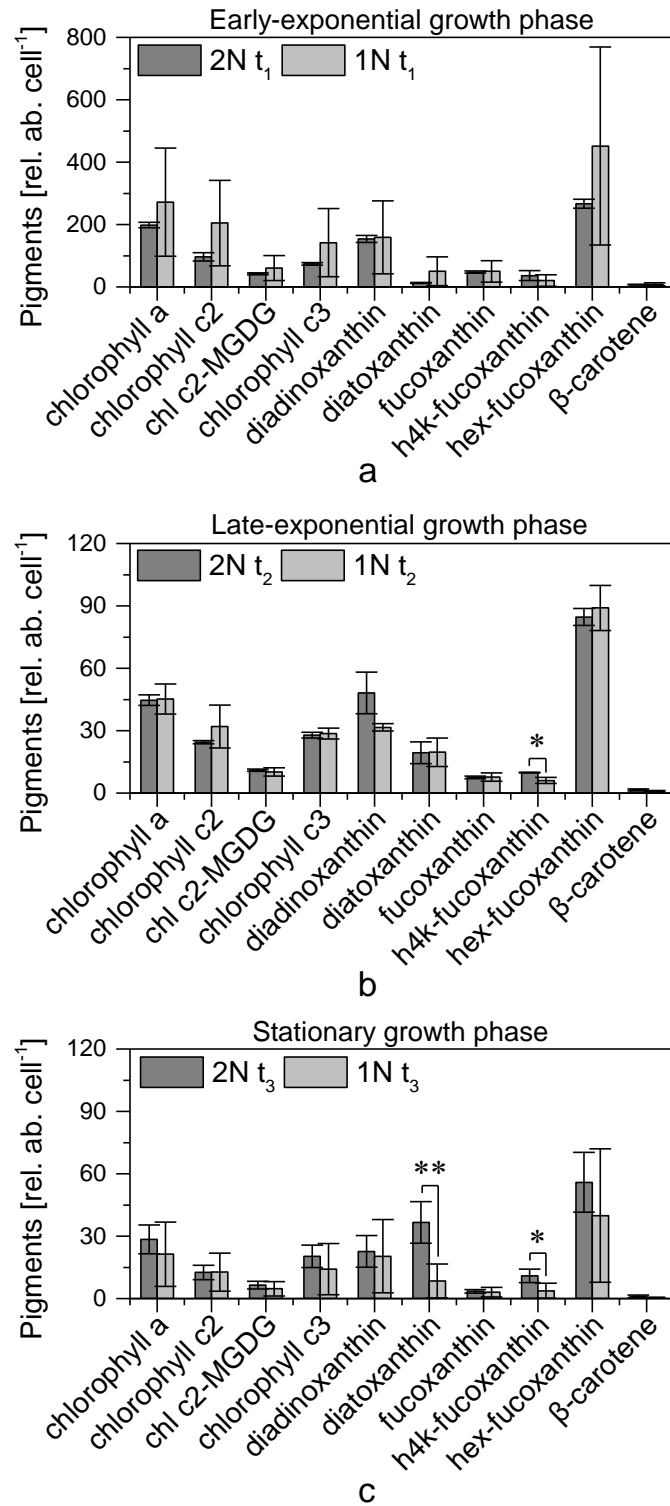
Figure 13: Relative pigment abundances per cell for *E. huxleyi* life-cycle stages harvested in different growth phases. Diploid (2N, dark grey) and haploid (1N, light grey) stages are shown. Cells harvested in (a) early-exponential phase (t_1), (b) late-exponential phase (t_2), (c) stationary phase (t_3). Note different scale of y-axis. Statistical differences between both life-cycle stages are indicated by asterisks, as determined via *t*-test (* indicates p-value ≤0.05, ** ≤0.01). Mean values and SD of two biological and two technical replicates are shown. Chl c2-MGDG, chlorophyll c2-monogalactosyldiacylglycerol.

The haploid stage generally showed a higher variability between biological replicates, as indicated by the higher standard deviation (SD). Comparison of both life-cycle stages in the individual growth phases revealed a similar pigment composition in the early-exponential growth phase, where not significant differences were observed (Figure 13 a). However, life-cycle specific differences were observed between both stages in the late-exponential and stationary phase, as the diploid stage contained significantly more h4k-fucoxanthin than the haploid stage in both later growth phases, as well as more diatoxanthin in the stationary phase (Figure 13 a, b).

Hex-fucoxanthin was a highly abundant pigment in both life-cycle stages. It was found in significantly higher abundance ($p \leq 0.05$) compared to chlorophyll a at all time points for the diploid stage, as well as in late-exponential phase for the haploid stage. However, as stated above, chlorophyll a gives a smaller detection response compared to fucoxanthin, which is why hex-fucoxanthin is not necessarily present in higher abundance than chlorophyll a. Direct comparison of fucoxanthin derivatives is possible due to high structural similarity. Hex-fucoxanthin comprised 76-87 % of total fucoxanthins in both life-cycle stages and all growth phases. In comparison, fucoxanthin (5-15 %) and h4k-fucoxanthin (4-15 %) proportions were minor.

The chlorophyll c derivatives are also comparable with regard to detection response. Chlorophyll c_2 and chlorophyll c_3 were the most abundant chlorophyll c pigments in both life-cycle stages, together making up 80-86 % of total chlorophyll c. In contrast, the proportion of chlorophyll c_2-MGDG was comparably small, amounting to 15-20 % of total chlorophyll c. The proportion of chlorophyll c_2 and c_3 varied slightly between growth phases and life-cycle stages. In the diploid stage, both chlorophyll c_2 and c_3 were similarly abundant in the early-exponential ($p=0.06$) and stationary phase ($p=0.09$), whereas the chlorophyll c_3 abundance was significantly higher in the late-exponential phase ($p=0.02$, 1.1-fold). This was not the case for the haploid stage, as no significant differences between chlorophyll c_2 and chlorophyll c_3 were observed.

To further examine growth phase-dependent changes in pigment composition in the individual life-cycle stages, the fold-change of cellular pigments was calculated, comparing pigment abundance of harvesting time points to the first harvesting time point (Figure 14).
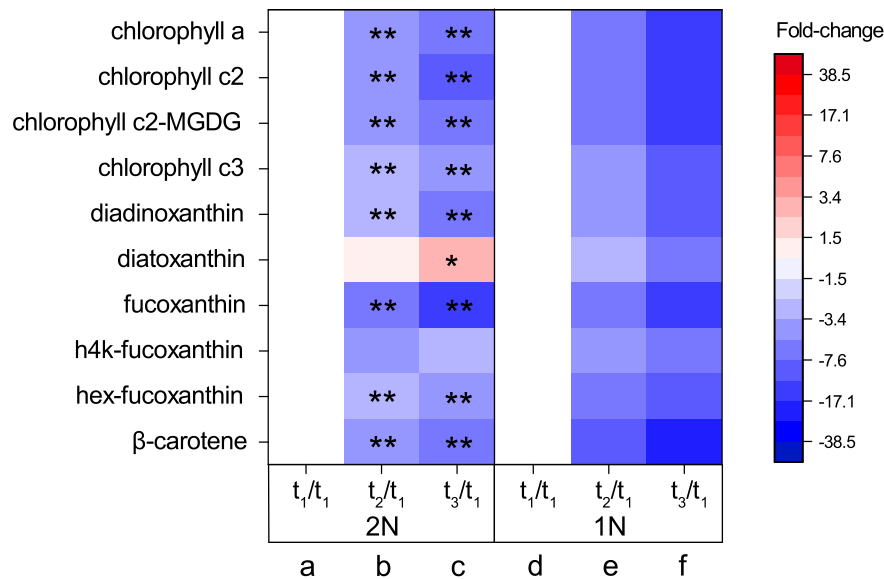
Figure 14: Heat map of the fold-changes of pigments per cell in *E. huxleyi* life-cycle stages, comparing growth phases. Diploid (2N) and haploid (1N) stages are shown. (a, d) Early-exponential growth phase (t1) compared to early-exponential growth phase (t1). (b, e) Late-exponential growth phase (t2) compared to early-exponential growth phase (t1). (c, f) Stationary growth phase (t3) compared to early-exponential growth phase (t1). Asterisks indicate p-value of t-test (* indicates ≤0.05, ** indicates ≤0.01). Fold-changes were calculated from mean values of two biological and two technical measurements.

In the diploid life-cycle stage (2N), nine of ten pigment abundances decreased in the late-exponential phase compared to the early-exponential phase (Figure 14 b). Eight of them were significantly decreased, including all chlorophylls, diadinoxanthin, fucoxanthin, hex-fucoxanthin and β-carotene (2.7-6.3-fold). Diatoxanthin increased non-significantly (1.5-fold). In the stationary phase, significant decreases were even more prominent for the same eight pigments (3.6-13.7-fold), compared to the early-exponential phase (Figure 14 c). Diatoxanthin was significantly increased (2.8-fold).

In the haploid-life cycle stage, the decreasing pattern of pigment abundances was similar, although the change was not significant, due to a higher SD. All pigment abundances non-significantly decreased (2.6-8.7-fold) from early to late-exponential phase (Figure 14 e). The decrease was more pronounced for all pigment abundances in the stationary phase compared to the early-exponential phase (6.0-21.3-fold), however again statistically non-significant (Figure 14 f).

Pigment abundances are often additionally normalized to chlorophyll a (Stolte, 2000; Zapata, 2004; Llewellyn, 2007; Lefebvre, 2010), which allows even more detailed interpretations of a cell's physiological status. The resulting pigment ratios are shown in Figure 15. Also, a de-epoxidation ratio can be calculated (Llewellyn, 2007; Ragni, 2008), which describes the activity of the xanthophyll cycle (photoprotection via non-photochemical quenching), in which diatoxanthin (dtx) and diadinoxanthin (ddx) are involved:

$$de - \text{epoxidation ratio} = \left(\frac{\text{dtx}}{(\text{dtx}+\text{ddx})}\right) \qquad \text{Eq. 6}$$

		t₁/t₁	t₂/t₁	t₃/t₁	t₁/t₁	t₂/t₁	t₃/t₁

Figure legend axis: 2N (a, b, c), 1N (d, e, f)
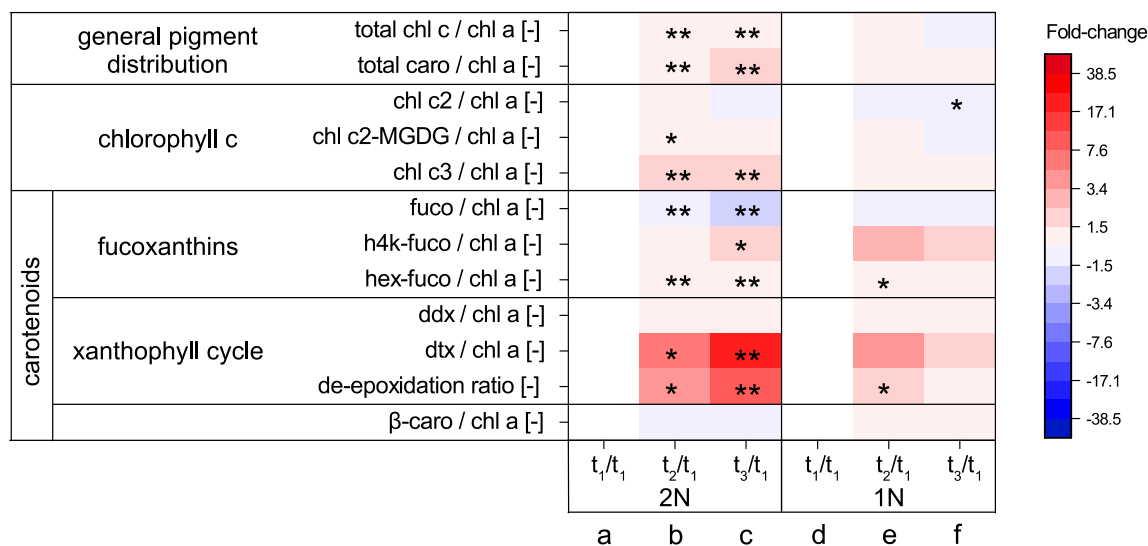
Figure 15: Heat map of the fold-changes of pigment to chlorophyll a ratios in *E. huxleyi* life-cycle stages, comparing growth phases. Diploid (2N) and haploid (1N) *E. huxleyi* life-cycle stages. (a, d) Late-exponential growth phase (t₂) compared to early-exponential growth phase (t₁). (b, e) Stationary phase (t₃) compared to early-exponential growth phase (t₁). (c, f) Stationary phase (t₃) compared to late-exponential growth phase (t₂). Asterisks indicate p-value of *t*-test (* indicates ≤0.05, ** indicates ≤0.01). Fold-changes were calculated from mean values of two biological and two technical measurements. Chl, chlorophyll; caro, carotenoids; MGDG, monogalactosylgdiacylglycerol; fuco, fucoxanthin; ddx, diadinoxanthin; dtx, diatoxanthin; β-caro, β-carotene.

As mentioned above, the abundance of chlorophyll a per cell decreased during growth in both life-cycle stages. Trends for pigment to chlorophyll a ratios were similar for both life-cycle stages, although most changes were non-significant for the haploid stage. Only significant changes will be mentioned hereafter, fold-changes in parenthesis are depicted for the late-exponential- and stationary phase, respectively.

Regarding the general pigment distribution, the ratio increased in the diploid stage for total chlorophyll c to chlorophyll a (both 1.3-fold) and carotenoids to chlorophyll a (1.2- and 1.5-fold) in the late-exponential and stationary phase, compared to the early exponential growth phase. Taking a more detailed look into the individual chlorophyll c pigments, the increase was especially caused by chlorophyll c_3 (1.7 and 1.9-fold). Furthermore, fucoxanthin abundance decreased in the diploid stage compared to chlorophyll a (1.4- and 2.0-fold), whereas both h4k-fucoxanthin (2.0-fold in stationary phase) and hex-fucoxanthin per chlorophyll a increased (1.4- and 1.5-fold).

Regarding the xanthophyll cycle carotenoids, the ratio of diatoxanthin to chlorophyll a especially increased in the diploid stage (6.6- and 19.3-fold), similar to the results on a cellular basis (Figure 14). Consequently, the calculated de-epoxidation ratio increased in the diploid stage in the late-exponential (3.7-fold) and even more in the stationary phase (7.9-fold), whereas it only increased in the late-exponential phase in haploid stage (2.1-fold in late-exponential phase). Absolute values for the de-epoxidation ratio are shown in Table 6. As mentioned above, increased de-epoxidation ratios indicate increased xanthophyll cycling and therefore a more intense photoprotection via non-photochemical quenching.

Table 6: The de-epoxidation ratio of xanthophyll cycle pigments for diploid (2N) and haploid (1N) *E. huxleyi* life-cycle stages harvested in three different growth phases. Mean value and SD of two biological and three technical measurements. Asterisks indicate significant difference of values at later growth phases compared to the early-exponential growth phase (p-value of *t*-test, * indicates ≤0.05, ** indicates ≤0.01).

	De-epoxidation ratio [-]	
Growth phase	**2N**	**1N**
early-exponential	0.08±0.003	0.18±0.08
late-exponential	0.29±0.10*	0.37±0.09*
stationary	0.62±0.03**	0.20±0.10

4.3.2 Lipid composition in different growth phases

The two lipid fractions, polar and neutral, were analyzed as FAMEs via GC-MS. The relative abundance was corrected via quadratic regression as discussed in section 4.1. This section is divided into two parts, according to the affiliation of fatty acids to either polar or neutral lipid fraction. For every part, the general fatty acid composition is presented first, including a comparison of both life-cycle stages. Secondly, growth phase-dependent changes are displayed.

4.3.2.1 Fatty acids associated with the polar lipid fraction

The applied FAME analysis method allowed elucidation of the fatty acid composition of polar lipids, which represent membrane lipids. In the fatty acid pool associated with the polar lipid fraction, fourteen chain lengths were identified, ranging from $C_{14:0}$ to $C_{22:6n3}$ (Figure 16). The odd-numbered $C_{15:0}$ has been reported for *E. huxleyi* previously (Volkman, 1981; Pond & Harris, 1996; Riebesell, 2000; Rontani, 2007; Evans, 2009; Fulton, 2014). Generally, the most abundant lipids were $C_{16:0}$, $C_{18:0}$, $C_{18:1n9c}$, $C_{18:3n3}$, $C_{18:4n3}$, $C_{22:6n3}$, although there were life-cycle stage- and growth phase-specific differences, as supported by *t*-test (p≤0.05).

The diploid stage contained a higher abundance of certain fatty acids compared to the haploid stage. For example, it contained a significantly higher abundance of $C_{14:0}$ in the early-exponential growth phase (Figure 16 a). The diploid stage also contained significantly more polyunsaturated fatty acids ($C_{18:1n9c}$, $C_{18:2n6c}$, $C_{18:3n3}$, $C_{18:4n3}$ and $C_{22:6n3}$) in all growth phases

(Figure 16 a, b, c) and a higher abundance of longer chain fatty acids ($C_{22:0}$, $C_{22:1n9}$ and $C_{22:6n3}$) in the late-exponential and stationary growth phase (Figure 16 b, c).
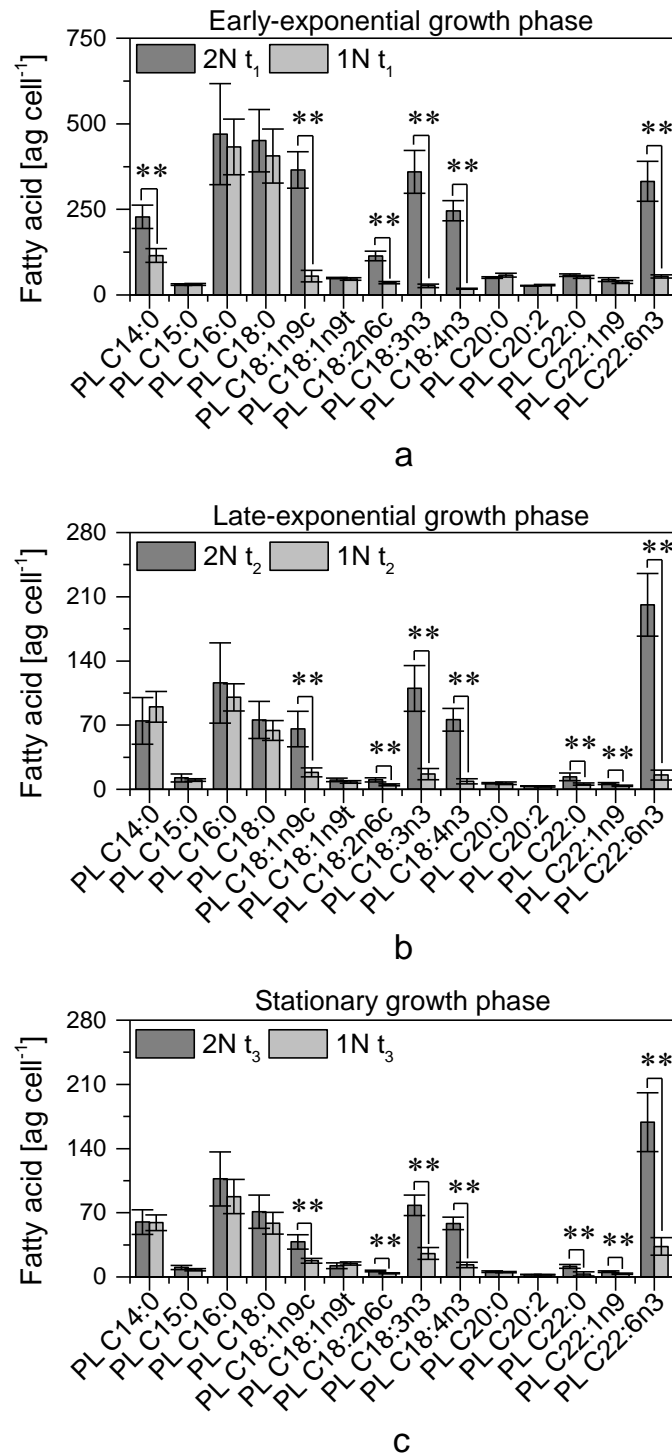
Figure 16: Fatty acid abundances [ag cell^{-1}] associated with the polar lipid fraction (PL) for *E. huxleyi* life-cycle stages harvested in different growth phases. Diploid (2N, dark grey) and haploid (1N, light grey) stages are shown. Cells harvested in (a) early-exponential phase (t_1), (b) late-exponential phase (t_2), (c) stationary phase (t_3). Note different scale of y-axis. Statistical differences between both life-cycle stages are indicated by asterisks, as determined via *t*-test (* indicates p-value ≤0.05, ** ≤0.01). Mean values and SD of two biological and three technical replicates are shown.

To further examine growth phase-dependent changes regarding polar lipids in the individual life-cycle stages, a fold-change was calculated, comparing cellular fatty acid abundance of specific harvesting time points, to those detected at the first harvesting time point (Figure 17).
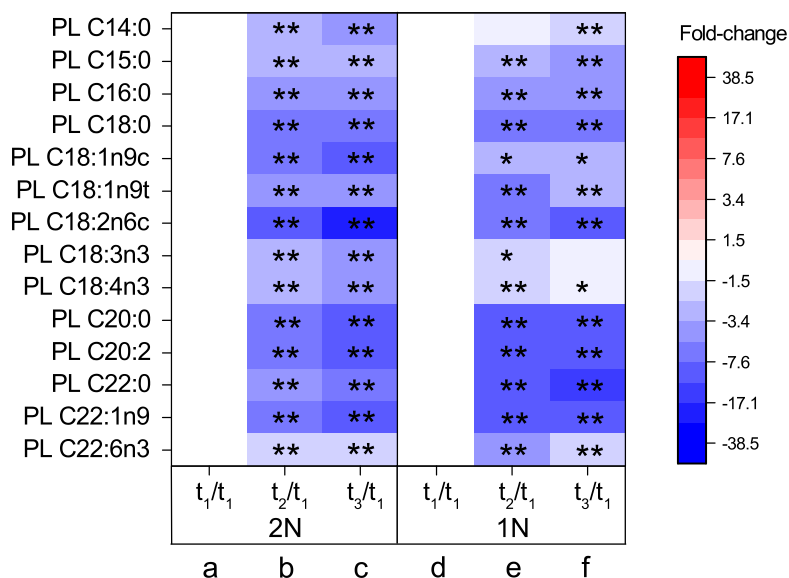
Figure 17: Heat map of the fold-changes of fatty acids per cell associated with the polar lipid fraction in *E. huxleyi* life-cycle stages, comparing growth phases. Diploid (2N) and haploid (1N) stages are shown.(a, d) Early-exponential growth phase (t_1) compared to early-exponential growth phase (t_1). (b, e) Late-exponential growth phase (t_2) compared to early-exponential growth phase (t_1). (c, f) Stationary growth phase (t_3) compared to early-exponential growth phase (t_1). Asterisks indicate p-value of *t*-test (* indicates ≤0.05, ** indicates ≤0.01). Fold-changes calculated from mean values of two biological and three technical measurements. In the diploid life-cycle stage, all fatty acid abundances significantly decreased in the late-exponential (1.7-11.0-fold) and stationary phase (2.0-17.9-fold), compared to the early-exponential growth phase (Figure 17 b, c). For certain fatty acids, the decrease was even more pronounced in the stationary phase. In the haploid life-cycle stage, significantly decreased fatty acid abundances were detected in the late-exponential growth phase for all fatty acids (1.6-10.0-fold) except for $C_{14:0}$, and in the stationary phase for all fatty acids (1.4-16.0-fold) except for $C_{18:3n3}$ (Figure 17 e, f). These results show that in the later growth phases, membrane production is decreased, in line with pigment production.

4.3.2.2 Fatty acids associated with the neutral lipid fraction

The results presented in this section represent fatty acids belonging to the neutral lipid fraction. This fraction is composed of free fatty acids, TAGs, PULCA as well as wax and sterol esters. However, the applied derivatization method only allows derivatization of free fatty acids and TAGs, as is further elucidated in the discussion (4.3.2). Therefore, all fatty acids presented in this section originate from free fatty acids and TAGs.

Ten different fatty acids could be identified in the neutral lipid fraction (Figure 18). Four fatty acids, previously detected in the polar lipid fraction, were not detected ($C_{14:0}$, $C_{20:0}$, $C_{20:2}$, $C_{22:1n9}$). In both stages, the most abundant fatty acids were $C_{16:0}$, $C_{18:0}$ and $C_{18:1n9c}$, followed by $C_{22:0}$ and $C_{22:6n3}$, depending on the growth phase. Both life-cycle stages had a relatively similar composition of fatty acids associated with the neutral lipid fraction (Figure 18), however, there were some significant differences between life-cycle stages in the individual growth phases (*t*-test, p≤0.05). In the early-exponential growth phase, the haploid stage contained a higher abundance of unsaturated fatty acids ($C_{16:0}$, $C_{18:0}$, $C_{22:0}$) and monounsaturated fatty acids ($C_{18:1n9c}$, $C_{18:1n9t}$), whereas the diploid stage contained significantly more $C_{22:6n3}$ (Figure 18 a). In the late-exponential growth phase, the diploid stage contained a higher abundance of unsaturated C_{18} fatty acids ($C_{18:1n9c}$, $C_{18:3n3}$ and $C_{18:4n3}$), and no $C_{18:1n9t}$, in contrast to the haploid stage (Figure 18 b). $C_{22:6n3}$ was not detected in any life-cycle stage at this time point. With respect to the neutral lipid fraction, there were no significant life-cycle specific differences in the stationary growth phase (Figure 18 c).
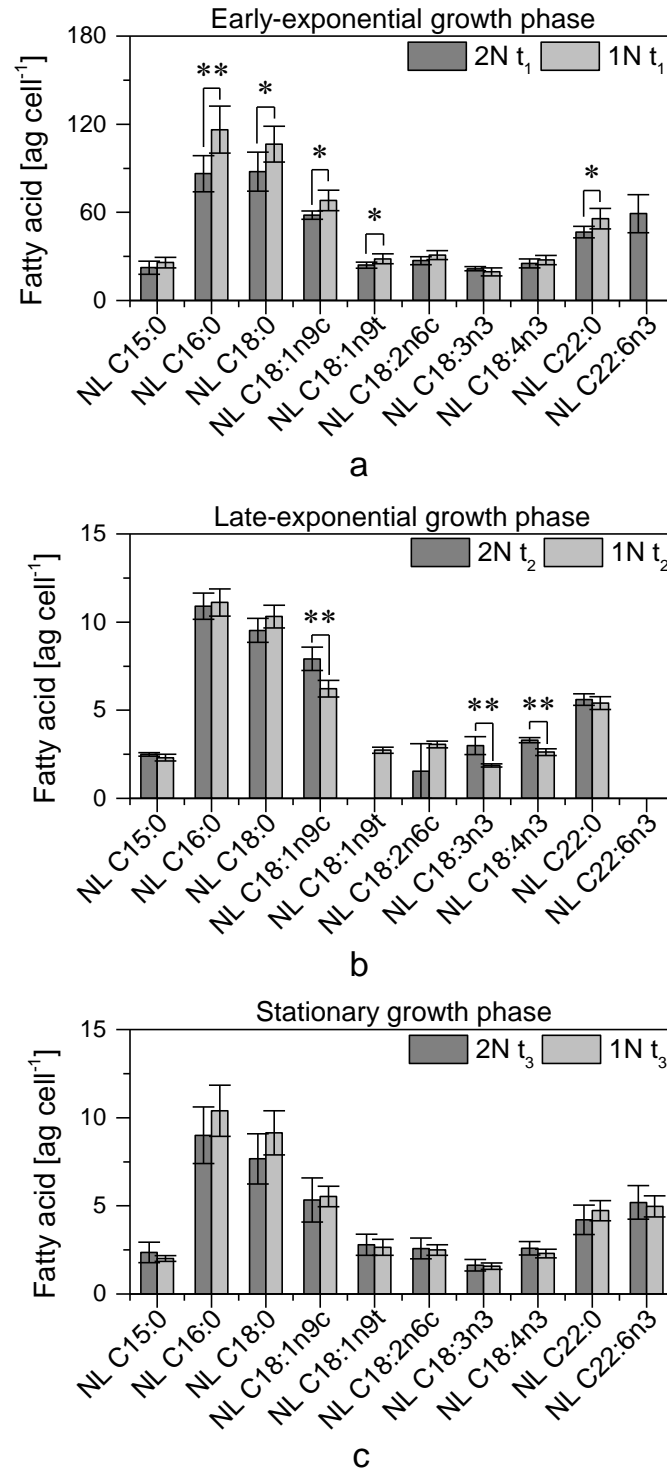
Figure 18: Fatty acid abundances [ag cell^{-1}] associated with the neutral lipid fraction (NL) for *E. huxleyi* life-cycle stages harvested in different growth phases. Diploid (2N, dark grey) and haploid (1N, light grey) stages are shown. Cells harvested in (a) early-exponential phase (t$_1$), (b) late-exponential phase (t$_2$), (c) stationary phase (t$_3$). Note different scale of y-axis. Statistical differences between both life-cycle stages are indicated by asterisks, as determined via *t*-test (* indicates p-value ≤0.05, ** ≤0.01). Mean values and SD of two biological and three technical replicates are shown.

To investigate growth phase-dependent changes of neutral lipid associated fatty acids in the individual life-cycle stages, the fold-change was calculated, representing changes of specific harvesting time points to the first harvesting time point (Figure 19). In cases where a fatty acid wasn't detected, calculation of fold-change was not possible. Here, the tendency of fold-change was set to the maximum/minimum of the scale to indicate either increase or decrease, and marked with a diagonal slash.
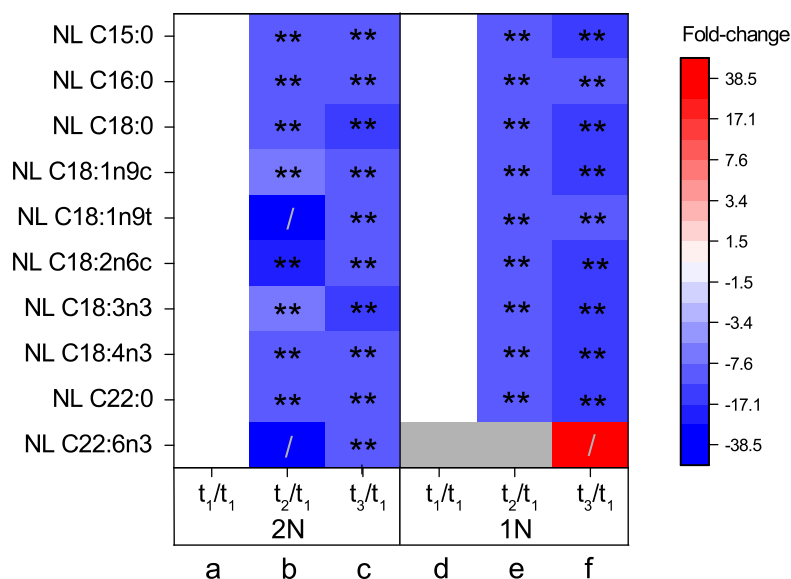
Figure 19: Heat map of the fold-changes of fatty acids per cell associated with the neutral lipid fraction in *E. huxleyi* life-cycle stages, comparing growth phases. Diploid (2N) and haploid (1N) stages are shown. (a, d) Early-exponential growth phase (t_1) compared to early-exponential growth phase (t_1). (b, e) Late-exponential growth phase (t_2) compared to early-exponential growth phase (t_1). (c, f) Stationary growth phase (t_3) compared to early-exponential growth phase (t_1). Asterisks indicate p-value of *t*-test (* indicates ≤0.05, ** indicates ≤0.01). The grey box indicates that component was not detected. Fatty acids detected in one treatment but not in the other were marked with /, indicating tendency of fold-change. The fold-changes calculated from mean values of two biological and three technical measurements.

In the diploid stage, all neutral lipid associated fatty acid abundances decreased significantly in the late-exponential (7.2-17.5-fold) and stationary phase (8.6-13.2-fold), compared to the early-exponential phase (Figure 19 b, c). $C_{18:1n9t}$ and $C_{22:6n3}$ were not detected in the late-exponential phase, therefore the fold-change tendency was set to the minimum of the scale, to indicate the decrease. The pattern was similar in the haploid stage, with nine fatty acid abundances significantly decreasing in the late-exponential (10.1-11.2-fold) and even more in the stationary phase (10.7-12.9-fold), compared to the early exponential phase (Figure 19 e, f). Here, $C_{22:6n3}$ was only detected in the stationary phase, not in the other two stages (marked by grey boxes), therefore also here the fold-change tendency was set to the maximum of the scale, to indicate the increase. These results show that neutral lipid fatty acids, here representing free

fatty acids and TAGs, decreased in the later growth phases (except for $C_{22:6n3}$ in the haploid stage) in line with pigments and polar lipid fatty acids.

An interesting target for industrial use from *E. huxleyi* is the ω-3 fatty acid $C_{22:6n3}$ (docosahexaenoic acid, DHA), which has been shown to be beneficent for human nutrition (Das, 2002; Voigt, 2002; Calder, 2003). The productivity of DHA was calculated per liter culture and day (Figure 20). Despite highest cellular abundances in the early-exponential growth phase, as reported above (Figure 16, Figure 18), the late-exponential phase was the ideal harvesting time point, as cell numbers were higher, leading to a higher productivity for DHA, especially in the polar lipid fraction of the diploid life-cycle stage.
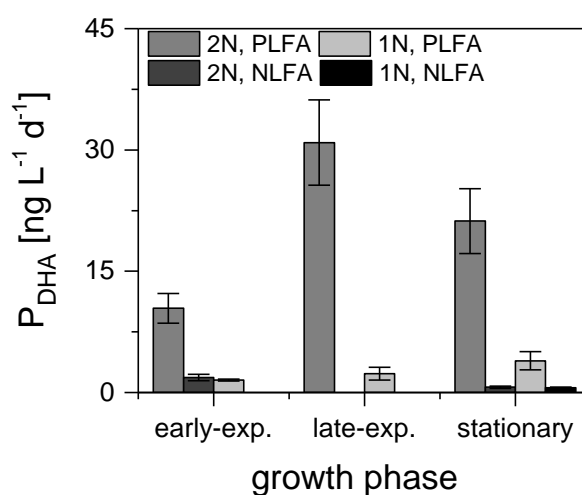
Figure 20: Growth phase dependent productivity of the industrially relevant ω-3 fatty acid DHA (docosahexaenoic acid, $C_{22:6n3}$) in the diploid (2N) and haploid (1N) *E. huxleyi* life-cycle stages. Productivity of DHA [ng L^{-1} d^{-1}] in the polar lipid fatty acids (PLFA) and neutral lipid fatty acids (NLFA). Mean values and SD of two biological and three technical replicates are shown.

4.4 Comprehensive metabolome analysis of *E. huxleyi* life-cycle stages under phosphorus- and nitrogen-starvation

The results described in this section were submitted as part of a manuscript:

> Wördenweber, R., Rokitta, S. D., Heidenreich, E., Corona, K., Kirschhöfer, F., Fahl, K., Klocke, J. L., Kottke, T., Brenner-Weiß, G., Rost, B., Mussgnug, J. H., Kruse, O. (submitted): Phosphorus and nitrogen starvation reveal life-cycle specific responses in the metabolome of Emiliania huxleyi (Haptophyta).

In nature, marine microalgae often have to cope with nutrient-starvation, as certain areas of the ocean are naturally limited by different nutrients, such as nitrogen, phosphorus, silica, iron and nickel (Moore, 2013; Palenik, 2015). Advancing climate change is proposed to enhanced nutrient limitation, due to increased thermal stratification in the upper layers of the ocean (Doney, 2006; Cermeno, 2008; Beman, 2011). The impact on microalgae is enhanced by concomitant ocean acidification, as nutrient and ion assimilation processes are perturbed (Shi, 2010; Beman, 2011). How phytoplankton cope with these changes will determine the fate of whole species and the ecosystem.

Comprehensive metabolome studies on *E. huxleyi* are rare to date. Furthermore, diploid stages have received the most attention, rendering haploid life-cycle stages poorly investigated. So far, three comprehensive studies have been conducted, focusing on GC-MS based metabolome analysis of a diploid strain (CCMP 1516) under nutrient-replete conditions (Obata, 2013), the effect of virus infection on the same strain (Rosenwasser, 2014), and GC-MS based metabolome analysis of *E. huxleyi* RCC 1216 and 1217 with regard to growth phases under nutrient-replete conditions (Mausz & Pohnert, 2015). In contrast, the study presented in this work is the first broad metabolome study including specific pigment and lipid analysis, and regarding nutrient-starvation responses.

In this work, diploid and haploid *E. huxleyi* life-cycle stages (RCC 1216 and 1217) were grown under P- and N-starvation, and metabolites, representative for several biochemical pathways, were analyzed by adapted GC-MS, GC-FID, LC-MS/MS, and HPLC methods.

To generate biomass for metabolomic analysis under nutrient-starved conditions, two separate cultivations were carried out. Both were conducted with nutrient-replete, as well as nutrient-limited ESAW medium, which contained 10 % of either P or N. Both life-cycle stages were inoculated at ~2000 cells mL^{-1} and grown for 7-8 days, reaching final cell numbers of ~2-3·10^6 cells mL^{-1} for nutrient-replete cultures and of ~1-2·10^6 cells mL^{-1} for nutrient-limited cultures (Figure 21 a, b). Samples for metabolome analysis were harvested during the exponential phase, as indicated by the arrows. Nutrient-replete controls of the haploid stage reached higher specific growth rates than the diploid stage during the exponential phase (P-

60

starvation setup: 1N: 0.86 ± 0.47 d^{-1} vs. 2N: 0.74 ± 0.34 d^{-1}; N-starvation setup: 1N: 0.92 ± 0.32 d^{-1} vs. 2N: 0.75 ± 0.12 d^{-1}). Cell numbers of starved cultures stalled from day six onwards compared to the nutrient-replete controls, which kept growing. At this point, respective limiting nutrients were not detectable in the supernatant, as they were consumed on day four (Figure 21 c, d). Nutrient-replete cultures were not limited at any time.

The total alkalinity, indicating availability of the C-source HCO_3^-, was analyzed at harvesting time point. It did not change in haploid cultures, but decreased due to calcification in diploid cultures, reaching values of ~1.2 mM, but was not depleted (Figure 21 e, f). There was also no difference between nutrient-replete and limited cultures, confirming that the only limitation stems from nutrient depletion. Therefore, metabolome sampling point for the starved cultures can be defined as the transition phase between late-exponential and stationary phase, at least for P-starved 2N and N-starved 1N.
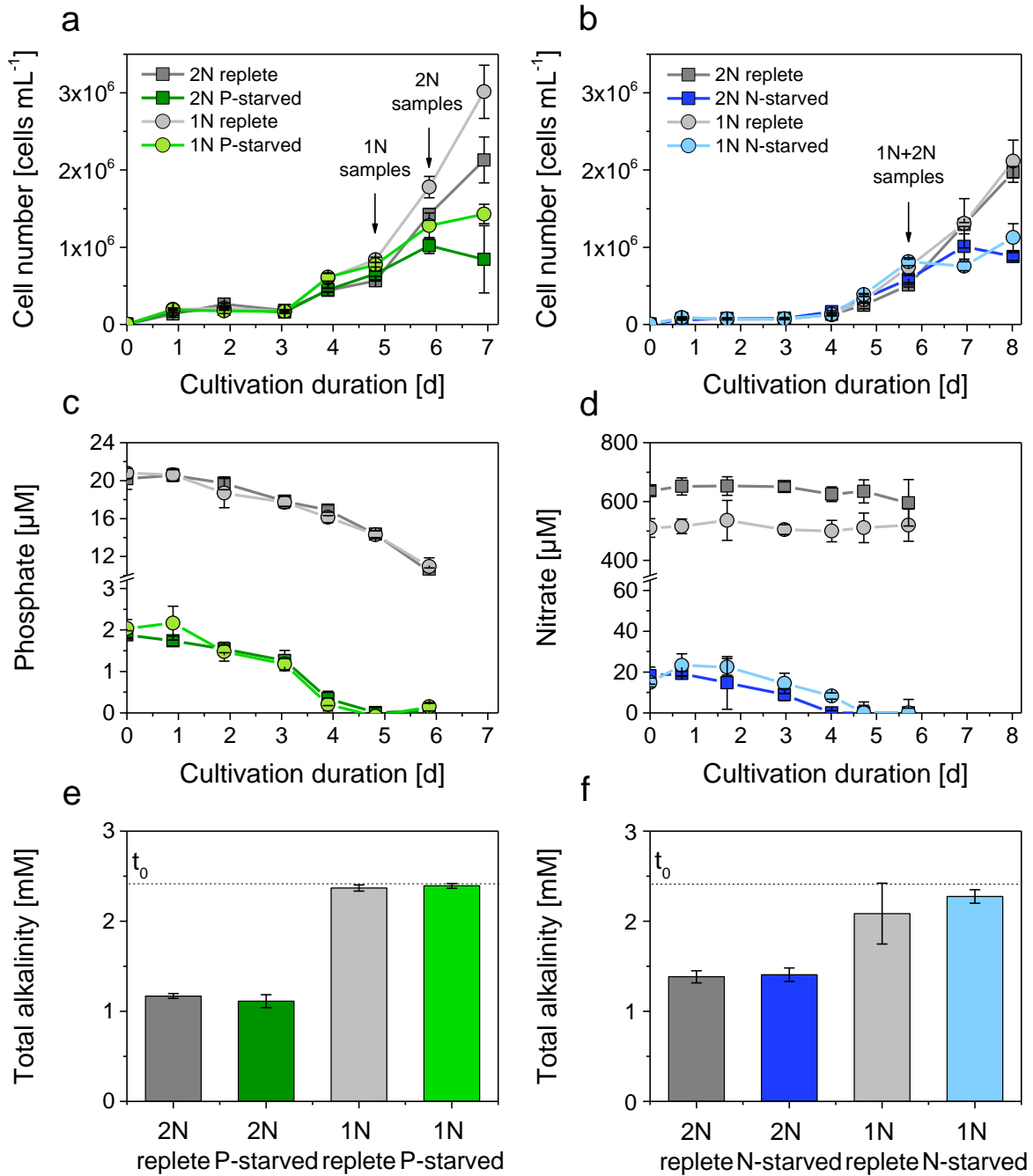
Figure 21: Growth characteristics for the diploid (2N) and haploid (1N) *E. huxleyi* life-cycle stages under nutrient starvation. (a) Cell numbers for the P-starvation setup with 2N (boxes) and 1N (circles), in nutrient-replete (grey) and P-limited ESAW media (green), arrows indicate metabolome sampling time points. (b) Cell numbers for the N-starvation setup with 2N (boxes) and 1N (circles), in nutrient-replete (grey) and N-limited ESAW media (blue), arrows indicate metabolome sampling time points. (c) Phosphate concentration in the media for the P-starvation setup. (d) Nitrate concentration in the media for the N-starvation setup. (e) Total alkalinity at the metabolome sampling time points, 2N and 1N under nutrient-replete (grey) and P-starved conditions (green). (f) Total alkalinity at the metabolome sampling time point, 2N and 1N under nutrient-replete (grey) and N-starved conditions (blue). The dotted line indicates the total alkalinity at the start of the cultivation (t_0). Mean values and SD of three biological and three technical measurements are shown.

Samples harvested at indicated time-points were analyzed with regard to their metabolome, applying eleven different analysis methods to investigate the effect of nutrient starvation on the metabolome of diploid and haploid *E. huxleyi* life-cycle stages. An overview of the applied methods is shown in Figure 22 for metabolome analyses and Figure 23, for pigment/lipid methods. Primary metabolite analysis was performed to detect changes in metabolites that can be derivatized to trimethylsilyl-esters, free amino acids, small carboxylic acids, osmolytes and polyamines. Pigments, as well as polar and neutral lipid associated fatty acids, were analyzed analogously to the growth phase experiment (4.3). Additionally, the neutral lipid fraction was further examined, with regard to whole triacylglyceride molecules, alkenes and alkenones. All methods as well as the detected metabolites are explained in more detail below.

LC-MS/MS measurements were performed by E. Heidenreich and F. Kirschhöfer (Analytical Biochemistry, Institute of Functional Interfaces, Karlsruhe Institute of Technology, Eggenstein-Leopoldshafen, Germany), GC-FID measurements were carried out by K. Fahl (Marine Geology and Paleontology, Alfred Wegener Institute, Helmholtz Centre for Polar and Marine Research, Bremerhaven, Germany).

GC-MS analysis of metabolites derivatized to trimethylsilyl-esters allowed identification of several primary metabolites in both *E. huxleyi* life-cycle stages. More specific compound classes were analyzed by LC-MS/MS measurements. Here four different derivatization and separation methods were applied to quantify free amino acids, small carboxylic acids, osmolytes and amines. Quantification was achieved with by external standard calibration and recovery of isotope-labeled or non-labeled internal standards. This way, three different osmolytes (dimethylsulfoniopropionate (DMSP), glycine betaine and homarine), six small carboxylic acids (α-ketoglutarate, citrate, lactate, malate, pyruvate, succinate), as well as 19 of the canonic proteinogenic amino acids were quantified. No amines were detected in the analyzed *E. huxleyi* life-cycle stages. The same is true for the osmolytes dimethylsulfonio-acetate, trimethylammonium propionate and trimethylammonium butyrate. UV-vis-HPLC measurements allowed detection of ten photosynthetic pigments. Furthermore, fatty acids of polar and neutral lipids were detected as FAME, measured via GC-MS.
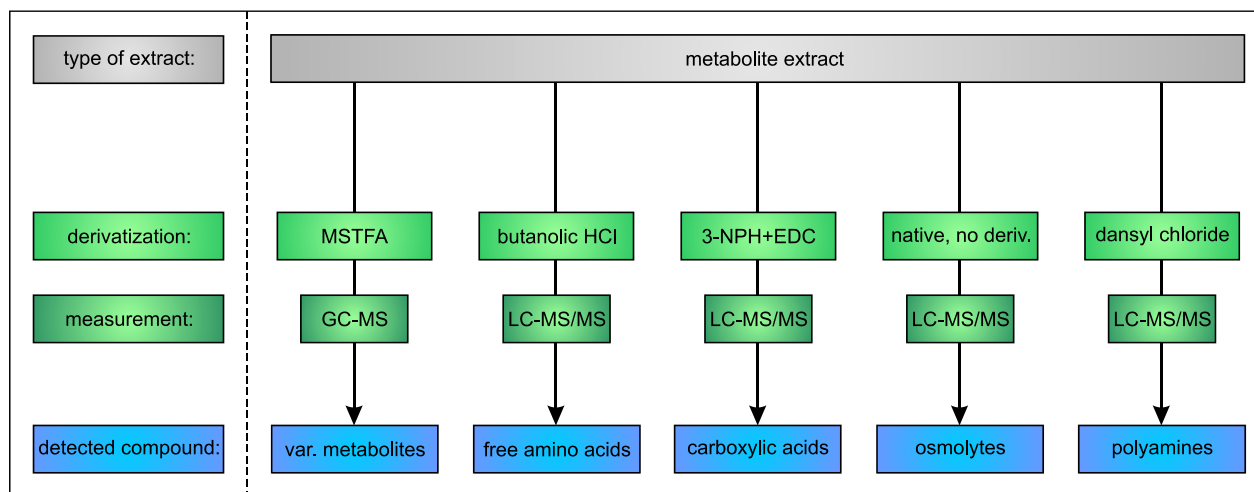
Figure 22: Workflow for metabolome analysis using different derivatization methods and measurement instruments to detect different metabolite classes. MSTFA, N-Methyl-N-(trimethylsilyl)trifluoroacetamide; 3-NPH, 3-nitrophenylhydrazine; EDC, 1-ethyl-3-(3-dimethylaminopropyl)carbodiimide hydrochloride.
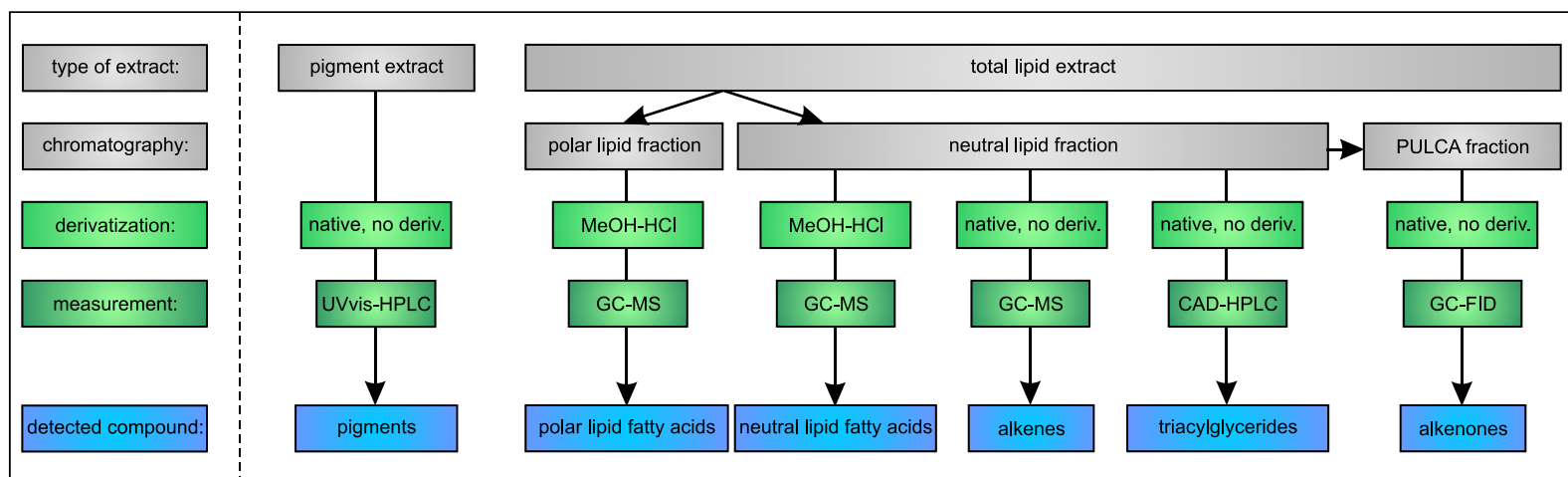
Figure 23: Workflow for pigment and lipid analysis using different derivatization methods and measurement instruments to detect different classes.

Whole TAG molecules were measured via CAD-HPLC, to get a more detailed insight into the composition of neutral storage lipids. Twenty peaks were detected, five of which were identified based on comparison with commercially available standards. Only TAG standards with three identical fatty acid chains attached to the glycerol backbone are available, such as even numbered $C_{8:0}$-$C_{24:0}$ fatty acids, as well as odd-numbered $C_{15:0}$-$C_{19:0}$ and unsaturated $C_{18:1}$ and $C_{18:3}$. However, natural TAGs often contain combinations of different fatty acids, which therefore cannot be identified with this method. The 15 unknown compounds were numbered consecutively. It was not possible to quantify TAGs with this method. A rough estimation was possible based on comparison with the internal standard $C_{17:0}$, but as different TAG standards showed different slopes when measuring external standard calibration curves, it was not possible to quantify all TAGs, as these curves were not available for the unknown TAGs.

The majority of *E. huxleyi*'s neutral lipid fraction consists of polyunsaturated long-chain alkenones, alkenoates and alkenes (PULCA) (Prahl & Wakeham, 1987; Sawada, 1996; Prahl, 2003; Eltgroth, 2005). Two isomers of a $C_{31:2}$ alkene were detected via GC-MS analysis of the non-derivatized neutral lipid fraction. This fraction also contained the alkenones, but proper detection was not possible, as other compounds coeluted. Therefore, this neutral lipid fraction was further purified by column chromatography, eluting alkenone compounds with dichloromethane. This fraction was subsequently analyzed via GC-FID. Six alkenones were detected, such as C_{37}-C_{38} polyunsaturated methyl and ethyl alkenones. Alkenoates, which differ from alkenones by an additional oxygen atom at the functional head group (COO-Me/Et vs. CO-Me/Et), were not detected in either life-cycle stage under these conditions. Different parameters can be calculated from alkenone data, which will be described in section 4.4.4.

The following section is divided into three parts. First, the metabolic profile of the nutrient-replete diploid and haploid *E. huxleyi* life-cycle stages are compared, to find possible similarities or exclusive patterns regarding ploidy. Secondly, the metabolic responses of both life-cycle stages are described with regard to P-starvation. Thirdly, the responses of these life-cycle stages are evaluated under N-starvation.

4.4.1 Comparison of life-cycle stages under nutrient-replete conditions
In order to reveal differences on metabolite levels between the diploid and haploid *E. huxleyi* life-cycle stages, nutrient-replete samples of both cultivation setups (Figure 21 a, b) were used. The quantified differences are shown in a heat map (Figure 24 a).
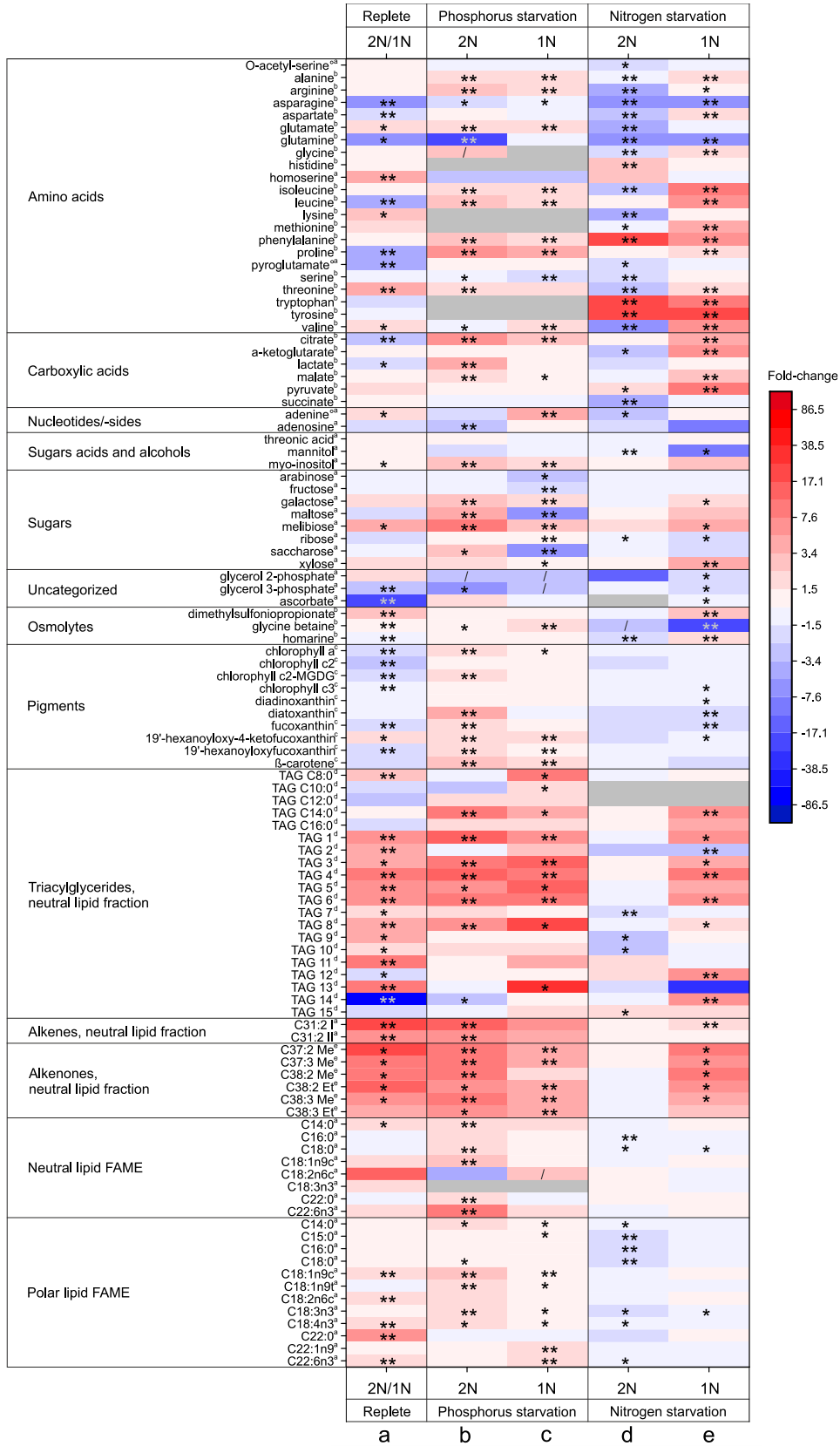
Figure 24: Heat map of the fold-changes of increased (red) or decreased (blue) metabolites for the diploid (2N) and haploid (1N) *E. huxleyi* life-cycle stage under macronutrient starvation. (a) Comparison of metabolite abundance between nutrient-replete 2N and 1N life-cycle stages, over both cultivation setups. (b, c) Fold-changes of metabolite abundance for P-starved 2N (b) and 1N (c) life-cycle stage compared to the respective nutrient-replete control. (d, e) Fold-changes of metabolite abundance for N-starved 2N (d) and 1N (e) cells compared to their respective replete control. Grey boxes indicate that the metabolite was not detected. Metabolites that were detected in one treatment, but not in the other, were marked with /,

indicating fold-change tendency, which was set to ±1.5. Asterisks represent p-values as determined via *t*-test (* represents p-values ≤0.05, ** represents p-values ≤0.01), grey color for some asterisks to facilitate visualization. Elevated letters denote the instrument used to detect the metabolite ([a]GC-MS, [b]LC-MS/MS, [c]UV-vis-HPLC, [d]CAD-HPLC, [e]GC-FID). Metabolites marked with ° were identified by data base comparison of m/z values (level 2, putatively identified compound), all other metabolites were additionally confirmed by measured standards (level 1, identified compound). Values represent fold-changes of mean values of six (a) or three (b-e) biological replicates measured in technical duplicates/triplicates. FAME, Fatty acid methyl ester; MGDG, monogalactosyldiacylglycerol.

Significant differences (*t*-test, p≤0.05) were found comparing the nutrient-replete metabolome profiles of both life-cycle stages (Figure 24 a). Of 105 detected metabolites, 66 were increased in abundance, compared to the haploid stage. Forty-five of these were at least 1.5-fold increased, the change being significant for 35 metabolites. Unless stated otherwise, only metabolites experiencing significant changes above 1.5-fold will be mentioned hereafter.

For example, abundances of glutamate, homoserine, lysine, threonine, valine, adenine, melibiose and DMSP were higher in the diploid stage (1.7-5.0-fold). H4k-fucoxanthin was found in higher abundance in the diploid stage (1.5-fold). Further pigment-associated evaluation approaches that were applied to this dataset, such as calculated de-epoxidation ratios and ratios of individual pigments to chlorophyll a will be described in section 4.4.5.

Several lipids were present in higher abundance in the diploid stage, such as polar lipid fatty acids, ($C_{18:1n9c}$, $C_{18:2n6c}$, $C_{18:4n3}$, $C_{22:0}$ and $C_{22:6n3}$ (1.5-6.0-fold)), neutral lipid fatty acids ($C_{14:0}$ (1.8-fold)), TAGs ($C_{8:0}$ and 12 unknown TAGs (1.9-9.1-fold)), alkenes (both $C_{31:2}$ isomers (17.0 and 5.4-fold)), and all alkenones (3.9-18.1-fold), except for $C_{38:3 \ Et}$, (increase non-significant).

The diploid stage also contained 39 metabolites in lower abundance than the haploid stage. Twenty-six of these were at least 1.5-fold changed, the change was significant of 17 metabolites. For example, the diploid stage contained a slightly lower abundance of aspartate, citrate, lactate and glycerol 3-phosphate (1.8-3.1-fold). Other differences were more pronounced, such as lower abundances of asparagine, glutamine, leucine, proline, pyroglutamate, ascorbate and two unknown TAGs (3.6-79.4-fold). The diploid stage also differed regarding its pigment composition, as it contained less chlorophyll a, chlorophyll c_2, chlorophyll c_2-MGDG, fucoxanthin and hex-fucoxanthin (1.7-2.3-fold) than the haploid stage.

4.4.2 The effect of P-starvation on *E. huxleyi* life-cycle stages

To examine the metabolic response of the two life-cycle stages regarding P-starvation, fold-changes of metabolites abundances from P-starved cultures compared to their respective nutrient-replete control were calculated (Figure 24 b, c). For both life-cycle stages, many detected metabolites increased under P-starvation, as visualized by the high proportion of red areas in the heatmap.

4.4.2.1 Metabolome changes under P-starvation in the diploid stage

In detail, 77 of 105 metabolites were increased in the diploid life-cycle stage under P-starvation (Figure 24 b). Fifty-six of these were increased at least 1.5-fold, the change being significant for 48 metabolites. Many amino acid abundances increased, such as alanine, arginine, glutamate, isoleucine, leucine, phenylalanine, and threonine (1.6-2.7-fold), the highest increase being detected for proline (5.1-fold). As glycine was not detected under replete conditions, it technically also increased under P-starvation, as marked by the diagonal slash. Further metabolites were increased in the range of 1.7-3.3-fold, such as malate, myo-inositol, galactose and saccharose, while others experienced a more distinct increase (4.2-11.3-fold), such as citrate, lactate, maltose and melibiose. All photosynthetic pigments were increased, with significant changes for chlorophyll a, chlorophyll c_2-MGDG, diatoxanthin, fucoxanthin, h4k-fucoxanthin, hex-fucoxanthin and β-carotene (1.6-4.0-fold). Many lipid compounds were increased under P-starvation in the diploid stage, including polar lipid fatty acids ($C_{14:0}$, $C_{18:1n9c}$, $C_{18:1n9t}$, $C_{18:3n3}$ and $C_{18:4n3}$ (1.6-2.3-fold)), neutral lipid fatty acids ($C_{14:0}$, $C_{18:0}$, $C_{18:1n9c}$, $C_{22:0}$ and $C_{22:6n3}$ (1.8-10.2-fold)), TAGs (TAG $C_{14:0}$ and six unknown TAGs (7.0-13.5-fold)), alkenes (both $C_{31:2}$ isomers (10.7- and 4.3-fold)) and all alkenones (7.0-10.6-fold).

Only 22 of 105 metabolites were decreased in abundance in the diploid stage under P-starvation. The change was at least 1.5-fold for ten of these, and significant for five metabolites. For example, asparagine, adenosine and one unknown TAG decreased 2.0-2.6-fold, while more noticeable decreases were observed for glutamine (17.2-fold) and glycerol 3-phosphate (5.7-fold).

4.4.2.2 Metabolome changes under P-starvation in the haploid stage

A similar pattern was detected for the haploid life-cycle stage under P-starvation (Figure 24 c). Seventy-nine of 105 detected metabolites increased, 45 metabolites experiencing a change of at least 1.5-fold, significant for 33 metabolites. Comparable to the results observed for the diploid stage, several amino acids were increased, such as alanine, arginine, glutamate, isoleucine, leucine, phenylalanine and valine (1.7-2.0-fold). The highest increase was again

found for proline (3.9-fold). Other metabolites, such as myo-inositol, galactose and glycine betaine, were found in moderately higher abundance (1.6-1.7-fold), while others, such as citrate, adenine and melibiose, increased more distinctively (2.5-3.5-fold). P-starvation also increased pigment abundance in the haploid stage, regarding h4k-fucoxanthin (2.0-fold) and β-carotene (1.6-fold). Similar to the diploid stage, P-starvation also resulted in increased lipid abundances, including polar lipid fatty acids ($C_{22:1n9}$ (1.7-fold), $C_{22:6n3}$ (1.6-fold)), TAGs (TAG $C_{10:0}$, TAG $C_{14:0}$, TAG $C_{8:0}$ and seven unknown TAGs (2.2-35.5-fold)) and all alkenones (3.7-5.0-fold), except for $C_{38:2\ Me}$, the increase being non-significant.

Only 19 of 105 metabolites were decreased in the haploid life-cycle stage under P-starvation. Six metabolites were changed more than 1.5-fold, the change being significant for five metabolites. Serine, arabinose, and fructose were moderately decreased in abundance (1.6-2.6-fold), whereas maltose and saccharose were decreased more prominently (5.6-6.3-fold). Technically P-containing metabolites glycerol 2- and glycerol 3-phosphate were also decreased under these conditions, as they were not detected (manually added fold-change tendency marked by diagonal slash).

4.4.3 The effect of N-starvation on *E. huxleyi* life-cycle stages

Fold-changes of metabolite abundances detected under N-starvation and the respective nutrient-replete control were calculated, allowing interpretation of N-starvation induced changes on both life-cycle stages (Figure 24 d, e). N-starvation resulted in generally decreased metabolite abundance in the diploid stage. A quite different pattern was observed for the haploid stage, where generally more metabolites were increased.

4.4.3.1 Metabolome changes under N-starvation in the diploid stage

In detail, 27 of 105 detected metabolites were increased in the diploid life-cycle stage (Figure 24 d). Ten of these changed more than 1.5-fold, six increasing significantly. In the range of 1.6-3.3 these included histidine, pyruvate and one unknown TAG, whereas the amino acids phenylalanine, tryptophan and tyrosine were increased more distinctly (18.5-24.7-fold).

In contrast, 75 of 105 metabolites decreased in this stage in response to N-starvation. Thirty-four metabolites were decreased at least 1.5-fold, 24 being significantly changed. Especially amino acids were affected, in varying ranges, such as O-acetyl-serine, glycine, pyroglutamate and serine (1.6-2.2-fold), arginine, aspartate, isoleucine and threonine (3.0-3.6-fold) and asparagine, glutamate, glutamine, lysine and valine (4.2-7.1-fold). Other metabolites were also found in lower abundance, such as α-ketoglutarate, succinate, adenine and homarine (1.6-3.5-fold). Technically, N-containing glycine betaine also decreased, as it was not detected under N-

starvation in contrast to nutrient-replete conditions (manually added fold-change tendency indicated by diagonal slash). All pigments were decreased under N-starvation, however changes were not significant. Several lipids were decreased, such as polar lipid fatty acids ($C_{15:0}$, $C_{16:0}$, $C_{18:0}$ and $C_{18:3n3}$ (1.6-1.8-fold)) and TAGs (three unknown TAGs (1.7-3.4-fold)), indicating that membrane lipids and storage of TAGs were impaired under N-starvation. Fatty acids of neutral lipids, alkenes or alkenones were not affected.

4.4.3.2 Metabolome changes under N-starvation in the haploid stage

As mentioned above, metabolite responses to N-starvation in the haploid stage did not follow the general decrease pattern observed in the diploid cells, with the exception of pigments (Figure 24 e). Rather, many metabolites were increased, similar to the responses of both life-cycle stages observed under P-starvation.

Fifty-eight of 105 metabolites were increased, 41 of them at least 1.5-fold, the change being significant for 35 metabolites. Several amino acids were increased, some only moderately (1.6-3.6-fold), such as alanine, aspartate, glycine, methionine, proline and threonine, others more prominently (7.3-8.5-fold), such as isoleucine, leucine, phenylalanine, tryptophan and valine. Tyrosine underwent the highest increase among amino acids (20.3-fold). Other metabolites were increased, such as malate, galactose, DMSP and homarine (2.1-3.3-fold) and citrate, α-ketoglutarate, pyruvate, melibiose and xylose (3.7-8.4-fold). Several lipids were increased under N-starvation in the haploid, such as TAGs (TAG $C_{14:0}$ and seven unknown TAGs (2.1-8.9-fold)), alkenes (one $C_{31:2}$ isomer (1.8-fold)) and all alkenones (4.0-10.5-fold), although the increase was non-significant for $C_{38:3 \text{ Et}}$.

Forty-five of 105 metabolites were decreased in the haploid stage under N-starvation. The change was at least 1.5-fold for 14 metabolites, 10 of which changed significantly. These included the N-rich amino acids asparagine and glutamine (5.4- and 5.7-fold, respectively). Further decreases were found for ribose, glycerol 2- and glycerol 3-phosphate (1.7-2.0-fold). Even more pronounced decreases were observed for mannitol and the N-containing osmolyte glycine betaine (9.8- and 18.9-fold, respectively). All pigment abundances were generally decreased, including significant changes for five pigments, of which diatoxanthin and fucoxanthin were decreased more than 1.5-fold (2.0- and 1.8-fold, respectively). Lipids and fatty acids were not impacted, except for one unknown TAG, which decreased in abundance (2.5-fold).

4.4.4 Calculation of alkenone-relevant parameters

Double bond positions of alkenones are influenced by temperature, for example a higher proportion of less unsaturated alkenones is produced at higher temperature (Brassell, 1986; Prahl & Wakeham, 1987). Therefore, the unsaturation ratio of C_{37} alkenones, the $U^{K'}_{37}$, can be used to estimate the temperature of the water in which the alkenone producing organism grew:

$$U^{K'}_{37} = \frac{C_{37:2}Me}{C_{37:2}Me + C_{37:3}Me} \qquad \text{Eq. 2}$$

As alkenones are also highly resistant to decomposition, this makes the $U^{K'}_{37}$ a valuable tool to estimate sea surface temperature (SST) in paleoceanography (Brassell, 1986; Prahl & Wakeham, 1987; Conte, 1998; Müller, 1998; Conte, 2006). Numerous studies have analyzed the relationship of alkenone composition and cultivation temperature (CT) for different *E. huxleyi* strains in the laboratory (Volkman, 1980b; Volkman, 1980a; Brassell, 1986; Prahl & Wakeham, 1987; Rontani, 1997; Conte, 1998; Epstein, 1998; Müller, 1998; Epstein, 2001; Sawada & Shiraiwa, 2004; Eltgroth, 2005; Conte, 2006; Ono, 2009), often with the result of strain-specific calibrations for the estimation of SST, which in this case equals CT. Therefore, the data gathered in this work can also be used to verify the relationship between unsaturation of alkenones and in this case the cultivation temperature (CT). The calculated values are shown in Table 7. As the first applied calibration (CT[1]) did not equal the applied CT of 20 °C, other calibrations specific for diploid *E. huxleyi* strains were applied to reach the best approximation.

Apart from the fact that alkenones were more abundant in the diploid stage under nutrient replete conditions, this stage also had a higher $U^{K'}_{37}$, and subsequently a higher calculated cultivation temperature. Although different calibrations were applied for CT calculation (CT[1], CT[2], CT[3]), values did not correspond to the applied cultivation temperature (20 °C). The nearest approximation was 17.1±1.4 °C for 2N and 13.5±1.1 °C for 1N.

Increased alkenone abundance in the diploid stage under P-starvation had no significant effect on the $U^{K'}_{37}$ or CT. In the haploid stage P-starvation induced alkenone accumulation resulted in a significantly higher $U^{K'}_{37}$ and CT. N-starvation didn't affect the diploid stage regarding these parameters, however the CT was significantly increased in the haploid stage under these conditions.

Table 7: Alkenone related parameters for *E. huxleyi* life-cycle stages under nutrient replete and nutrient starvation conditions. Unsaturation index (U$^{K'}_{37}$), calculated cultivation temperature (CT) based on three different calibrations for sea surface temperature (SST) for both separate cultivations, as well as the pooled replete replicates from both cultivations. Mean values and standard deviations (SD) of n=3 are denoted. Asterisk indicates statistical significance (* represent p-value ≤0.05, ** ≤0.01) of limitation to replete control, or in case of all replete replicates, of the two different life-cycle stages.

Setup		U$^{K'}_{37}$ [-]	CT[1] [°C]	CT[2] [°C]	CT[3] [°C]
P-starvation	2N	0.3±0.02	9.0±0.54	12.7±0.55	16.4±0.51
	2N -P	0.3±0.02	9.0±0.66	12.7±0.66	16.3±0.62
	1N	0.2±0.02	7.2±0.47	10.7±0.55	14.5±0.50
	1N -P	0.3±0.01**	8.4±0.40**	12.0±0.42**	15.8±0.39**
N-starvation	2N	0.4±0.06	10.8±1.71	14.3±1.70	17.9±1.59
	2N -N	0.4±0.02	11.5±0.66	15.1±0.58	18.6±0.55
	1N	0.2±0.02	5.6±0.59	8.7±0.81	12.7±0.72
	1N -N	0.3±0.02**	9.3±0.52**	12.9±0.52**	16.6±0.49**
All replete	2N	0.3±0.05**	9.9±1.55**	13.5±1.50**	17.1±1.41**
	1N	0.2±0.03	6.3±0.95	9.6±1.21	13.5±1.09

[1]Summer SST calibration for 1-30 °C, global core-top compilation (Müller, 1998),
[2]SST calibration for *E. huxleyi* B92/21 (Conte, 1998),
[3]Conte SST calibration for *E. huxleyi* G1779Ga (Conte, 1998).

4.4.5 Calculation of pigment and de-epoxidation ratios

Complex pigment compositions that change under application of external stressors can help determine the physiological response of a photosynthetically active cell. As shown above for the growth phase experiment, ratios of individual chlorophylls to chlorophyll a and the de-epoxidation ratio, allow further interpretation.

As mentioned above, chlorophyll a abundance increased significantly for both life-cycle stages under P-starvation, compared to the nutrient-replete control. In contrast, total chlorophylls to chlorophyll a decreased, significantly in the diploid stage (Figure 25). This decrease was caused by a significant decrease of all three chlorophylls, especially chlorophyll c_2 and chlorophyll c_3. Although carotenoids did not change regarded as total carotenoids, individual carotenoids did. For example, fucoxanthin and hex-fucoxanthin significantly decreased relative to chlorophyll a in the diploid stage, h4k-fucoxanthin increased non-significantly. In the haploid stage, the decrease for fucoxanthin was non-significant, however, h4k-fucoxanthin increased significantly here. Furthermore, diatoxanthin per chlorophyll a increased significantly in the diploid stage, leading to a significantly increased de-epoxidation ratio, as also shown in Table 8. This indicates activate xanthophyll cycle-mediated photoprotection in response to P-starvation in the diploid stage, which is absent in the haploid stage. In both life-cycle stages, β-carotene per chlorophyll a increased significantly.Under N-starvation, changes were not very pronounced and seldom significant. In the diploid stage diatoxanthin to chlorophyll a and subsequently the de-epoxidation ratio were significantly

decreased (Table 8), indicating that photoprotection via xanthophyll cycle-mediated non-photochemical quenching cannot function under N-starvation. This was also the case in the haploid stage. Here the chlorophyll c_2 to chlorophyll a ratio was significantly increased in the haploid stage.
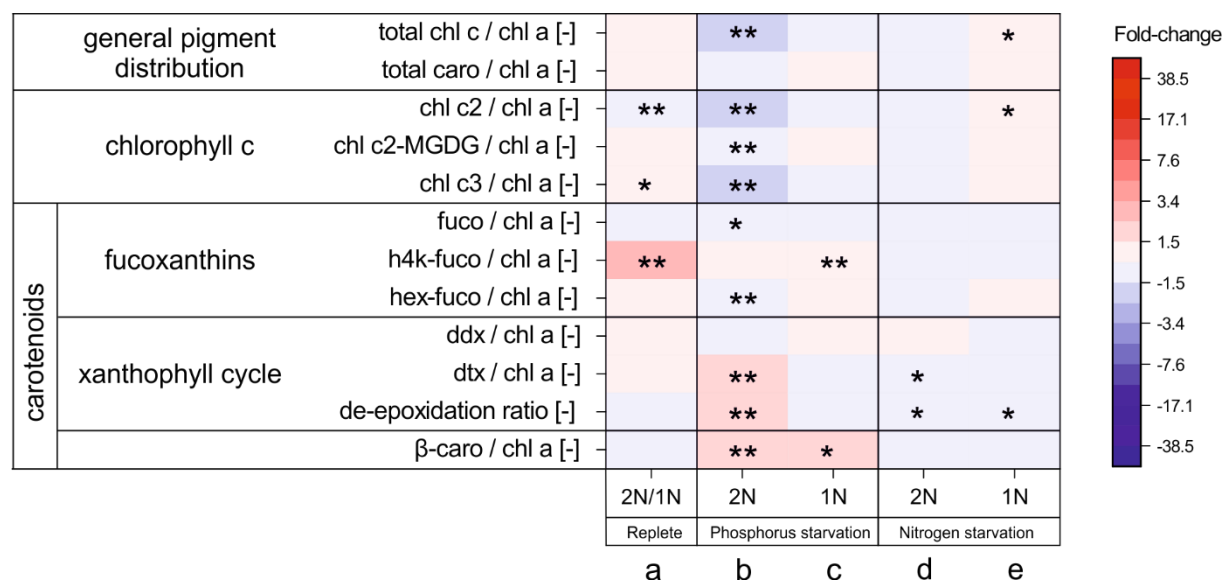
Figure 25: Heat map of the fold-changes of pigment ratios for diploid (2N) and haploid (1N) *E. huxleyi* life-cycle stages under nutrient-replete and nutrient-starvation conditions. (a) Nutrient-replete 2N compared to nutrient-replete 1N. (b, c) P-starved 2N (b) or 1N (c) compared to their respective nutrient-replete control. (d, e) N-starved 2N (d) or 1N (e) compared to their respective nutrient-replete control. Asterisks indicate p-value of *t*-test (* indicates ≤0.05, ** ≤0.01). Fold-changes were calculated from mean values of three biological and two technical measurements. Chl, chlorophyll; caro, carotenoids; MGDG, monogalactosyldiacylglycerol; fuco, fucoxanthin; ddx, diadinoxanthin; dtx, diatoxanthin; β-caro, β-carotene.

Table 8: The de-epoxidation ratio of xanthophyll cycle pigments for diploid (2N) and haploid (1N) *E. huxleyi* life-cycle stages grown under nutrient-replete or P-/N-starved conditions. Mean value and SD of three biological and two technical replicates. Asterisk indicates statistical significance (* represent p-value ≤0.05, ** ≤0.01) of limitation to replete control, or in case of all replete replicates, of the two different life-cycle stages.

Setup	Life-cycle stage	Nutrient status	De-epoxidation ratio [-]
P-starvation	2N	replete	0.25±0.11
		P-starved	0.51±0.12**
	1N	replete	0.25±0.21
		P-starved	0.19±0.03
N-starvation	2N	replete	0.22±0.05
		N-starved	0.17±0.02*
	1N	replete	0.28±0.03
		N-starved	0.22±0.04*
All replete	2N	replete	0.24±0.05
	1N		0.26±0.11

5. Discussion

5.1 Non-linearity of individual FAMEs measured via GC-MS (ITQ) requires correction of data post-run

Lipids are often detected as their respective fatty acid methyl esters (FAME), which are easily detectable via GC-FID or GC-MS (Dodds, 2005). The latter is advantageous due to the additional spectral information for FAME identification, circumventing misinterpretation due to occurring artefacts, which can happen with GC-FID (Roach, 2000; Mjøs, 2003). Regardless of the chosen instrument, FAME calibration is necessary, as the detector's response varies with carbon and double bond number (Ackman & Sipos, 1964; Ulberth, 1999; Ackman, 2002; Dodds, 2005).

The GC-MS instrument used in this work (TraceGC gas chromatograph and ITQ ion trap mass spectrometer, Thermo Scientific) delivered highly variable responses for individual FAMEs, which additionally were non-linear at low concentrations (Figure 6, Supplementary Figure 1). This has been observed previously regarding quadrupole and ion trap GC-MS instruments, as well as GC-FID (Dodds, 2005). To obtain the correct amount, correction of FAME abundances via second degree polynomial regression was necessary (Figure 8, Supplementary Table 1). The detection was also especially sensitive towards short-chain fatty acids, which were not detected at low concentrations, in contrast to the other fatty acids (Figure 7, Supplementary Figure 1). Particularly regarding complex biological samples this can lead to misinterpretation of shorter fatty acid chains.

This is also true when comparing TAG containing short-chain fatty acids, measured via CAD-HPLC, and the respective FAME, measured via GC-MS (Figure 9). The HPLC was able to detect TAG in lower concentration ranges. This problem has been reported before (Holcapek, 2005; Lísa, 2007). However, the comparison of instruments was further complicated by the dilution step introduced by FAME derivatization, so that technically concentrations were lower for GC-MS measurements. Another issue is the higher volatility of short-chain fatty acids, which can lead to partial evaporation both pre-derivatization and as FAME (Ulberth, 1999; Schreiner, 2006). Therefore, observations about short-chain fatty acids need to be treated with caution.

5.2 Similar cellular content of life-cycle stages on FTIR level

The results discussed in this section were submitted as part of a manuscript:

> Wördenweber, R., Rokitta, S. D., Heidenreich, E., Corona, K., Kirschhöfer, F., Fahl, K., Klocke, J. L., Kottke, T., Brenner-Weiß, G., Rost, B., Mussgnug, J. H., Kruse, O. (submitted): Phosphorus and nitrogen starvation reveal life-cycle specific responses in the metabolome of *Emiliania huxleyi* (Haptophyta).

FTIR is a valuable tool for quick non-invasive overview of the most important cellular components (Naumann, 1991; Giordano, 2001; Johnson, 2004). In this experiment, the cellular composition of the diploid and haploid *E. huxleyi* life-cycle stages was elucidated using FTIR.

On this level of analysis, no big differences between proteins, carbohydrates and lipids were found regarding ploidy (Figure 11), although the diploid stage indicated slightly higher alkenone abundance (1.1-fold). The general cellular composition is comparable with previous FTIR analyses for diploid cells (Domenighini & Giordano, 2009; Pelusi, 2016).

This is the first report of haploid FTIR analysis for *E. huxleyi*, therefore, results can only be compared with other analysis methods. The haploid stage has long been overlooked by research. There are no reports of protein abundance in the haploid stage, the same is true for carbohydrates. Certain phospholipids were found in slightly higher abundance in the haploid stage, such as PDPT and PE (Hunter, 2015), in contrast to the suggestions from the FTIR measurement. However, detailed lipid analysis in the following parts of this thesis will further elucidate differences between both life-cycle stages. Alkenones have been reported to be slightly higher in a different *E. huxleyi* stage, compared to its haploid stage, in a comparable growth phase (Bell & Pond, 1996). Alkenones have been proposed to be storage lipids (Bell & Pond, 1996; Epstein, 2001; Prahl, 2003; Eltgroth, 2005; Pan & Sun, 2011), which was confirmed by Tsuji (2015). Sawada and Shiraiwa (2004) found them particularly associated with the coccolith vesicle fraction, which could explain the higher abundance in the calcifying, diploid stage, compared to the non-calcifying haploid stage, which does not contain coccolith vesicles (Paasche, 2001). However, this role of alkenones is still under debate, as Eltgroth and coworkers (2005) did not find alkenones associated with the coccolith vesicle, but packaged into lipid bodies. Furthermore, they have been suggested to influence buoyancy (Fernández, 1994; Fernández, 1996; Paasche, 2001), which could explain a higher abundance in the non-motile diploid stage.

5.3 Growth phase-dependent metabolome analysis of *E. huxleyi* life-cycle stages

Metabolic analysis of microalgal cells is highly dependent on the growth phase. The exponential phase is typically the most active phase, as many primary metabolites are produced in high abundance, to ensure efficient cell division (Vidoudez & Pohnert, 2012; Mausz & Pohnert, 2015). The transitional and stationary growth phases are characterized by cessation of growth, and accumulation of assimilation products, such as lipids and sugars, has been observed (Hodgson, 1991; Kluender, 2009; Vidoudez & Pohnert, 2012). To allow physiological observations, for example comparison of calcifying and non-calcifying *E. huxleyi* life-cycle stages, is therefore important to analyze the metabolome during different growth phases.

In this experiment, the diploid and haploid *E. huxleyi* life-cycle stages (RCC 1216, RCC 1217) were grown under nutrient-replete conditions. Samples for pigment and lipid analysis were harvested at three different time points, to assess metabolic composition of these compounds with respect to the early-exponential, late-exponential and stationary growth phase. Both life-cycle stages grew comparably (Figure 12), with no significant difference of maximum growth rate, as observed before (Houdan, 2005; Rokitta & Rost, 2012; Mausz & Pohnert, 2015; Rokitta, 2016). Diploid cells shed their coccoliths in stationary phase, typical for this life-cycle stage (Holligan, 1983; Balch, 1996; Vardi, 2012; Lehahn, 2014). As ESAW medium contains high levels of nutrients (Berges, 2001), which are typically not depleted during growth, (as seen for P and N in results section 4.4), the cell's stationary phase entry was probably caused by a different factor, possibly changes in pH or total alkalinity.

5.3.1 Pigment abundance and composition changes with growth

In both life-cycle stages ten photosynthetic pigments could be identified (Figure 13), such as chlorophyll a, three different chlorophylls c (c_2, c_2-MGDG, c_3), and the carotenoids fucoxanthin, h4k-fucoxanthin, hex-fucoxanthin, diadinoxanthin, diatoxanthin and β-carotene. The presence of these pigments is in line with reports of the exact same life-cycle stages harvested in mid-exponential phase (van Lenning, 2004; Houdan, 2005).

No α-carotene was detected, as observed by Houdan and coworkers (2005). This might be due to concentrations below the detection limit, as the α-carotene concentration is known to be lower than the β-carotene concentration, which was close to the detection limit. Furthermore, α-carotene has been observed to accumulate only under low light intensities in the diploid *E. huxleyi* strain CCMP 370, whereas β-carotene is present under both high and low light (425 vs. 18 μmol m^{-2} s^{-1}) (Garrido, 2016). As relatively high light intensities were applied in this experiment (350 μmol m^{-2} s^{-1}), this could explain the absence of α-carotene. Furthermore, both

carotenes are precursor for all carotenoids (Lohr & Wilhelm, 1999; DellaPenna, 2004; Tanaka, 2008; Takaichi, 2011). The low concentration (or absence) of both precursors indicates that these carotenes do not *per se* have a relevant function in photoprotection in *E. huxleyi*. The flux is rather directed towards conversion into other carotenoids. This has also been observed for other diploid *E. huxleyi* strains (Stolte, 2000; Zapata, 2004; Zapata, 2006; Garrido, 2016).

Over the course of cultivation, the abundance of all pigments decreased, except for diatoxanthin, which even showed increases (Figure 14). A decrease of cellular pigment content in the stationary growth phase has been reported for the diploid *E. huxleyi* strains CCMP 1516 (Llewellyn, 2007) and *E. huxleyi* PLY-61/7/3 (Llewellyn & Gibb, 2000), as well as for other microalgae (Conover, 1975; Roy, 1988; Llewellyn & Gibb, 2000; Ruivo, 2011). In some cases, pigment content decreased before cell numbers stalled, indicating shut down of pigment synthesis before other cellular components.

From a metabolical point of view, the early to mid-exponential growth phase is the most active one, characterized by high rates of photosynthesis and carbon assimilation, allowing accumulation of carbon, biomass and energy storage compounds (Raven & Beardall, 2003; Mausz & Pohnert, 2015). In this stage, as suggested by the results of this work, pigment abundance is highest, possibly implying a larger antenna size, to absorb as many photons as possible. However, antenna size is not correlated directly with efficiency. Increased absorption is only effective as long as the reaction center can function efficiently, as energy from excessive photons is lost as heat or, more severely, leads to the formation of triplet chlorophyll, which either reacts with molecular oxygen to produce radical oxygen species, or needs to be quenched by a carotenoid to return to its ground state (Pogson, 2005; Croce & van Amerongen, 2014). The exponential growth phase ends when cells are limited by any essential component. After a short transitional phase, cells enter stationary phase, ceasing cell division. It is likely that decreased pigment abundances signify downscaling of light harvesting to minimize energy generation, adapting to the lowered requirements of the non-dividing cell. All residual energy goes into metabolism maintenance (Raven & Beardall, 2016) and the metabolism is streamlined. This could explain why most pigment abundances decreased in the later growth phases of this experiment.

In the following part, the results for individual pigments will be discussed regarding their relevance in *E. huxleyi*. Pigment profiles of both life-cycle stages were highly similar. Therefore, changes will be discussed mainly for the diploid stage and differences will be discussed comprehensively at the end of the chapter.

Hex-fucoxanthin was highly abundant in most growth phases and life-cycle stages (Figure 13), and comprised a major proportion of total fucoxanthins (76-87 %). Over the course of cultivation, the cellular abundance of all fucoxanthins decreased (Figure 14). The relative proportion of hex-fucoxanthin and h4k-fucoxanthin increased compared to chlorophyll a, at the expense of fucoxanthin (Figure 15).

Quantification of the exact amount of hex-fucoxanthin was not possible due to limiting concentration of the standard. This is common for pigment analysis in marine microalgae, as uncommon pigment standards are difficult to obtain in pure form and sufficient concentration (Egeland, 2011). As analytes can give variable responses in UV-vis-spectrometers, especially when they contain different numbers of chromophores, it is possible that the abundance of one pigment is not necessarily comparable to another pigment (Jeffrey, 1997; Smith, 2004). However, fucoxanthin derivatives have been shown to give a similar response to fucoxanthin (Egeland, 2011), whereas chlorophyll a gives a smaller response compared to fucoxanthin (Jeffrey, 1997). Therefore, it is difficult to state whether hex-fucoxanthin was present in higher abundance than chlorophyll a in this work. However, Houdan (2005) was able to quantify hex-fucoxanthin and showed that hex-fucoxanthin was just as abundant as chlorophyll a in the same diploid *E. huxleyi* life-cycle stage (2N: 1.02-fold), whereas it was lower in the haploid stage (1N 0.86-fold). A higher abundance of hex-fucoxanthin compared to chlorophyll a has also been found in the diploid strains CS-57 (1.51-fold) and CS-282 (1.14-fold) (Zapata, 2004), here authors quantified using self-isolated standards. This was also observed for other haptophytes, such as *Chrysochromulina polylepsis* (CCMP 286, 1.11-fold), *Phaeocystis antarctica* (DE 12.1, 1.05-fold) (Zapata, 2004). Other diploid *E. huxleyi* strains typically have a hex-fucoxanthin or fucoxanthin to chlorophyll a ratio under one, indicating strain-specific differences (Haxo, 1985; Stolte, 2000; Zapata, 2004; Garrido, 2016).

The observed decreases of cellular fucoxanthin abundance in the later growth phases, as well as shifts towards higher hex-fucoxanthin and h4k-fucoxanthin ratios to chlorophyll a, at the expense of fucoxanthin, are well in line with results for the diploid *E. huxleyi* strains CCMP 1516 (Llewellyn, 2007), CCMP 370 (Garrido, 2016) and another haptophyte, *Phaeocystis* sp. (Buma, 1991).

Different *E. huxleyi* strains vastly differ in their fucoxanthin composition, highlighting the differences between strains of the *E. huxleyi* species complex. For example, strains can have either fucoxanthin or hex-fucoxanthin as their major carotenoid (Zapata, 2004). Furthermore, only strains belonging to the coccolith morphotype A and R contain h4k-fucoxanthin, others have but-fucoxanthin (van Lenning, 2004; Zapata, 2004; Cook, 2011). These morphotypes

divide *E. huxleyi* into different categories based on coccolith structure. In contrast to lightly calcifying types, type A and R form heavier calcified elements (Hagino, 2011; Read, 2013). The life-cycle stages analyzed in this work belong to the morphotype R (van Lenning, 2004). It is assumed that differences regarding fucoxanthin composition and coccolith morphology reflect environmental adaptation of strains in the *E. huxleyi* species complex (Cook, 2011).

In order to explain these growth-dependent changes and strain-dependent differences, it is necessary to understand the function of different fucoxanthin derivatives in photosynthesis. Fucoxanthins are accessory pigments that participate effectively in light harvesting (Siefermann-Harms, 1987; Jeffrey & Anderson, 2000; Llewellyn, 2007; Takaichi, 2011). They are especially important in *E huxleyi*'s natural habitat, as irradiance is limited to blue-green light below 600 nm in depths lower than 12 m (Kirk, 2011; Blankenship, 2014; Croce & van Amerongen, 2014). Light of this range cannot be absorbed by chlorophyll a (or b), which is why haptophytes, diatoms and other marine microalgae of the `red lineage´ (Falkowski, 2004) generally contain chlorophyll c, as well as a high proportion fucoxanthins (Haxo, 1960; Govindjee & Braun, 1974; Zapata, 2006; Lepetit, 2012; Blankenship, 2014).

Fucoxanthin is proposed to be the biosynthetic precursor for hex-fucoxanthin and h4k-fucoxanthin (Lohr & Wilhelm, 1999; Stolte, 2000; Llewellyn, 2007). The different derivatives differ only slightly in their absorption spectrum. However, structural changes in a pigment within direct vicinity of its chromophore are assumed to lead to conformational changes in the protein complex, which in turn alter light harvesting and excitation energy transfer capacity (Croce & van Amerongen, 2014). This has been assumed to happen in *E. huxleyi*, as fucoxanthin interconversion occurs in response to increasing light intensity (Garde & Cailliau, 2000; Schlüter, 2000; Stolte, 2000; Lefebvre, 2010). Therefore, results of this experiment indicate that *E. huxleyi* most likely uses interconversions of fucoxanthins in the later growth phases, to alter the absorption spectrum in line with photoprotection, to reduce light absorption in the minimized photosystems.

E. huxleyi strains from different geographical origins have most likely adapted their fucoxanthin composition with respect to the ecological composition of their individual niche, and this could be manifested genetically (Falkowski & Chen, 2003; Cook, 2011). On the other hand, strains with hex-fucoxanthin as main carotenoid could be a result of temporary adaption to specific light conditions, as hex-fucoxanthin has been shown to be a special blue-light harvester in *E. huxleyi* (Schlüter, 2000; Garrido, 2016). Enhanced blue light conditions can occur when using white light-emitting diode (LED) lamps (Garrido, 2016), as these naturally enriched in blue light, relative to fluorescent lamps (Piasecki, 2010). As a cool white fluorescent

lamps were used in this work, it is unlikely that the fucoxanthin composition was influenced by the light source. The lamp's absorption spectrum is shown in Supplementary Figure 2, including comparison with an LED source.

The high abundance of hex-fucoxanthin or fucoxanthin compared to chlorophyll a, indicated by this work and confirmed for the diploid strain by Houdan (2005), is unusual. However, as stated above, hex-fucoxanthin concentration has even been reported to be higher than chlorophyll a concentration for certain diploid *E. huxleyi* strains and other haptophytes (Zapata, 2004). Chlorophyll a is typically the most abundant pigment, involved in light-harvesting, excited electron transport, and charge separation in the reaction centers (Croce & van Amerongen, 2011; Songaila, 2013). One purpose for higher hex-fucoxanthin abundance could be the optimization of energy transfer efficiency, the underlying reason being the limited light-harvesting capacity of carotenoids (Polivka & Frank, 2010; Croce & van Amerongen, 2014). As carotenoid excited-state lifetime is very short (~10 ps), excitations can get lost if not immediately transferred to a nearby chlorophyll a (Polivka & Frank, 2010; Croce & van Amerongen, 2014). For this reason, a high carotenoid to chlorophyll a ratio is found in dinoflagellates, as their peridinin-chlorophyll a-binding protein contains eight peridinins surrounding two chlorophyll a molecules (Hofmann, 1996; Schulte, 2009). Diatoms and haptophytes, including *E. huxleyi*, contain a similar protein in their light-harvesting antenna, a fucoxanthin-chlorophyll a/c-binding protein (FCP) (Caron, 1996; McKew, 2013a). In the diatom *Cyclotella meneghiniana*, FCPs have been reported to contain four chlorophyll a, four fucoxanthin and one chlorophyll c (Papagiannakis, 2005). Another study even suggested there might be double as many pigments per FCP (Premvardhan, 2010). However, including additional chlorophyll a required for energy transport and charge separation, this results in a higher overall proportion of chlorophyll a compared to fucoxanthin.

Therefore, in line with results from Houdan (2005) and Zapata (2004) (hex-fucoxanthin/chlorophyll a ≥1), it is possible that certain diploid *E. huxleyi* strains, including the diploid stage analyzed in this work, and some other haptophytes, could have a higher ratio of fucoxanthin, or in this case, hex-fucoxanthin, to chlorophyll a in FCPs. This could enable more efficient light harvesting. However, this assumption is not supported by further evidence, as analysis of FCP composition in haptophytes is lacking. In general, FCPs are the most recalcitrant and least understood of all light harvesting complexes (Larkum, 2016). In contrast, plant and chlorophyte LHCs contain less carotenoids compared to chlorophyll, with 14 chlorophylls and 3-4 carotenoids per LHC (Liu, 2004; Grewe, 2014; Natali & Croce, 2015), therefore shifting the absorption spectrum to higher wavelengths (Hildebrand, 2013).

Chlorophyll a was also highly abundant both life-cycle stages and all growth phases (Figure 13). As mentioned above, chlorophyll a has a smaller response in UV-vis detection (Egeland, 2011), which is why it is probably more abundant than it seemed by relative abundance in this work, possibly similarly abundant as hex-fucoxanthin, as observed by Houdan (2005) for the same life-cycle stages. On a cellular basis, chlorophyll a decreased in the two later growth phases (Figure 14). This has been shown to occur after the early- or mid-exponential growth phase for different diploid *E. huxleyi* strains (van Bleijswijk, 1994; Pond & Harris, 1996; Llewellyn, 2007) and other algae (Conover, 1975; Roy, 1988; Fidalgo, 1998; Llewellyn & Gibb, 2000; Ruivo, 2011), implying a reduced antenna size in less metabolically active phases. These results emphasize the importance of choosing the right harvesting time point, as conclusions drawn from late-exponential phase pigment compositions can differ from those harvested earlier. This could happen easily, as it is sometimes difficult to estimate the time point of transitional phases in an ongoing cultivation.

Among all chlorophyll c pigments, depending on the growth stage, chlorophyll c_2 and chlorophyll c_3 were similarly abundant, while chlorophyll c_2-MGDG only made up ~20 % of total chlorophyll c (Figure 13). Pigment abundances of these chlorophylls were not quantified due to limited concentration of available standards, however it is often assumed that all three derivatives have a similar response in UV-vis detection (Egeland, 2011; Garrido, 2016), which is why their abundance can probably be compared among each other. The cellular abundance of all chlorophyll c derivatives decreased in the two later growth phases (Figure 14). However, relative to chlorophyll a, total chlorophyll c pigments increased in the later growth phases, mainly due to chlorophyll c_3 (Figure 15). Other *E. huxleyi* strains are reported to contain either chlorophyll c_2 (Stolte, 2000; Zapata, 2004; Zapata, 2006; Mizoguchi, 2011) or chlorophyll c_3 (Stolte, 2000; Zapata, 2004) as their main chlorophyll c. Here again, the chosen time point for harvest could be biasing this conclusion.

Chlorophyll c pigments are accessory pigments, participating in light harvesting, with special importance in the limited light spectrum reaching aquatic environments (Croce & van Amerongen, 2014). The different derivatives differ marginally in absorption spectra (Jeffrey, 1972; Fawley, 1989; Saitoh, 1993). Similar to fucoxanthins, interconversion of chlorophyll c derivatives alters the architecture of pigment-protein complexes (Melkozernov & Blankenship, 2006), thereby changing spectral absorption properties (Garrido, 1995). This has been observed under red light for the diploid *E. huxleyi* strain CCMP 370, where ratios of chlorophyll c_2 and chlorophyll c_3 to chlorophyll a increased compared to white light (Garrido, 2016). Therefore, the observed interconversions in the later growth phases could indicate structural changes of

light harvesting proteins, leading to alterations of the absorption spectrum as a means of photoprotection, as observed for fucoxanthin derivatives in this work.

Diadinoxantin abundance was comparable in both life-cycle stages (Figure 13). In line with the light harvesting pigments, it decreased in the later growth phases (Figure 14). However, relative to chlorophyll a, the proportion increased (Figure 15). Two diadinoxanthin pools are assumed to exist (Stolte, 2000), one involved in the xanthophyll cycle, where conversion of diadinoxanthin to diatoxanthin results in non-photochemical quenching, dissipating excess energy (Demmig-Adams & Adams III, 1993; Llewellyn, 2007), and one as substrate for fucoxanthin synthesis (Goericke & Welschmeyer, 1992; Stolte, 2000; Bertrand, 2010). As mentioned above, fucoxanthin is the precursor for hex-fucoxanthin (Lohr & Wilhelm, 1999; Stolte, 2000; Llewellyn, 2007). Following these premises, sufficient diadinoxanthin needs to be available, to ensure a high level of hex-fucoxanthin synthesis via fucoxanthin, and at the same time the cell needs to guarantee efficient photoprotection via conversion of diadinoxanthin to diatoxanthin at short notice, explaining relatively constant diadinoxanthin proportion in the cell in all growth phases.

Diatoxanthin abundance was minor in the early-exponential phase, compared to the other pigments (Figure 13), although here again it must be noted that abundance was not quantified, due to limited concentration of available standard. With progressing growth, diatoxanthin abundance increased per cell (Figure 14) and regarding chlorophyll a (Figure 15). This suggests an intensification of the xanthophyll cycle, as reflected by the increasing calculated de-epoxidation ratio (Table 6). This type of photoprotection is typically observed under high light stress, also in diploid *E. huxleyi* strains (PLY 92, B11, CCMP 370) (Harris, 2005; Ragni, 2008; Garrido, 2016). Increases de-epoxidation ratios have been observed previously in the stationary growth phase, for the diploid *E. huxleyi* strain PLY-61/7/3, nine other haptophytes and ten diatoms (Llewellyn & Gibb, 2000), as well as other microalgal classes, such as chlorophytes (*Dunaliella salina* and *Tetraselmis suecica*), dinoflagellates (*Amphidinium carterae, Heterocapsa* sp. and *Gymnodinium catenatum*) and bacillariophytes (*Cylindrotheca closterium*) (Latasa & Berdalet, 1994; Ruivo, 2011).

Cells in late-exponential and stationary growth phases contain decreased overall pigment abundance, therefore probably a smaller light-harvesting antenna, as discussed above. As the light intensity is unchanged, the antenna need to absorb more photons per light harvesting pigment. The xanthophyll cycle is activated in response to reactive oxygen species (ROS) stress and/or electron pressure on the photosynthetic chain (Pogson, 2005). The principle is illustrated in Figure 26. These results are in line with the increased α-tocopherol abundance (antioxidant,

ROS scavenger) in the stationary and declining growth phases for the same life-cycle stages (Mausz & Pohnert, 2015).

The fact that diatoxanthin was detected in the early-exponential phase confirms that the diadinoxanthin de-epoxidase is also active under non-stressed conditions in the diadinoxanthin-based xanthophyll cycle (Jakob, 2001), in contrast to the violaxanthin de-epoxidase in violaxanthin-based xanthophyll cycle (Hager, 1975; Bratt, 1995).
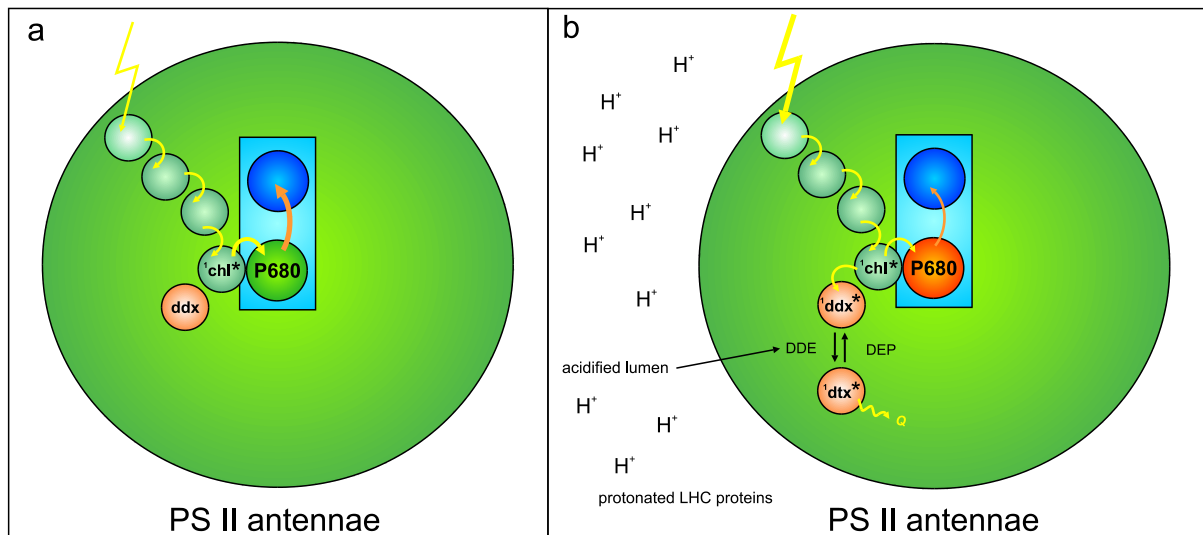
Figure 26: Simplified schematic representation of xanthophyll cycle mediated quenching in photosystem II as a response to higher light availability. (a) An accessory pigment absorbs a photon and excitation energy is transferred to the reaction center P680 via chlorophyll a, where charge separation occurs. (b) Upon stress stimulation (light, temperature, drought), photochemistry is saturated (red P680). To avoid the excited singlet chlorophyll (^{1}chl*) crossing over into the dangerous triplet state (^{3}chl*), diatinoxanthin in *E. huxleyi* quenches the singlet chlorophyll, which emits fluorescence and relaxes into its ground state. The excited diadinoxanthin is epoxidated by the diadinoxanthin de-epoxidase (DDE), which has been activated due to the decreased pH from the acidified lumen, as protons accumulate here, because the ATP synthase is stalled. Epoxidation results in diatoxanthin, which emits heat (Q) in the process of non-photochemical quenching. It can be converted back to diadinoxanthin via the diatoxanthin epoxidase (DEP).

The question remains why growth-dependent pigment responses in the haploid life-cycle stage exhibited the same pattern as in the diploid stage, but were seldom significant (Figure 14, Figure 15). Also, both stages activated xanthophyll-cycling in the late-exponential phase, but the diploid stage was able to increase photoprotection further in the stationary phase, whereas xanthophyll-cycling ceased in haploid stage (Table 6).

The diploid life-cycle stage of this particular *E. huxleyi* strain has been shown to perform more efficiently in photosynthesis. For example, a higher photosynthetic capacity has been shown for the diploid stage under normal light intensities (Rokitta & Rost, 2012). This stage additionally showed no signs of photoinhibition up to light intensities of 1000 µmol m^{-2} s^{-1}, whereas the haploid stage was inhibited at 400-500 µmol m^{-2} s^{-1} (Houdan, 2005). Also, the diploid stage contained a higher hex-fucoxanthin to chlorophyll a ratio (Houdan, 2005),

indicating more specialized absorption of light, as discussed above. The results of this work further expand the knowledge with regard to the diploid stage's superior photosynthetic efficiency, as it displayed a higher ability to activate and sustain xanthophyll cycle-mediated non-photochemical quenching during later growth stages.

Both life-cycle stages are thought to occupy distinct niches (Frada, 2008; von Dassow, 2009; Rokitta, 2011). Information about the haploid life-cycle stage in nature is rare, often only few individuals are found in diploid dominated blooms (Frada, 2012). This difference in photosynthetic endurance could be connected to the proposed difference in niche-occupation for the life-cycle stages (von Dassow, 2009; Rokitta, 2011).

5.3.2 Lipid abundance and composition change with growth

The lipid composition of microalgal cells is known to be highly dependent on their growth phase, as for example storage lipids can accumulate when cell growth ceases (Sukenik 1990, Hodgson 1991). The knowledge of this growth phase-dependent composition allows conclusions about the cell's physiology. In this experiment, the abundance of fatty acids associated with the polar and neutral lipid fraction were assessed during the early-exponential, late-exponential and stationary growth phase of a diploid and haploid *E. huxleyi* life cycle stage, grown under nutrient-replete conditions. The applied lipid-detection method via FAME derivatization allowed elucidation of the fatty acid composition of polar lipids (i.e., membrane lipids such as glyco-, phospho-, sphingo- and betaine lipids), as well as the fatty acids from neutral lipids (i.e., TAGs, free fatty acids).

In both life-cycle stages, fourteen different fatty acids were detected in *E. huxleyi*'s polar lipid fraction (Figure 16), while ten were found in the neutral lipid fraction (Figure 18). Chain lengths ranged from $C_{14:0}$ to $C_{22:6n3}$. The odd-numbered fatty acid $C_{15:0}$ was undoubtedly detected in both fractions, and was not detected in the lipid isolation blanks or measurements blanks. The occurrence of odd-chain fatty acids in eukaryotes, which typically contain even-chain lengths, is unusual. However, $C_{15:0}$ has been reported for numerous different *E. huxleyi* strains (Volkman, 1981; Bell & Pond, 1996; Pond & Harris, 1996; Riebesell, 2000; Rontani, 2007; Evans, 2009) and has been localized as one possible fatty acid chain of the phospholipid phosphatidylethanolamine (PE) in the diploid *E. huxleyi* strain CCMP 374 (Fulton, 2014). Furthermore, C_{15} to C_{29} or even longer chain lengths up to C_{47} have been detected in certain other microalgae (Douglas, 1969; Gillan, 1981; Řezanka, 1983; Řezanka & Podojil, 1984; Gelin, 1997; Fidalgo, 1998; Allard & Templier, 2001; Kalacheva, 2002; Řezanka & Sigler, 2009; Schwarzhans, 2015).

In the following two sections, results will be discussed in more detail for fatty acids of the polar and neutral lipid fraction, respectively. In each section, the fatty acid composition in general will be discussed first, then life-cycle specific differences will be addressed, and in a last step growth phase-dependent changes will be elucidated.

5.3.2.1 Fatty acids associated with the polar lipid fraction

Several polar lipid fatty acids were highly abundant in all three growth phases, such as saturated ($C_{14:0}$, $C_{16:0}$, $C_{18:0}$), mono- ($C_{18:1n9c}$) and polyunsaturated fatty acids ($C_{18:3n3}$, $C_{18:4n3}$, $C_{22:6n3}$) (Figure 16). These results are in line with a previous study analyzing the same strain (Fiorini, 2010), with the exception of $C_{18:0}$, which was only found in trace amounts. In the haploid stage, only the saturated fatty acids were present as major fatty acids in all growth phases (Figure 16). This general trend for the haploid stage was confirmed by Fiorini's results, although the difference was not as pronounced (Fiorini, 2010).

Most of the fatty acids detected in this strain have been reported as components of polar lipids identified in other diploid and haploid *E. huxleyi* strains (Bell & Pond, 1996; Fulton, 2014), such as glycolipids (MGDG, DGDG, SQDG), phospholipids (PC, PDPT, PG, PE), betaine lipids (DGCC, BLL, DGTS) and sphingolipids (GSL). However, there seem to be strain-specific differences regarding the fatty acid composition of polar lipids. For example, $C_{18:2n6c}$ was detected in both life-cycle stages of *E. huxleyi* (RCC 1216 and RCC 1217) in this work, which is in line with Fiorini and coworkers (2010). Intriguingly, this fatty acid is often not reported in other *E. huxleyi* strains, with the exception of trace amounts in DWN 61/81/5 (Bell & Pond, 1996) and CCMP 1516 (Evans, 2009). Furthermore, other *E. huxleyi* strains contain high abundances of $C_{18:5n3}$ (Volkman, 1981; Bell & Pond, 1996; Pond & Harris, 1996; Dijkman & Kromkamp, 2006; Evans, 2009), identified as the major fatty acid found in thylakoid membrane lipids MGDG and DGDG (Bell & Pond, 1996; Fulton, 2014). This polyunsaturated fatty acid was not detected in either life-cycle stage in this work, in line with previous results, where it was not detected in the diploid, and only found in trace amounts in the haploid stage (Fiorini, 2010).

One reason for the absence of $C_{18:5n3}$ could be the oxidation of fatty acids during sample preparation. Especially polyunsaturated fatty acids and their methyl esters are susceptible to oxidation (Frankel, 1980; Knothe & Dunn, 2003). However, as Fiorini and coworkers (2010) also found similar results for these life-cycle stages, and other polyunsaturated fatty acids, such as $C_{22:6n3}$ and $C_{18:4}$, are highly abundant in this work, this is probably not the reason.

A more plausible reason for the absence of $C_{18:5n3}$ could be related to the cultivation temperature. At lower temperatures, membrane lipid fatty acids are more unsaturated, thereby

maintaining membrane fluidity due to looser packaging of fatty acids, mediated by the rigid kink of the cis double bond (Mansilla, 2004; van Wagenen, 2012). In all studies cited as comparison for *E. huxleyi* strains containing $C_{18:5n3}$, the cultivation temperature was 15 °C (Volkman, 1981; Bell & Pond, 1996; Pond & Harris, 1996; Dijkman & Kromkamp, 2006; Evans, 2009), whereas is was 19 °C in Fiorini's work (2010) and 20 °C in this work. Therefore, it is possible that this fatty acid is absent in this work and Fiorini's work (2010), due to the higher cultivation temperature. Increased fatty acid unsaturation ratios with lower temperature have been observed for many microalgal species (Ackman, 1968; Thompson, 1992; Renaud, 2002; van Wagenen, 2012). This would also explain the relatively high proportion of unsaturated fatty acids and the occurrence of $C_{18:2n6}$ found in this work, as saturated, mono- and diunsaturated fatty acids are consequently present in higher abundance at higher temperatures.

However, the ω-3-fatty acid $C_{22:6n3}$ did not seem to be affected, as it was detected in high abundance in the diploid stage. This has been observed previously for *Isochrysis* sp., where $C_{18:5n3}$ abundance increased at lower temperatures, whereas $C_{22:6n3}$ abundance increased with higher temperatures (Renaud, 2002). Next to $C_{18:5n3}$, $C_{22:6n3}$ and $C_{18:4n3}$ also represent polyunsaturated fatty acids in the typical thylakoid lipids MGDG and DGDG (Bell & Pond, 1996; Fulton, 2014). Therefore, it is possibly that these fatty acids compensate the loss of $C_{18:5n3}$, to maintain thylakoid membrane structure at higher temperatures, applied in this work.

The low abundance of polyunsaturated polar lipid fatty acids in the haploid stage revealed differences between life-cycle stages (Figure 16). This was also reflected in the total abundance of polar lipid fatty acids, which was twice as high for the diploid compared to the haploid stage, at every harvesting time point (Supplementary Table 3, Supplementary Table 4). As stated above, polyunsaturated fatty acids have been reported to be major components of thylakoid membrane glycolipids in *E. huxleyi* (Bell & Pond, 1996; Fulton, 2014). The composition of thylakoid membranes directly influences photosynthesis, as thylakoid lipids form the lipid bilayer and aid in folding and assembly of protein subunits (Murata, 1998; Kobayashi, 2016). Therefore, low abundance of polyunsaturated fatty acids in the haploid stage probably reflect thylakoid membrane differences. This could be connected to the less efficient photosynthesis, which has been reported for this life-cycle stage (Houdan, 2005; Rokitta & Rost, 2012). This assumption is supported by Fiorini and coworkers (2010), who also observed a higher abundance of $C_{18:4n3}$ in the diploid stage and connected it to less efficient photoabsorption and photosynthetic activity in the haploid stage. Reconstruction of polar lipid data from Bell and Pond (1996) showed a higher $C_{18:4n3}$, $C_{18:5n3}$ and $C_{22:6n3}$ abundance in thylakoid membrane glycolipids of the diploid stage of *E. huxleyi* DWN 61/81/5, compared to its haploid stage,

further supporting this theory. In addition, untargeted glycerolipid analysis revealed four thylakoid-associated lipids selectively indicative for the same haploid stage as analyzed in this work, all containing saturated or monounsaturated fatty acids (Hunter, 2015). Therefore, it is highly likely that the haploid stage has a different thylakoid membrane composition, with tighter packaging of less unsaturated fatty acids, influencing structure and stability of this membrane (Murphy, 1982; Demé, 2014), and in turn possibly influencing photosynthetic efficiency (Kobayashi, 2016).

Furthermore, the observed differences could reflect differences regarding non-photosynthetic, extraplastidial membranes of both stages. For example, the diploid stage contained a much higher amount of $C_{22:6n3}$ than the haploid stage. In *E. huxleyi* this polyunsaturated ω-3 fatty acid is present in all glycosyl-glycerides (MGDG, DGDG, SQDG), phosphoglycerides (PC, PDPT, PE, except PG) and betaine lipids (DGCC, DGTS, BLL) (Bell & Pond, 1996; Fulton, 2014). Next to the aforementioned differences regarding thylakoid membranes, this suggests differences in other membrane structures, of which phospho- and betaine lipids are major components (Bell & Pond, 1996; Khozin-Goldberg, 2016). Less $C_{22:6n3}$ in the haploid's membrane could result in a more rigid bilayer formation. This could be connected to the fact that the cell is only covered by organic scales, not protected by coccoliths. Coccoliths have been proven to protect diploid cells against hydrostatic pressure (Jaya, 2016). Another reason for the higher abundance of phospholipid related fatty acids in the diploid stage could be the need for additional membrane lipid structures for the coccolith forming endomembraneous apparatus and vacuole-like compartments for preconcentration of Ca^{2+} ions (Eltgroth, 2005; Sviben, 2016). The membrane composition of these organelles has not been completely elucidated, but polar lipids have been found associated with the coccolith vesicle fraction (Sawada & Shiraiwa, 2004; Eltgroth, 2005). These compartments are absent in the haploid stage, as it does not calcify (Paasche, 2001), which could explain why general polar lipid abundance was lower in this stage. The $C_{22:6n3}$ containing betaine lipid DGTS was 2-fold higher in the same diploid stage as analyzed in this work, compared to the haploid stage (Hunter, 2015), which could partly explain the differences observed in this work. However, this lipid can also be found in thylakoid membranes, in addition to extraplastidial membrane structures (Murata, 1998; Khozin-Goldberg, 2016). Interestingly, authors also found sialic glycosphingolipid (sGSL) exclusively in the diploid stage (Hunter, 2015). This lipid is a marker for viral susceptibility in *E. huxleyi* (Fulton, 2014) and is not found in the haploid stage (Hunter, 2015), due to resistance of this stage against infection (Frada, 2008). It contains $C_{22:0}$, not $C_{22:6n3}$, according to Fulton (2014). In this work, no significant difference between life-cycle

stages was detected for $C_{22:0}$. However, this fatty acid is also found in another GSL (Fulton, 2014), only present in the haploid stage (Hunter, 2015). These results highlight viral susceptibility as a reason for different cell membrane composition between both life-cycle stages. The haploid stage may be less photosynthetically efficient than the diploid stage (Houdan, 2005; Rokitta & Rost, 2012), but it represents an `escape mechanism´ for *E. huxleyi*, as viral infection can induce changes from diploid to haploid life-cycle stages, thereby ensuring survival of the species, when all diploid stages are killed (Frada, 2008).

For both life-cycle stages the polar lipid fatty acid abundance was highest in the early-exponential phase, decreasing in the late-exponential and stationary phase (Figure 17). This is in line with decreasing MGDG and PE abundance observed in the same life-cycle stages with ongoing growth (Hunter, 2015). In the diploid *E. huxleyi* strain CCMP 1516, the fatty acid content also decreased in late-exponential phase, although in that particular study total fatty acids were analyzed (Evans, 2009). One other study showed more variable responses for different diploid *E. huxleyi* strains regarding polar lipid abundance, which either increased, decreased or did not change at all from exponential to stationary growth phase (Pond & Harris, 1996). The same contradicting results can be found for other microalgae (Dunstan, 1993; Lombardi & Wangersky, 1995; Fidalgo, 1998; Edvardsen, 2000; Fujiwara, 2001).

Nonetheless, the observed decrease in polar lipid fatty acid abundance in the later growth phases of both life-cycle stages analyzed in this work could be explained by the aforementioned theory of decreased photosynthesis, as a means to adapt to the lowered energy demand of non-dividing cells. It is highly likely that polar lipid and pigment abundances are co-regulated, because polar lipids are important components of the chloroplast thylakoid membrane, directly influencing photosynthesis, as they form the thylakoid membranes and aid in folding and assembly of protein subunits (Murata, 1998; Kobayashi, 2016).

Furthermore, there is a direct connection between pigments and polar lipids in *E. huxleyi*, due to the pigment chlorophyll c_2-MGDG. The chlorophyll c_2 moiety is esterified to a MGDG, which predominantly contains $C_{14:0}$ and $C_{18:4}$ fatty acids in the diploid *E. huxleyi* strain CCMP 370 (Garrido, 2000). In this work, pigments were inevitably co-isolated with the lipid extraction (Li-Beisson, 2016) and eluted in the polar lipid fraction. The fatty acids of chlorophyll c_2-MGDG were subsequently derivatized and analyzed as FAME. In line with the decreasing chlorophyll c_2-MGDG abundance (Figure 14), the polar lipid fatty acids $C_{14:0}$ and $C_{18:4}$ also decreased in abundance with ongoing growth (Figure 16), indicating connections between pigment and polar lipid fatty acid abundance.

5.3.2.2 Fatty acids associated with the neutral lipid fraction

E. huxleyi's neutral lipids consist of alkenones, alkenoates, alkenes, free fatty acids, triacylglycerides (TAGs), wax and sterol esters. These accumulate in lipid bodies in chloroplasts and cytoplasm (Eltgroth, 2005). The applied method of fatty acid methyl ester (FAME) derivatization of the neutral lipid fraction, allowed the elucidation of the fatty acid composition of TAGs and free fatty acids via GC-MS. As alkenones, alkenoates and alkenes contain an acetyl group (CH_3OH) instead of a carboxyl group ($COOH$), they were not esterified with this method. However, their composition in both life-cycle stages was assessed with a separate method for the nutrient starvation experiment, discussed in section 5.4. Furthermore, fatty acids of wax and sterol esters, which occur in small amounts in *E. huxleyi* (Volkman, 1981), were not detected here, as they require base-catalyzed methylation (Kanya, 2007; Christie, 2011c; Christie, 2011b).

Major fatty acids associated with the neutral lipid fraction of both life-cycle stages were $C_{16:0}$, $C_{18:0}$, $C_{18:1n9c}$, $C_{22:0}$ and $C_{22:6n3}$, the latter two depending on the growth phase (Figure 18). In contrast to the polar lipid fraction the fatty acids $C_{14:0}$, $C_{20:0}$, $C_{20:2}$, $C_{22:1n9}$ were not detected. It is possible that $C_{14:0}$ was not detected due to the sensitivity of the detector towards low-abundant short-chain fatty acids, as discussed in section 4.1. Unfortunately, no information on exact fatty acid composition is available for the neutral lipid fraction of *E. huxleyi*, let alone the haploid stage, as the focus is usually on alkenones.

For both life-cycle stages and all growth phases, the total abundance of neutral lipid fatty acids was ~6-fold lower than that detected for the polar lipid fatty acids (Supplementary Table 3, Supplementary Table 4). This indicates that neutral lipid fatty acids only comprise a small proportion of *E. huxleyi*'s lipids, in line with reports for TAG and free fatty acids, which have both shown to comprise ~2 % of total lipids under nutrient-replete conditions (Volkman, 1986; Bell & Pond, 1996; Pond & Harris, 1996; Rosenwasser, 2014; Malitsky, 2016). *E. huxleyi* has been shown to have the capacity to produce up to 20 % TAGs of total lipids, as observed under viral infection (Malitsky, 2016). Results from these studies were either stated as total free fatty acids/TAGs, or as the sum of all three fatty acids for TAG (125 possible combinations, ranging from $C_{42:0}$ to $C_{60:11}$), therefore not allowing fatty acid specific comparison with the data obtained in this work.

Comparison of both life-cycle stages showed slight differences in the abundance of individual neutral lipid fatty acids (Figure 18). These especially regard the ω-3 fatty acid $C_{22:6n3}$ and will therefore be discussed together with changes of this fatty acid in the polar lipid fraction at the end of this chapter.

The neutral lipid fatty acids decreased markedly in the late-exponential and stationary growth phase (Figure 19), in line with pigments (Figure 14) and polar lipid fatty acids (Figure 17) and the general decrease of metabolism activity associated with these growth phases (Raven & Beardall, 2003; Mausz & Pohnert, 2015). Comparison with other *E. huxleyi* strains to this regard is challenging, as changes are typically assessed regarding PULCA, which can markedly increase in the later growth phases in some diploid strains (Pond & Harris, 1996). Studies have shown that even including PULCA, growth phase-dependent changes in diploid *E. huxleyi* strain's neutral lipids are highly strain-dependent, as they either increase, decrease or do not change at all, dependent on analyzed strain (Pond & Harris, 1996).

However, results from the nutrient starvation experiment (4.3) showed that cells harvested in late-exponential phase contained a comparably high amount of PULCA (Supplementary Table 5, Supplementary Table 6). Therefore, it can be assumed that while TAG and free fatty acid abundances decrease in the later growth phases, PULCA increases, in line with the assumption of being a storage lipid (Bell & Pond, 1996; Epstein, 2001; Tsuji, 2015).

The fatty acid $C_{22:6n3}$ (docosahexaenoic acid, DHA) belongs to the ω-3 fatty acids, which are of commercial interest, as they are essential for human nutrition (Das, 2002; Voigt, 2002; Calder, 2003). The overall proportion of DHA in total lipids (polar and neutral fatty acids) for the early-exponential, late-exponential and stationary growth phase, respectively, was 11.8 %, 25.7 % and 26.6 % in the diploid stage and 4 %, 4 % and 10 % in the haploid stage. These results are comparable with other diploid *E. huxleyi* strains, where the proportion of DHA in total lipids ranged from 20-36 % in the exponential phase (Pond & Harris, 1996; Evans, 2009; Fulton, 2014; Boelen, 2016) to 16-38 % in the stationary phase (Pond & Harris, 1996; Evans, 2009; Boelen, 2016). Bell and Pond (1996) confirmed the lower abundance of DHA in polar lipids in the haploid stage of *E. huxleyi* DWN 61/81/5, compared to its diploid stage. Reasons for these life-cycle specific differences have been discussed in detail above (4.3.2.1). This proportion of DHA in *E. huxleyi* is comparably high, higher than six other microalgae, including the diatoms *Phaeodactylum tricornutum*, *Thalassiosira weissflogii*, *Thalassiosira pseudonana* and *Skeletonema costatum*, the haptophyte *Isochrysis galbana* and the cryptomonad *Rhodomonas salina* (Boelen, 2016).

The achieved DHA productivity in this cultivation was maximal in the late-exponential growth phase, amounting to 33.2 ng L^{-1} d^{-1} in diploid stage, when adding productivities for polar and neutral lipids (Figure 20). Only one other study mentions DHA productivity in a further undefined diploid *E. huxleyi* stage, resulting in 164 µg L^{-1} d^{-1} DHA (Boelen, 2013). Differences could be strain-specific, or based on the fact that authors only analyzed one

replicate and did not specifically quantify DHA, but estimated based on the internal standard $C_{19:0}$. Higher productivities have been reported for other haptophytes, such as *Pavlova lutheri*, which produces DHA (1.3 mg L^{-1} d^{-1}), and the ω-3 fatty acid EPA (eicosapentaenoic acid, $C_{20:5n3}$, 3.6 mg L^{-1} d^{-1}) when grown in continuous culture with 0.5 % CO_2 (Carvalho & Malcata, 2005). Nonetheless, commercial DHA production is typically performed with heterotrophically growing microalgae and marine protists, as they reach higher biomass and therefore DHA productivity (Ward & Singh, 2005; Martins, 2013). For example, the heterotrophically growing dinoflagellate *Crypthecodinium cohnii* has been reported to produce 33 % DHA of total lipids in a 220 h fed-batch cultivation with ethanol as a C-source, producing 83 g dry biomass L^{-1}, resulting in a productivity of 1.3 g L^{-1} d^{-1} (de Swaaf, 2003). This microalga is used for commercial DHA production, in addition to marine stramenopiles (Thraustochytriaceae) *Ulkenia* sp. and *Schizochytrium* sp. (Martins, 2013), which produce DHA in similar productivity ranges (Ward & Singh, 2005).

In both the polar and neutral lipid fraction, DHA exhibited a pattern (Figure 16, Figure 18), often involving high abundances of DHA in the early-exponential phase, which decreased in the late-exponential phase, and increased again in the stationary phase. Not all three steps of this pattern are realized for all life-cycle stages and lipid fractions, i.e. DHA did not increase again in stationary phase in the diploid's polar lipids, and DHA was not detected in the haploid's neutral lipid fraction in early-exponential growth phase. The accumulation of DHA in the stationary phase has been reported for different diploid and haploid *E. huxleyi* strains before (Bell & Pond, 1996; Pond & Harris, 1996; Boelen, 2016), in one study also along with higher concentrations in the early exponential phase (Bell & Pond, 1996). However, these studies only assessed DHA in the polar or total lipid fraction. The link between high DHA concentrations and the stationary growth phase has also been observed for other algae (Dunstan, 1993; Fidalgo, 1998). In algae that produce EPA and DHA, EPA selectively increased in the later growth phases (Boelen, 2016).

The selective accumulation of ω-3 fatty acids in the stationary phase, while all other fatty acids decrease, could indicate an energy storage function of this fatty acid. For this experiment this would imply that cells used as inoculum still contained relatively high amounts of DHA, which was metabolized for more energy in the growth phase (late-exponential phase). When cell growth ceased, superfluous energy was stored in form of this fatty acid, resulting in decreased abundances of precursor fatty acids. Although accumulation of ω-3 fatty acids has been linked to the stationary phase, as indicated by the references above, the hypothesis of it being a storage fatty acid has not been stated before and is not supported by further evidence.

Nonetheless, knowledge of growth phase-dependent accumulation of ω-3 fatty acids can be of advantage for the use of microalgae as aquacultural feed (Bell & Pond, 1996; Sayanova, 2011; Boelen, 2016).

In summary, the results of this work highlight the importance of analyzing more than one time point for physiological studies, as the metabolome and therefore the physiological status of the cell can differ prominently with regard to growth stage.

5.4 Comprehensive metabolome analysis of *E. huxleyi* under phosphorus- and nitrogen-starvation reveals life-cycle specific responses

The results discussed in this section were submitted as part of a manuscript:

> Wördenweber, R., Rokitta, S. D., Heidenreich, E., Corona, K., Kirschhöfer, F., Fahl, K., Klocke, J. L., Kottke, T., Brenner-Weiß, G., Rost, B., Mussgnug, J. H., Kruse, O. (submitted): Phosphorus and nitrogen starvation reveal life-cycle specific responses in the metabolome of *Emiliania huxleyi* (Haptophyta).

The aim of this work was to analyze the effect of P- and N-starvation on the intracellular metabolome of diploid and haploid *E. huxleyi* life-cycle stages. As these limitation scenarios are very common in the ocean (Moore, 2013; Palenik, 2015), and are proposed to enhance with advancing climate change (Doney, 2006; Cermeno, 2008; Beman, 2011), this dataset facilitates the understanding of how the different life-cycle stages cope with nutrient starvation.

To generate biomass for metabolome analysis, two separate cultivations were performed, each with nutrient replete controls and either P- or N-starvation. Both *E. huxleyi* life-cycle stages grow comparably under nutrient-replete conditions (Figure 21 a, b). In the P-starvation setup, replete cultures reached slightly higher cell numbers at the end of the cultivation, compared to nutrient replete cultures in the N-starvation setup. Achieved growth rates were comparable with those of the growth phase experiment (4.3) and those reported previously for the same life-cycle stages (Houdan, 2005; Rokitta & Rost, 2012; Mausz & Pohnert, 2015; Rokitta, 2016). At harvesting time point, nutrient-replete cultures were in mid-exponential growth phase and not limited by nutrients or C-source (Figure 21 c-f). In contrast, cell numbers of both life-cycle stages, starved by P or N, stalled on day six, and entered stationary phase. This deceleration of growth was induced by the respective nutrient limitation, which was detected in the supernatant on day four, for either P or N. The exact time point at which an extracellular limitation was reached intracellularly, is difficult to clarify. However, clearly the limitation had already affected the cells, as seen by the setbacks in growth and the significant metabolome differences (Figure 24).

Thirty primary metabolite were identified in this work via GC-MS after TMS-derivatization, some of them putatively via database comparison, as the standard was lacking. However, for metabolites that were additionally identified via LC-MS/MS, LC-MS/MS values were chosen, as these were quantified with internal partly labeled and external standards, therefore signifying higher data confidence. Nonetheless, the number of identified primary metabolites via GC-MS is in line with Obata (2013), who identified 26 metabolites with the same method for the diploid *E. huxleyi* strain CCMP 1516.

5.4.1 Life-cycle-specific metabolite patterns under nutrient-replete conditions

The comparison of life-cycle stages under nutrient-replete conditions, revealed a 50 % difference regarding significantly and at least 1.5-fold difference of metabolite abundance (Figure 24 a), of which the majority was found in higher abundance in the diploid stage (67 %). Main distinctions were higher lipid and DMSP abundances in the diploid stage. In this section, life-cycle specific differences under nutrient-replete conditions will be discussed in more detail.

DMSP is an osmolyte with cryoprotective and antioxidative properties (Sunda, 2002). It has been detected in *E. huxleyi* strains previously (Turner, 1988; Keller, 1999; Spielmeyer, 2011; Gebser & Pohnert, 2013), and is suggested to play an important role in the global sulfur cycle (Bates, 1987; Malin, 1996). Among all osmolytes, DMSP was the most abundant in both life-cycle stages (Supplementary Table 5, Supplementary Table 6) and was present in significantly higher abundance in the diploid stage (Figure 24 a). When focusing on the replete cultivations separately, nutrient-replete diploid strains contained 11.5-fold more DMSP than haploid cells in the P-starvation setup (304 ± 23 fg cell^{-1} vs. 32 ± 12 fg cell^{-1}, respectively) and 1.7-fold more in the N-starvation setup (678 ± 88 fg cell^{-1} vs. 402 ± 65 fg cell^{-1}, respectively). Divergences in this order of magnitude have been reported before (Keller, 1999) and possibly derive from slightly offset harvesting time points.

DMSP has been reported as the most abundant osmolyte in the same diploid *E. huxleyi* life-cycle stage previously (Gebser & Pohnert, 2013), along with smaller amounts of glycine betaine and homarine, in line with the results of this work. Minor concentrations of dimethylsulfonio-acetate, trimethylammonium propionate and trimethylammonium butyrate have been reported (Gebser & Pohnert, 2013). These osmolytes were not detected in this work, possibly due to detection limits. The absolute amount of DMSP was comparable with previous reports for the same strain (Spielmeyer, 2011; Gebser & Pohnert, 2013). The higher abundance observed in the diploid life-cycle stage has been reported previously for the same strain (2N: 580 fg cell^{-1} vs. 1N: 380 fg cell^{-1}) (Spielmeyer, 2011). In a first approximation, this could mean that the diploid stage relies on a higher DMSP abundance to maintain osmotic balance. The coccolith production, occuring only in this life-cycle stage, requires large amounts of Ca^{2+} and HCO_3^- to be imported into the coccolith forming endomembraneous apparatus. Ca^{2+} ions are pre-concentrated in a vacuole-like compartment (Sviben, 2016), which could possibly require stronger intracellular osmoregulation.

Comparison of carboxylic acids in both life-cycle stages under nutrient-replete conditions revealed a higher citrate concentration in the haploid stage (Figure 24 a). This has been reported for the same strain previously (Mausz & Pohnert, 2015). In addition, the haploid stage contained

more lactate and less succinate than the diploid stage. These metabolites are associated with the TCA and energy metabolism. Transcriptomic studies of the same life-cycle stages indicated a higher transcript abundance of genes coding for proteins involved in these processes (Rokitta, 2011). Based on this evidence, it was hypothesized that the haploid life-cycle stage requires more energy to fuel its flagellar apparatus (Rokitta, 2011). This could partially explain the increased abundance of citrate and lactate in the haploid stage.

The pigment composition of both life-cycle stages under nutrient-replete conditions differed significantly (Figure 24 a). The diploid stage contained a higher abundance of h4k-fucoxantin, and a lower amount of various chlorophylls (chlorophyll a, chlorophyll c_2, chlorophyll c_2-MGDG) and carotenoids (fucoxanthin, hex-fucoxanthin). In general, the pigment profile was similar to that obtained in the growth phase experiment (Figure 13). The absolute pigment abundance was comparable to the late-exponential and stationary phase of the growth phase experiment. The higher abundance of h4k-fucoxanthin in the diploid stage is confirmed by the results of the growth phase experiment (late-exponential and stationary growth phase). However, other than that, life-cycle specific differences were not necessarily comparable between both experiments. Also, in contrast to the observations in the growth phase experiment, where total pigment abundance was similar for both stages in the late-exponential growth phase, the total pigment abundance was higher in the haploid stage in this experiment. Additionally, less variability was detected in the pigment abundance of the haploid stage in this experiment, as indicated by SD. As this experiment reflects two separate cultivations with nutrient replete control cultures, it can be assumed that the haploid stage does contain a higher abundance of pigments per cell compared to the diploid stage. Houdan and coworkers (2005) found no significant difference between pigment abundances of these life-cycle stages. However, this measurement only represented one biological replicate measured in technical triplicate (Houdan, 2005), therefore not representing biological variability, which clearly needs to be considered when analyzing *E. huxleyi*'s pigment abundance, as shown in this work. Generally, it is possible that both life-cycle stages were not in exactly the same growth phase in all experiments, which could also explain differences in pigment abundance. Nevertheless, results regarding photoprotection via xanthophyll cycle-mediated non-photochemical quenching (Table 8) showed active photoprotection in both stages, confirming results from the growth phase experiment, as values were comparable with the de-epoxidation ratios in the late-exponential growth phase (Table 6), which represented increased photoprotection compared to the early-exponential phase in both stages.

The general composition of neutral lipid fatty acids was comparable to that observed in the growth phase experiment (Figure 18), main lipids being $C_{16:0}$, $C_{18:0}$, $C_{18:1n9c}$ and $C_{22:6n3}$, depending on the setup (Supplementary Table 5, Supplementary Table 6). The short-chain fatty acid $C_{14:0}$ was detected in this experiment, in contrast to the growth phase experiment. As mentioned above, this is probably due to underestimation of short-chain fatty acids via GC-MS (4.1). Some neutral lipid fatty acids were not detected in comparison to the growth phase experiment, such as $C_{15:0}$, $C_{18:1n9t}$ and $C_{18:4n3}$. Here it is also possible that abundances were below detection limit, as these compounds were found only in small abundance in the growth phase experiment, or not at all (no $C_{18:1n9t}$ in 2N in late-exponential phase, Figure 18 b). As stated above, no reference data is available for *E. huxleyi*'s neutral lipid fatty acid composition. On level of neutral lipid fatty acids, the diploid stage contained significantly higher abundance of $C_{14:0}$, compared to the haploid stage (Figure 24 a). This was not observed in the growth phase experiment, as this short-chain fatty acid was not detected. Life-cycle specific differences of neutral lipid fatty acids observed in the growth phase experiment were not observed here, indicating variability in neutral lipid fatty acid abundance in the different experiments.

In contrast to neutral lipid FAME analysis, CAD-HPLC analysis allowed direct observations regarding TAG storage lipids. Five TAGs with identical fatty acids were identified, along with 15 unknown TAGs, which probably comprised combinations of different fatty acids (Figure 24 a). Various medium-chain TAGs were found, such as $C_{8:0}$-$C_{12:0}$, which could be of interest as biofuel components (Knothe, 2009), as these chain lengths are rare in biological systems. As discussed in section 4.1, there was a certain discrepancy between these short-chain TAGs and detected neutral lipid fatty acids, due to the different analysis instruments. Therefore, $C_{8:0}$-$C_{12:0}$ are detected as TAG, but not as neutral lipid fatty acids via GC-MS measurement as FAME. However, it can be assumed that the unknown TAGs are comprised of combinations of detected neutral lipid fatty acids. Comparison of TAG data with other *E. huxleyi* strains is not possible, as TAG is typically only reported as total TAG (Volkman, 1986; Bell & Pond, 1996; Pond & Harris, 1996; Rosenwasser, 2014), or as the sum of all three fatty acids for TAG (125 possible combinations, ranging from $C_{42:0}$ to $C_{60:11}$) (Malitsky, 2016).

The diploid stage showed a significantly higher total abundance of TAGs compared to the haploid stage (2.9-fold, Supplementary Table 5, Supplementary Table 6). This could indicate a generally higher capacity of this life-cycle stage to store energy in this form. Furthermore, the lower abundance in the haploid stage could be connected to the transcriptome derived

postulation that this stage has a higher respiratory activity, thereby intensely using fatty compounds to fuel mitochondrial energy generation for flagellar movement (Rokitta, 2011).

Furthermore, the diploid stage contained a significantly higher abundance of alkenones and alkenes (Figure 24 a). This confirms the significantly higher amount for alkenones detected via FTIR for this stage (Figure 1). Bell and Pond (1994) also reported a slightly higher alkenone abundance in the diploid stage of *E. huxleyi* DWN 61/81/5 compared to its haploid stage, at a comparable growth phase. PULCA have been found in various membrane fractions, but they were found especially associated with coccolith forming vesicles in *E. huxleyi* (Sawada & Shiraiwa, 2004), which could explain the higher abundance in the diploid stage. However, another study did not find any alkenones with the coccolith vesicle fraction, therefore this role of PULCA is still under debate (Eltgroth, 2005). Furthermore, alkenones have been suggested to enhance buoyancy (Fernández, 1994; Fernández, 1996; Paasche, 2001). The haploid stage contains flagella and is motile, but the diploid stage is non-motile (Green, 1996; Paasche, 2001). Therefore, the diploid stage possibly contains more alkenones to counteract sinking. In addition, alkenone unsaturation ratios were low under nutrient-replete conditions, indicating a high proportion of triunsaturated alkenones (Table 7). The majority of reports on unsaturation indices for other diploid *E. huxleyi* strains in exponential growth phase is higher, around ~0.5-0.7 (Conte, 1998; Müller, 1998; Prahl, 2003). Reference values for haploid stages are lacking. Nonetheless, similarly low values have been reported for various diploid strains (Conte, 1998), once again highlighting strain specific differences of this species. Calculated cultivation temperatures did not match the actual cultivation temperature (20 °C), even though different calibrations were applied (Table 7). The nearest approximation was 17.1±1.4 °C for 2N and 13.5±1.1 °C for 1N. Discrepancies between calculated CT or SST have been reported for clonal microalgal cultures before and highlight the difficulty of transferring laboratory derived assumptions to natural systems (Conte, 1995; Conte, 1998; Eltgroth, 2005).

The general composition of polar lipids (Supplementary Table 5, Supplementary Table 6) for nutrient-replete cultures was comparable to that observed for the diploid stage in the growth phase experiment (Figure 16), with $C_{14:0}$, $C_{16:0}$, $C_{18:0}$, $C_{18:1n9c}$, $C_{18:3n3}$, $C_{18:4n3}$ and $C_{22:6n3}$ as major fatty acids. The odd-numbered fatty acid $C_{15:0}$ was also identified here. Two fatty acids were not detected, such as $C_{20:0}$ and $C_{20:2}$. This could again be due to the concentration being below detection range, as these fatty acids were only found in low abundance in the growth phase experiment. Confirming results from the growth phase experiment, $C_{18:2n9c}$ was present, whereas $C_{18:5n3}$ was not. The total abundance of polar lipid fatty acids for nutrient-replete cultures was generally higher in the diploid stage (Figure 24 a), especially with regard to

$C_{18:1n9c}$, $C_{18:2n6c}$, $C_{18:4n3}$, $C_{22:0}$ and $C_{22:6n3}$, indicating differences in membrane composition. These results confirm observations from the growth phase experiment (Figure 16), underlining life-cycle specific differences in membrane composition. As mentioned in the discussion of the growth phase experiment, one reason for this could be the additional endomembraneous structures in the diploid life-cycle stage, required for calcium carbonate pre-concentration and precipitation for coccolith production (Sviben, 2016). Furthermore, differences could also be coupled to differences in thylakoid membrane composition, as well as viral susceptibility, as discussed above (5.3.2.1).

Apart from the higher osmolyte, polar lipid fatty acid and alkenone abundance in the diploid stage, which could possibly be connected to the calcification process in this stage, no specific metabolites were identified that could be termed `key metabolites´ for calcification. It is possible that such metabolites were either not identified, below concentration limits or not detectable with the applied analysis methods. On the other hand, it is possible that no such metabolite exists.

5.4.2 P-starvation boosts metabolite contents in both life-cycle stages

The effect of nutrient starvation has been analyzed for other *E. huxleyi* strains with respect to either lipids or pigments (Stolte, 2000; van Mooy, 2009; Loebl, 2010; McKew, 2015; Malitsky, 2016; Shemi, 2016). Comprehensive metabolome studies, comparable to the approach in this work, have not been conducted for nutrient limitation scenarios. One transcriptomic study exists, analyzing the effect of P- and N-starvation on the same life-cycle stages used in this work (Rokitta, 2016). Based on these results, authors proposed a metabolic model, with which the results from this work will be compared. Observations from transcriptomic studies cannot necessarily directly be compared with metabolome data, as further regulatory processes involved on post-transcriptional/-translational level (Feder & Walser, 2005). At the end of the following N-starvation section (5.4.3), the agreements or disagreements of metabolic data from this work with the proposed model are visualized (Figure 27, page 109).

Under P-starvation, 50.5 % of all detected metabolites were significantly changed more than 1.5-fold for the diploid stage, and 36.2 % for the haploid stage (Figure 24 b, c). Most these changed metabolites were increased in both stages (90.6 % and 86.8 %, respectively). This indicated a status of `metabolic overflow´ compared to nutrient-replete conditions.

Although there was a 24 h offset in the metabolite sampling time of both life-cycle stages, nutrient limitation was clearly sensed intracellularly. Transcriptomic studies for these life-cycle stages showed that early and later P-starvation responses answer in an `all or nothing´ manner, differing not qualitatively but quantitatively (Rokitta, 2016).

In both stages, P-starvation resulted in the increase of several amino acid abundances (Figure 24 b,c). This could indicate that amino acids are no longer build into proteins, or that proteins are recycled under these starvation conditions. The shutdown of cell cycling and protein synthesis have been proposed from transcriptomic data for these life-cycle stages under P-starvation (Rokitta, 2016). In agreement, the protein abundance has been shown to decrease under P-starvation in the diploid *E. huxleyi* strain CCMP 1516 (McKew, 2015).

Proline was especially increased in both life-cycle stages under P-starvation (Figure 24 b, c), indicating a special role of this amino acid in nutrient stress response. On transcriptomic level, a prominent increase of mitochondrial amino acid oxidation was observed under P-starvation, which proposedly leads to high levels of ammonia (Rokitta, 2016). Transcripts of genes encoding for ornithine-urea cycle enzymes were decreased (Rokitta, 2016). This cycle takes place over the mitochondrial membrane and removes ammonia and CO_2, thereby producing arginine and polyamines (Wünschiers, 2012b). Cessation of parts of this cycle could lead to accumulation of intermediates, of which proline is proposed to be formed (Miller, 2009; Szabados & Savoure, 2010). Furthermore, a prominent increase of transcript abundance of the gene coding for proline oxidase was observed under P-starvation (Rokitta, 2016). Authors hypothesized that this enzyme, which catalyzes mitochondrial proline oxidation (Phang, 2012), plays a superior regulatory role in cell-cycle arrest, possibly by inducing mitochondrial oxidative stress and related signaling (Rokitta, 2016). The increase of proline observed in this work could confirm these hypotheses on metabolic level.

DMSP abundance did not change under P-starvation in either life-cycle stage, still being the most abundant osmolyte (Figure 24 b, c, Supplementary Table 5, Supplementary Table 6), indicating continuous production of this osmolyte during P-starvation. A study analyzing *E. huxleyi* in seawater mesocosm enclosures in a Norwegian fjord with P-limited water also showed no difference in cellular DMSP, compared to mesocosms supplemented with P (Wilson, 1998). The betaine osmolyte glycine betaine, however, increased significantly in both life-cycle stages in this work. As *E. huxleyi* replaces phospholipids with betaine lipids under P-starvation (van Mooy, 2009; Abida, 2014; Shemi, 2016), it can be assumed that betaine compounds, such as glycine betaine and homarine, are also used for betaine lipid synthesis under these conditions.

The generally high lactate content (*D* and/or *L*) (Supplementary Table 5, Supplementary Table 6) increased in both life-cycle stages under P-starvation, although non-significantly in the haploid stage (Figure 24 b, c). On transcriptome level, increases were observed for genes encoding *D*-lactate dehydrogenases for both life-cycle stages under P-starvation (Rokitta, 2016). In combination with other increased transcripts, authors hypothesized an upregulation

of the methylglyoxal pathway, with *L*-lactate as an intermediate, occurring under starvation and during cell-cycle arrest (Rokitta, 2016). Next to production of cytostatic methylglyoxal, this pathway represents an alternative way to synthesize cytoplasmic ATP under conditions where glycolytic flux is disturbed (Inoue, 1985; Chakraborty, 2014). The presence of the glycolytic bypass under P-starvation has been hypothesized for the diatom *Thalassiosira pseudonana* (Dyhrman, 2012), the pelagophyte *Aureococcus anophagefferens* (Wurch, 2011) and the chlorophyte *Selenastrum minutum* (Theodorou, 1991). The increased lactate content observed on metabolome level in this work could further supports this theory. However, as accumulation of an intermediate is not necessarily indicative of an upregulated pathway, flux-based analysis is necessary to confirm this theory.

Apart from lactate, cellular contents of small carboxylic acids doubled under P-starvation in both life-cycle stages (Supplementary Table 5, Supplementary Table 6), including metabolites from the tricarboxylic acid cycle, e.g. citrate and malate. Transcript abundance of genes encoding enzymes involved in the respiratory electron-transfer chain was decreased under P-starvation (Rokitta, 2016). Therefore, it is likely that malate and citrate accumulated because of decreased mitochondrial respiratory activity. Furthermore, increased transcript abundance of genes encoding malate-quinone-oxidoreductase was observed under P-starvation in both life-cycle stages (Rokitta, 2016). Authors hypothesized that under these conditions, electron transport to the respiratory chain via this enzyme is increased, in line with the higher malate abundance observed in this work. An increased lipid turnover was further hypothesized based on increased transcript abundances of genes encoding for enzymes involved in lipid buildup and breakdown (Rokitta, 2016). This could further explain increased citrate abundances observed in this work, as citrate can be converted to acetyl-CoA, which is proposed to be used for de-novo fatty acid synthesis (Bellou & Aggelis, 2012; Mühlroth, 2013; Avidan & Pick, 2015).

Under P-starvation, several pigment abundances significantly increased per cell in both life-cycle stages (Figure 24 b, c). For the diploid stage, two chlorophylls (chlorophyll a, chlorophyll c_2-MGDG) and five carotenoids (diatoxanthin, fucoxanthin, h4k-fucoxanthin, hex-fucoxanthin, β-carotene) were concerned, whereas in the haploid stage one chlorophyll (chlorophyll a) and three carotenoids (h4kfucoxanthin, hex-fucoxanthin, β-carotene) were affected. These results indicate increased light harvesting by chlorophyll and accessory pigments, as well as increased photoprotection via carotenoids. The diatoxanthin increase in the diploid stage was reflected by the significantly increased de-epoxidation ratio (Table 8), indicating an upregulation of the xanthophyll cycle and therefore photoprotection via non-

photochemical quenching under P-starvation. This was not observed for the haploid stage. As mentioned above, this type of photoprotection is typically observed under high light stress, also in diploid *E. huxleyi* strains (PLY 92, B11, CCMP 370) (Harris, 2005; Ragni, 2008; Garrido, 2016). The results from the growth phase experiment suggest that the diploid *E. huxleyi* strain RCC 1216 also uses this mechanism to fine tune its photosynthesis with regard to growth phase (5.3.1) and, in light of this experiment, in response to P-starvation. Furthermore the increased β-carotene abundance in both stages could be increased because of its precursor function for the other carotenoids (Lohr & Wilhelm, 1999; DellaPenna, 2004; Tanaka, 2008; Takaichi, 2011), or it could be involved in direct quenching of triplet chlorophylls or singlet oxygen species (Pogson, 2005) under these conditions.

Increased chlorophyll a concentration has been observed before in the diploid *E. huxleyi* strain CCMP 1516 under P-starvation (McKew, 2015). No data for haploid stages is available. In general, the response of microalgae towards P-starvation seems to be highly strain-specific. For example, P-starvation resulted in decreased pigment abundance in the dinoflagellate *Heterocapsa* sp. (Latasa & Berdalet, 1994), whereas in *Chlorella vulgaris* chlorophyll a was unchanged and photoprotective carotenoids increased (Kozlowska-Szerenos, 2004). In *Chlamydomonas reinhardtii* CS-51 chlorophyll a and photoprotective carotenoids were unchanged during the growth phase, except for one time point, where they were slightly higher than the nutrient-replete control (late-exponential growth phase) (Kamalanathan, 2016).

The connection between P-starvation and higher non-photochemical quenching has been shown for the chlorophyte *Dunaliella tertiolecta* (Petrou, 2008) and for rice (Xu, 2007). On a molecular level, activation of the xanthophyll cycle typically occurs in the presence of reactive oxygen species stress and electron pressure in the photosynthetic chain (Pogson, 2005). This can occur in *E. huxleyi* in response to P-starvation, as the increased number of pigments in the light harvesting antenna capture more photons. In this case, similar to high light intensities, the increased amount of transferred excitation energy leads to photochemical saturation of the P680 chlorophyll in the reaction center of photosystem II. To prevent excited chlorophylls from going into dangerous triplet states, xanthophyll cycle pigments effectively quench the energy, emitting it as heat, and the chlorophyll returns to its ground state (Pogson, 2005), as visualized in Figure 26 (5.3.1). The fact that these changes were not observed for the haploid stage under P-starvation once more emphasizes the difference between these two stages, and highlights possible differences in niche-occupation, as suggested previously (von Dassow, 2009; Rokitta, 2011). These results also explain the higher photosynthetic endurance of the diploid strain observed under P-starvation (Rokitta, 2016) and expand the knowledge regarding the diploid

stage's success in P-limited waters (Riegman, 1992; Egge & Heimdal, 1994; Tyrrell & Taylor, 1996; Riegman, 2000).

On transcriptomic level, P-starvation also resulted in differences regarding photosynthesis (Rokitta, 2016). However, these results do not necessarily match the observations of this work on metabolomic level. Authors observed decreased transcript abundances for genes encoding several enzymes involved in photosynthesis, xanthophyll cycle, as well as the synthesis of pigments, photosystems and plastidic ATP under P-starvation (Rokitta, 2016). Only few transcript abundances were increased, i.e. a transcript for a fucoxanthin chlorophyll a-c binding protein that protects against photooxidative stress (McKew, 2013a), indicating increased photoprotection. While this transcriptomic data suggested a general decrease of plastidic activity under P-starvation, the results of this work show that on metabolome level, functional pathways are increased, leading to an increase of pigment abundance. Pigment production is not influenced by the low P availability, in contrast to N-starvation (Figure 24 d, e), which is much more hampered, because chlorophyll precursor molecules and enzymatic machinery depend on N. Therefore, despite decreased levels of relevant transcripts, pigment synthesis pathways seem functional and even overproduce. This assumption is supported by the evidence on proteomic level, as increased light harvesting proteins were observed under P-starvation in *E. huxleyi* CCMP 1516 (McKew, 2015).

Many lipids increased in abundance under P-starvation in both life-cycle stages, including polar and neutral lipid fatty acids, and especially neutral storage lipids such as TAGs and PULCA (Figure 24 b, c). Glycerol 3-phosphate, a product from glycolysis, was significantly decreased or not detected in both stages. This metabolite is needed for glycerolipid synthesis (Sanjaya, 2013; Li-Beisson, 2016), and could be decreased due to increased lipid synthesis, or decreased glycolytic flux. This trend is in agreement with data for the diploid *E. huxleyi* strain CCMP 1516 under P-starvation, where polar lipids (McKew, 2015; Shemi, 2016) and neutral lipid abundance increased (McKew, 2015). However, these publications do not allow comparison of individual lipids or fatty acids, as they only state the total lipid amount. It is possible that the polar lipid increase is reflected in thylakoid membrane lipids, as especially unsaturated fatty acids were affected, which are major components of the thylakoid membrane lipids in *E. huxleyi* (Bell & Pond, 1996; Fulton, 2014). In line with the aforementioned theory of co-regulation of pigments and thylakoid lipids, it can be assumed that increases of thylakoid membrane lipids are connected to the observed increased pigment abundance, as thylakoid membrane lipids play an important role in photosynthesis (Murata, 1998; Kobayashi, 2016).

Under prolonged P-starvation, an accumulation of coccoliths has been observed (Paasche & Brubak, 1994; Paasche, 1998; Kayano & Shiraiwa, 2009; Satoh, 2009). Therefore, it could be possible that additional coccolith vesicles are needed, explaining increased abundances of polar lipid fatty acids. However, the increased coccolith production has been observed to be coupled to ceased cell division (Shiraiwa, 2003). In the later phases of P-starvation, when cells stop dividing, coccolith production continues in an undisturbed manner, resulting in additional layers of coccoliths around the cell (Shiraiwa, 2003). Therefore, it is unlikely that the increased polar lipid fatty acid abundance is explained by higher amounts of coccolith vesicles, as only one coccolith is produced at a time, the same as for dividing cells (Paasche, 2001).

With regard to lipids, transcriptomic data also indicated an increased metabolic carbon flow through the metabolism (Rokitta, 2016). It is likely that cells use lipogenesis under starvation conditions to dissipate photosynthate and reduction equivalents. This has been observed in other microalgae, e. g. *Chlamydomonas reinhardtii* under N- and P-starvation (Kamalanathan, 2016). Furthermore, a shift from phospholipids to betaine lipids can be anticipated, as this has been observed for *E. huxleyi* and other phytoplankton under P-starvation conditions (van Mooy, 2009; McKew, 2015; Shemi, 2016), in agreement with the increased abundance of betaine compounds, such as glycine betaine (Figure 24 b, c).

Observations regarding the alkenone unsaturation index indicate that the calculation of alkenone relevant parameters is highly influenced by nutrient starvation, as the $U^{K'}_{37}$ value increased significantly for the haploid stage under both P- and N-starvation (Table 7). Nutrient-starvation induced changes of $U^{K'}_{37}$ have been observed for diploid *E. huxleyi* strains previously, as stationary phase mediated N-starvation lead to an increased $U^{K'}_{37}$ value in strain CCMP 372 (Epstein, 1998), whereas stationary phase mediated P- and N-starvation lead to a decrease of $U^{K'}_{37}$ in strain NEPCC 55a (Prahl, 2003). No data is available for haploid life-cycle stages. These results imply that caution should be applied in reconstruction of past sea surface temperatures, if the possibility exists that waters were nutrient limited, as stated previously (Epstein, 1998; Prahl, 2003).

In summary, many metabolic responses of both life-cycle stages under P-starvation confirmed the transcriptome-based model (Rokitta, 2016), with regard to central carbon metabolism, cell-cycle arrest, activation of glycolytic bypass, as well as increased lipid turnover and decreased mitochondrial oxidation. However, pigment synthesis and plastid activity were increased on the metabolome level, because N-containing precursors were not lacking. The validation of the proposed model by the metabolome data of this work is shown in Figure 27 (page 109). Comparison of the metabolome data presented in this work and the previously

published transcriptome data of the same *E. huxleyi* life-cycle stages under P- and N-starvation once again highlights that conclusions derived from different omics-levels can diverge strongly (Feder & Walser, 2005). In response to nutrient starvation, gene expression patterns triggered by cells set the boundary conditions. Nevertheless, the instantaneous molecular fluxes and metabolic equilibria dominate the phenotype and therefore may not be neglected. Transcriptomic settings can result in very different phenotypes, depending on metabolite flux and precursor production.

E. huxleyi is known to efficiently scavenge inorganic P from dissolved organic matter under P-starvation, using highly efficient alkaline phosphatases, which are upregulated under these conditions and cleave 5'-phosphate groups from DNA, RNA, nucleotides and proteins by hydrolysis of phosphate-ester bonds (Riegman, 2000; McKew, 2015; Shemi, 2016). Furthermore, marine microalgae, including *E. huxleyi*, efficiently cycle polyphosphate and substitute phospholipids by non-phosphorus containing lipids (van Mooy, 2009; Martin, 2014). The results of this work expand knowledge of *E. huxleyi*'s P-starvation response to the metabolomic level, showing that its phosphorus recycling is efficient enough to lead to upregulation of certain metabolites, such as pigments, to prolong survival and fend of cell death as long as possible. These results contribute to the explanation of the diploid *E. huxleyi*'s success in P-limited waters (Riegman, 1992; Egge & Heimdal, 1994; Tyrrell & Taylor, 1996; Riegman, 2000).

5.4.3 Life-cycles cope differently with N-starvation

Diverging results were obtained for N-starvation in both stages, suggesting a life-cycle stage specific response (Figure 24 d, e). So far, studies have focused exclusively on the diploid stage with regard to specific metabolite classes under N-starvation (Turner, 1988; Keller, 1999; Stolte, 2000; Loebl, 2010; McKew, 2015; Malitsky, 2016).

Regarding significantly and at least 1.5-fold changes metabolites (28.6 and 42.9 % for 2N and 1N, respectively), the majority was decreased in the diploid stage (80.0 %), and increased in the haploid stage (77.8 %) (Figure 24 d, e). General metabolites decreased in both life-cycle stages, e.g. N-rich amino acids asparagine and glutamine, however, other metabolites increased selectively in the haploid stage, such as various carbon-rich amino acids and small carboxylic acids.

Especially metabolites containing several nitrogen atoms were decreased in abundance, such as nucleotides and nucleosides. Here adenine was decreased significantly in the diploid stage, adenosine was decreased in both stages, although non-significantly so (Figure 24 d, e). This suggests impaired DNA and RNA synthesis, as well as decreased cofactor abundance

(ATP, NAD, FAD) in response to N-starvation. Transcriptome data support this assumption, as transcript abundance of genes coding for synthesis of nucleic acid bases was significantly decreased under N-starvation (Rokitta, 2014; Rokitta, 2016). Authors further drew the connection to cell-cycle arrest under starvation, which can be assumed to take place in this work.

One of the most abundant metabolites in the dataset was mannitol, a sugar alcohol with osmoprotective properties (Supplementary Table 5, Supplementary Table 6). This is confirmed by previous studies, where it was suggested to play a role in carbon and reductant storage (Obata, 2013; Mausz & Pohnert, 2015; Tsuji, 2015). In contrast to the non-significant decreases observed under P-starvation, decreases were significant in both life-cycle stages under N-starvation (Figure 24 d, e, 1.3- and 9.8-fold for 1N and 2N, respectively). A decrease of mannitol abundance has been observed in the stationary growth phase for these *E. huxleyi* life-cycle stages (Mausz & Pohnert, 2015). These results indicate that mannitol is used to fuel carbohydrate metabolism when photosynthetic production is impaired, to mobilize reduction equivalents such as NADH and to maintain redox homeostasis in the cytoplasm.

Several amino acids decreased in the diploid stage under N-starvation (Figure 24 d). All proteinogenic amino acids contain N and are primarily affected if N is limiting (Barsanti & Gualtieri, 2006). This influences protein abundance, which has been shown to decrease under N-starvation in the diploid *E. huxleyi* strain CCMP 1516, in line with increased proteins involved in degradation (McKew, 2015). In the haploid stage, several amino acid abundances were increased (Figure 24 e), hinting towards life-cycle specific prioritizations of metabolic pathways. However, N-rich amino acids, such as asparagine and glutamine, were also decreased in the haploid stage, indicating that N-starvation did affect this stage on level of amino acid biosynthesis.

Similar to the observations under P-starvation, proline increased in both life-cycle stages under N-starvation, although only significantly for the haploid stage. This is in line with the transcriptomic-based hypothesis of increased proline oxidation and throttled ornithine urea cycle pathways under N-starvation (Phang, 2012; Rokitta, 2014; Rokitta, 2016), as mentioned above for P-starvation. The increase of proline under both P- and N-starvation indicates a superior role of these pathways in regulating cellular growth, and potentially linking the nitrogen metabolism to the mitochondrial activity of the cell and producing toxic ROS.

The osmolyte composition further highlighted the differences of both life-cycle stages in coping with N-starvation. Osmolytes containing N, such as glycine betaine and homarine, significantly decreased or were undetectable in the diploid stage, whereas N-independent

DMSP was unchanged (Figure 24 d, e). In the haploid stage, N-containing glycine betaine decreased, whereas DMSP and homarine significantly increased. These differences could indicate different capabilities and prioritizations of the life-cycle stages regarding N shuttling and recycling into different pathways. Controversial trends regarding DMSP abundance under N-starvation have been reported for different diploid *E. huxleyi* strains. For a further undefined diploid strain, a 50 % increase was observed (Turner, 1988), whereas DMSP abundance decreased for the diploid *E. huxleyi* strain CCMP 378, along with glycine betaine (Keller, 1999). Data for haploid life-cycle stages under N-starvation has not been available until this work. Increases of DMSP under N-starvation have been reported for the marine prasinophyte *Tetraselmis subcordiformis* (Gröne & Kirst, 1992) and phytoplankton communities have been shown to produce more DMSP under N-starvation (Turner, 1988).

DMSP has been proposed to replace N-containing compatible solutes, such as glycine betaine (Turner, 1988; Gröne & Kirst, 1991) or proline (Bucciarelli & Sunda, 2003) under N-starvation. However, these hypotheses have not been proven. The data of this work indicates that replacement of proline by DMSP does not happen in *E. huxleyi* under N-starvation, as proline is increased in abundance, as discussed above. Replacement of glycine betaine by DMSP could be true for the haploid stage. However, as methionine is suggested to be the biosynthetic precursor for DMSP (Gröne & Kirst, 1992; Gage, 1997), an increased DMSP abundance could simply be the result of increased methionine abundance, which could occur due to enhanced protein degradation under N-starvation (McKew, 2015), increased methionine uptake or lowered methionine consumption (Gröne & Kirst, 1992). The results of this work support this theory, as methionine abundance was significantly increased in the haploid stage (3.9-fold) under N-starvation, in line with increased DMSP abundance (Figure 24 d). This was not the case in the diploid stage, further emphasizing the differential pathway priorities of the life-cycle stages.

In both life-cycle stages, pigment abundances were decreased under N-starvation (Figure 24 d, e), although not significantly for every pigment. Diatoxanthin and various fucoxanthins were decreased more than 1.5-fold in both life-cycle stages, significant decreases were found for the haploid stage regarding chlorophyll c_3, diadinoxanthin, diatoxanthin, fucoxanthin and h4k-fucoxanthin. The de-epoxidation ratio significantly decreased in both life-cycle stages (Table 8), indicating that photoprotection via xanthophyll cycle-mediated non-photochemical quenching was not possible under N-starvation. Decreased pigment abundance under N-starvation has been reported previously for other *E. huxleyi* strains (Stolte, 2000; Loebl, 2010) and other microalgae (Latasa & Berdalet, 1994; Li, 2008; Ördög, 2012; Zhang,

2013). Furthermore, it was suggested that N-rich chlorophylls could be recycled under N-starvation to support further growth (Li, 2008; Ördög, 2012).

Missing N directly affects chlorophyll synthesis, which relies on N-containing precursors, such as glutamine (Porra, 1997; Wilhelm, 2006), which was significantly decreased in both life-cycle stages in this work (Figure 24 d, e). Also, the diploid stage has been shown to be more efficient regarding photosynthesis under these conditions, as F_v/F_m values stayed constant for the diploid stage under N-starvation, while they dropped for the haploid stage (Rokitta, 2014). F_v/F_m describes the normalized ratio of variable fluorescence to maximum fluorescence, therefore allowing estimations of the maximum quantum efficiency of photosystem II photochemistry (Baker & Oxborough, 2004). This could explain the more distinct decreases of pigments for the haploid stage, again pointing out different capabilities of the two life-cycle stages.

The results from this work are in line with transcriptome data for the same life-cycle stages, where N-starvation resulted in decreased transcript abundances for genes encoding several critical components of the photosystem, such as light harvesting antenna, the xanthophyll cycle, as well as plastidic ATP and chlorophyll synthesis (Rokitta, 2014). Differences between life-cycle stages were also observed, as transcript abundances for genes encoding fucoxanthin-chlorophyll a-c binding proteins increased in the diploid stage. As these proteins are typically increased for photoprotection under high light (McKew, 2013b), this could also explain the less severe pigment decreases (Figure 24 d, e) and better photosynthetic performance observed in the diploid stage (Rokitta, 2014). These results suggest that, in contrast to P-starvation, N-starvation results in decreased metabolic flux of N-containing precursors into pigment synthesis pathways. Subsequently, pigment content in the light harvesting antenna is decreased, lowering light harvesting and photosynthetic efficiency.

Certain lipids were decreased under N-starvation in the diploid stage, such as polar and neutral lipid fatty acids and TAGs (Figure 24 d, e), in agreement with other studies analyzing total lipid classes (McKew, 2015). Some fatty acids were decreased in both life-cycle stages, such as $C_{18:0}$ in the neutral lipid fraction and $C_{18:3n3}$ in the polar lipid fraction, indicating lipid rearrangements in both stages. This was also predicted from transcriptomic data (Rokitta, 2014). It is also possible that thylakoid membrane lipids were impaired in the diploid stage, as polyunsaturated fatty acids, typical for thylakoid membranes in *E. huxleyi* (Bell & Pond, 1996; Fulton, 2014), were decreased. Again, this could be connected to the decreased pigment abundance, as discussed above. However, life-cycle specific differences in coping with N-starvation were also observed, as most polar fatty acid abundances were unchanged in the

haploid stage, indicating that membrane lipids were not impaired under these conditions. Also this stage increased TAGs and PULCA, in line with decreased glycerol 3-phosphate, indicating a need to build up neutral storage lipids under N-starvation, in contrast to the diploid stage. Increases of TAG have been observed under N-starvation, however in a different diploid strain (Malitsky, 2016).

In summary, N-starvation had a more severe impact on the metabolome than P-starvation, as missing N directly impaired amino acid and pigment synthesis. Generally speaking, the changes observed on metabolomic level under N-starvation confirmed those predicted from transcriptomic data for the same life-cycle stages (Rokitta, 2014; Rokitta, 2016), with some exceptions. Figure 27 shows the validation of the transcriptome-based model under P- and N-starvation with the metabolic data of this work.
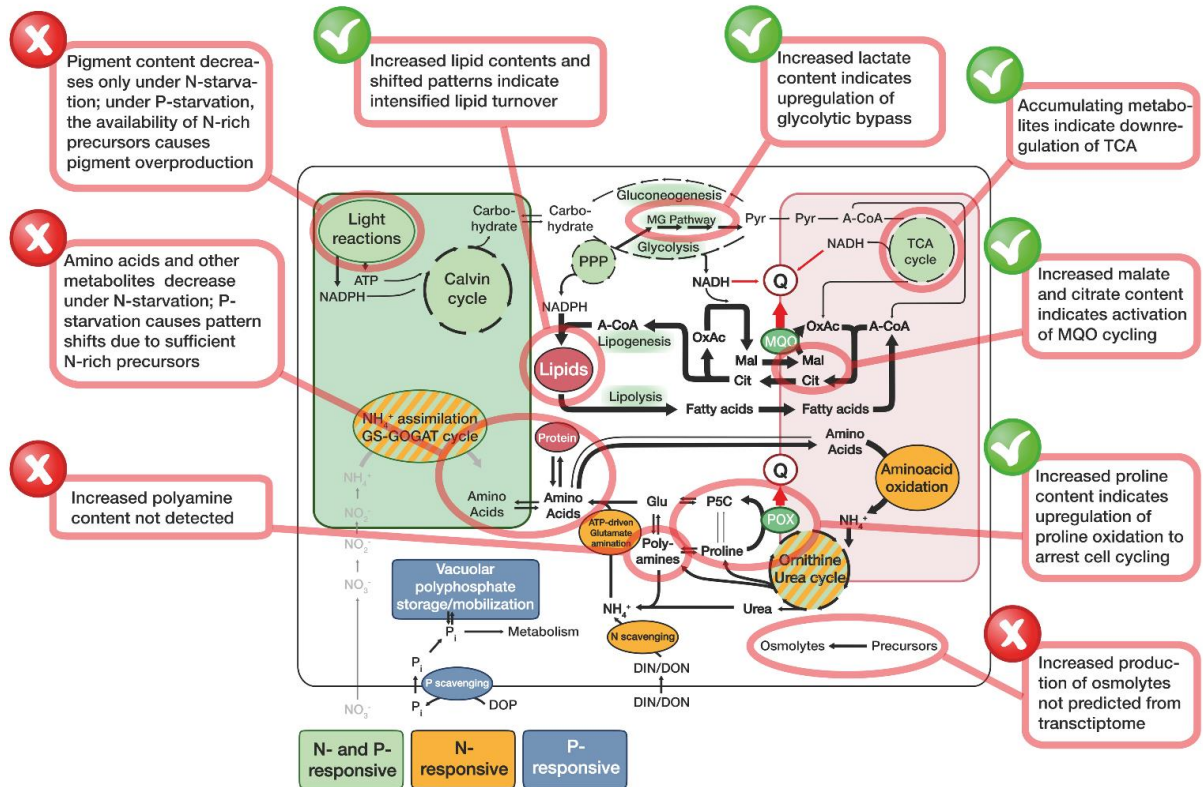
Figure 27: Validation of a generalized metabolic model of the *E. huxleyi* metabolism under P- and N-starvation, derived from transcriptomic data (Rokitta, 2016), with metabolomic data gathered in this work. ✓ **indicates that assumption from transcriptomic data was verified by metabolic data, X indicates that is was not verified**. **In more detail, Rokitta and coworkers (2016) predicted the following metabolic changes based on transcriptomic data. Under both P- and N-starvation, photosynthetic light reactions and carbon fixation are decreased, minimizing carbon flux into glycolysis and tricarboxylic acid cycle (TCA). The citrate shuttle is strongly induced, suggesting increased export of acetyl-CoA (A-CoA) into the cytoplasm. Lipid synthesis and turnover are increased, providing sinks for reduction equivalents. Cells increase malate-quinone-oxidoreductase (MQO), contributing to electron input for oxidative phosphorylation (quinone-pool, Q). Under N-starvation, mitochondrial amino acid oxidation is increased, together with cytoplasm-based glutamate amination. Ornithine-urea cycle (OUC) enzymes are throttled, possibly resulting an accumulation of OUC intermediates, especially proline and polyamines. Proline oxidase (POX) is increased under both P- and N-starvation, suggesting that oxidation of proline to pyrroline-5-carboxylate (P5C) delivers reductants into the mitochondria for Q. Especially the diploid stage increases scavenging of dissolved inorganic/organic nitrate (DIN/DON) under N-starvation, where nitrate uptake and subsequently nitrate assimilation via the GC-GOGAT (glutamine synthase-glutamine oxoglutarate aminotransferase) cycle are decreased. This stage also especially increases dissolved organic phosphate (DOP) scavenging (Rokitta, 2016). See text in boxes for validation of this transcriptomic derived model with the metabolomic data of this work. Cit, citrate; Mal, malate; Glu, glutamic acid; MG, methylglyoxal; OxAc, oxaloacetate; PPP, pentose phosphate pathway; Pyr, pyruvate. This figure was modified from Rokitta (2016), image license CC BY 4.0.**

6. Conclusion

Metabolomics is a powerful tool which can provide novel insights to understanding microalgae physiology. By applying different analytical methods, a comprehensive metabolome analysis was conducted for a calcifying, diploid and a non-calcifying, haploid *E. huxleyi* life-cycle stage. On the level of proteins, carbohydrates and lipids, no significant difference was observed between both stages, analyzed by FTIR. However, in-depth metabolomic analyses highlighted differences between both life-cycle stages, especially regarding pigments, osmolytes as well as membrane and storage lipid associated fatty acids. These life-cycle specific differences can partly be attributed to general physiological differences between stages. For example, the higher abundance of the osmolyte DMSP in the diploid, calcifying stage could be necessary to regulate osmolarity due to the preconcentration of Ca^{2+} in special vacuole-like compartments (Sviben, 2016). The higher abundance of polar lipid fatty acids could in turn be connected to the formation of these vesicles, as well as coccolith vesicles, which are absent in the haploid, non-calcifying stage. The higher abundance of alkenones (neutral storage lipids) could be connected to coccolith vesicles, however this is still under debate (Sawada & Shiraiwa, 2004; Eltgroth, 2005). The haploid stage was characterized by a higher abundance of carboxylic acids, which could be linked to the driving of flagellar motion only present in the haploid stage. The more efficient photoprotection via the xanthophyll cycle in the diploid stage, regarding later growth phases and P-starvation, could be attributed this stage's high light tolerance (Nanninga & Tyrrell, 1996; Ragni, 2008; Loebl, 2010) and success in P-limited waters (Riegman, 1992; Egge & Heimdal, 1994; Tyrrell & Taylor, 1996; Riegman, 2000), as well as to differences in niche occupation, suggested for these life-cycle stages (Frada, 2008; von Dassow, 2009; Rokitta, 2011).

Metabolome analysis at three different harvesting time points revealed growth phase-dependent differences regarding pigments and fatty acids. Results implied that photosynthesis and thylakoid membrane abundance decrease in the late-exponential and stationary growth phase, compared to the early-exponential growth phase, in line with the lower energy demand of the non-dividing cell. The gathered data underlines the importance of analyzing more than one time point in physiological studies. This can also be important with regard to biotechnologically relevant products, such as the ω-3 fatty acid DHA or the uncommon pigment hex-fucoxanthin.

Metabolome analysis under P-starvation and N-starvation allowed observations on how *E. huxleyi* copes with nutrient starvation, which is a common scenario in the ocean (Moore, 2013; Palenik, 2015). While both starvation scenarios eventually result in cell death, both life-

cycle stages coped exceptionally well with P-starvation, which caused a `metabolic overflow´. N-starvation hampered many metabolic processes, resulting in decreases for many metabolites, especially in the diploid stage. Under both scenarios, amino acids were recycled, especially with respect to proline, and mannitol and neutral lipids served as carbon and reductant storage.

It is interesting to speculate where the different starvation scenarios are sensed and integrated. Under P-starvation, ATP synthesis is decreased, resulting in an increased H^+ gradient in the plastid (and in the mitochondria), leading to a possible over-reduction of the electron transfer chain. Under N-starvation, the photosynthetic electron transfer chain is over-reduced, due to missing plastidary nitrate assimilation, therefore not dissipating electrons from reduced ferredoxin (Rokitta, 2014). Thus, it is likely that these starvation scenarios are sensed and integrated at the same points, namely mitochondria and plastids.

Transcriptomic studies showed very similar responses toward both starvation scenarios (Rokitta, 2011; Rokitta, 2014; Rokitta, 2016), however, the metabolomic data obtained in this work highlight that there are further regulatory processes involved on post-transcriptional/-translational level (Feder & Walser, 2005), as P- and N-starvation result in very different phenotypes on metabolome level. N-starvation also has more severe effects on biochemical processes, impairing nucleotide and amino acid biosynthesis, as well as enzymatic machinery. P-starvation mainly affects nucleoside-triphosphate synthesis, therefore the energy budget and DNA/RNA synthesis, as well as enzyme phosphorylation. Therefore, even though decreased transcript levels of genes encoding pigment biosynthesis were observed under both nutrient starvation scenarios (Rokitta, 2014; Rokitta, 2016), the enzyme content and metabolic flux of precursors are still adequate under P-starvation, resulting in high pigment production, whereas N-starvation directly constrains pigment precursor synthesis. These results highlight the importance of instantaneous biochemical metabolite flux, which can influence metabolite production in the same way as transcriptomically rearranged pathway patterns.

Limitations of this work are reflected in the limited number of detected metabolites, which did not enable complete metabolic pathway reconstruction. This is a typical problem with metabolomics, as current analytical instrumentation does not allow quantitative analysis of all metabolites (Dettmer, 2007; Villas-Bôas, 2007). Next steps could include feeding isotope-labeled precursors, therefore enabling detailed metabolite flux analysis (Buescher, 2015).

The metabolomic data obtained in this work allowed retracing of major reconstellations in biochemical pathways, resulting in a converging picture of cellular reactions with regard to life-cycle stages, growth phase and nutrient starvation. The gathered data can be used to concretize existing metabolic models (Knies, 2015) and offers valuable clues on how eukaryotic cells react

to nutrient stress. The broad array of applied metabolomic analysis methods can easily be adapted to assess a wide range of metabolites in other microalgae.

List of publications

Published papers:

- Lauersen, K. J., Baier, T., Wichmann, J., **Wördenweber, R.**, Mussgnug, J. H., Hübner, W., Huser, T., Kruse, O. (2016): Efficient phototrophic production of a high-value sesquiterpenoid from the eukaryotic microalga *Chlamydomonas reinhardtii. Metab. Engin.* **38**, 331–343, doi: 10.1016/j.ymben.2016.07.013.

- Jaeger, D., Pilger, C., Hachmeister, H., Oberländer, E., **Wördenweber, R.**, Wichmann, J., Mussgnug, J. H., Huser, T., Kruse, O. (2016): Label-free *in vivo* analysis of intracellular lipid droplets in the oleaginous microalga *Monoraphidium neglectum* by coherent Raman scattering microscopy. *Sci. Rep.* **6**, 35340, doi:10.1038/srep35340.

Submitted papers:

- **Wördenweber, R.**, Rokitta, S. D., Heidenreich, E., Corona, K., Kirschhöfer, F., Fahl, K., Klocke, J. L., Kottke, T., Brenner-Weiß, G., Rost, B., Mussgnug, J. H., Kruse, O. (submitted): Phosphorus and nitrogen starvation reveal life-cycle specific responses in the metabolome of *Emiliania huxleyi* (Haptophyta).

- Chaudhari, S., Blifernez-Klassen, O., Klassen, V., **Wördenweber, R.**, Steffens, T., Cholewa, D., Kruse, O. (submitted): Systematic metabolic characterization of *Botryococcus braunii* CCAP 807/2 (race A) reveals distinct growth and hydrocarbon/carbohydrate-production phases.

List of tables

List of figures

Appendix

Supplementary Figure 1: Calibration curves of individual commercial fatty acid methyl esters standards measured via ion trap GC-MS. Note fixed y-axis. In all cases, linear regression did not result in accurate description, whereas second degree polynomic fit accurately described the curves, as shown in Supplementary Table 1. Mean values and standard deviation of four replicates are shown.

Supplementary Table 1: Coefficients for calibration of FAME concentrations, derived from second degree polynomic fit with the equation $y = a \cdot x^2 + b \cdot x + c$, x being concentration [µg mL^{-1}] and y being peak area [-]. Valid for the given peak area region, grouped by color.

FAME	a	b	c	R^2	lower limit peak area	upper limit peak area
C8:0	764.77	131,277.41	-250,741.02	1.0000	2.68E+05	1.08E+07
C10:0	1,156.84	261,766.13	-186,287.87	1.0000	1.09E+05	2.04E+07
C12:0	2,679.32	384,500.22	-286,046.58	1.0000	1.62E+05	3.37E+07
C14:0	4,170.00	550,583.00	-295,214.00	0.9999	4.10E+04	4.97E+07
C15:0	9,259.60	583,011.00	-170,896.00	0.9999	1.70E+04	2.67E+07
C16:0	4,295.20	723,538.00	-638,521.00	0.9999	4.30E+05	1.03E+08
C16:1n5	16,064.00	649,451.00	-219,154.00	0.9999	3.22E+04	3.52E+07
C17:0	9,526.90	527,983.00	-260,185.00	0.9999	8.50E+04	2.51E+07
C18:0	8,121.50	884,677.95	-499,388.78	0.9999	4.91E+04	8.53E+07
C18:1n9c	19,703.01	2,107,362.18	-1,319,062.59	0.9999	6.66E+05	2.04E+08
C18:1n9t	16,134.56	1,050,560.86	-283,997.70	0.9999	2.63E+04	4.76E+07
C18:2n6c	18,598.00	886,690.00	-316,190.00	0.9999	4.75E+04	4.49E+07
C18:3n3	21,832.00	716,059.00	-171,914.00	0.9998	3.03E+04	4.22E+07
C20:0	4,803.43	463,682.52	-292,386.98	0.9999	2.99E+04	4.68E+07
C20:1	10,623.64	1,057,173.64	-691,597.01	0.9999	5.43E+04	1.05E+08
C20:2	20,937.50	1,012,005.50	-385,322.75	0.9998	3.12E+04	5.07E+07
C20:3	20,139.20	937,730.20	-345,609.24	0.9999	3.37E+04	4.79E+07
C20:4n6	22,065.15	774,337.56	-512,720.40	0.9999	8.69E+04	4.45E+07
C20:5n3	17,214.85	868,381.25	-547,990.13	0.9999	8.30E+04	4.28E+07
C22:0	12,161.15	1,202,058.58	-848,477.52	0.9999	5.64E+04	1.20E+08
C22:1n9	25,019.74	1,329,297.30	-486,382.64	0.9999	4.02E+04	6.46E+07
C22:6n3	21,352.84	680,523.28	-519,674.21	0.9999	3.33E+04	4.10E+07
C24:0	14,328.93	1,229,555.93	-930,989.75	0.9999	6.29E+04	1.30E+08
C24:1	33,400.57	1,036,607.14	-440,521.15	0.9998	3.09E+04	6.36E+07

Supplementary Table 2: Retention time (RT) at 440 nm and characteristic absorption maximum of commercial pigment standards measured via UV-vis-HPLC. Note that absorption of isolated pigments differs from pigments *in vivo*, also dependent on used solvent. Pigments that were detected in *E. huxleyi* RCC 1216 (2N) and 1217 (1N) are shaded in grey. Asterisk indicates carotenoid with light harvesting function in different *E. huxleyi* strains.

Type of pigment	Pigment	Solvent	RT [min]	Absorption maxima [nm]
chlorophyll	chlorophyll c_3	90 % acetone	5.55	459
chlorophyll	chlorophyll c_2	90 % acetone	8.66	449
carotenoid	peridinin	ethanol	10.21	475/629
carotenoid*	but-fucoxanthin	ethanol	11.87	448/472
carotenoid*	fucoxanthin	ethanol	14.42	452/463
carotenoid*	h4k-fucoxanthin	ethanol	15.75	448/469
carotenoid*	hex-fucoxanthin	ethanol	16.92	449/469
carotenoid	neoxanthin	ethanol	17.13	414/437/465
carotenoid	violaxanthin	ethanol	24.18	417/440/469/630
carotenoid	diadinoxanthin	ethanol	34.43	447
carotenoid	antheraxanthin	ethanol	37.22	446/474
carotenoid	diatoxanthin	ethanol	43.27	453/480
carotenoid	canthaxanthin, trans	ethanol	43.43	474
carotenoid	lutein	acetone	43.62	445/455
carotenoid	zeaxanthin	acetone	44.54	455/479
chlorophyll	chlorophyll b	acetone	49.34	465/642
carotenoid	echinenone	ethanol	52.63	463
chlorophyll	chlorophyll c_2-MGDG	90 % acetone	54.41	456
chlorophyll	chlorophyll a	acetone	56.70	430/651/664
carotenoid	lycopene	acetone	57.78	447/473/503
carotenoid	α-carotene	acetone	64.29	448/475
carotenoid	β-carotene	acetone	65.09	454/479
carotenoid	pheophytin	acetone	67.09	409

Supplementary Table 3: Metabolome data for diploid *E. huxleyi* life-cycle stage in growth phase experiment. Abundance of pigments and fatty acids per cell for nutrient-replete cells harvested in different growth phases (early-exponential (t_1), late-exponential (t_2) and stationary phase (t_3)). Mean values and standard deviation of two biological and three technical replicates are shown.

Class	Metabolite	2N					
		t_1	SD	t_2	SD	t_3	SD
pigments [(rel. abund. cell^{-1}) 10^3]	chlorophyll a	198.24	8.87	44.67	2.49	28.42	6.94
	chlorophyll c_2	96.08	13.18	24.46	0.84	12.59	3.47
	chlorophyll c_2-MGDG	41.99	2.72	10.95	0.53	6.50	1.88
	chlorophyll c_3	73.76	3.87	27.80	1.39	20.29	5.35
	diadinoxanthin	153.88	11.52	48.17	10.03	22.69	7.65
	diatoxanthin	13.18	1.42	19.36	5.23	36.63	9.99
	fucoxanthin	47.50	3.57	7.49	0.63	3.48	0.80
	h4k-fucoxanthin	36.39	15.82	9.84	0.16	10.88	3.24
	hex-fucoxanthin	266.54	14.63	84.68	4.05	55.90	14.42
	β-carotene	7.28	0.48	1.53	0.45	1.07	0.55
polar lipid fatty acids (FAME) [ag cell^{-1}]	C14:0	228.30	33.89	74.58	25.57	59.89	13.44
	C15:0	30.45	1.96	12.46	4.31	10.39	2.34
	C16:0	469.74	147.86	116.03	43.82	106.89	29.31
	C18:0	450.80	91.00	75.66	20.31	71.02	18.17
	C18:1n9c	364.87	53.10	65.88	19.37	38.20	7.89
	C18:1n9t	49.42	1.97	10.23	1.86	12.29	3.15
	C18:2n6c	113.63	13.87	10.34	2.17	6.36	0.91
	C18:3n3	359.29	62.46	110.11	24.88	78.02	11.21
	C18:4n3	245.77	29.44	75.84	12.31	58.25	6.81
	C20:0	50.64	2.46	6.68	0.62	5.71	0.88
	C20:2	26.88	0.76	3.54	0.34	2.59	0.31
	C22:0	57.94	3.39	13.59	4.12	11.41	2.11
	C22:1n9	44.83	6.00	6.33	1.09	5.69	0.94
	C22:6n3	331.91	58.56	201.20	34.31	168.79	31.94
neutral lipid fatty acids (FAME) [ag cell^{-1}]	C14:0	0.00	0.00	0.00	0.00	0.00	0.00
	C15:0	22.37	4.48	2.50	0.10	2.36	0.58
	C16:0	86.37	12.29	10.90	0.75	9.01	1.61
	C18:0	87.70	13.35	9.53	0.68	7.67	1.42
	C18:1n9c	58.09	2.76	7.91	0.66	5.33	1.25
	C18:1n9t	24.07	2.09	0.00	0.00	2.79	0.59
	C18:2n6c	27.10	2.74	1.55	1.56	2.58	0.59
	C18:3n3	21.60	1.39	2.99	0.50	1.64	0.32
	C18:4n3	25.26	3.00	3.30	0.15	2.60	0.38
	C22:0	46.57	3.99	5.61	0.32	4.21	0.83
	C22:6n3	59.13	12.98	0.00	0.00	5.19	0.95

Supplementary Table 4: Metabolome data for haploid _E. huxleyi_ life-cycle stage in growth phase experiment. Abundance of pigments and fatty acids per cell for nutrient-replete cells harvested in different growth phases (early-exponential (t_1), late-exponential (t_2) and stationary phase (t_3)). Mean values and standard deviations (SD) of two biological and three technical replicates are shown.

Class	Metabolite	1N					
		t_1	SD	t_2	SD	t_3	SD
pigments [(rel. abund. cell^{-1})·10^3]	chlorophyll a	271.71	173.06	45.23	7.25	21.33	15.50
	chlorophyll c_2	204.70	136.98	32.01	10.31	12.72	9.10
	chlorophyll c_2-MGDG	60.57	40.15	10.12	2.01	4.70	3.50
	chlorophyll c_3	141.93	109.01	28.63	2.67	14.08	12.30
	diadinoxanthin	159.01	117.31	31.57	1.76	20.35	17.59
	diatoxanthin	50.45	46.15	19.66	6.82	8.47	8.17
	fucoxanthin	49.75	34.71	7.70	2.00	3.04	2.31
	h4k-fucoxanthin	20.46	18.41	6.05	1.46	3.75	3.65
	hex-fucoxanthin	451.67	317.61	89.02	10.79	39.91	32.14
	β-carotene	8.32	4.54	0.96	0.22	0.39	0.29
polar lipid fatty acids (FAME) [ag cell^{-1}]	C14:0	115.31	20.12	89.97	16.72	59.11	8.57
	C15:0	30.87	2.57	10.15	1.47	7.74	1.21
	C16:0	432.78	81.22	100.28	14.90	87.61	18.72
	C18:0	405.92	78.89	64.20	10.86	58.57	11.73
	C18:1n9c	55.42	16.91	18.58	4.91	17.66	2.60
	C18:1n9t	46.75	3.71	7.95	1.36	14.53	1.72
	C18:2n6c	36.01	3.65	4.83	1.12	4.00	0.52
	C18:3n3	27.00	5.17	16.59	6.11	25.52	6.39
	C18:4n3	18.07	1.60	8.76	2.84	13.20	3.01
	C20:0	57.73	5.68	6.57	1.28	5.21	0.77
	C20:2	29.03	2.12	3.08	0.67	2.55	0.33
	C22:0	52.87	4.28	5.65	1.20	3.30	2.37
	C22:1n9	37.77	4.37	3.82	0.77	3.48	0.62
	C22:6n3	54.21	4.28	15.54	5.33	33.25	9.63
neutral lipid fatty acids (FAME) [ag cell^{-1}]	C14:0	0.00	0.00	0.00	0.00	0.00	0.00
	C15:0	25.87	3.56	2.31	0.19	2.01	0.17
	C16:0	116.29	15.96	11.11	0.77	10.39	1.45
	C18:0	106.41	12.21	10.31	0.64	9.14	1.26
	C18:1n9c	68.16	6.94	6.22	0.47	5.53	0.58
	C18:1n9t	28.40	3.40	2.73	0.18	2.66	0.45
	C18:2n6c	30.93	3.04	3.06	0.19	2.50	0.30
	C18:3n3	19.53	2.76	1.87	0.10	1.58	0.18
	C18:4n3	27.55	3.20	2.62	0.19	2.30	0.25
	C22:0	55.75	6.98	5.40	0.37	4.73	0.57
	C22:6n3	0.00	0.00	0.00	0.00	4.97	0.59

Supplementary Table 5: Metabolite abundances for the P-starvation setup. Diploid (2N) and haploid (1N)
E. huxleyi **life-cycle stages under replete (R) and phosphate-starved (-P) conditions. Mean values and standard deviations (SD) of three biological and two/three technical replicates are shown. Asterisks indicate putatively identified metabolites. n.d., not detected; glycerol 2-p, glycerol 2-phosphate; glycerol 3-P; glycerol 3-phosphate.**

Class	Metabolite	2N R	SD	2N -P	SD	1N R	SD	1N -P	SD
					Phosphate starvation				
Metabolites (TMS-derivatives, GC-MS) [(rel. abund. cell^{-1})·10^{10}]	O-acetyl-serine*	1.57	0.62	1.37	0.64	2.15	0.28	1.77	0.34
	homoserine	0.28	0.13	0.11	0.04	0.48	0.25	0.18	0.05
	pyroglutamate*	1.18	0.67	1.69	1.29	7.95	1.45	8.63	1.18
	adenine*	5.89	2.69	3.19	1.62	1.58	0.26	5.46	1.77
	adenosine	0.84	0.16	0.36	0.16	0.38	0.04	0.43	0.04
	threonic acid	0.94	0.52	0.95	0.32	2.09	0.34	1.58	0.22
	mannitol	31.72	10.95	17.24	3.33	12.02	2.50	10.13	1.21
	myo-inositol	0.80	0.39	2.60	0.60	1.06	0.04	1.65	0.24
	arabinose	0.08	0.04	0.08	0.02	0.19	0.05	0.07	0.04
	fructose	0.47	0.17	0.39	0.09	0.57	0.05	0.37	0.07
	galactose	2.12	0.89	5.27	1.11	3.17	0.51	5.49	0.78
	maltose	0.25	0.09	1.18	0.39	1.42	0.20	0.25	0.04
	melibiose	0.14	0.03	1.54	0.58	0.15	0.02	0.39	0.10
	ribose	0.35	0.14	0.48	0.13	0.83	0.10	1.16	0.15
	saccharose	1.07	0.33	2.53	0.88	2.40	0.42	0.36	0.81
	xylose	0.07	0.03	0.14	0.05	0.15	0.01	0.22	0.05
	glycerol 2-P	0.21	0.07	n.d.	-	0.95	0.13	n.d.	-
	glycerol 3-P	0.94	0.26	0.17	0.06	4.05	2.15	n.d.	-
	ascorbic acid	0.55	0.45	1.22	0.59	5.09	0.22	4.57	0.59
amino acids (LC-MS/MS) [fg cell^{-1}]	alanine	0.85	0.19	1.36	0.22	0.83	0.28	1.59	0.30
	arginine	1.13	0.43	2.77	0.66	4.17	0.49	6.95	1.13
	asparagine	0.68	0.26	0.35	0.06	2.49	0.21	2.01	0.42
	aspartate	2.60	0.63	2.83	0.54	5.92	0.54	5.85	0.63
	glutamate	11.27	1.34	18.60	1.89	8.80	1.23	16.36	2.76
	glutamine	2.19	1.52	0.13	0.18	3.10	1.83	2.91	0.90
	glycine	n.d.	-	0.06	0.11	n.d.	-	n.d.	-
	histidine	n.d.	-	n.d.	-	n.d.	-	n.d.	-
	isoleucine	0.18	0.03	0.32	0.05	0.58	0.04	1.13	0.19
	leucine	0.07	0.01	0.19	0.03	0.80	0.08	1.42	0.21
	lysine	n.d.	-	n.d.	-	n.d.	-	n.d.	-
	methionine	n.d.	-	n.d.	-	n.d.	-	n.d.	-
	phenylalanine	0.03	0.00	0.09	0.02	0.15	0.03	0.26	0.03
	proline	0.14	0.04	0.72	0.09	0.30	0.07	1.18	0.42
	serine	2.17	0.56	1.45	0.36	2.99	0.79	1.65	0.39
	threonine	1.06	0.42	1.77	0.31	0.41	0.78	0.82	1.07
	tryptophan	n.d.	-	n.d.	-	n.d.	-	n.d.	-
	tyrosine	n.d.	-	n.d.	-	n.d.	-	n.d.	-
	valine	0.93	0.08	0.79	0.11	1.11	0.09	1.96	0.27
osmolytes (LC-MS/MS) [fg cell^{-1}]	DMSP	304.1	23.45	325.3	32.5	32.21	12.32	32.93	15.21
	GBT	19.32	2.69	28.33	10.3	17.91	5.97	28.09	3.95
	homarine	10.53	1.12	11.48	3.48	17.96	3.93	19.67	4.14
small carboxylic acids (LC-MS/MS) [ag cell^{-1}]	citrate	115.4	27.43	606.7	67.0	353.2	125.5	901.2	199.2
	α-ketoglutarate	7.67	1.60	8.68	1.27	13.10	1.31	18.51	8.35
	lactate	33.02	11.01	138.3	47.2	90.60	31.61	99.24	23.19
	malate	12.26	1.41	21.30	2.49	17.14	2.22	23.25	5.06
	pyruvate	4.91	1.54	5.56	2.00	7.03	2.56	8.92	4.07
	succinate	13.71	4.09	13.09	3.85	20.96	18.14	14.80	9.76
polyamines (LC-MS/MS) [ag cell^{-1}]	cadaverine	n.d.	-	n.d.	-	n.d.	-	n.d.	-
	putrescine	n.d.	-	n.d.	-	n.d.	-	n.d.	-
	spermidine	n.d.	-	n.d.	-	n.d.	-	n.d.	-

Supplementary Table 5: Continued table. n.d., not detected; Chl c2-MGDG, chlorophyll c2-mono-galactosyldiacylglycerol; fuco, fucoxanthin; FAME, fatty acid methyl ester; NLF, neutral lipid fraction.

Class	Metabolite	Phosphate starvation							
		2N R	SD	2N -P	SD	1N R	SD	1N -P	SD
pigments [(rel. abund. cell^{-1}) 10^3]	chlorophyll a	21.94	1.99	41.54	4.97	42.04	3.93	47.72	2.18
	chlorophyll c$_2$	17.89	1.04	20.84	3.05	41.01	3.94	46.15	4.08
	chl c$_2$-MGDG	6.55	0.59	10.48	1.82	9.94	3.58	13.65	0.53
	chlorophyll c$_3$	19.30	1.57	19.85	2.49	27.14	2.52	28.52	2.00
	diadinoxanthin	13.56	4.17	17.46	2.75	17.53	6.15	22.57	2.15
	diatoxanthin	4.55	2.02	18.35	4.23	5.95	4.91	5.30	0.42
	fucoxanthin	6.31	0.99	9.47	1.65	10.28	1.00	11.11	0.71
	h4k-fuco	4.95	0.28	9.86	1.32	2.82	0.34	4.53	0.25
	hex-fuco	49.32	1.61	76.59	10.71	80.82	6.73	94.87	2.76
	β-carotene	0.33	0.07	0.99	0.18	0.38	0.16	0.77	0.20
polar lipid fatty acids (FAME) [ag cell^{-1}]	C14:0	181.47	46.88	335.93	93.22	240.92	52.19	340.05	47.35
	C15:0	17.77	5.79	20.99	5.45	20.62	5.10	29.91	4.31
	C16:0	279.26	97.71	392.61	93.49	310.88	58.76	408.26	78.93
	C18:0	207.47	58.68	299.50	60.96	265.97	51.89	315.99	54.01
	C18:1n9c	127.29	30.37	297.61	58.96	115.63	15.63	169.83	25.28
	C18:1n9t	17.75	4.12	28.36	5.53	26.36	4.71	33.88	5.21
	C18:2n6c	31.14	19.22	56.31	24.06	26.79	4.56	33.22	6.28
	C18:3n3	190.06	63.38	363.83	74.37	184.14	41.76	271.10	52.82
	C18:4n3	139.86	42.66	232.49	49.72	86.15	14.45	111.82	19.91
	C22:0	19.42	5.39	15.01	3.30	4.69	2.20	4.60	3.26
	C22:1n9	7.58	1.69	9.74	1.46	8.32	1.29	13.83	2.63
	C22:6n3	397.31	135.32	436.80	78.54	212.31	52.40	334.35	65.80
neutral lipid fatty acids (FAME) [ag cell^{-1}]	C14:0	3.64	0.88	7.21	0.85	4.49	2.18	7.57	2.41
	C16:0	13.28	1.44	20.10	6.27	25.61	2.60	33.29	8.15
	C18:0	6.61	1.01	13.30	1.43	12.69	1.55	16.34	6.08
	C18:1n9c	4.23	0.68	12.15	1.57	6.62	0.90	9.59	2.67
	C18:2n6c	11.22	23.61	3.19	3.27	n.d.	n.d.	2.92	6.52
	C18:3n3	n.d.	n.d.	n.d.	n.d.	n.d.	n.d.	n.d.	n.d.
	C22:0	4.48	0.70	7.94	0.62	7.71	0.98	7.68	3.69
	C22:6n3	3.96	2.83	40.49	5.22	7.01	1.62	13.06	5.31
triacyl-glycerides (NLF) [(rel. abund. cell^{-1})·10^{10}]	TAG C8:0	3.09	1.61	2.22	2.67	0.89	0.18	9.08	6.50
	TAG C10:0	1.25	0.74	0.40	0.40	2.46	0.90	5.50	2.20
	TAG C12:0	6.83	3.11	12.57	7.45	21.52	4.43	39.59	28.14
	TAG C14:0	2.10	1.70	22.66	10.37	3.63	1.58	14.20	6.17
	TAG C16:0	3.24	1.27	5.61	2.19	8.08	0.85	12.54	5.92
	TAG 1	22.89	19.34	280.06	69.60	7.49	1.34	49.36	14.08
	TAG 2	0.89	0.47	0.70	0.28	0.24	0.17	0.68	0.47
	TAG 3	16.63	17.09	167.17	53.90	2.98	1.74	36.17	17.99
	TAG 4	12.62	9.91	170.65	54.78	3.54	0.36	28.27	9.74
	TAG 5	5.75	6.17	39.99	20.79	0.45	0.38	5.31	3.40
	TAG 6	24.33	24.26	222.36	60.66	6.14	2.39	50.70	14.54
	TAG 7	7.32	5.22	13.81	6.14	7.57	2.42	10.14	2.38
	TAG 8	4.88	6.28	35.27	14.71	0.25	0.12	4.39	2.55
	TAG 9	0.31	0.32	0.40	0.16	0.30	0.21	0.36	0.36
	TAG 10	1.38	0.93	2.90	1.31	2.49	0.60	3.94	1.84
	TAG 11	2.98	1.93	3.96	1.54	0.28	0.14	1.21	1.00
	TAG 12	3.57	2.07	4.10	2.43	5.32	0.66	6.51	1.80
	TAG 13	1.60	0.52	1.30	0.40	0.22	0.16	7.84	5.19
	TAG 14	0.17	0.09	0.07	0.04	13.42	4.01	14.15	7.06
	TAG 15	1.66	0.45	1.65	1.12	3.89	1.92	7.70	3.71
alkenes (NLF) [rel. ab. cell^{-1}]	C31:2 a	11.14	5.28	142.77	25.63	3.17	4.50	18.16	15.24
	C31:2 b	45.29	21.55	233.81	48.12	9.68	13.76	38.71	29.17
alkenones (NLF) [fg cell^{-1}]	C37:2 Me	0.87	0.67	8.45	2.83	0.20	0.06	0.99	0.36
	C37:3 Me	1.90	1.33	19.94	7.04	0.65	0.15	2.49	0.88
	C38:2 Me	0.23	0.18	2.42	0.87	0.13	0.17	0.30	0.12
	C38:2 Et	0.13	0.09	0.99	0.42	0.03	0.01	0.17	0.05
	C38:3 Me	0.59	0.41	5.96	2.17	0.22	0.06	0.81	0.30
	C38:3 Et	0.18	0.12	1.26	0.52	0.07	0.02	0.27	0.07

Supplementary Table 6: Metabolite abundances for the N-starvation setup. Diploid (2N) and haploid (1N) *E. huxleyi* life-cycle stages under replete (R) and nitrogen-starved (-N) conditions. Mean values and standard deviations (SD) of three biological and two/three technical replicates are shown. Asterisks indicate putatively identified metabolites. n.d., not detected; glycerol 2-p, glycerol 2-phosphate; glycerol 3-P; glycerol 3-phosphate.

Class	Metabolite	Nitrate starvation							
		2N R	SD	2N -N	SD	1N R	SD	1N -N	SD
Metabolites (TMS-derivatives, GC-MS) [(rel. abund. cell^{-1})·10^{10}]	O-acetyl-serine*	8.61	2.16	5.03	1.98	6.01	0.69	5.95	0.76
	homoserine	1.77	0.46	5.91	6.82	0.09	0.02	0.07	0.01
	pyroglutamate*	2.43	0.26	1.45	0.72	11.22	5.03	7.94	1.17
	adenine*	8.65	3.22	3.73	1.42	5.39	1.23	7.47	1.50
	adenosine	0.70	0.33	0.32	0.18	2.19	2.66	0.28	0.17
	threonic acid	16.98	3.05	13.32	4.59	15.08	1.55	15.94	2.40
	mannitol	185.25	16.33	145.16	19.41	189.11	104.18	19.34	4.20
	myo-inositol	1.55	0.14	1.83	0.46	0.74	0.10	1.79	1.69
	arabinose	0.27	0.04	0.26	0.06	0.31	0.07	0.26	0.10
	fructose	2.32	0.24	2.18	0.54	2.86	1.03	2.11	1.37
	galactose	16.54	2.38	13.27	4.51	6.98	1.46	15.58	3.19
	maltose	1.33	0.44	1.69	0.80	1.63	0.86	4.87	2.62
	melibiose	2.54	0.60	4.05	2.11	0.44	0.13	1.80	0.56
	ribose	1.22	0.19	0.88	0.22	1.71	0.42	1.02	0.09
	saccharose	4.58	1.07	4.48	1.47	5.22	2.05	3.38	0.93
	xylose	0.70	0.16	0.85	0.14	0.32	0.09	1.16	0.17
	glycerol 2-P	5.59	11.14	0.46	0.27	2.11	0.59	1.07	0.27
	glycerol 3-P	1.95	0.54	1.50	0.63	5.32	0.68	2.88	1.29
	ascorbic acid	n.d.	n.d.	n.d.	n.d.	4.14	0.65	2.95	0.37
amino acids (LC-MS/MS) [fg cell^{-1}]	alanine	2.78	0.40	2.07	0.38	2.72	0.37	4.82	0.92
	arginine	11.30	1.59	3.12	0.26	7.92	1.49	9.50	1.06
	asparagine	3.80	0.62	0.69	0.06	26.61	12.87	4.94	0.83
	aspartate	4.86	0.98	1.48	0.39	7.78	1.64	12.93	1.92
	glutamate	52.44	2.97	12.47	1.62	31.18	5.47	30.49	6.59
	glutamine	22.38	6.97	4.23	0.60	160.85	96.92	28.01	6.12
	glycine	0.72	0.21	0.44	0.17	0.59	0.08	0.95	0.10
	histidine	0.84	0.11	2.57	0.29	0.80	0.38	1.00	0.11
	isoleucine	1.54	0.15	0.49	0.10	1.07	0.31	9.16	0.93
	leucine	0.50	0.07	0.54	0.14	1.54	0.34	11.38	1.34
	lysine	7.02	1.66	1.60	0.16	2.81	1.30	3.91	0.83
	methionine	0.98	0.13	0.84	0.08	0.56	0.10	2.16	0.23
	phenylalanine	0.44	0.07	10.14	0.76	0.33	0.14	2.38	0.07
	proline	0.17	0.05	0.17	0.02	0.92	0.41	1.62	0.15
	serine	5.80	0.44	2.70	0.30	5.67	2.58	6.29	1.33
	threonine	3.55	0.53	1.20	0.12	0.84	0.27	1.64	0.22
	tryptophan	0.16	0.04	3.90	0.42	0.35	0.23	2.79	0.15
	tyrosine	0.18	0.08	3.25	0.94	0.20	0.07	4.13	0.18
	valine	5.57	1.57	0.78	0.21	2.07	0.47	15.60	1.99
osmolytes (LC-MS/MS) [fg cell^{-1}]	DMSP	678.10	87.56	633.20	51.30	401.98	65.41	1091.68	237.34
	GBT	28.60	5.22	n.d.	n.d.	18.05	1.01	0.96	0.77
	homarine	15.90	4.18	10.21	3.13	19.36	4.09	40.14	12.04
small carboxylic acids (LC-MS/MS) [ag cell^{-1}]	citrate	74.35	10.42	75.30	10.15	166.80	28.63	770.28	95.07
	α-ketoglutarate	39.79	19.37	17.59	5.68	19.63	11.65	118.82	37.35
	lactate	38.71	25.19	21.02	14.19	26.77	13.56	39.35	19.57
	malate	24.49	8.66	18.23	1.19	15.26	2.55	50.81	9.90
	pyruvate	33.44	24.37	58.69	14.41	10.09	5.64	85.09	27.36
	succinate	44.16	22.84	12.53	5.25	17.87	10.18	17.50	8.70
polyamines (LC-MS/MS) [ag cell^{-1}]	cadaverine	n.d.	-	n.d.	-	n.d.	-	n.d.	-
	putrescine	n.d.	-	n.d.	-	n.d.	-	n.d.	-
	spermidine	n.d.	-	n.d.	-	n.d.	-	n.d.	-

Supplementary Table 6: Continued table. Chl c₂-MGDG, chlorophyll c₂-monogalactosyldiacylglycerol; fuco, fucoxanthin; FAME, fatty acid methyl ester; NLF, neutral lipid fraction.

Class	Metabolite	Nitrate starvation							
		2N R	SD	2N -N	SD	1N R	SD	1N -N	SD
pigments [(rel. abund. cell⁻¹) 10³]	chlorophyll a	19.42	4.89	15.23	0.87	34.56	5.80	23.32	2.86
	chlorophyll c₂	13.20	2.47	8.73	0.06	28.97	5.05	22.68	2.14
	chl c₂-MGDG	3.74	0.66	2.54	0.00	8.98	1.44	6.08	0.72
	chlorophyll c₃	10.86	1.87	7.45	0.34	18.06	1.38	13.52	1.27
	diadinoxanthin	3.85	1.06	3.45	0.54	8.87	0.96	6.15	0.98
	diatoxanthin	1.10	0.27	0.71	0.07	3.37	0.31	1.73	0.34
	fucoxanthin	4.47	1.06	2.37	0.07	12.68	1.13	7.06	1.11
	h4k-fuco	2.15	0.37	1.38	0.04	2.25	0.18	1.53	0.15
	hex-fuco	30.52	4.70	20.74	0.20	55.31	8.68	41.48	4.61
	β-carotene	0.30	0.14	0.22	0.08	0.96	0.22	0.49	0.12
polar lipid fatty acids (FAME) [ag cell⁻¹]	C14:0	316.90	74.82	214.10	64.85	184.34	11.62	156.25	43.88
	C15:0	15.52	2.93	8.99	2.30	9.59	1.94	7.22	1.94
	C16:0	264.51	49.46	167.57	45.14	136.20	17.14	126.54	34.87
	C18:0	174.14	28.65	103.14	25.89	89.10	14.69	67.04	19.55
	C18:1n9c	170.78	41.65	130.30	35.78	75.37	5.53	96.82	26.18
	C18:1n9t	14.77	3.53	10.27	2.79	15.54	2.33	11.78	3.11
	C18:2n6c	36.91	7.30	29.34	7.58	11.15	0.94	13.95	3.43
	C18:3n3	336.34	70.95	211.78	61.73	242.75	19.86	180.61	47.73
	C18:4n3	138.11	24.21	103.46	23.36	62.91	4.00	56.87	15.14
	C22:0	22.16	11.90	12.39	3.20	1.72	0.28	2.31	0.58
	C22:1n9	3.50	0.53	3.33	1.95	1.74	0.10	1.65	0.52
	C22:6n3	467.40	99.53	331.54	90.46	226.80	27.26	202.39	51.17
neutral lipid fatty acids (FAME) [ag cell⁻¹]	C14:0	7.88	2.52	7.40	2.57	1.90	0.23	2.34	0.64
	C16:0	14.08	1.93	10.22	1.73	6.86	1.36	5.97	1.90
	C18:0	13.72	3.10	9.84	1.65	7.82	1.00	5.81	1.52
	C18:1n9c	9.49	2.74	9.02	3.03	2.32	0.36	2.69	0.79
	C18:2n6c	3.27	1.00	3.37	1.07	0.99	0.17	0.84	0.12
	C18:3n3	3.62	0.76	4.55	3.95	1.80	0.46	1.62	0.51
	C22:0	2.99	0.37	3.03	0.94	1.56	0.19	1.57	0.20
	C22:6n3	12.49	4.21	9.36	1.88	2.94	0.26	4.28	1.39
triacyl-glycerides (NLF) [(rel. abund. cell⁻¹)· 10¹⁰]	TAG C8:0	7.88	1.56	6.03	1.50	2.90	0.21	3.21	0.93
	TAG C10:0	n.d.	-	n.d.	-	n.d.	-	n.d.	-
	TAG C12:0	n.d.	-	n.d.	-	n.d.	-	n.d.	-
	TAG C14:0	2.42	1.27	3.03	1.15	0.47	0.32	3.14	0.55
	TAG C16:0	1.88	0.56	1.94	0.91	0.05	0.09	0.19	0.15
	TAG 1	83.56	11.22	79.48	15.32	9.49	2.65	55.72	25.79
	TAG 2	1.31	0.91	0.46	0.08	0.30	0.09	0.12	0.08
	TAG 3	33.93	24.29	38.63	8.31	11.04	3.29	37.67	17.84
	TAG 4	55.16	3.56	57.43	5.00	3.91	1.22	34.71	9.36
	TAG 5	17.15	8.02	16.43	3.48	2.66	0.96	9.34	5.95
	TAG 6	49.52	5.02	46.52	4.25	5.78	2.96	34.59	3.97
	TAG 7	20.76	2.08	11.99	4.29	7.20	3.68	5.98	2.71
	TAG 8	14.30	2.13	12.94	1.78	3.70	1.02	7.72	3.44
	TAG 9	2.37	0.54	1.01	0.95	0.37	0.20	0.53	0.28
	TAG 10	5.85	1.35	1.74	2.41	1.29	0.35	0.98	0.31
	TAG 11	1.60	1.34	2.50	1.44	0.26	0.16	0.18	0.20
	TAG 12	1.08	0.53	2.40	1.65	2.87	1.31	17.19	6.72
	TAG 13	1.93	1.23	1.11	0.64	0.22	0.27	0.01	0.02
	TAG 14	0.01	0.02	0.01	0.02	1.23	1.32	7.91	2.37
	TAG 15	0.57	0.19	0.91	0.27	0.22	0.14	0.47	0.35
alkenes (NLF) [rel. ab. cell⁻¹]	C31:2 a	114.83	35.59	134.40	32.22	2.22	0.35	3.93	0.90
	C31:2 b	173.42	50.60	205.68	43.65	19.89	4.99	25.65	9.48
alkenones (NLF) [fg cell⁻¹]	C37:2 Me	12.34	6.80	13.95	3.33	0.53	0.16	5.54	2.80
	C37:3 Me	20.67	11.83	22.05	4.40	2.26	0.72	12.38	6.58
	C38:2 Me	2.68	1.49	2.66	0.63	0.16	0.07	1.50	0.79
	C38:2 Et	1.80	1.37	1.63	0.61	0.11	0.05	0.67	0.37
	C38:3 Me	5.04	2.89	4.78	0.96	0.87	0.35	3.43	1.83
	C38:3 Et	1.41	1.04	1.18	0.27	0.33	0.14	0.83	0.48
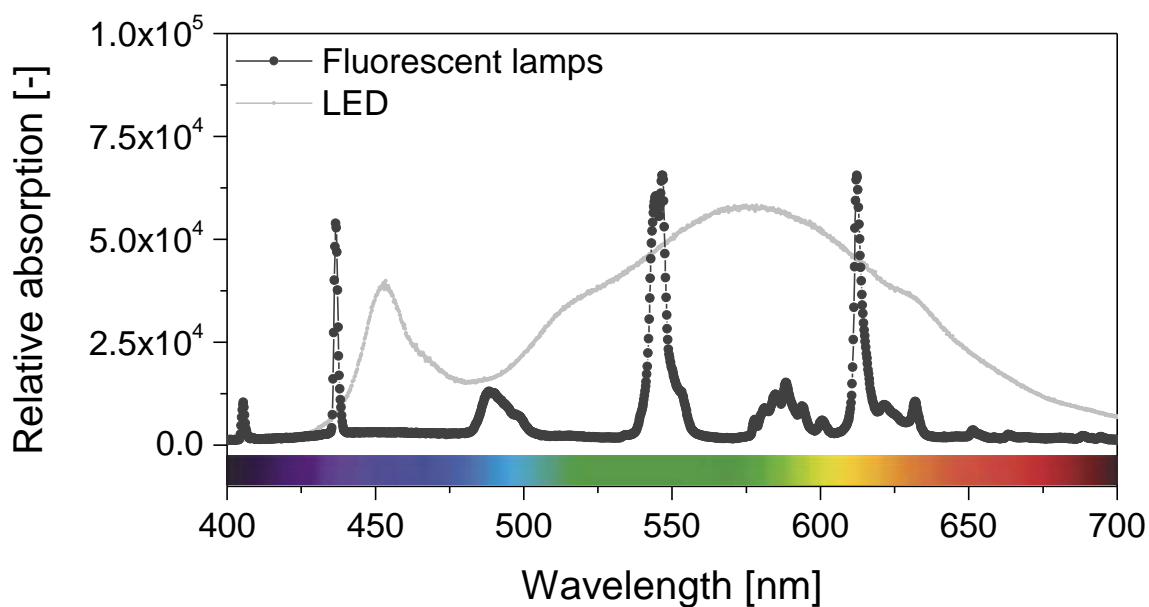
a
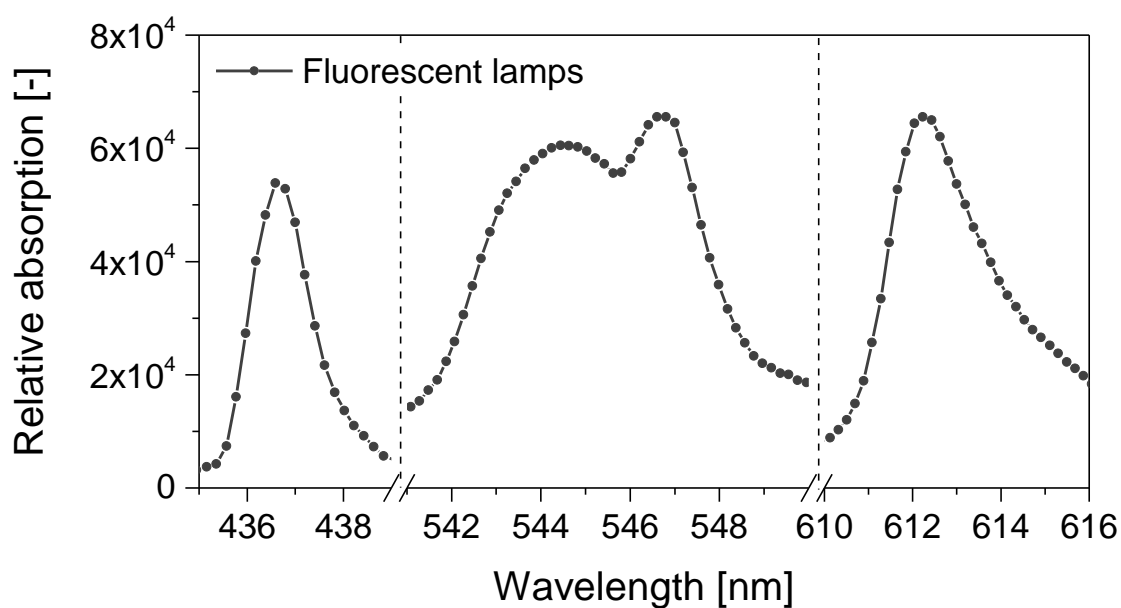
b

Supplementary Figure 2: Absorption of fluorescent lamps (TL-D 18W/840 Master, Philips) used to illuminate *E. huxleyi* cultures during growth. (a) Complete spectrum for fluorescent lamps, with LED spectrum to facilitate comparison (SMD-LED, NSSL 757, warm white, Nichia corporation, Japan). (b) Fluorescent lamp spectrum, zoomed sections of the three biggest peaks, note interruptions in x-axis. The spectrum was measured with a portable spectrometer (USB 4000, Ocean optics) and the software SpectraSuite (Ocean optics).

References

Abida, H., Dolch, L.-J., Meï, C., Villanova, V., Conte, M., Block, M. A., Finazzi, G., Bastien, O., Tirichine, L., Bowler, C., Rébeillé, F., Petroutsos, D., Jouhet, J., Maréchal, E. (2014): Membrane glycerolipid remodeling triggered by nitrogen and phosphorus starvation in *Phaeodactylum tricornutum. Plant Physiol.* **167**, 118–136, doi:10.1104/pp.114.252395.

Ackman, R. G. (1990): Misidentification of fatty acid methyl ester peaks in liquid canola shortening. *J. Am. Oil Chem. Soc.* **67**, 1028, doi:10.1007/BF02541870.

Ackman, R. G. (2002): The gas chromatograph in practical analyses of common and uncommon fatty acids for the 21st century. *Anal. Chim. Acta* **465**, 175–192, doi:10.1016/S0003-2670(02)00098-3.

Ackman, R. G., Sipos, J. C. (1964): Application of specific response factors in the gas chromatographic analysis of methyl esters of fatty acids with flame ionization detectors. *J. Am. Oil Chem. Soc.* **41**, 377–378, doi:10.1007/BF02654818.

Ackman, R. G., Tocher, C. S., McLachlan, J. (1968): Marine phytoplankter fatty acids. *J. Fish. Res. Bd. Can.* **25**, 1603–1620, doi:10.1139/f68-145.

Airs, R. L., Llewellyn, C. A. (2006): Improved detection and characterization of fucoxanthin-type carotenoids: Novel pigments in *Emiliania huxleyi* (Prymnesiophyceae). *J. Phycol.* **42**, 391–399, doi:10.1111/j.1529-8817.2006.00199.x.

Alcolombri, U., Ben-Dor, S., Feldmesser, E., Levin, Y., Tawfik, D. S., Vardi, A. (2015): Marine sulfur cycle. Identification of the algal dimethyl sulfide-releasing enzyme: A missing link in the marine sulfur cycle. *Science (New York, N.Y.)* **6242**, 1466–1469, doi:10.1126/science.aab1586.

Allard, B., Templier, J. (2001): High molecular weight lipids from the trilaminar outer wall (TLS)-containing microalgae *Chlorella emersonii*, *Scenedesmus conmmunis* and *Tetraedron minimum. Phytochemistry* **57**, 459–467.

Antia, N. J., Berland, B. R., Bonin, D. J., Maestrini, S. Y. (1975): Comparative evaluation of certain organic and inorganic sources of nitrogen for phototrophic growth of marine microalgae. *J. Mar. Biol. Ass.* **55**, 519–539, doi:10.1017/S0025315400017239.

Avidan, O., Pick, U. (2015): Acetyl-CoA synthetase is activated as part of the PDH-bypass in the oleaginous green alga *Chlorella desiccata. J. Exp. Botany* **66**, 7287–7298, doi:10.1093/jxb/erv424.

Baker, N. R., Oxborough, K. (2004): *Chlorophyll fluorescence as a probe of photosynthetic productivity*. In *Chlorophyll a fluorescence: A signature of photosynthesis*. Eds. Papageorgiou, G.C., Govindjee, Kluwer Academic, Dordrecht, Netherlands, 65–82.

Balch, W. M., Kilpatrick, K. A., Holligan, P., Harbour, D., Fernandez, E. (1996): The 1991 coccolithophore bloom in the central North Atlantic. 2. Relating optics to coccolith concentration. *Limnol. Oceanogr.* **41**, 1684–1696, doi:10.4319/lo.1996.41.8.1684.

Bao, X., Pollard, M., Ohlrogge, J. (1998): The biosynthesis of erucic acid in developing embryos of *Brassica rapa. Plant Physiol.* **118**, 183–190.

Barsanti, L., Gualtieri, P. (2006): *Algae: Anatomy, biochemistry, and biotechnology*, CRC Press, Boca Raton, FL, US.

Bates, T. S., Charlson, R. J., Gammon, R. H. (1987): Evidence for the climatic role of marine biogenic sulphur. *Nature* **329**, 319–321, doi:10.1038/329319a0.

Beardall, J., Raven, J. A. (2016): *Carbon acquisition by microalgae*. In *The Physiology of Microalgae*, 1st ed. Eds. Borowitzka, M.A., Beardall, J., Raven, J.A., Springer International Publishing, Cham, Switzerland.

Bell, M. V., Pond, D. (1996): Lipid composition during growth of motile and coccolith forms of *Emiliania huxleyi*. *Phytochemistry* **41**, 465–471, doi:10.1016/0031-9422(95)00663-X.

Bellou, S., Aggelis, G. (2012): Biochemical activities in *Chlorella* sp. and *Nannochloropsis salina* during lipid and sugar synthesis in a lab-scale open pond simulating reactor. *J. Biotechnol.* **164**, 318–329, doi:10.1016/j.jbiotec.2013.01.010.

Beman, J. M., Chow, C.-E., King, A. L., Feng, Y., Fuhrman, J. A., Andersson, A., Bates, N. R., Popp, B. N., Hutchins, D. A. (2011): Global declines in oceanic nitrification rates as a consequence of ocean acidification. *PNAS* **108**, 208–213, doi:10.1073/pnas.1011053108.

Berges, J. A., Charlebois, D. O., Mauzerall, D. C., Falkowski, P. G. (1996): Differential effects of nitrogen limitation on photosynthetic efficiency of photosystems I and II in microalgae. *Plant Physiol.* **110**, 689–696.

Berges, J. A., Franklin, D. J., Harrison, P. J. (2001): Evolution of an artificial seawater medium: Improvements in enriched seawater, artificial water over the last two decades. *J. Phycol.* **37**, 1138–1145, doi:10.1046/j.1529-8817.2001.01052.x.

Bertrand, M. (2010): Carotenoid biosynthesis in diatoms. *Photosynth. Res* **106**, 89–102, doi:10.1007/s11120-010-9589-x.

Bijma, J., Altabet, M., Conte, M., Kinkel, H., Versteegh, G. J. M., Volkman, J. K., Wakeham, S. G., Weaver, P. P. (2001): Primary signal: Ecological and environmental factors-Report from Working Group 2. *Geochem. Geophys. Geosyst.* **2**, n/a-n/a, doi:10.1029/2000GC000051.

Billard, C. (1994): *Life cycles*. In *The Haptophyte algae*. Eds. Green, J.C., Leadbeater, B.S.C., Clarendon Press, Oxford, UK, 167–186.

Blankenship, R. E. (2014): *Molecular mechanisms of photosynthesis*, 2. ed., Wiley Blackwell, Chichester, UK.

Bligh, E., Dyer, W. (1959): A rapid method of total lipid extraction and purification. *Can. J. Biochem. Physiol.* **37**, 911–917, doi:10.1139/o59-099.

Bochenek, M., Etherington, G. J., Koprivova, A., Mugford, S. T., Bell, T. G., Malin, G., Kopriva, S. (2013): Transcriptome analysis of the sulfate deficiency response in the marine microalga *Emiliania huxleyi*. *New Phytol.* **199**, 650–662, doi:10.1111/nph.12303.

Boelen, P., van Dijk, R., Sinninghe Damste, J. S., Rijpstra, W. I. C., Buma, A. G. (2013): On the potential application of polar and temperate marine microalgae for EPA and DHA production. *AMB Express* **3**, 26, doi:10.1186/2191-0855-3-26.

Boelen, P., van Mastrigt, A., van de Bovenkamp, H. H., Heeres, H. J., Buma, A. G. J. (August 25, 2016): Growth phase significantly decreases the DHA-to-EPA ratio in marine microalgae. *Aquacult. Int.*, doi:10.1007/s10499-016-0053-6.

Bogen, C., Klassen, V., Wichmann, J., La Russa, M., Doebbe, A., Grundmann, M., Uronen, P., Kruse, O., Mussgnug, J. H. (2013): Identification of *Monoraphidium contortum* as a promising species for liquid biofuel production. *Biores. Techn.* **133**, 622–626, doi:10.1016/j.biortech.2013.01.164.

Brassell, S. C., Eglinton, G., Marlowe, I. T., Pflaumann, U., Sarnthein, M. (1986): Molecular stratigraphy: A new tool for climatic assessment. *Nature* **320**, 129–133, doi:10.1038/320129a0.

Bratbak, G., Egge, J. K., Heldal, M. (1993): Viral mortality of the marine alga *Emiliania huxleyi* (Haptophyceae) and termination of algal blooms. *Mar. Ecol. Prog. Ser.* **93**, 39–48, doi:10.3354/meps093039.

Bratbak, G., Wilson, W., Heldal, M. (1996): Viral control of *Emiliania huxleyi* blooms? *J. Mar. Syst.* **9**, 75–81, doi:10.1016/0924-7963(96)00018-8.

Bratt, C. E., Arvidsson, P. O., Carlsson, M., Akerlund, H. E. (1995): Regulation of violaxanthin de-epoxidase activity by pH and ascorbate concentration. *Photosynth. Res.* **45**, 169–175, doi:10.1007/BF00032588.

Brown, C. W., Yoder, J. A. (1994): Distribution pattern of coccolithophorid blooms in the western North Atlantic Ocean. *Cont. Shelf Res.* **14**, 175–197, doi:10.1016/0278-4343(94)90012-4.

Bruhn, A., Laroche, J., Richardson, K. (2010): *Emiliania huxleyi* (Prymnesiophyceae): Nitrogen-metabolism genes and their expression in response to external nitrogen sources. *J. Phycol.* **46**, 266–277, doi:10.1111/j.1529-8817.2010.00809.x.

Brunet, C., Johnsen, G., Lavaud, J., Roy, S. (2011): *Pigments and photoacclimation processes*. In *Phytoplankton pigments: Characterization, chemotaxonomy, and applications in oceanography*, 1 ed. Eds. Roy, S., Llewellyn, C.A., Egeland, E.S., Johnsen, G., Cambridge University Press, Cambridge, New York, US, 445–471.

Bucciarelli, E., Sunda, W. G. (2003): Influence of CO_2, nitrate, phosphate, and silicate limitation on intracellular dimethylsulfoniopropionate in batch cultures of the coastal diatom *Thalassiosira* pseudonana. *Limnol. Oceanogr.* **48**, 2256–2265, doi:10.4319/lo.2003.48.6.2256.

Buchanan, B. B., Gruissem, W., Jones, R. L. (2015): *Biochemistry and molecular biology of plants*, 2nd ed., Wiley Blackwell, Chichester, UK.

Buescher, J. M., Antoniewicz, M. R., Boros, L. G., Burgess, S. C., Brunengraber, H., Clish, C. B., DeBerardinis, R. J., Feron, O., Frezza, C., Ghesquiere, B., Gottlieb, E., Hiller, K., Jones, R. G., Kamphorst, J. J., Kibbey, R. G., Kimmelman, A. C., Locasale, J. W., Lunt, S. Y., Maddocks, O. D. K., Malloy, C., Metallo, C. M., Meuillet, E. J., Munger, J., Noh, K., Rabinowitz, J. D., Ralser, M., Sauer, U., Stephanopoulos, G., St-Pierre, J., Tennant, D. A., Wittmann, C., Vander Heiden, M. G., Vazquez, A., Vousden, K., Young, J. D., Zamboni, N., Fendt, S.-M. (2015): A roadmap for interpreting ^{13}C metabolite labeling patterns from cells. *Curr. Opin. Biotechn.*, 189–201, doi:10.1016/j.copbio.2015.02.003.

Buma, A., Bano, N., Veldhuis, M., Kraay, G. W. (1991): Comparison of the pigmentation of two strains of the prymnesiophyte *Phaeocystis* sp. *Neth. J. Sea Res.* **27**, 173–182, doi:10.1016/0077-7579(91)90010-X.

Caldeira, K. (2005): Ocean model predictions of chemistry changes from carbon dioxide emissions to the atmosphere and ocean. *J. Geophys. Res.* **110**, doi:10.1029/2004JC002671.

Calder, P. C. (2003): n−3 Polyunsaturated fatty acids and inflammation: From molecular biology to the clinic. *Lipids* **38**, 343–352, doi:10.1007/s11745-003-1068-y.

Caron, L., Douady, D., Quinet-Szely, M., Goër, S. de, Berkaloff, C. (1996): Gene structure of a chlorophyll a/c-binding protein from a brown alga: Presence of an intron and phylogenetic implications. *J. Mol. Evol.* **43**, 270–280, doi:10.1007/BF02338835.

Carvalho, A. P., Malcata, F. X. (2005): Optimization of omega-3 fatty acid production by microalgae: crossover effects of CO_2 and light intensity under batch and continuous cultivation modes. *Mar. Biotechnol.* **7**, 381–388, doi:10.1007/s10126-004-4047-4.

Casetta, B., Tagliacozzi, D., Shushan, B., Federici, G. (2000): Development of a method for rapid quantitation of amino acids by liquid chromatography-tandem mass spectrometry (LC-MSMS) in plasma. *Clin. Chem. Lab. Med.* **38**, 391–401, doi:10.1515/CCLM.2000.057.

Cermeno, P., Dutkiewicz, S., Harris, R. P., Follows, M., Schofield, O., Falkowski, P. G. (2008): The role of nutricline depth in regulating the ocean carbon cycle. *PNAS* **105**, 20344–20349, doi:10.1073/pnas.0811302106.

Chakraborty, S., Karmakar, K., Chakravortty, D. (2014): Cells producing their own nemesis: Understanding methylglyoxal metabolism. *IUBMB Life* **66**, 667–678, doi:10.1002/iub.1324.

Charlson, R. J., Lovelock, J. E., Andreae, M. O., Warren, S. G. (1987): Oceanic phytoplankton, atmospheric sulphur, cloud albedo and climate. *Nature* **326**, 655–661, doi:10.1038/326655a0.

Chen, W., Zhang, C., Song, L., Sommerfeld, M., Hu, Q. (2009): A high throughput Nile red method for quantitative measurement of neutral lipids in microalgae. *J. Microbiol. Meth.* **77**, 41–47, doi:10.1016/j.mimet.2009.01.001.

Christie, W. W. (2011a): Thin-Layer Chromatography of Lipids. AOCS Lipid Library. http://lipidlibrary.aocs.org/Analysis/content.cfm?ItemNumber=40388 (05.01.2017)

Christie, W. W. (2011b): Methylation of fatty acids: A beginner's guide. AOCS Lipid Library. http://lipidlibrary.aocs.org/History/content.cfm?ItemNumber=40363 (18.12.2016)

Christie, W. W. (2011c): Preparation of ester derivatives of fatty acids for chromatographic analysis. AOCS Lipid Library. http://lipidlibrary.aocs.org/Analysis/content.cfm?ItemNumber=40374 (18.12.2016)

Christie, W. W. (2013): What is a Lipid? AOCS Lipid Library. http://lipidlibrary.aocs.org/Primer/content.cfm?ItemNumber=39371 (15.01.2017)

Christie, W. W., Han, X. (2010): *Lipid analysis: Isolation, separation, identification and lipidomic analysis*, 4. ed., Oily Press, Bridgwater, UK.

Conover, S. A. M. (1975): Partitioning of nitrogen and carbon in cultures of the marine diatom *Thalassiosira fluviatilis* supplied with nitrate, ammonium, or urea. *Mar. Biol.* **32**, 231–246, doi:10.1007/BF00399203.

Conte, M. H., Sicre, M.-A., Rühlemann, C., Weber, J. C., Schulte, S., Schulz-Bull, D., Blanz, T. (2006): Global temperature calibration of the alkenone unsaturation index (UK$'_{37}$) in surface waters and comparison with surface sediments. *Geochem. Geophys. Geosyst.* **7**, 1-22, doi:10.1029/2005GC001054.

Conte, M. H., Thompson, A., Eglinton, G., Green, J. C. (1995): Lipid biomarker diversity in the coccolithophorid *Emiliania huxleyi* (Prymnesiophyceae) and the related species *Gephyrocapsa oceanica*. *J. Phycol.* **31**, 272–282, doi:10.1111/j.0022-3646.1995.00272.x.

Conte, M. H., Thompson, A., Lesley, D., Harris, R. P. (1998): Genetic and physiological influences on the alkenone/alkenoate versus growth temperature relationship in *Emiliania huxleyi* and *Gephyrocapsa oceanica*. *Geochim. Cosmochim. Acta* **62**, 51–68, doi:10.1016/S0016-7037(97)00327-X.

Cook, S. S., Whittock, L., Wright, S. W., Hallegraeff, G. M. (2011): Photosynthetic pigment and genetic differences between two southern ocean morphotypes of *Emiliania huxleyi* (Haptophyta). *J. Phycol.* **47**, 615–626, doi:10.1111/j.1529-8817.2011.00992.x.

Croce, R., van Amerongen, H. (2011): Light-harvesting and structural organization of Photosystem II: From individual complexes to thylakoid membrane. *J. Photochem. Photobiol. B* **104**, 142–153, doi:10.1016/j.jphotobiol.2011.02.015.

Croce, R., van Amerongen, H. (2014): Natural strategies for photosynthetic light harvesting. *Nat. Chem. Biol.* **10**, 492–501, doi:10.1038/nchembio.1555.

Das, U. N. (2002): The lipids that matter from infant nutrition to insulin resistance. *Prostagland. Leuk. Essent. Fatty Acids* **67**, 1–12.

de Swaaf, M. E., Pronk, J. T., Sijtsma, L. (2003): Fed-batch cultivation of the docosahexaenoic-acid-producing marine alga *Crypthecodinium cohnii* on ethanol. *Appl. Microbiol. Biotechnol.* **61**, 40–43, doi:10.1007/s00253-002-1118-1.

de Vrind-de Jong, E. W., van Emburg, P. R., Vrind, J. de (1994): *Mechanisms of calcification: Emiliania huxleyi as a model system*. In *The Haptophyte algae*. Eds. Green, J.C., Leadbeater, B.S.C., Clarendon Press, Oxford, UK, 149–166.

de Vrind-de Jong, E. W., Vorman, A. H., Thierry, R., Westbroek, P., Grünter, M., Kamerling, J. P. (1986): *Calcification in the coccolithophorids Emiliania huxleyi and Pleuchrysis carterae. II. Biochemical aspects*. In *Biomineralization in lower plants and animals*. Eds. Leadbeater, B.S.C., Riding, R.S., Clarendon Press, Oxford, UK, 205–217.

DellaPenna, D. (2004): *Carotenoid synthesis and function in plants: Insights from mutant studies in Arabidopsis thaliana*. In *The Photochemistry of Carotenoids*. Eds. Frank, H.A., Young, A.J., Britton, G., Cogdell, R.J., Kluwer Academic Publishers, Dordrecht, Netherlands.

Demé, B., Cataye, C., Block, M. A., Marechal, E., Jouhet, J. (2014): Contribution of galactoglycerolipids to the 3-dimensional architecture of thylakoids. *FASEB J.* **28**, 3373–3383, doi:10.1096/fj.13-247395.

Demmig-Adams, B., Adams III, W. W. (1993): *The xanthophyll cycle*. In *Carotenoids in Photosynthesis*, 1rst Ed. Eds. Young, A.J., Britton, G., Springer, Dordrecht, Netherlands, 206–251.

Dettmer, K., Aronov, P. A., Hammock, B. D. (2007): Mass spectrometry-based metabolomics. *Mass Spectrom. Rev.* **26**, 51–78, doi:10.1002/mas.20108.

Dettmer, K., Hammock, B. D. (2004): Metabolomics -a new exciting field within the "omics" sciences. *Env. Health Persp.* **112**, A396-7.

Dickson, A. G. (1981): An exact definition of total alkalinity and a procedure for the estimation of alkalinity and total inorganic carbon from titration data. *Deep Sea Res. A* **28**, 609–623, doi:10.1016/0198-0149(81)90121-7.

Didymus, J. M., Oliver, P., Mann, S., DeVries, A. L., Hauschka, P. V., Westbroek, P. (1993): Influence of low-molecular-weight and macromolecular organic additives on the morphology of calcium carbonate. *J. Chem. Soc. Faraday Trans.* **89**, 2891–2900, doi:10.1039/ft9938902891.

Dijkman, N. A., Kromkamp, J. C. (2006): Phospholipid-derived fatty acids as chemotaxonomic markers for phytoplankton: Application for inferring phytoplankton composition. *Mar. Ecol. Prog. Ser.* **324**, 113–125, doi:10.3354/meps324113.

Dixon, R. W., Peterson, D. S. (2002): Development and testing of a detection method for liquid chromatography based on aerosol charging. *Anal. Chem.* **74**, 2930–2937.

Dodds, E. D., McCoy, M. R., Rea, L. D., Kennish, J. M. (2005): Gas chromatographic quantification of fatty acid methyl esters: Flame ionization detection vs. electron impact mass spectrometry. *Lipids* **40**, 419–428, doi:10.1007/s11745-006-1399-8.

Doebbe, A., Keck, M., La Russa, M., Mussgnug, J. H., Hankamer, B., Tekçe, E., Niehaus, K., Kruse, O. (2010): The interplay of proton, electron, and metabolite supply for photosynthetic H_2 production in *Chlamydomonas reinhardtii*. *J. Biol. Chem.* **285**, 30247–30260, doi:10.1074/jbc.M110.122812.

Domenighini, A., Giordano, M. (2009): Fourier transfrom infrared spectroscopy of microalgae as a novel tool for biodiversity studies, species identification and the assessment of water quality. *J. Phycol.* **45**, 522–531, doi:10.1111/j.1529-8817.2009.00662.x.

Doney, S. C. (2006): The dangers of ocean acidification. *Sci. Am.* **294**, 58–65.

Douglas, A. G., Douraghi-Zadeh, K., Eglinton, G. (1969): The fatty acids of the alga *Botryococcus braunii*. *Phytochemistry* **8**, 285–293, doi:10.1016/S0031-9422(00)85826-4.

Dugdale, R. C. (1967): Nutrient limitation in the sea: Dynamics, identification and significance. *Limnol. Oceanogr.* **12**, 685–695, doi:10.4319/lo.1967.12.4.0685.

Dunstan, G. A., Volkman, J. K., Barrett, S. M., Garland, C. D. (1993): Changes in the lipid composition and maximisation of the polyunsaturated fatty acid content of three microalgae grown in mass culture. *J. Appl. Phycol.* **5**, 71–83, doi:10.1007/BF02182424.

Durak, G. M., Taylor, A. R., Walker, C. E., Probert, I., Vargas, C. de, Audic, S., Schroeder, D., Brownlee, C., Wheeler, G. L. (February 4th, 2016): A role for diatom-like silicon transporters in calcifying coccolithophores. *Nat. Commun.*, doi:10.1038/ncomms10543.

Dyhrman, S. T., Jenkins, B. D., Rynearson, T. A., Saito, M. A., Mercier, M. L., Alexander, H., Whitney, L. P., Drzewianowski, A., Bulygin, V. V., Bertrand, E. M., Wu, Z., Benitez-Nelson, C., Heithoff, A., Santos, P. (2012): The transcriptome and proteome of the diatom *Thalassiosira pseudonana* reveal a diverse phosphorus stress response. *PLoS ONE* **7**, e33768, doi:10.1371/journal.pone.0033768.

Dyhrman, S. T., Palenik, B. (2003): Characterization of ectoenzyme activity and phosphate-regulated proteins in the coccolithophorid *Emiliania huxleyi*. *J. Plankton Res.* **25**, 1215–1225, doi:10.1093/plankt/fbg086.

Dyhrman, S. T., Palenik, B. P. (1997): The identification and purification of a cell-surface alkaline phosphatase from the dinoflagellate *Prorocentrum minimum* (Dinophyceae). *J. Phycol.* **33**, 602–612, doi:10.1111/j.0022-3646.1997.00602.x.

Edvardsen, B., Eikrem, W., Green, J. C., Andersen, R. A., Moon-van der Staay, S. Y., Medlin, L. K. (2000): Phylogenetic reconstructions of the Haptophyta inferred from 18S ribosomal DNA sequences and available morphological data. *Phycologia* **39**, 19–35, doi:10.2216/i0031-8884-39-1-19.1.

Egeland, E. S. (2011): *Data sheets aiding identification of phytoplankton carotenoids and chlorophylls*. In *Phytoplankton pigments: Characterization, chemotaxonomy, and applications in oceanography*, 1 ed. Eds. Roy, S., Llewellyn, C.A., Egeland, E.S., Johnsen, G., Cambridge University Press, Cambridge, New York, US, 665–822.

Egeland, E. S., Garrido, J. L., Zapata, M., Maestro, M. A., Liaaen-Jensen, S. (2000): Algal carotenoids. Part 64. Structure and chemistry of 4-keto-19'-hexanoyloxyfucoxanthin with a novel carotenoid end group. *J. Chem. Soc. Perkin 1* **8**, 1223–1230, doi:10.1039/A910345G.

Egge, J. K., Heimdal, B. R. (1994): Blooms of phytoplankton including *Emiliania huxleyi* (Haptophyta). Effects of nutrient supply in different N:P ratios. *Sarsia* **79**, 333–348, doi:10.1080/00364827.1994.10413565.

Eltgroth, M. L., Watwood, R. L., Wolfe, G. V. (2005): Production and cellular localization of neutral long-chain lipid in the haptophyte algae *Isochrysis galbana* and *Emiliania huxleyi*. *J. Phycol.* **41**, 1000–1009, doi:10.1111/j.1529-8817.2005.00128.x.

Epstein, B. L., D'Hondt, S., Quinn, J. G., Zhang, J., Hargraves, P. E. (1998): An effect of dissolved nutrient concentrations on alkenone-based temperature estimates. *Paleoceanography* **13**, 122–126, doi:10.1029/97PA03358.

Epstein, B. L., D'Hondt, S., Hargraves, P. E. (2001): The possible metabolic role of C37 alkenones in *Emiliania huxleyi*. *Org. Geochem.* **32**, 867–875, doi:10.1016/S0146-6380(01)00026-2.

Escribano, M. I., Legaz, M. E. (1988): High performance liquid chromatography of the dansyl derivatives of putrescine, spermidine, and spermine. *Plant Physiol.* **87**, 519–522, doi:10.1104/pp.87.2.519.

Evans, C., Pond, D. W., Wilson, W. H. (2009): Changes in *Emiliania huxleyi* fatty acid profiles during infection with *E. huxleyi* virus 86: Physiological and ecological implications. *Aquat. Microb. Ecol.* **55**, 219–228, doi:10.3354/ame01295.

Fabris, M., Matthijs, M., Rombauts, S., Vyverman, W., Goossens, A., Baart, G. J. E. (2012): The metabolic blueprint of *Phaeodactylum tricornutum* reveals a eukaryotic Entner-Doudoroff glycolytic pathway. *Plant J.* **70**, 1004–1014, doi:10.1111/j.1365-313X.2012.04941.x.

Falkowski, P. G. (1997): Evolution of the nitrogen cycle and its influence on the biological sequestration of CO_2 in the ocean. *Nature* **387**, 272–275, doi:10.1038/387272a0.

Falkowski, P. G., Chen, Y.-B. (2003): *Photoacclimation of light harvesting systems in eukaryotic algae*. In *Light-harvesting antennas in photosynthesis*. Eds. Green, B.R., Parson, W.W., Kluwer Academic, Dordrecht, Netherlands, 423–447.

Falkowski, P. G., Raven, J. A. (2007): *An introduction to photosynthesis in aquatic systems*. In *Aquatic Photosynthesis*, 2nd edition. Eds. Falkowski, P.G., Raven, J.A., Princeton University Press, Princeton, NJ, US, 1–43.

Falkowski, P. G., Schofield, O., Katz, M. E., van de Schootbrugge, B., Knoll, A. H. (2004): *Why is the land green and the ocean red?* In *Coccolithophores: From molecular processes to global impact*, 1rst Ed. Eds. Thierstein, H.R., Young, J.R., Springer, Heidelberg, Germany, 429–453.

Falkowski, P. G., Sukenik, A., Herzig, R. (1989): Nitrogen limitation in *Isochrysis galbana* (Haptophaceae). II. Relative abundance of chloroplast proteins. *J. Phycol.* **25**, 471–478, doi:10.1111/j.1529-8817.1989.tb00252.x.

Fawley, M. W. (1989): A new form of chlorophyll c involved in light-harvesting. *Plant Phys.* **91**, 727–732.

Feder, M. E., Walser, J.-C. (2005): The biological limitations of transcriptomics in elucidating stress and stress responses. *J. Evol. Biol.* **18**, 901–910, doi:10.1111/j.1420-9101.2005.00921.x.

Fernández, E., Balch, W. M., Maranon, E., Holligan, P. M. (1994): High rates of lipid biosynthesis in cultured, mesocosm and coastal populations of the coccolithophore *Emiliania huxleyi*. *Mar. Ecol. Prog. Ser.* **117**, 13–22, doi:10.3354/meps114013.

Fernández, E., Marañón, E., Balch, W. M. (1996): Intracellular carbon partitioning in the coccolithophorid *Emiliania huxleyi*. *J. Mar. Syst.* **9**, 57–66, doi:10.1016/0924-7963(96)00016-4.

Fidalgo, J., Cid, A., Torres, E., Sukenik, A., Herrero, C. (1998): Effects of nitrogen source and growth phase on proximate biochemical composition, lipid classes and fatty acid profile of the marine microalga *Isochrysis galbana*. *Aquaculture* **1166**, 105–116, doi:10.1016/S0044-8486(98)00278-6.

Fiehn, O. (2002): Metabolomics - the link between genotyopes and phenotypes. *Plant Mol. Biol.* **48**, 155–171.

Field, Behrenfeld, Randerson, Falkowski (1998): Primary production of the biosphere: integrating terrestrial and oceanic components. *Science* **281**, 237–240.

Fiorini, S., Gattuso, J.-P., van Rijswijk, P., Middelburg, J. (2010): Coccolithophores lipid and carbon isotope composition and their variability related to changes in seawater carbonate chemistry. *J. Exp. Mar. Biol. Ecol.* **394**, 74–85, doi:10.1016/j.jembe.2010.07.020.

Folch, J., Lees, M., Sloane Stanley, G. H. (1957): A simple method for isolation and purification of total lipids from animal tissues. *J. Biol. Chem.* **226**, 497–509.

Forcisi, S., Moritz, F., Kanawati, B., Tziotis, D., Lehmann, R., Schmitt-Kopplin, P. (2013): Liquid chromatography-mass spectrometry in metabolomics research: mass analyzers in ultra high pressure liquid chromatography coupling. *J. Chromatogr. A* **1292**, 51–65, doi:10.1016/j.chroma.2013.04.017.

Frada, M., Probert, I., Allen, M. J., Wilson, W. H., Vargas, C. de (2008): The "Cheshire Cat" escape strategy of the coccolithophore Emiliania huxleyi in response to viral infection. *PNAS* **105**, 15944–15949, doi:10.1073/pnas.0807707105.

Frada, M. J., Bidle, K. D., Probert, I., Vargas, C. de (2012): In situ survey of life cycle phases of the coccolithophore *Emiliania huxleyi* (Haptophyta). *Environm. Microbiol.* **14**, 1558–1569, doi:10.1111/j.1462-2920.2012.02745.x.

Frankel, E. N. (1980): Lipid oxidation. *Progr. Lipid Res.* **19**, 1–22, doi:10.1016/0163-7827(80)90006-5.

Frankignoulle, M., Canon, C., Gattuso, J.-P. (1994): Marine calcification as a source of carbon dioxide: Positive feedback of increasing atmospheric CO_2. *Limnol. Oceanogr.* **39**, 458–462, doi:10.4319/lo.1994.39.2.0458.

Friend, A. D., Geider, R. J., Behrenfeld, M. J., Still, C. J. (2009): *Photosynthesis in global-scale models*. In *Photosynthesis in silico: Understanding complexity from molecules to ecosystems*. Eds. Laisk, A., Nedbal, K, Govindjee, Springer Netherlands, Dordrecht, Netherlands, 465–497.

Frommolt, R., Goss, R., Wilhelm, C. (2001): The de-epoxidase and epoxidase reactions of *Mantoniella squamata* (Prasinophyceae) exhibit different substrate-specific reaction kinetics compared to spinach. *Planta* **213**, 446–456, doi:10.1007/s004250100589.

Fuchs, B., Suss, R., Teuber, K., Eibisch, M., Schiller, J. (2011): Lipid analysis by thin-layer chromatography - A review of the current state. *J. Chromatogr. A* **1218**, 2754–2774, doi:10.1016/j.chroma.2010.11.066.

Fujita, A., Cheng, J., Fujimoto, T. (2010): Quantitative electron microscopy for the nanoscale analysis of membrane lipid distribution. *Nat. Protoc.* **5**, 661–669, doi:10.1038/nprot.2010.20.

Fujiwara, S., Tsuzuki, M., Kawachi, M., Minaka, N., Inouye, I. (2001): Molecular phylogeny of the Haptophyta based on the rbcL gene and sequence variation in the spacer region of the RUBISCO operon. *J. Phycol.* **37**, 121–129, doi:10.1046/j.1529-8817.2001.037001121.x.

Fulton, J. M., Fredricks, H. F., Bidle, K. D., Vardi, A., Kendrick, B. J., DiTullio, G. R., Van Mooy, B. A. S. (2014): Novel molecular determinants of viral susceptibility and resistance in the lipidome of *Emiliania huxleyi*. *Environm. Microbiol.* **16**, 1137–1149, doi:10.1111/1462-2920.12358.

Gage, D. A., Rhodes, D., Nolte, K. D., Hicks, W. A., Leustek, T., Cooper, A. J., Hanson, A. D. (1997): A new route for synthesis of dimethylsulphoniopropionate in marine algae. *Nature* **387**, 891–894, doi:10.1038/43160.

Gao, K., Helbling, E. W., Häder, D. P., Hutchins, D. A. (2012): Responses of marine primary producers to interactions between ocean acidification, solar radiation, and warming. *Mar. Ecol. Prog. Ser.* **470**, 167–189, doi:10.3354/meps10043.

Gao, K., Ruan, Z., Villafañe, V. E., Gattuso, J.-P., Helbling, E. W. (2009): Ocean acidification exacerbates the effect of UV radiation on the calcifying phytoplankter *Emiliania huxleyi*. *Limnol. Oceanogr.* **54**, 1855–1862, doi:10.4319/lo.2009.54.6.1855.

Garde, K., Cailliau, C. (2000): The impact of UV-B radiation and different PAR intensities on growth, uptake of ^{14}C, excretion of DOC, cell volume, and pigmentation in the marine prymnesiophyte, *Emiliania huxleyi*. *J. Exp. Mar. Biol. Ecol.* **247**, 99–112, doi:10.1016/S0022-0981(00)00145-3.

Garrido, J. L., Brunet, C., Rodriguez, F. (June 27, 2016): Pigment variations in *Emiliania huxleyi* (CCMP370) as a response to changes in light intensity or quality. *Environm. Microbiol.*, doi:10.1111/1462-2920.13373.

Garrido, J. L., Otero, J., Maestro, M. A., Zapata, M. (2000): The main nonpolar chlorophyll c from *Emiliania huxleyi* (Prymnesiophyceae) is a chlorophyll c_2-monogalactosyldiacylglyceride ester: a mass spectrometry study. *J. Phycol.* **36**, 497–505, doi:10.1046/j.1529-8817.2000.99135.x.

Garrido, J. L., Zapata, M., Muniz, S. (1995): Spectral characterization of new chlorophyll c pigments isolated from *Emiliania huxleyi* (Prymnesiophyceae) by high-performance liquid chromatography. *J. Phycol*. **31**, 761–768, doi:10.1111/j.0022-3646.1995.00761.x.

Gebser, B., Pohnert, G. (2013): Synchronized regulation of different zwitterionic metabolites in the osmoadaption of phytoplankton. *Mar. Drugs* **11**, 2168–2182, doi:10.3390/md11062168.

Geider, R. J., Roche, J., Greene, R. M., Olaizola, M. (1993): Response of the photosynthetic apparatus of *Phaeodactylum tricornutum* (Bacillariophyceae) to nitrate, phosphate, or iron starvation. *J. Phycol.* **29**, 755–766, doi:10.1111/j.0022-3646.1993.00755.x.

Gelin, F., Volkman, J. K., Leeuw, J. W. de, Sinninghe Damsté, J. S. (1997): Mid-chain hydroxy long-chain fatty acids in microalgae from the genus *Nannochloropsis*. *Phytochemistry* **45**, 641–646, doi:10.1016/S0031-9422(97)00068-X.

Gillan, F. T., Mcfadden, G. I., Wetherbee, R., Johns, R. B. (1981): Sterols and fatty acids of an antarctic sea ice diatom, *Stauroneis amphioxys*. *Phytochemistry* **20**, 1935–1937, doi:10.1016/0031-9422(81)84038-1.

Giordano, M., Kansiz, M., Heraud, P., Beardall, J., Wood, B., McNaughton, D. (2001): Fourier Transform Infrared Spectroscopy as a novel tool to investigate changes in intracellular macromolecular pools in the marine microalga *Chaetoceros muellerii* (Bacillariophyceae). *J. Phycol.* **31**, 271–279, doi:10.1046/j.1529-8817.2001.037002271.x.

Glauert, A. M. (1968): Electron microscopy of lipids and membranes. *J. Royal. Microsc. Soc.* **88**, 49–70, doi:10.1111/j.1365-2818.1968.tb00597.x.

Goericke, R., Welschmeyer, N. A. (1992): Pigment turnover in the marine diatom *Thalassiosira weissflogii*. II. The $^{14}CO_2$-labeling kinetics of carotenoids. *J. Phycol.* **28**, 507–517, doi:10.1111/j.0022-3646.1992.00507.x.

Gorzolka, K., Kolling, J., Nattkemper, T. W., Niehaus, K. (2016): Spatio-temporal metabolite profiling of the barley germination process by MALDI MS imaging. *PLoS ONE* **11**, e0150208, doi:10.1371/journal.pone.0150208.

Govindjee, Braun, B. Z. (1974): *Light absorption, emission and photosynthesis*. In *Algal physiology and biochemistry*. Eds. Stewart, W., Blackwell Scientific Publication Ltd, Oxford, UK, 346–390.

Green, B. R., Durnford, D. G. (1996): The chlorophyll-carotenoid proteins of oxygenic photosynthesis. *Annu. Rev. Plant Physiol. Plant Mol. Biol.* **47**, 685–714, doi:10.1146/annurev.arplant.47.1.685.

Green, D. H., Echavarri-Bravo, V., Brennan, D., Hart, M. C. (January 30th, 2015): Bacterial diversity associated with the coccolithophorid algae *Emiliania huxleyi* and *Coccolithus pelagicus* f. *braarudii*. *BioMed Res. Int.*, doi:10.1155/2015/194540.

Green, J. C., Course, P. A., Tarran, G. A. (1996): The life-cycle of *Emiliania huxleyi:* A brief review and a study of relative ploidy levels analysed by flow cytometry. *J. Mar. Syst.* **9**, 33–44, doi:10.1016/0924-7963(96)00014-0.

Grewe, S., Ballottari, M., Alcocer, M., D'Andrea, C., Blifernez-Klassen, O., Hankamer, B., Mussgnug, J. H., Bassi, R., Kruse, O. (2014): Light-harvesting complex protein LHCBM9 is critical for photosystem II activity and hydrogen production in *Chlamydomonas reinhardtii*. *Plant Cell* **26**, 1598–1611, doi:10.1105/tpc.114.124198.

Gröne, T., Kirst, G. O. (1991): Aspects of dimethylsulfoniopropionate effects on enzymes isolated from the marine phytoplankter *Tetraselmis subcordiformis* (Stein). *J. Plant Phys.* **138**, 85–91, doi:10.1016/S0176-1617(11)80735-2.

Gröne, T., Kirst, G. O. (1992): The effect of nitrogen deficiency, methionine and inhibitors of methionine metabolism on the DMSP contents of *Tetraselmis subcordiformis* (Stein). *Mar. Biol.* **112**, 497–503, doi:10.1007/BF00356296.

Gross, J. H. (2004): *Mass Spectrometry: A Textbook*, Springer-Verlag, Berlin, Germany.

Guan, W., Gao, K. (2010): Enhanced calcification ameliorates the negative effects of UV radiation on photosynthesis in the calcifying phytoplankter *Emiliania huxleyi*. *Chin. Sci. Bull.* **55**, 588–593, doi:10.1007/s11434-010-0042-5.

Guschina, I. A., Harwood, J. L. (2006): Lipids and lipid metabolism in eukaryotic algae. *Prog. Lipid Res.* **45**, 160–186, doi:10.1016/j.plipres.2006.01.001.

Hager, A. (1975): Die reversiblen, lichtabhängigen Xanthophyllumwandlungen im Chloroplasten. *Ber. Dtsch. Bot. Ges.* **88**, 27–44.

Hagino, K., Bendif, E. M., Young, J. R., Kogame, K., Probert, I., Takano, Y., Horiguchi, T., Vargas, C. de, Okada, H. (2011): New evidence for morphological and genetic variation in the cosmopolitan coccolithophore *Emiliania huxleyi* (Prymnesiophyceae) from the COX1b-ATP4 genes. *J. Phycol.* **47**, 1164–1176, doi:10.1111/j.1529-8817.2011.01053.x.

Han, J., Gagnon, S., Eckle, T., Borchers, C. H. (2013): Metabolomic analysis of key central carbon metabolism carboxylic acids as their 3-nitrophenylhydrazones by UPLC/ESI-MS. *Electrophoresis* **34**, 2891–2900, doi:10.1002/elps.201200601.

Han, X., Gross, R. W. (2005): *Toward total cellular lipidome analysis by ESI mass spectrometry from a crude lipid extract*. In *Modern methods for lipid analysis by liquid chromatography/mass spectrometry and related techniques*. Eds. Byrdwell, W.C., AOCS Press, Champaign, Ill, US, 488–509.

Hansen, F. C., Witte, H. J., Passarge, J. (1996): Grazing in the heterotrophic dinoflagellate *Oxyrrhis marina*: Size selectivity and preference for calcified *Emiliania huxleyi* cells. *Aquat. Microb. Ecol.* **10**, 307–313, doi:10.3354/ame010307.

Harder, U., Koletzko, B., Peissner, W. (2011): Quantification of 22 plasma amino acids combining derivatization and ion-pair LC–MS/MS. *J. Chromatogr. B* **879**, 495–504, doi:10.1016/j.jchromb.2011.01.010.

Harris, G. N., Scanlan, D. J., Geider, R. J. (2005): Acclimation of *Emiliania huxleyi* (Prymnesiophyceae) to photon flux density. *J. Phycol.* **41**, 851–862, doi:10.1111/j.1529-8817.2005.00109.x.

Hart-Smith, G., Blanksby, S. J. (2012): *Mass analysis*. In *Mass spectrometry in polymer chemistry*. Eds. Barner-Kowollik, C., Wiley-VCH, Weinheim, Germany, 5–32.

Harwood, J. L. (1998): *Membrane lipids in algae*. In *Lipids in photosynthesis: Structure, function, and genetics*. Eds. Siegenthaler, P.A., Murata, N., Kluwer Academic Publishers, Dordrecht, Netherlands, 53–64.

Haxo, F. T. (1960): *Photosynthesis in algae containing special pigments*. In *The assimilation of carbon dioxide: 2 parts*. Eds. Pirson, A., Springer Berlin Heidelberg, Berlin, Germany, 1363–1377.

Haxo, F. T. (1985): Photosynthetic action spectrum of the coccolithophorid, *Emiliania huxleyi* (Haptophyceae): 19'hexanoyloxyfucoxanthin as antenna pigment. *J. Phycol.* **21**, 282–287, doi:10.1111/j.0022-3646.1985.00282.x.

Henriksen, K., Stipp, S., Young, J. R., Marsh, M. E. (2005): Biological control on calcite crystallization: AFM investigation of coccolith polysaccharide function. *Am. Mineralog.* **89**, 1709–1716, doi:10.2138/am-2004-11-1217.

Hildebrand, M., Abbriano, R. M., Polle, J. E. W., Traller, J. C., Trentacoste, E. M., Smith, S. R., Davis, A. K. (2013): Metabolic and cellular organization in evolutionarily diverse microalgae as related to biofuels production. *Curr. Opin. Chem. Biol.* **17**, 506–514, doi:10.1016/j.cbpa.2013.02.027.

Hipkin, C. R., Thomas, R. J., Syrett, P. J. (1983): Effects of nitrogen deficiency on nitrate reductase, nitrate assimilation and photosynthesis in unicellular marine algae. *Mar. Biol.* **2**, 101–105, doi:10.1007/BF00396306.

Hirokawa, Y., Fujiwara, S., Suzuki, M., Akiyama, T., Sakamoto, M., Kobayashi, S., Tsuzuki, M. (2008): Structural and physiological studies on the storage beta-polyglucan of haptophyte *Pleurochrysis haptonemofera*. *Planta* **227**, 589–599, doi:10.1007/s00425-007-0641-9.

Hodgson, P. A., Henderson, R. J., Sargent, J. R., Leftley, J. W. (1991): Patterns of variation in the lipid class and fatty acid composition of *Nannochloropsis oculata* (Eustigmatophyceae) during batch culture. *J. Appl. Phycol.* **3**, 169–181, doi:10.1007/BF00003699.

Hoffmann, R., Kirchlechner, C., Langer, G., Wochnik, A. S., Griesshaber, E., Schmahl, W. W., Scheu, C. (2015): Insight into *Emiliania huxleyi* coccospheres by focused ion beam sectioning. *Biogeosciences* **12**, 825–834, doi:10.5194/bg-12-825-2015.

Hofmann, E., Wrench, P. M., Sharples, F. P., Hiller, R. G., Welte, W., Diederichs, K. (1996): Structural basis of light harvesting by carotenoids: Peridinin-chlorophyll-protein from *Amphidinium carterae*. *Science* **272**, 1788–1791, doi:10.1126/science.272.5269.1788.

Holcapek, M., Lisa, M., Jandera, P., Kabatova, N. (2005): Quantitation of triacylglycerols in plant oils using HPLC with APCI-MS, evaporative light-scattering, and UV detection. *J. Sep. Sci.* **28**, 1315–1333.

Holligan, P. M., Fernández, E., Aiken, J., Balch, W. M., Boyd, P., Burkill, P. H., Finch, M., Groom, S. B., Malin, G., Muller, K., Purdie, D. A., Robinson, C., Trees, C. C., Turner, S. M., van der Wal, P. (1993): A biogeochemical study of the coccolithophore, *Emiliania huxleyi* , in the North Atlantic. *Global Biogeochem. Cycles* **7**, 879–900, doi:10.1029/93GB01731.

Holligan, P. M., Viollier, M., Harbour, D. S., Camus, P., Champagne-Philippe, M. (1983): Satellite and ship studies of coccolithophore production along a continental shelf edge. *Nature* **304**, 339–342, doi:10.1038/304339a0.

Hoober, J., Eggink, L. L. (2001): A potential role of chlorophylls b and c in assembly of light-harvesting complexes. *FEBS Letters* **489**, 1–3, doi:10.1016/S0014-5793(00)02410-8.

Horn, P. J., Chapman, K. D. (2014): Lipidomics in situ: insights into plant lipid metabolism from high resolution spatial maps of metabolites. *Prog. Lipid Res.* **54**, 32–52, doi:10.1016/j.plipres.2014.01.003.

Hou, J., Huang, B., Cao, Z., Chen, J., Hong, H. (2007): Effects of nutrient limitation on pigments in *Thalassiosira weissflogii* and *Prorocentrum donghaiense*. *J. Integr. Plant Biol.* **49**, 686–697, doi:10.1111/j.1744-7909.2007.00449.x.

Houdan, A., Probert, I., van Lenning, K., Lefebvre, S. (2005): Comparison of photosynthetic responses in diploid and haploid life-cycle phases of *Emiliania huxleyi* (Prymnesiophyceae). *Mar. Ecol. Prog. Ser.* **292**, 139–146, doi:10.3354/meps292139.

Houdan, A., Probert, I., Zatylyn, C., Véron, B., Billard, C. (2006): Ecology of oceanic coccolithophores. I. Nutritional preferences of the two stages in the life cycle of *Coccolithus braarudii* and *Calcidiscus leptoporus*. *Aquat. Microb. Ecol.* **44**, 291–301.

Hu, Q., Sommerfeld, M., Jarvis, E., Ghirardi, M., Posewitz, M., Seibert, M., Darzins, A. (2008): Microalgal triacylglycerols as feedstocks for biofuel production: Perspectives and advances. *Plant. J.* **54**, 621–639, doi:10.1111/j.1365-313X.2008.03492.x.

Hunter, J. E., Frada, M. J., Fredricks, H. F., Vardi, A., Van Mooy, B. A. S. (October 13, 2015): Targeted and untargeted lipidomics of *Emiliania huxleyi* viral infection and life cycle phases highlights molecular biomarkers of infection, susceptibility, and ploidy. *Front. Mar. Sci.*, doi:10.3389/fmars.2015.00081.

Ietswaart, T., Schneider, P. J., Prins, R. A. (1994): Utilization of organic nitrogen sources by two phytoplankton species and a bacterial isolate in pure and mixed cultures. *Appl. Environm. Microbiol.* **60**, 1554–1560.

Iglesias-Rodriguez, M. D., Halloran, P. R., Rickaby, R. E. M., Hall, I. R., Colmenero-Hidalgo, E., Gittins, J. R., Green, D. R. H., Tyrrell, T., Gibbs, S. J., Dassow, P. von, Rehm, E., Armbrust, E. V., Boessenkool, K. P. (2008): Phytoplankton calcification in a high-CO_2 world. *Science*, doi:10.1126/science.1154122.

Iglesias-Rodríguez, M. D., Brown, C. W., Doney, S. C., Kleypas, J., Kolber, D., Kolber, Z., Hayes, P. K., Falkowski, P. G. (2002): Representing key phytoplankton functional groups in ocean carbon cycle models: Coccolithophorids. *Global Biogeochem. Cycles* **16**, 47-1-47-20, doi:10.1029/2001GB001454.

Inoue, Y., Watanabe, K., Shimosaka, M., Saikusa, T., Fukuda, Y., Murata, K., Kimura, A. (1985): Metabolism of 2-oxoaldehydes in yeasts. *Eur. J. Biochem.* **153**, 243–247, doi:10.1111/j.1432-1033.1985.tb09293.x.

Jaeger, D., Pilger, C., Hachmeister, H., Oberländer, E., Wördenweber, R., Wichmann, J., Mussgnug, J. H., Huser, T., Kruse, O. (September 28, 2016): Label-free *in vivo* analysis of intracellular lipid droplets in the oleaginous microalga *Monoraphidium neglectum* by coherent Raman scattering microscopy. *Sci. Rep.*, doi:10.1038/srep35340.

Jahn, M., Jahn, D. (2012): *Electron transfer reactions and oxidative phosphorylation*. In *Biochemical pathways: an atlas of biochemistry and molecular biology*, 2. ed. Eds. Michal, G., Wiley, Hoboken, NJ, US.

Jakob, T., Goss, R., Wilhelm, C. (2001): Unusual pH-dependence of diadinoxanthin de-epoxidase activation causes chlororespiratory induced accumulation of diatoxanthin in the diatom *Phaeodactylum tricornutum*. *J. Plant Phys.* **158**, 383–390, doi:10.1078/0176-1617-00288.

Jaya, B. N., Hoffmann, R., Kirchlechner, C., Dehm, G., Scheu, C., Langer, G. (2016): Coccospheres confer mechanical protection: New evidence for an old hypothesis. *Acta Biomater.* **42**, 258–264, doi:10.1016/j.actbio.2016.07.036.

Jeffrey, S. W. (1972): Preparation and some properties of crystalline chlorophyll c_1 and c_2 from marine algae. *Biochim. Biophys. Acta* **279**, 15–33, doi:10.1016/0304-4165(72)90238-3.

Jeffrey, S. W., Anderson, J. M. (2000): *Emiliania huxleyi* (Haptophyta) holds promising insights for photosynthesis. *J. Phycol.* **36**, 449–452, doi:10.1046/j.1529-8817.2000.00ag3.x.

Jeffrey, S. W., Mantoura, R., Wright, S. W. (1997): *Phytoplankton pigments in oceanography: guidelines to modern methods*, 1rst ed, Unesco Publishing, Paris, France.

Johnson, H. E., Broadhurst, D., Kell, D. B., Theodorou, M. K., Merry, R. J., Griffith, G. W. (2004): High-throughput metabolic fingerprinting of legume silage fermentations via Fourier transform infrared spectroscopy and chemometrics. *Appl. Environm. Microbiol.* **70**, 1583–1592, doi:10.1128/AEM.70.3.1583-1592.2004.

Johnson, X., Alric, J. (2013): Central carbon metabolism and electron transport in *Chlamydomonas reinhardtii*: metabolic constraints for carbon partitioning between oil and starch. *Euk. Cell* **12**, 776–793, doi:10.1128/EC.00318-12.

Jones, B. M., Edwards, R. J., Skipp, P. J., O'Connor, C. D., Iglesias-Rodriguez, M. D. (2011): Shotgun proteomic analysis of *Emiliania huxleyi*, a marine phytoplankton species of major biogeochemical importance. *Mar. Biotech.* **13**, 496–504, doi:10.1007/s10126-010-9320-0.

Jones, B. M., Iglesias-Rodriguez, M. D., Skipp, P. J., Edwards, R. J., Greaves, M. J., Young, J. R., Elderfield, H., O'Connor, C. D. (April 12, 2013): Responses of the *Emiliania huxleyi* proteome to ocean acidification. *PLoS ONE*, doi:10.1371/journal.pone.0061868.

Kaczmarzyk, D., Fulda, M. (2010): Fatty acid activation in cyanobacteria mediated by acyl-acyl carrier protein synthetase enables fatty acid recycling. *Plant Physiol.* **152**, 1598–1610, doi:10.1104/pp.109.148007.

Kaffes, A., Thoms, S., Trimborn, S., Rost, B., Langer, G., Richter, K.-U., Köhler, A., Norici, A., Giordano, M. (2010): Carbon and nitrogen fluxes in the marine coccolithophore *Emiliania huxleyi* grown under different nitrate concentrations. *J. Exp. Mar. Biol. Ecol.* **393**, 1–8, doi:10.1016/j.jembe.2010.06.004.

Kail, B. W., Link, D. D., Morreale, B. D. (2012): Determination of free fatty acids and triglycerides by gas chromatography using selective esterification reactions. *J. Chromatogr. Sci.* **50**, 934–939, doi:10.1093/chromsci/bms093.

Kalacheva, G. S., Zhila, N. O., Volova, T. G. (2002): Lipid and hydrocarbon compositions of a collection strain and a wild sample of the green microalga *Botryococcus*. *Aquat. Ecol.* **36**, 317–331, doi:10.1023/A:1015615618420.

Kamalanathan, M., Pierangelini, M., Shearman, L. A., Gleadow, R., Beardall, J. (2016): Impacts of nitrogen and phosphorus starvation on the physiology of *Chlamydomonas reinhardtii*. *J. Appl. Phycol.* **28**, 1509–1520, doi:10.1007/s10811-015-0726-y.

Kanya, T., Rao, L, J., Sastry, M. (2007): Characterization of wax esters, free fatty alcohols and free fatty acids of crude wax from sunflower seed oil refineries. *Food Chem.* **4**, 1552–1557.

Kayano, K., Saruwatari, K., Kogure, T., Shiraiwa, Y. (2011): Effect of coccolith polysaccharides isolated from the coccolithophorid, *Emiliania huxleyi*, on calcite crystal formation in in vitro $CaCO_3$ crystallization. *Mar. Biotechnol.* **13**, 83–92, doi:10.1007/s10126-010-9272-4.

Kayano, K., Shiraiwa, Y. (2009): Physiological regulation of coccolith polysaccharide production by phosphate availability in the coccolithophorid *Emiliania huxleyi*. *Plant Cell Physiol.* **50**, 1522–1531, doi:10.1093/pcp/pcp097.

Ke, B. (2001): *Photosynthesis: Photobiochemistry and photobiophysics*, Kluwer Academic Publishers, Dordrecht, Boston.

Keller, D. M., Kiene, P. R., Matrai, A. P., Bellows, K. W. (1999): Production of glycine betaine and dimethylsulfoniopropionate in marine phytoplankton. I. Batch cultures. *Mar. Biol.* **135**, 237–248, doi:10.1007/s002270050621.

Khozin-Goldberg, I. (2016): *Lipid metabolism in microalgae*. In *The Physiology of Microalgae*, 1st ed. Eds. Borowitzka, M.A., Beardall, J., Raven, J.A., Springer International Publishing, Cham, Switzerland, 413–484.

Kim, S. M., Jung, Y.-J., Kwon, O.-N., Cha, K. H., Um, B.-H., Chung, D., Pan, C.-H. (2012): A potential commercial source of fucoxanthin extracted from the microalga *Phaeodactylum tricornutum*. *Appl. Biochem. Biotechn.* **166**, 1843–1855, doi:10.1007/s12010-012-9602-2.

Kirk, J. T. O. (2011): *Light and photosynthesis in aquatic ecosystems*, 3. ed., Cambridge University Press, Cambridge, UK.

Klaveness, D. (1972a): *Coccolithus huxleyi* (Lohman) Kaptner. I. Morphological investigations on the vegetative cell and the process of coccolith formation. *Protistologica* **8**, 335–346.

Klaveness, D. (1972b): *Coccolithus huxleyi* (Lohm.) Kamptn II. The flagellate cell, aberrant cell types, vegetative propagation and life cycles. *Br. Phycol. J.* **7**, 309–318, doi:10.1080/00071617200650321.

Klaveness, D., Paasche, E. (1971): Two different *Coccolithus huxleyi* cell types incapable of coccolith formation. *Archiv. Mikrobiol.* **75**, 382–385, doi:10.1007/BF00407700.

Klein, U. (1986): Compartmentation of glycolysis and of the oxidative pentose-phosphate pathway in *Chlamydomonas reinhardii*. *Planta* **167**, 81–86, doi:10.1007/BF00446372.

Klöck, G., Kreuzberg, K. (1991): Compartmented metabolite pools in protoplasts from the green alga *Chlamydomonas reinhardtii*: Changes after transition from aerobiosis to anaerobiosis in the dark. *Biochim. Biophys. Acta* **1073**, 410–415.

Kluender, C., Sans-Piché, F., Riedl, J., Altenburger, R., Härtig, C., Laue, G., Schmitt-Jansen, M. (2009): A metabolomics approach to assessing phytotoxic effects on the green alga *Scenedesmus vacuolatus*. *Metabolomics* **5**, 59–71, doi:10.1007/s11306-008-0139-x.

Knies, D., Wittmüß, P., Appel, S., Sawodny, O., Ederer, M., Feuer, R. (2015): Modeling and simulation of optimal resource management during the diurnal cycle in *Emiliania huxleyi* by genome-scale reconstruction and an extended flux balance analysis approach. *Metabolites* **5**, 659–676, doi:10.3390/metabo5040659.

Knothe, G., Cermak, S. C., Evangelista, R. L. (2009): Cuphea oil as source of biodiesel with improved fuel properties caused by high content of methyl decanoate. *Energy Fuels* **23**, 1743–1747, doi:10.1021/ef800958t.

Knothe, G., Dunn, R. O. (2003): Dependence of oil stability index of fatty compounds on their structure and concentration and presence of metals. *J. Amer. Oil Chem. Soc.* **80**, 1021–1026, doi:10.1007/s11746-003-0814-x.

Kobayashi, K., Endo, K., Wada, H. (2016): *Roles of Lipids in Photosynthesis*. In *Lipids in plant and algae development*. Eds. Nakamura, Y., Li-Beisson, Y., Springer International Publishing, Cham, Switzerland, 21–49.

Kolber, Z., Zehr, J., Falkowski, P. (1988): Effects of growth irradiance and nitrogen limitation on photosynthetic energy conversion in photosystem II. *Plant Physiol.* **88**, 923–929, doi:10.1104/pp.88.3.923.

Kopka, J., Schauer, N., Krueger, S., Birkemeyer, C., Usadel, B., Bergmuller, E., Dormann, P., Weckwerth, W., Gibon, Y., Stitt, M., Willmitzer, L., Fernie, A. R., Steinhauser, D. (2005): GMD@CSB.DB: the Golm Metabolome Database. *Bioinformatics* **21**, 1635–1638, doi:10.1093/bioinformatics/bti236.

Kottmeier, D. M., Rokitta, S. D., Rost, B. (2016): Acidification, not carbonation, is the major regulator of carbon fluxes in the coccolithophore *Emiliania huxleyi*. *New Phytol.* **211**, 126–137, doi:10.1111/nph.13885.

Kozlowska-Szerenos, B., Bialuk, I., Maleszewski, S. (2004): Enhancement of photosynthetic O_2 evolution in *Chlorella vulgaris* under high light and increased CO_2 concentration as a sign of acclimation to phosphate deficiency. *Plant Physiol. Biochem.* **42**, 403–409, doi:10.1016/j.plaphy.2004.02.010.

Kroth, P. G., Chiovitti, A., Gruber, A., Martin-Jezequel, V., Mock, T., Parker, M. S., Stanley, M. S., Kaplan, A., Caron, L., Weber, T., Maheswari, U., Armbrust, E. V., Bowler, C. (2008): A model for carbohydrate metabolism in the diatom *Phaeodactylum tricornutum* deduced from comparative whole genome analysis. *PLoS ONE* **3**, e1426, doi:10.1371/journal.pone.0001426.

Kruve, A., Rebane, R., Kipper, K., Oldekop, M.-L., Evard, H., Herodes, K., Ravio, P., Leito, I. (2015): Tutorial review on validation of liquid chromatography-mass spectrometry methods: Part I. *Anal. Chim. Acta* **870**, 29–44, doi:10.1016/j.aca.2015.02.017.

Kuenzler, E. J., Perras, J. P. (1965): Phosphatates of marine algae. *Biol. Bull.* **128**, 271–284, doi:10.2307/1539555.

Kühlbrandt, W., Wang, D. N., Fujiyoshi, Y. (1994): Atomic model of plant light-harvesting complex by electron crystallography. *Nature* **367**, 614–621, doi:10.1038/367614a0.

Landry, D. M., Gaasterland, T., Palenik, B. P. (2006): Molecular characerization of a phosphate-regulated cell-surface protein from the coccolithophorid, *Emiliania huxleyi* (Prymnesiophyceae). *J. Phycol.* **42**, 814–821, doi:10.1111/j.1529-8817.2006.00247.x.

Larkum, A. W. (2016): *Photosynthesis and light harvesting in algae*. In *The Physiology of Microalgae*, 1st ed. Eds. Borowitzka, M.A., Beardall, J., Raven, J.A., Springer International Publishing, Cham, Switzerland, 67–87.

Larkum, A. W., Scaramuzzi, C., Cox, G. C., Hiller, R. G., Turner, A. G. (1994): Light-harvesting chlorophyll c-like pigment in *Prochloron*. *PNAS* **91**, 679–683.

Latasa, M., Berdalet, E. (1994): Effect of nitrogen or phosphorus starvation on pigment composition of cultured *Heterocapsa* sp. *J. Plankton Res.* **16**, 83–94, doi:10.1093/plankt/16.1.83.

Le Williams, P. J., del Giorgio, P. A. (2005): *Respiration in aquatic ecosystems: history and background*. In *Respiration in aquatic ecosystems*. Eds. Del Giorgio, P.A., Williams, P.J.l., Oxford University Press, Oxford, NY, US, 1–18.

Lecourt, M., Muggli, D. L., Harrison, P. J. (1996): Comparison of growth and sinking rates of non-coccolith- and coccolith-forming strains of *Emiliania huxleyi* (Prymnesiophyceae) grown under different irradiances and nitrogen sources. *J. Phycol.* **32**, 17–21, doi:10.1111/j.0022-3646.1996.00017.x.

Lee, R. B. Y., Mavridou, D. A. I., Papadakos, G., McClelland, H. L. O., Rickaby, R. E. M. (2016): The uronic acid content of coccolith-associated polysaccharides provides insight into coccolithogenesis and past climate. *Nat. Commun.*, doi:10.1038/ncomms13144.

Lee, R. E. (2008): *Phycology*, 4th ed., Cambridge University Press, Cambridge, UK.

Lefebvre, S. C., Harris, G., Webster, R., Leonardos, N., Geider, R. J., Raines, C. A., Read, B. A., Garrido, J. L. (2010): Characterization and expression analysis of the *Lhcf* gene family in *Emiliania huxleyi* (Haptophyta) reveals differential responses to light and CO_2. *J. Phycol.* **46**, 123–134, doi:10.1111/j.1529-8817.2009.00793.x.

Lehahn, Y., Koren, I., Schatz, D., Frada, M., Sheyn, U., Boss, E., Efrati, S., Rudich, Y., Trainic, M., Sharoni, S., Laber, C., DiTullio, G. R., Coolen, M. J. L., Martins, A. M., Van Mooy, B. A. S., Bidle, K. D., Vardi, A. (2014): Decoupling physical from biological processes to assess the impact of viruses on a mesoscale algal bloom. *Curr. Biol.* **24(17)**, 2041–2046, doi:10.1016/j.cub.2014.07.046.

Lepetit, B., Goss, R., Jakob, T., Wilhelm, C. (2012): Molecular dynamics of the diatom thylakoid membrane under different light conditions. *Photosynth. Res.* **111**, 245–257, doi:10.1007/s11120-011-9633-5.

Lessard, E. J., Merico, A., Tyrrell, T. (2005): Nitrate:Phosphate ratios and *Emiliania huxleyi* blooms. *Limnol. Oceanogr.* **50**, 1020–1024, doi:10.4319/lo.2005.50.3.1020.

Li, Y., Horsman, M., Wang, B., Wu, N., Lan, C. Q. (2008): Effects of nitrogen sources on cell growth and lipid accumulation of green alga *Neochloris oleoabundans*. *Appl. Microbiol. Biotechnol.* **81**, 629–636, doi:10.1007/s00253-008-1681-1.

Liaud, M.-F., Lichtlé, Christiane, Apt, Kirk, Martin, W., Cerff, R. (2000): Compartment-specific isoforms of TPI and GAPDH are imported into diatom mitochondria as a fusion protein: Evidence in favor of a mitochondrial origin of the eukaryotic glycolytic pathway. *Mol. Biol. Evol.* **17**, 213–223.

Li-Beisson, Y., Beisson, F., Riekhof, W. (2015): Metabolism of acyl-lipids in *Chlamydomonas reinhardtii*. *Plant J.* **82**, 504–522, doi:10.1111/tpj.12787.

Li-Beisson, Y., Nakamura, Y., Harwood, J. (2016): *Lipids: From Chemical Structures, Biosynthesis, and Analyses to Industrial Applications*. In *Lipids in plant and algae development*. Eds. Nakamura, Y., Li-Beisson, Y., Springer International Publishing, Cham, Switzerland, 1–18.

Linschooten, C., Bleijswijk, J. D. L., Emburg, P. R., Vrind, J. P. M., Kempers, E. S., Westbroek, P., Vrind-de Jong, E. W. (1991): Role of the light-dark cycle and medium composition on the production onf coccoliths by *Emiliania huxleyi* (Haptophyceae). *J. Phycol.* **27**, 82–86, doi:10.1111/j.0022-3646.1991.00082.x.

Lísa, M., Lynen, F., Holcapek, M., Sandra, P. (2007): Quantitation of triacylglycerols from plant oils using charged aerosol detection with gradient compensation. *J. Chromatogr. A* **1176**, 135–142, doi:10.1016/j.chroma.2007.10.075.

Liu, Z., Yan, H., Wang, K., Kuang, T., Zhang, J., Gui, L., An, X., Chang, W. (2004): Crystal structure of spinach major light-harvesting complex at 2.72 Å resolution. *Nature* **428**, 287–292, doi:10.1038/nature02373.

Llewellyn, C. A., Evans, C., Airs, R. L., Cook, I., Bale, N., Wilson, W. H. (2007): The response of carotenoids and chlorophylls during virus infection of *Emiliania huxleyi* (Prymnesiophyceae). *J. Exp. Mar. Biol. Ecol.* **344**, 101–112, doi:10.1016/j.jembe.2006.12.013.

Llewellyn, C. A., Gibb, S. W. (2000): Intra-class variability in the carbon, pigment and biomineral content of prymnesiophytes and diatoms. *Mar. Ecol. Prog. Ser.* **193**, 33–44.

Loebl, M., Cockshutt, A. M., Campbell, D. A., Finkel, Zoe V. (2010): Physiological basis for high resistance to photoinhibition under nitrogen depletion in *Emiliania huxleyi*. *Limn. Oceanogr.* **55**, 2150–2160, doi:10.4319/lo.2010.55.5.2150.

Lohr, M., Wilhelm, C. (1999): Algae displaying the diadinoxanthin cycle also possess the violaxanthin cycle. *PNAS* **96**, 8784–8789, doi:10.1073/pnas.96.15.8784.

Lombardi, A. T., Wangersky, P. J. (1995): Particulate lipid class composition of three marine phytoplankters *Chaetoceros gracilis*, *Isochrysis galbana* (Tahiti) and *Dunaliella tertiolecta* grown in batch culture. *Hydrobiologia* **306**, 1–6, doi:10.1007/BF00007853.

Malin, G. (1996): *The role of DMSP and DMS in the global sulfur cycle and climate regulation*. In *Biological and environmental chemistry of DMSP and related sulfonium compounds*. Eds. Keller, M.D., Kiene, R.P., Kirst, G.O., Visscher, P.T., Springer US, Boston, MA, US, 177–189.

Malin, G., Steinke, M. (2004): *Dimethyl sulfide production: what is the contribution of the coccolithophores?* In *Coccolithophores: From molecular processes to global impact*, 1rst Ed. Eds. Thierstein, H.R., Young, J.R., Springer, Heidelberg, Germany, 127–164.

Malitsky, S., Ziv, C., Rosenwasser, S., Zheng, S., Schatz, D., Porat, Z., Ben-Dor, S., Aharoni, A., Vardi, A. (2016): Viral infection of the marine alga *Emiliania huxleyi* triggers lipidome remodeling and induces the production of highly saturated triacylglycerol. *New Phytol.* **210**, 88–96, doi:10.1111/nph.13852.

Mann, S., Sparks, N. H. C. (1988): Single crystalline nature of coccolith elements of the marine alga *Emiliania huxleyi* as determined by electron diffraction and high-resolution transmission. *Proc. Royal Soc. B* **1277**, 441–453, doi:10.1098/rspb.1988.0057.

Mansilla, M. C., Cybulski, L. E., Albanesi, D., Mendoza, D. de (2004): Control of membrane lipid fluidity by molecular thermosensors. *J. Bacteriol.* **186**, 6681–6688, doi:10.1128/JB.186.20.6681-6688.2004.

Margalef, R. (1978): Life-forms of phytoplankton as survival alternatives in an unstable environment. *Oceanol. Acta* **1**, 493–509.

Marriott, P. J. (2004): *Gas chromatography*. In *Chromatography: Fundamentals and applications of chromatography and related differential migration methods*, 6th ed. Eds. Heftmann, E., Elsevier, Amsterdam, Netherlands, 319–368.

Martin, P., Dyhrman, S. T., Lomas, M. W., Poulton, N. J., Van Mooy, B. A. S. (2014): Accumulation and enhanced cycling of polyphosphate by Sargasso Sea plankton in response to low phosphorus. *PNAS* **111**, 8089–8094, doi:10.1073/pnas.1321719111.

Martins, D. A., Custodio, L., Barreira, L., Pereira, H., Ben-Hamadou, R., Varela, J., Abu-Salah, K. M. (2013): Alternative sources of n-3 long-chain polyunsaturated fatty acids in marine microalgae. *Mar. Drugs* **11**, 2259–2281, doi:10.3390/md11072259.

Mausz, M. A., Pohnert, G. (2015): Phenotypic diversity of diploid and haploid *Emiliania huxleyi* cells and of cells in different growth phases revealed by comparative metabolomics. *J. Plant Physiol.* **172**, 137–148, doi:10.1016/j.jplph.2014.05.014.

McKew, B. A., Davey, P., Finch, S. J., Hopkins, J., Lefebvre, S. C., Metodiev, M. V., Oxborough, K., Raines, C. A., Lawson, T., Geider, R. J. (2013a): The trade-off between the light-harvesting and photoprotective functions of fucoxanthin-chlorophyll proteins dominates light acclimation in *Emiliania huxleyi* (clone CCMP 1516). *New Phytol.* **200**, 74–85, doi:10.1111/nph.12373.

McKew, B. A., Lefebvre, S. C., Achterberg, E. P., Metodieva, G., Raines, C. A., Metodiev, M. V., Geider, R. J. (2013b): Plasticity in the proteome of *Emiliania huxleyi* CCMP 1516 to extremes of light is highly targeted. *New Phytol.* **200**, 61–73, doi:10.1111/nph.12352.

McKew, B. A., Metodieva, G., Raines, C. A., Metodiev, M. V., Geider, R. J. (2015): Acclimation of *Emiliania huxleyi* (1516) to nutrient limitation involves precise modification of the proteome to scavenge alternative sources of N and P. *Environ. Microbiol.* **17**, 4050–4062, doi:10.1111/1462-2920.12957.

Melkozernov, A. N., Blankenship, R. E. (2006): *Photosynthetic functions of chlorophylls*. In *Chlorophylls and bacteriochlorophylls: Biochemistry, biophysics, functions and applications*. Eds. Grimm, B., Porra, R.J., Rüdiger, W., Scheer, H., Springer, Dordrecht, Netherlands, 397–412.

Miller, G., Honig, A., Stein, H., Suzuki, N., Mittler, R., Zilberstein, A. (2009): Unraveling delta1-pyrroline-5-carboxylate-proline cycle in plants by uncoupled expression of proline oxidation enzymes. *J. Biol. Chem.* **284**, 26482–26492, doi:10.1074/jbc.M109.009340.

Mizoguchi, T., Kimura, Y., Yoshitomi, T., Tamiaki, H. (2011): The stereochemistry of chlorophyll-c_3 from the haptophyte *Emiliania huxleyi*: The (13^2R)-enantiomers of chlorophylls-c are exclusively selected as the photosynthetically active pigments in chromophyte algae. *Biochim. Biophys. Acta* **1807**, 1467–1473, doi:10.1016/j.bbabio.2011.07.008.

Mjøs, S. A. (2003): Identification of fatty acids in gas chromatography by application of different temperature and pressure programs on a single capillary column. *J. Chromatogr. A* **1015**, 151–161, doi:10.1016/S0021-9673(03)01240-8.

Mohan, R., Mergulhao, L. P., Guptha, M., Rajakumar, A., Thamban, M., AnilKumar, N., Sudhakar, M., Ravindra, R. (2008): Ecology of coccolithophores in the Indian sector of the Southern Ocean. *Mar. Micropaleont.* **67**, 30–45, doi:10.1016/j.marmicro.2007.08.005.

Moheimani, N. R., Webb, J. P., Borowitzka, M. A. (2012): Bioremediation and other potential applications of coccolithophorid algae: A review. *Algal Res.* **2**, 120–133, doi:10.1016/j.algal.2012.06.002.

Moore, C. M., Mills, M. M., Arrigo, K. R., Berman-Frank, I., Bopp, L., Boyd, P. W., Galbraith, E. D., Geider, R. J., Guieu, C., Jaccard, S. L., Jickells, T. D., La Roche, J., Lenton, T. M., Mahowald, N. M., Marañón, E., Marinov, I., Moore, J. K., Nakatsuka, T., Oschlies, A., Saito, M. A., Thingstad, T. F., Tsuda, A., Ulloa, O. (2013): Processes and patterns of oceanic nutrient limitation. *Nature Geosci.* **6**, 701–710, doi:10.1038/ngeo1765.

Moreau, R. A. (2006): The analysis of lipids via HPLC with a charged aerosol detector. *Lipids* **41**, 727–734, doi:10.1007/s11745-006-5024-7.

Mouzdahir, A., Grossi, V., Bakkas, S., Rontani, J.-F. (2001): Visible light-dependent degradation of long-chain alkenes in killed cells of *Emiliania huxleyi* and *Nannochloropsis salina*. *Phytochemistry* **56**, 677–684, doi:10.1016/S0031-9422(00)00468-4.

Mühlroth, A., Li, K., Rokke, G., Winge, P., Olsen, Y., Hohmann-Marriott, M. F., Vadstein, O., Bones, A. M. (2013): Pathways of lipid metabolism in marine algae, co-expression network, bottlenecks and candidate genes for enhanced production of EPA and DHA in species of Chromista. *Mar. Drugs* **11**, 4662–4697, doi:10.3390/md11114662.

Müller, P. J., Kirst, G., Ruhland, G., Storch, I. von, Rosell-Melé, A. (1998): Calibration of the alkenone paleotemperature index $U_{37}^{K'}$ based on core-tops from the eastern South Atlantic and the global ocean (60°N-60°S). *Geochim. Cosmochim. Acta* **62**, 1757–1772, doi:10.1016/S0016-7037(98)00097-0.

Muller-Feuga, A. (2000): The role of microalgae in aquaculture: situation and trends. *J. Appl. Phycol.* **12**, 527–534, doi:10.1023/A:1008106304417.

Murata, N. (1998): *Lipids in photosynthesis: An overview*. In *Lipids in photosynthesis: Structure, function, and genetics*. Eds. Siegenthaler, P.A., Murata, N., Kluwer Academic Publishers, Dordrecht, Netherlands, 1–20.

Murphy, D. J. (1982): The importance of non-planar bilayer regions in photosynthetic membranes and their stabilisation by galactolipids. *FEBS Letters* **150**, 19–26, doi:10.1016/0014-5793(82)81297-0.

Murphy, S. A., Nicolaou, A. (2013): Lipidomics applications in health, disease and nutrition research. *Mol. Nutr. Food Res.* **57**, 1336–1346, doi:10.1002/mnfr.201200863.

Myklestad, S. M. (1989): Production, chemical structure, metabolism, and biological function of the (1→3)-linked, β-D-glucans in diatoms. *Biol. Oceanogr.* **6**, 313–326.

Nanninga, H. J., Tyrrell, T. (1996): Importance of light for the formation of algal blooms by *Emiliania huxleyi*. *Mar. Ecol. Prog. Ser.* **136**, 195–203, doi:10.3354/meps136195.

Natali, A., Croce, R. (2015): Characterization of the major light-harvesting complexes (LHCBM) of the green alga *Chlamydomonas reinhardtii*. *PLoS ONE* **10**, e0119211, doi:10.1371/journal.pone.0119211.

Naumann, D. (2001): FT-Infrared and FT-Raman Spectroscopy in biomedical research. *Appl. Spectrosc. Rev.* **36**, 239–298, doi:10.1081/ASR-100106157.

Naumann, D., Helm, D., Labischinski, H. (1991): Microbiological characterizations by FT-IR spectroscopy. *Nature* **351**, 81–82, doi:10.1038/351081a0.

Nejstgaard, J. C., Gismervik, I., Solberg, P. T. (1997): Feeding and reproduction by *Calanus finmarchicus*, and microzooplankton grazing during mesocosm blooms of diatoms and the coccolithophore *Emiliania huxleyi*. *Mar. Ecol. Prog. Ser.* **147**, 197–217, doi:10.3354/meps147197.

Niessen, W. (2004): *Combined techniques*. In *Chromatography: Fundamentals and applications of chromatography and related differential migration methods*, 6th ed. Eds. Heftmann, E., Elsevier, Amsterdam, Netherlands, 403–430.

Obata, T., Schoenefeld, S., Krahnert, I., Bergmann, S., Scheffel, A., Fernie, A. R. (2013): Gas-chromatography mass-spectrometry (GC-MS) based metabolite profiling reveals mannitol as a major storage carbohydrate in the coccolithophorid alga *Emiliania huxleyi*. *Metabolites* **3**, 168–184, doi:10.3390/metabo3010168.

Oesterhelt, D., Wachtveitl, J. (2012): *Photosynthesis*. In *Biochemical pathways: an atlas of biochemistry and molecular biology*, 2. ed. Eds. Michal, G., Wiley, Hoboken, NJ, US, 188–193.

Okada, H., McIntyre, A. (1979): Seasonal distribution of modern coccolithophores in the western North Atlantic Ocean. *Mar. Biol.* **54**, 319–328, doi:10.1007/BF00395438.

Ono, M., Sawada, K., Kubota, M., Shiraiwa, Y. (2009): Change of the unsaturation degree of alkenone and alkenoate during acclimation to salinity in *Emiliania huxleyi* and *Gephyrocapsa oceanica* with reference to palaeosalinity indicator. *Res. Org. Geochem.* **25**, 53–60.

Ördög, V., Stirk, W. A., Bálint, P., van Staden, J., Lovász, C. (2012): Changes in lipid, protein and pigment concentrations in nitrogen-stressed *Chlorella minutissima* cultures. *J. Appl. Phycol.* **24**, 907–914, doi:10.1007/s10811-011-9711-2.

Paasche, E. (1962): Coccolith formation. *Nature* **193**, 1094–1095, doi:10.1038/1931094b0.

Paasche, E. (1998): Roles of nitrogen and phosphorus in coccolith formation in *Emiliania huxleyi* (Prymnesiophyceae). *Eur. J. Phycol.* **33**, 33–42.

Paasche, E. (2001): A review of the coccolithophorid *Emiliania huxleyi* (Prymnesiophyceae), with particular reference to growth, coccolith formation, and calcification-photosynthesis interactions. *Phycologia* **40**, 503–529, doi:10.2216/i0031-8884-40-6-503.1.

Paasche, E., Brubak, S. (1994): Enhanced calcification in the coccolithophorid *Emiliania huxleyi* (Haptophyceae) under phosphorus limitation. *Phycologia* **33**, 324–330, doi:10.2216/i0031-8884-33-5-324.1.

Palenik, B. (2015): Molecular mechanisms by which marine phytoplankton respond to their dynamic chemical environment. *Ann. Rev. Mar. Sci.* **7**, 325–340, doi:10.1146/annurev-marine-010814-015639.

Palenik, B., Henson, S. E. (1997): The use of amides and other organic nitrogen sources by the phytoplankton *Emiliania huxleyi* . *Limnol. Oceangr.* **42**, 1544–1551.

Pan, H., Sun, M.-Y. (2011): Variations of alkenone based paleotemperature index ($U^{K'}_{37}$) during *Emiliania huxleyi* cell growth, respiration (auto-metabolism) and microbial degradation. *Org. Geochem.* **42**, 678–687, doi:10.1016/j.orggeochem.2011.03.024.

Papagiannakis, E., van H M Stokkum, I., Fey, H., Buchel, C., van Grondelle, R. (2005): Spectroscopic characterization of the excitation energy transfer in the fucoxanthin-chlorophyll protein of diatoms. *Photosynth. Res.* **86**, 241–250, doi:10.1007/s11120-005-1003-8.

Passarelli, M. K., Winograd, N. (2011): Lipid imaging with time-of-flight secondary ion mass spectrometry (ToF-SIMS). *Biochim. Biophys. Acta* **1811**, 976–990, doi:10.1016/j.bbalip.2011.05.007.

Pelusi, A., Hanawa, Y., Araie, H., Suzuki, I., Giordano, M., Shiraiwa, Y. (2016): Rapid detection and quantification of haptophyte alkenones by Fourier transform infrared spectroscopy (FTIR). *Algal Research* **19**, 48–56, doi:10.1016/j.algal.2016.07.006.

Petrou, K., Doblin, M. A., Smith, R. A., Ralph, P. J., Shelly, K., Beardall, J. (2008): State transitions and nonphotochemical quenching during a nutrient-induced fluorescence transient in phosphorus-starved *Dunaliella tertiolecta*. *J. Phycol.* **44**, 1204–1211, doi:10.1111/j.1529-8817.2008.00585.x.

Phang, J. M., Liu, W., Hancock, C., Christian, K. J. (June 21, 2012): The proline regulatory axis and cancer. *Front. Oncol.*, doi:10.3389/fonc.2012.00060.

Piasecki, T., Breadmore, M. C., Macka, M. (2010): White LEDs as broad spectrum light sources for spectrophotometry: demonstration in the visible spectrum range in a diode-array spectrophotometric detector. *Electrophoresis* **31**, 3737–3744, doi:10.1002/elps.201000341.

Plaxton, W. C., Carswell, M. C. (1999): *Metabolic aspects of the phosphate starvation response in plants*. In *From phytohormones to genome reorganization*. Eds. Lerner, H.R., Dekker, New York, US, 349–372.

Pogson, B. J., Rissler, H. M., Frank, H. A. (2005): *The role of carotenoids in energy quenching*. In *Photosystem II: The light-driven water:plastoquinone oxidoreductase*. Eds. Wydrzynski, T.J., Satoh, K., Springer, Dordrecht, Netherlands, 515–537.

Polivka, T., Frank, H. A. (2010): Molecular factors controlling photosynthetic light harvesting by carotenoids. *Acc. Chem. Res* **43**, 1125–1134, doi:10.1021/ar100030m.

Pond, D. W., Harris, R. P. (1996): The lipid composition of the coccolithophore *Emiliania huxleyi* and its possible ecophysiological significance. *J. Mar. Biol. Assoc. UK* **76**, 579–594, doi:10.1017/S0025315400031295.

Porra, R. J. (1997): Recent progress in porphyrin and chlorophyll biosynthesis. *Photochem. Photobiol.* **65**, 492–516, doi:10.1111/j.1751-1097.1997.tb08596.x.

Poulton, A. J., Adey, T. R., Balch, W. M., Holligan, P. M. (2007): Relating coccolithophore calcification rates to phytoplankton community dynamics: Regional differences and implications for carbon export. *Deep Sea Res. Part 2 Top. Stud. Oceanogr.* **54**, 538–557, doi:10.1016/j.dsr2.2006.12.003.

Prahl, F. G., Sparrow, M. A., Wolfe, G. V. (April 9, 2003): Physiological impacts on alkenone paleothermometry. *Paleoceanography*, doi:10.1029/2002PA000803.

Prahl, F. G., Wakeham, S. G. (1987): Calibration of unsaturation patterns in long-chain ketone compositions for palaeotemperature assessment. *Nature* **330**, 367–369, doi:10.1038/330367a0.

Premvardhan, L., Robert, B., Beer, A., Buchel, C. (2010): Pigment organization in fucoxanthin chlorophyll a/c_2 proteins (FCP) based on resonance Raman spectroscopy and sequence analysis. *Biochim. Biophys. Acta B* **1797**, 1647–1656, doi:10.1016/j.bbabio.2010.05.002.

Quinn, P. K., Bates, T. S. (2011): The case against climate regulation via oceanic phytoplankton sulphur emissions. *Nature* **480**, 51–56, doi:10.1038/nature10580.

Raghothama, K. G. (1999): Phosphate acquisition. *Ann. Rev. Plant Physiol. Plant Mol. Biol.* **50**, 665–693, doi:10.1146/annurev.arplant.50.1.665.

Ragni, M., Airs, R. L., Leonardos, N., Geider, R. J. (2008): Photoinhibition of PSII in *Emiliania huxleyi* (Haptophyta) under high light stress: The roles of photoacclimation, photoprotection, and photorepair. *J. Phycol.* **44**, 670–683, doi:10.1111/j.1529-8817.2008.00524.x.

Raven, J. A., Beardall, J. (2003): *Carbohydrate Metabolism and Respiration in Algae*. In *Photosynthesis in Algae*. Eds. Larkum, A.W.D., Douglas, S.E., Raven, J.A., Springer, Dordrecht, Netherlands, 205–224.

Raven, J. A., Beardall, J. (2016): *Dark respiration and organic carbon loss*. In *The Physiology of Microalgae*, 1st ed. Eds. Borowitzka, M.A., Beardall, J., Raven, J.A., Springer International Publishing, Cham, Switzerland, 129–140.

Raven, J. A., Crawfurd, K. (2012): Environmental controls on coccolithophore calcification. *Mar. Ecol. Prog. Ser.* **470**, 137–166, doi:10.3354/meps09993.

Read, B. A., Kegel, J., Klute, M. J., Kuo, A., Lefebvre, S. C., Maumus, F., Mayer, C., Miller, J., Monier, A., Salamov, A., Young, J., Aguilar, M., Claverie, J.-M., Frickenhaus, S., Gonzalez, K., Herman, E. K., Lin, Y.-C., Napier, J., Ogata, H., Sarno, A. F., Shmutz, J., Schroeder, D., de Vargas, C., Verret, F., von Dassow, P., Valentin, K., van de Peer, Y., Wheeler, G., Emiliania huxleyi Annotation Consortium, Dacks, J. B., Delwiche, C. F., Dyhrman, S. T., Glockner, G., John, U., Richards, T., Worden, A. Z., Zhang, X., Grigoriev, I. V. (2013): Pan genome of the phytoplankton *Emiliania* underpins its global distribution. *Nature* **499**, 209–213, doi:10.1038/nature12221.

Reitan, K. I., Rainuzzo, J. R., Olsen, Y. (1994): Effect of nutrient limitation on fatty acid and lipid content of marine microalgae. *J. Phycol.* **30**, 972–979, doi:10.1111/j.0022-3646.1994.00972.x.

Renaud, S. M., Thinh, L.-V., Lambrinidis, G., Parry, D. L. (2002): Effect of temperature on growth, chemical composition and fatty acid composition of tropical Australian microalgae grown in batch cultures. *Aquaculture* **1-4**, 195–214, doi:10.1016/S0044-8486(01)00875-4.

Reyes-Prieto, A., Weber, A. P. M., Bhattacharya, D. (2007): The origin and establishment of the plastid in algae and plants. *Annu. Rev. Genet.* **41**, 147–168, doi:10.1146/annurev.genet.41.110306.130134.

Řezanka, T., Podojil, M. (1984): The very long chain fatty acids of the green alga, *Chlorella kessleri*. *Lipids* **19**, 472–473, doi:10.1007/BF02537412.

Řezanka, T., Sigler, K. (2009): Odd-numbered very-long-chain fatty acids from the microbial, animal and plant kingdoms. *Prog. Lipid Res.* **48**, 206–238, doi:10.1016/j.plipres.2009.03.003.

Řezanka, T., Vokoun, J., Slavíček, J., Podojil, M. (1983): Determination of fatty acids in algae by capillary gas chromatography-mass spectrometry. *J. Chrom. A* **268**, 71–78, doi:10.1016/S0021-9673(01)95388-9.

Rhiel, E., Krupinska, K., Wehrmeyer, W. (1986): Effects of nitrogen starvation on the function and organization of the photosynthetic membranes in *Cryptomonas maculata* (Cryptophyceae). *Planta* **169**, 361–369, doi:10.1007/BF00392132.

Riebesell, U., Zondervan, I., Rost, B., Tortell, P. D., Zeebe, R. E., Morel, F. M. M. (2000): Reduced calcification of marine plankton in response to increased atmospheric CO_2. *Nature* **407**, 364–367, doi:10.1038/35030078.

Riegman, R., Noordeloos, A. A. M., Cadée, G. C. (1992): *Phaeocystis* blooms and eutrophication of the continental coastal zones of the North Sea. *Mar. Biol.* **112**, 479–484, doi:10.1007/BF00356293.

Riegman, R., Stolte, W., Noordeloos, A. A. M., Slezak, D. (2000): Nutrient uptake and alkaline phosphatase (ec 3:1:3:1) activity of *Emiliania huxleyi* (Prymnesiophyceae) during growth under N and P limitation in continuous cultures. *J. Phycol.* **36**, 87–96, doi:10.1046/j.1529-8817.2000.99023.x.

Riekhof, W. R., Sears, B. B., Benning, C. (2005): Annotation of genes involved in glycerolipid biosynthesis in *Chlamydomonas reinhardtii*: Discovery of the betaine lipid synthase BTA1$_{Cr}$. *Euk. Cell* **4**, 242–252, doi:10.1128/EC.4.2.242-252.2005.

Roach, J. A. G., Yurawecz, M. P., Kramer, J. K. G., Mossoba, M. M., Eulitz, K., Ku, Y. (2000): Gas chromatography-high resolution selected-ion mass spectrometric identification of trace 21:0 and 20:2 fatty acids eluting with conjugated linoleic acid isomers. *Lipids* **35**, 797–802, doi:10.1007/s11745-000-0588-9.

Rodolfi, L., Chini Zittelli, G., Bassi, N., Padovani, G., Biondi, N., Bonini, G., Tredici, M. R. (2009): Microalgae for oil: strain selection, induction of lipid synthesis and outdoor mass cultivation in a low-cost photobioreactor. *Biotechnol. Bioeng.* **102**, 100–112, doi:10.1002/bit.22033.

Roessner, U., Wagner, C., Kopka, J., Trethewey, R. N., Willmitzer, L. (2000): Technical advance: simultaneous analysis of metabolites in potato tuber by gas chromatography-mass spectrometry. *Plant J.* **23**, 131–142.

Rokitta, S. D., de Nooijer, L. J., Trimborn, S., de Vargas, C., Rost, B., John, U. (2011): Transcriptome analyses reveal differential gene expression patterns between the life-cycle stages of *Emiliania huxleyi* (Haptophyta) and reflect specialization to different ecological niches. *J. Phycol.* **47**, 829–838, doi:10.1111/j.1529-8817.2011.01014.x.

Rokitta, S. D., Rost, B. (2012): Effects of CO_2 and their modulation by light in the life-cycle stages of the coccolithophore *Emiliania huxleyi*. *Limnol. Oceanogr.* **57**, 607–618, doi:10.4319/lo.2012.57.2.0607.

Rokitta, S. D., von Dassow, P., Rost, B., John, U. (December 2, 2014): *Emiliania huxleyi* endures N-limitation with an efficient metabolic budgeting and effective ATP synthesis. *BMC Genomics*, doi:10.1186/1471-2164-15-1051.

Rokitta, S. D., von Dassow, P., Rost, B., John, U. (June 30, 2016): P- and N-depletion trigger similar cellular responses to promote senescence in eukaryotic phytoplankton. *Front. Mar. Sci.*, doi:10.3389/fmars.2016.00109.

Rontani, J.-F., Cuny, P., Grossi, V., Beker, B. (1997): Stability of long-chain alkenones in senescing cells of *Emiliania huxleyi*: Effect of photochemical and aerobic microbial degradation on the alkenone unsaturation ratio ($U^{K'}_{37}$). *Org. Geochem.* **26**, 503–509, doi:10.1016/S0146-6380(97)00023-5.

Rontani, J.-F., Jameson, I., Christodoulou, S., Volkman, J. K. (2007): Free radical oxidation (autoxidation) of alkenones and other lipids in cells of *Emiliania huxleyi*. *Phytochemistry* **68**, 913–924, doi:10.1016/j.phytochem.2006.12.013.

Roscoff Culture Collection (2017): Strain information for *Emiliania huxleyi* RCC 1216. http://roscoff-culture-collection.org/rcc-strain-details/1216 (20.01.2017)

Rosenwasser, S., Mausz, M. A., Schatz, D., Sheyn, U., Malitsky, S., Aharoni, A., Weinstock, E., Tzfadia, O., Ben-Dor, S., Feldmesser, E., Pohnert, G., Vardi, A. (2014): Rewiring host lipid metabolism by large viruses determines the fate of *Emiliania huxleyi*, a bloom-forming alga in the ocean. *Plant Cell* **26**, 2689–2707, doi:10.1105/tpc.114.125641.

Rost, B., Riebesell, U. (2004): *Coccolithophores and the biological pump: responses to environmental changes*. In *Coccolithophores: From molecular processes to global impact*, 1rst Ed. Eds. Thierstein, H.R., Young, J.R., Springer, Heidelberg, Germany.

Roy, S. (1988): Effects of changes in physiological condition on HPLC-defined chloropigment composition of *Phaeodactylum tricornutum* (Bohlin) in batch and turbidostat cultures. *J. Exp. Mar. Biol. Ecol.* **188**, 137–149, doi:10.1016/0022-0981(88)90236-5.

Ruivo, M., Amorim, A., Cartaxana, P. (2011): Effects of growth phase and irradiance on phytoplankton pigment ratios: Implications for chemotaxonomy in coastal waters. *J. Plankton Res.* **33**, 1012–1022, doi:10.1093/plankt/fbr019.

Saitoh, K., Awaka, I., Suzuki, N. (1993): Separation of chlorophyll c_1 and c_2 by reversed-phase high-performance liquid chromatography. *J. Chrom. A* **653**, 247–251, doi:10.1016/0021-9673(93)83181-Q.

Sakshaug, E., Granéli, E., Elbrächter, M., Kayser, H. (1984): Chemical composition and alkaline phosphatase activity of nutrient-saturated and P-deficient cells of four marine dinoflagellates. *J. Exp. Mar. Biol. Ecol.* **77**, 241–254, doi:10.1016/0022-0981(84)90122-9.

Salter, I., Lampitt, R. S., Sanders, R., Poulton, A., Kemp, A. E., Boorman, B., Saw, K., Pearce, R. (2007): Estimating carbon, silica and diatom export from a naturally fertilised phytoplankton bloom in the Southern Ocean using PELAGRA: A novel drifting sediment trap. *Deep Sea Res. Part 2 Top. Stud. Oceanogr.* **54**, 2233–2259, doi:10.1016/j.dsr2.2007.06.008.

Sanjaya, Miller, R., Durrett, T. P., Kosma, D. K., Lydic, T. A., Muthan, B., Koo, A. J. K., Bukhman, Y. V., Reid, G. E., Howe, G. A., Ohlrogge, J., Benning, C. (2013): Altered lipid composition and enhanced nutritional value of *Arabidopsis* leaves following introduction of an algal diacylglycerol acyltransferase 2. *Plant Cell* **2**, 677–693, doi:10.1105/tpc.112.104752.

Sarazin, G., Michard, G., Prevot, F. (1999): A rapid and accurate spectroscopic method for alkalinity measurements in sea water samples. *Water Res.* **33**, 290–294, doi:10.1016/S0043-1354(98)00168-7.

Saruwatari, K., Ozaki, N., Nagasawa, H., Kogure, T. (2008): Comparison of crystallographic orientations between living (*Emiliania huxleyi* and *Gephyrocapsa oceanica*) and fossil (*Watznaueria barnesiae*) coccoliths using electron microscopes. *Am. Mineral.* **93**, 1670–1677, doi:10.2138/am.2008.2924.

Satoh, M., Iwamoto, K., Suzuki, I., Shiraiwa, Y. (2009): Cold stress stimulates intracellular calcification by the coccolithophore, *Emiliania huxleyi* (Haptophyceae) under phosphate-deficient conditions. *Mar. Biotech.* **11**, 327–333, doi:10.1007/s10126-008-9147-0.

Sawada, K., Handa, N., Shiraiwa, Y., Danbara, A., Montani, S. (1996): Long-chain alkenones and alkyl alkenoates in the coastal and pelagic sediments of the northwest North Pacific, with special reference to the reconstruction of *Emiliania huxleyi* and *Gephyrocapsa oceanica* ratios. *Org. Geochem.* **24**, 751–764, doi:10.1016/S0146-6380(96)00087-3.

Sawada, K., Shiraiwa, Y. (2004): Alkenone and alkenoic acid compositions of the membrane fractions of *Emiliania huxleyi*. *Phytochemistry* **65**, 1299–1307, doi:10.1016/j.phytochem.2004.03.015.

Sayanova, O., Haslam, R. P., Venegas Calerón, M., Ruiz López, N., Worthy, C., Rooks, P., Allen, M. J., Napier, J. A. (2011): Identification and functional characterisation of genes encoding the omega-3 polyunsaturated fatty acid biosynthetic pathway from the coccolithophore *Emiliania huxleyi*. *Phytochemistry* **72**, 594–600, doi:10.1016/j.phytochem.2011.01.022.

Schlüter, L., Møhlenberg, F., Havskum, H., Larsen, S. (2000): The use of phytoplankton pigments for identifying and quantifying phytoplankton groups in coastal areas: Testing the influence of light and nutrients on pigment/chlorophyll a ratios. *Mar. Ecol. Prog. Ser.* **192**, 49–63, doi:10.3354/meps192049.

Schreiner, M. (2006): *Principles for the analysis of omega-3 fatty acids*. In *Omega 3 fatty acid research*. Eds. Teale, M.C., Nova Science Publ, New York, US, 1–25.

Schroeder, D. C., Oke, J., Malin, G., Wilson, W. H. (2002): Coccolithovirus (Phycodnaviridae): characterisation of a new large dsDNA algal virus that infects *Emiliana huxleyi*. *Arch. Virol.* **147**, 1685–1698, doi:10.1007/s00705-002-0841-3.

Schulte, T., Niedzwiedzki, D. M., Birge, R. R., Hiller, R. G., Polivka, T., Hofmann, E., Frank, H. A. (2009): Identification of a single peridinin sensing Chl-a excitation in reconstituted PCP by crystallography and spectroscopy. *PNAS* **106**, 20764–20769, doi:10.1073/pnas.0908938106.

Schwarzhans, J.-P., Cholewa, D., Grimm, P., Beshay, U., Risse, J.-M., Friehs, K., Flaschel, E. (2015): Dependency of the fatty acid composition of *Euglena gracilis* on growth phase and culture conditions. *J. Appl. Phycol.* **27**, 1389–1399, doi:10.1007/s10811-014-0458-4.

Scott, S. A., Davey, M. P., Dennis, J. S., Horst, I., Howe, C. J., Lea-Smith, D. J., Smith, A. G. (2010): Biodiesel from algae: Challenges and prospects. *Curr. Opin. Biotechn.* **21**, 277–286, doi:10.1016/j.copbio.2010.03.005.

Shaw, G. E. (1983): Bio-controlled thermostasis involving the sulfur cycle. *Climatic Change* **5**, 297–303, doi:10.1007/BF02423524.

Shemi, A., Schatz, D., Fredricks, H. F., Van Mooy, B. A. S., Porat, Z., Vardi, A. (2016): Phosphorus starvation induces membrane remodeling and recycling in *Emiliania huxleyi*. *New Phytol.* **211**, 886–898, doi:10.1111/nph.13940.

Shevchenko, A., Simons, K. (2010): Lipidomics: coming to grips with lipid diversity. *Nat. Rev. Mol. Cell Biol.* **11**, 593–598, doi:10.1038/nrm2934.

Shi, D., Xu, Y., Hopkinson, B. M., Morel, F. M. M. (2010): Effect of ocean acidification on iron availability to marine phytoplankton. *Science* **327**, 676–679, doi:10.1126/science.1183517.

Shiraiwa, Y. (2003): Physiological regulation of carbon fixation in the photosynthesis and calcification of coccolithophorids. *Comp. Biochem. Physiol. B Biochem. Mol. Biol.* **136**, 775–783, doi:10.1016/S1096-4959(03)00221-5.

Siefermann-Harms, D. (1987): The light-harvesting and protective functions of carotenoids in photosynthetic membranes. *Physiol. Plant.* **69**, 561–568, doi:10.1111/j.1399-3054.1987.tb09240.x.

Sikes, C. S., Wilbur, K. M. (1982): Functions of coccolith formation. *Limnol. Oceanogr.* **27**, 18–26, doi:10.4319/lo.1982.27.1.0018.

Smith, R. M. (2004): *Column liquid chromatography*. In *Chromatography: Fundamentals and applications of chromatography and related differential migration methods*, 6th ed. Eds. Heftmann, E., Elsevier, Amsterdam, Netherlands, 95–138.

Smith, S. R., Abbriano, R. M., Hildebrand, M. (2012): Comparative analysis of diatom genomes reveals substantial differences in the organization of carbon partitioning pathways. *Algal Res.* **1**, 2–16, doi:10.1016/j.algal.2012.04.003.

Solomon, S., Qin, D., Manning, M., Chen, Z., Marquis, M., Averyt, K. B., Tignor, M., Miller, H. L. (2007): *Climate change 2007: The physical science basis. Contribution of working group I to the fourth assessment report of the intergovernmental panel on climate change*, Cambridge University Press, Cambridge, UK.

Solovchenko, A. E., Khozin-Goldberg, I., Didi-Cohen, S., Cohen, Z., Merzlyak, M. N. (2008): Effects of light and nitrogen starvation on the content and composition of carotenoids of the green microalga *Parietochloris incisa*. *Russ. J. Plant Physiol.* **55**, 455–462, doi:10.1134/S1021443708040043.

Songaila, E., Augulis, R., Gelzinis, A., Butkus, V., Gall, A., Büchel, C., Robert, B., Zigmantas, D., Abramavicius, D., Valkunas, L. (2013): Ultrafast energy transfer from chlorophyll c_2 to chlorophyll a in fucoxanthin–chlorophyll protein complex. *J. Phys. Chem. Lett.* **4**, 3590–3595, doi:10.1021/jz401919k.

Spielmeyer, A., Gebser, B., Pohnert, G. (2011): Dimethylsulfide sources from microalgae: Improvement and application of a derivatization-based method for the determination of dimethylsulfoniopropionate and other zwitterionic osmolytes in phytoplankton. *Mar. Chem.* **124**, 48–56, doi:10.1016/j.marchem.2010.12.001.

Stebbins, G. L., Hill, G. J. C. (1980): Did multicellular plants invade the land? *Am. Nat.* **115**, 342–353, doi:10.1086/283565.

Stehfest, K., Toepel, J., Wilhelm, C. (2005): The application of micro-FTIR spectroscopy to analyze nutrient stress-related changes in biomass composition of phytoplankton algae. *Plant Phys. Biochem.* **43**, 717–726, doi:10.1016/j.plaphy.2005.07.001.

Stolte, W., Kraay, G. W., Noordeloos, A. A. M., Riegman, R. (2000): Genetic and physiological variation in pigment composition of *Emiliania huxleyi* (Prymnesiophyceae) and the potential use of its pigment ratios as a quantitative physiological marker. *J. Phycol.* **36**, 529–539, doi:10.1046/j.1529-8817.2000.99158.x.

Sumner, L. W., Amberg, A., Barrett, D., Beale, M. H., Beger, R., Daykin, C. A., Fan, T. W.-M., Fiehn, O., Goodacre, R., Griffin, J. L., Hankemeier, T., Hardy, N., Harnly, J., Higashi, R., Kopka, J., Lane, A. N., Lindon, J. C., Marriott, P., Nicholls, A. W., Reily, M. D., Thaden, J. J., Viant, M. R. (2007): Proposed minimum reporting standards for chemical analysis. *Metabolomics* **3**, 211–221, doi:10.1007/s11306-007-0082-2.

Sunda, W., Kieber, D. J., Kiene, R. P., Huntsman, S. (July 18, 2002): An antioxidant function for DMSP and DMS in marine algae. *Nature*, doi:10.1038/nature00851.

Sviben, S., Gal, A., Hood, M. A., Bertinetti, L., Politi, Y., Bennet, M., Krishnamoorthy, P., Schertel, A., Wirth, R., Sorrentino, A., Pereiro, E., Faivre, D., Scheffel, A. (April 14, 2016): A vacuole-like compartment concentrates a disordered calcium phase in a key coccolithophorid alga. *Nat. Commun.*, doi:10.1038/ncomms11228.

Szabados, L., Savoure, A. (2010): Proline: A multifunctional amino acid. *Trends Plant Sci.* **15**, 89–97, doi:10.1016/j.tplants.2009.11.009.

Takaichi, S. (2011): Carotenoids in algae: distributions, biosyntheses and functions. *Mar. Drugs* **9**, 1101–1118, doi:10.3390/md9061101.

Tanabe, Y., Shitara, T., Kashino, Y., Hara, Y., Kudoh, S. (2011): Utilizing the effective xanthophyll cycle for blooming of *Ochromonas smithii* and *O. itoi* (Chrysophyceae) on the snow surface. *PLoS ONE* **6**, e14690, doi:10.1371/journal.pone.0014690.

Tanaka, Y., Sasaki, N., Ohmiya, A. (2008): Biosynthesis of plant pigments: anthocyanins, betalains and carotenoids. *Plant J.* **54**, 733–749, doi:10.1111/j.1365-313X.2008.03447.x.

Theodorou, M. E., Elrifi, I. R., Turpin, D. H., Plaxton, W. C. (1991): Effects of phosphorus limitation on respiratory metabolism in the green alga *Selenastrum minutum*. *Plant Physiol.* **95**, 1089–1095, doi:10.1104/pp.95.4.1089.

Thierstein, H. R., Geitzenauer, K. R., Molfino, B., Shackleton, N. J. (1977): Global synchroneity of late Quaternary coccolith datum levels validation by oxygen isotopes. *Geol.* **5**, 400, doi:10.1130/0091-7613(1977)5<400:GSOLQC>2.0.CO;2.

Thompson, P. A., Guo, M.-x., Harrison, P. J., Whyte, J. N. C. (1992): Effects of variation in temperature. II. On the fatty acid composition of eight species of marine phytoplankton. *J. Phycol.* **28**, 488–497, doi:10.1111/j.0022-3646.1992.00488.x.

Tsuji, Y., Yamazaki, M., Suzuki, I., Shiraiwa, Y. (2015): Quantitative analysis of carbon flow into photosynthetic products functioning as carbon storage in the marine coccolithophore, *Emiliania huxleyi*. *Mar. Biotech.* **17**, 428–440, doi:10.1007/s10126-015-9632-1.

150

Turner, S. M., Malin, G., Liss, P. S., Harbour, D. S., Holligan, P. M. (1988): The seasonal variation of dimethyl sulfide and dimethylsulfoniopropionate concentrations in nearshore waters. *Limnol. Oceanogr.* **33**, 364–375, doi:10.4319/lo.1988.33.3.0364.

Twining, B. S., Nuñez-Milland, D., Vogt, S., Johnson, R. S., Sedwick, P. N. (2010): Variations in *Synechococcus* cell quotas of phosphorus, sulfur, manganese, iron, nickel, and zinc within mesoscale eddies in the Sargasso Sea. *Limnol. Oceanogr.* **55**, 492–506, doi:10.4319/lo.2010.55.2.0492.

Tyrrell, T., Merico, A. (2004): *Emiliania huxleyi: Bloom observations and the conditions that induce them*. In *Coccolithophores: From molecular processes to global impact*, 1rst Ed. Eds. Thierstein, H.R., Young, J.R., Springer, Heidelberg, Germany, 75–97.

Tyrrell, T., Taylor, A. (1996): A modelling study of *Emiliania huxleyi* in the NE atlantic. *J. Mar. Systems* **9**, 83–112, doi:10.1016/0924-7963(96)00019-X.

Tyson, R. V., Funnell, B. M. (1987): European cretaceous shorelines, stage by stage. *Palaeogeogr. Palaeoclimatol. Palaeoecol.* **59**, 69–91, doi:10.1016/0031-0182(87)90075-7.

Ulberth, F., Gabernig, R. G., Schrammel, F. (1999): Flame-ionization detector response to methyl, ethyl, propyl, and butyl esters of fatty acids. *J. Amer. Oil Chem. Soc.* **76**, 263–266, doi:10.1007/s11746-999-0228-7.

van Bleijswijk, J. D. L., Kempers, R. S., Veldhuis, M. J., Westbroek, P. (1994): Cell and growth characteristics of types A and B of *Emiliania huxleyi* (Prymnesiophyceae) as determined by flow cytometry and chemical analyses. *J. Phycol.* **30**, 230–241, doi:10.1111/j.0022-3646.1994.00230.x.

van der Meeren, P., Vanderdeelen, J. (2013): *Preparative high-performance liquid chromatography of lipids*. In *Advances in lipid methodology*. Eds. Christie, W.W., Woodhead Publishing, Cambridge, UK, 83–118.

van der Wal, P., Jong, E. W. de, Westbroek, P., Bruijn, W. C. de, Mulder-Stapel, A. A. (1983): Ultrastructural polysaccharide localization in calcifying and naked cells of the coccolithophorid *Emiliania huxleyi*. *Protoplasma* **118**, 157–168, doi:10.1007/BF01293073.

van der Wal, P., Kempers, R. S., Veldhuis, M. J. W. (1995): Production and downward flux of organic matter and calcite in a North Sea bloom of the coccolithophore *Emiliania huxleyi*. *Mar. Ecol. Prog. Ser.* **126**, 247–265.

van Etten, J. L., Graves, M. V., Muller, D. G., Boland, W., Delaroque, N. (2002): Phycodnaviridae - large DNA algal viruses. *Arch. Virol.* **147**, 1479–1516, doi:10.1007/s00705-002-0822-6.

van Gulik, W. M. (2010): Fast sampling for quantitative microbial metabolomics. *Curr. Opin. Biotechn.* **21**, 27–34, doi:10.1016/j.copbio.2010.01.008.

van Lenning, K., Probert, I., Latasa, M., Estrada, M., Young, J. R. (2004): *Pigment diversity of coccolithophores in relation to taxonomy, phylogeny and ecological preferences*. In *Coccolithophores: From molecular processes to global impact*, 1rst Ed. Eds. Thierstein, H.R., Young, J.R., Springer, Heidelberg, Germany, 51–73.

van Mooy, B. A., Fredricks, H. F., Pedler, B. E., Dyhrman, S. T., Karl, D. M., Koblizek, M., Lomas, M. W., Mincer, T. J., Moore, L. R., Moutin, T., Rappe, M. S., Webb, E. A. (2009): Phytoplankton in the ocean use non-phosphorus lipids in response to phosphorus scarcity. *Nature* **458**, 69–72, doi:10.1038/nature07659.

van Oostende, N., Moerdijk-Poortvliet, T. C. W., Boschker, H. T. S., Vyverman, W., Sabbe, K. (2013): Release of dissolved carbohydrates by *Emiliania huxleyi* and formation of transparent exopolymer particles depend on algal life cycle and bacterial activity. *Environm. Microbiol.* **15**, 1514–1531, doi:10.1111/j.1462-2920.2012.02873.x.

van Wagenen, J., Miller, T. W., Hobbs, S., Hook, P., Crowe, B., Huesemann, M. (2012): Effects of light and temperature on fatty acid production in *Nannochloropsis salina*. *Energies* **5**, 731–740, doi:10.3390/en5030731.

Vardi, A., Haramaty, L., Van Mooy, B. A. S., Fredricks, H. F., Kimmance, S. A., Larsen, A., Bidle, K. D. (): Host-virus dynamics and subcellular controls of cell fate in a natural coccolithophore population. *PNAS*, doi:10.1073/pnas.1208895109.

Vårum, K. M., Kvam, B. J., Myklestad, S., Paulsen, B. S. (1986): Structure of a food-reserve β-D-glucan produced by the haptophyte alga *Emiliania huxleyi* (Lohmann) Hay and Mohler. *Carbohydr. Res.* **152**, 243–248, doi:10.1016/S0008-6215(00)90304-5.

Vehovec, T., Obreza, A. (2010): Review of operating principle and applications of the charged aerosol detector. *J. Chromatogr. A* **1217**, 1549–1556, doi:10.1016/j.chroma.2010.01.007.

Vidoudez, C., Pohnert, G. (2012): Comparative metabolomics of the diatom *Skeletonema marinoi* in different growth phases. *Metabolomics* **8**, 654–669, doi:10.1007/s11306-011-0356-6.

Villas-Bôas, S. G., Roessner, U., Hansen, M. A. E., Smedsgaard, J., Nielsen, J. (2007): *Metabolome Analysis: An Introduction*, John Wiley & Sons, Hoboken, NJ, USA.

Voigt, R. G., Jensen, C. L., Fraley, J. K., Rozelle, J. C., Brown, F. R. 3., Heird, W. C. (2002): Relationship between omega3 long-chain polyunsaturated fatty acid status during early infancy and neurodevelopmental status at 1 year of age. *J. Hum. Nutr. Diet* **15**, 111–120.

Volkman, J. K., Eglinton, G., Corner, E., Sargent, J. R. (1980a): Novel unsaturated straight-chain C37-C39 methyl and ethyl ketones in marine sediments and a coccolithophore *Emiliania huxleyi*. *Phys. Chem. Earth* **12**, 219–227, doi:10.1016/0079-1946(79)90106-X.

Volkman, J. K., Eglinton, G., Corner, E. D., Forsberg, T. (1980b): Long-chain alkenes and alkenones in the marine coccolithophorid *Emiliania huxleyi*. *Phytochemistry* **19**, 2619–2622, doi:10.1016/S0031-9422(00)83930-8.

Volkman, J. K., Everitt, D. A., Allen, D. I. (1986): Some analyses of lipid classes in marine organisms, sediments and seawater using thin-layer chromatography-flame ionisation detection. *J. Chromatogr. A* **356**, 147–162, doi:10.1016/S0021-9673(00)91474-2.

Volkman, J. K., Smith, D. J., Eglinton, G., Forsberg, T. E. V., Corner, E. D. S. (1981): Sterol and fatty acid composition of four marine haptophycean algae. *J. Mar. Biol. Ass.* **02**, 509, doi:10.1017/S0025315400047111.

von Dassow, P., John, U., Ogata, H., Probert, I., Bendif, E. M., Kegel, J. U., Audic, S., Wincker, P., Da Silva, C., Claverie, J.-M., Doney, S., Glover, D. M., Flores, D. M., Herrera, Y., Lescot, M., Garet-Delmas, M.-J., de Vargas, C. (2015): Life-cycle modification in open oceans accounts for genome variability in a cosmopolitan phytoplankton. *ISME J* **9**, 1365–1377, doi:10.1038/ismej.2014.221.

von Dassow, P., Ogata, H., Probert, I., Wincker, P., Da, S. C., Audic, S., Claverie, J. M., Vargas, C. de (2009): Transcriptome analysis of functional differentiation between haploid and diploid cells of *Emiliania huxleyi*, a globally significant photosynthetic calcifying cell. *Genome Biol.* **10**, R114, doi:10.1186/gb-2009-10-10-r114.

Ward, O. P., Singh, A. (2005): Omega-3/6 fatty acids: Alternative sources of production. *Proc. Biochem.* **40**, 3627–3652, doi:10.1016/j.procbio.2005.02.020.

Welti, R., Li, W., Li, M., Sang, Y., Biesiada, H., Zhou, H.-E., Rajashekar, C. B., Williams, T. D., Wang, X. (2002): Profiling membrane lipids in plant stress responses. Role of phospholipase D alpha in freezing-induced lipid changes in *Arabidopsis*. *J. Biol. Chem.* **277**, 31994–32002, doi:10.1074/jbc.M205375200.

Westbroek, P., Brown, C. W., van Bleijswijk, J., Brownlee, C., Brummer, G. J., Conte, M., Egge, J., Fernández, E., Jordan, R., Knappertsbusch, M., Stefels, J., Veldhuis, M., van der Wal, P., Young, J. (1993): A model system approach to biological climate forcing. The example of *Emiliania huxleyi*. *Glob. Planet. Change* **8**, 27–46, doi:10.1016/0921-8181(93)90061-R.

Westbroek, P., Jong, E. W. de, van der Wal, P., Borman, A. H., Vrind, J. P. M. de, Kok, D., Bruijn, W. C. de, Parker, S. B. (1984): Mechanism of calcification in the marine alga *Emiliania huxleyi* [and Discussion]. *Phil. Transact. Royal Soc. B* **1121**, 435–444, doi:10.1098/rstb.1984.0037.

Wilhelm, C., Buchel, C., Fisahn, J., Goss, R., Jakob, T., Laroche, J., Lavaud, J., Lohr, M., Riebesell, U., Stehfest, K., Valentin, K., Kroth, P. G. (2006): The regulation of carbon and nutrient assimilation in diatoms is significantly different from green algae. *Protist* **157**, 91–124, doi:10.1016/j.protis.2006.02.003.

Wilson, W. H., Tarran, G. A., Schroeder, D., Cox, M., Oke, J., Malin, G. (2002): Isolation of viruses responsible for the demise of an *Emiliania huxleyi* bloom in the English Channel. *J. Mar. Biol. Ass.* **82**, 369–377, doi:10.1017/S002531540200560X.

Wilson, W. H., Turner, S., Mann, N. H. (1998): Population dynamics of phytoplankton and viruses in a phosphate-limited mesocosm and their effect on DMSP and DMS production. *Estuar. Coast. Shelf Sci.* **46**, 49–59, doi:10.1006/ecss.1998.0333.

Winter, A., Jordan, R., Roth P.H. (1994): *Biogeography of living coccolithophores in ocean waters*. In *Coccolithophores*. Eds. Winter, A., Siesser, W.G., Cambridge University Press, Cambridge, New York, US, 161–177.

Wolf-Gladrow, D. A., Zeebe, R. E., Klaas, C., Körtzinger, A., Dickson, A. G. (2007): Total alkalinity: The explicit conservative expression and its application to biogeochemical processes. *Mar. Chem.* **106**, 287–300, doi:10.1016/j.marchem.2007.01.006.

Wünschiers, R. (2012): *Carbohydrate metabolism and citrate cycle*. In *Biochemical pathways: an atlas of biochemistry and molecular biology*, 2. ed. Eds. Michal, G., Wiley, Hoboken, NJ, US, 37–57.

Wünschiers, R. (2012): *Amino acids and derivatives*. In *Biochemical pathways: an atlas of biochemistry and molecular biology*, 2. ed. Eds. Michal, G., Wiley, Hoboken, NJ, US, 58–81.

Wünschiers, R. (2012): *Lipids and glycolipids*. In *Biochemical pathways: an atlas of biochemistry and molecular biology*, 2. ed. Eds. Michal, G., Wiley, Hoboken, NJ, US, 93–106.

Wurch, L. L., Bertrand, E. M., Saito, M. A., Van Mooy, B. A. S., Dyhrman, S. T. (2011): Proteome changes driven by phosphorus deficiency and recovery in the brown tide-forming alga *Aureococcus anophagefferens*. *PLoS ONE* **6**, e28949, doi:10.1371/journal.pone.0028949.

Xu, H. X., Weng, X. Y., Yang, Y. (2007): Effect of phosphorus deficiency on the photosynthetic characteristics of rice plants. *Russ. J. Plant Physiol.* **54**, 741–748, doi:10.1134/S1021443707060040.

Xu, J., Bach, L. T., Schulz, K. G., Zhao, W., Gao, K., Riebesell, U. (2016): The role of coccoliths in protecting *Emiliania huxleyi* against stressful light and UV radiation. *Biogeosciences* **13**, 4637–4643, doi:10.5194/bg-13-4637-2016.

Yamamoto, M., Shiraiwa, Y., Inouye, I. (2000): Physiological responses of lipids in *Emiliania huxleyi* and *Gephyrocapsa oceanica* (Haptophyceae) to growth status and their implications for alkenone paleothermometry. *Org. Geochem.* **31**, 799–811, doi:10.1016/S0146-6380(00)00080-2.

Yoon, K., Han, D., Li, Y., Sommerfeld, M., Hu, Q. (2012): Phospholipid:diacylglycerol acyltransferase is a multifunctional enzyme involved in membrane lipid turnover and degradation while synthesizing triacylglycerol in the unicellular green microalga *Chlamydomonas reinhardtii*. *Plant Cell* **24**, 3708–3724, doi:10.1105/tpc.112.100701.

Young, Davis, Bown, Mann (1999): Coccolith ultrastructure and biomineralisation. *J. Struct. Biol.* **126**, 195–215, doi:10.1006/jsbi.1999.4132.

Young, J. R. (1994): *Functions of coccoliths*. In *Coccolithophores*. Eds. Winter, A., Siesser, W.G., Cambridge University Press, Cambridge, New York, US, 63–82.

Young, J. R. (2003): Biomineralization within vesicles: The calcite of coccoliths. *Rev. Mineral. Geochem.* **54**, 189–215, doi:10.2113/0540189.

Young, J. R., Didymus, J. M., Brown, P. R., Prins, B., Mann, S. (1992): Crystal assembly and phylogenetic evolution in heterococcoliths. *Nature* **356**, 516–518, doi:10.1038/356516a0.

Zapata, M., Garrido, J. L., Jeffrey, S. W. (2006): *Chlorophyll c pigments: current status*. In *Chlorophylls and bacteriochlorophylls: Biochemistry, biophysics, functions and applications*. Eds. Grimm, B., Porra, R.J., Rüdiger, W., Scheer, H., Springer, Dordrecht, Netherlands, 39–53.

Zapata, M., Jeffrey, S. W., Wright, S. W., Rodríguez, F., Garrido, J. L., Clementson, L. (2004): Photosynthetic pigments in 37 species (65 strains) of Haptophyta. *Mar. Ecol. Prog. Ser.* **270**, 83–102, doi:10.3354/meps270083.

Zhang, X., Gamarra, J., Castro, S., Carrasco, E., Hernandez, A., Mock, T., Hadaegh, A. R., Read, B. A. (2016): Characterization of the small RNA transcriptome of the marine coccolithophorid, *Emiliania huxleyi*. *PLoS ONE* **11**, e0154279, doi:10.1371/journal.pone.0154279.

Zhang, Y.-M., Chen, H., He, C.-L., Wang, Q. (2013): Nitrogen starvation induced oxidative stress in an oil-producing green alga *Chlorella sorokiniana* C3. *PLoS ONE* **8**, e69225, doi:10.1371/journal.pone.0069225.

Zhao, Y., Yu, Z., Song, X., Cao, X. (2009): Biochemical compositions of two dominant bloom-forming species isolated from the Yangtze River estuary in response to different nutrient conditions. *J. Exp. Mar. Biol. Ecol.* **368**, 30–36, doi:10.1016/j.jembe.2008.09.023.

Danksagung